UNIVERSITA' DEGLI STUDI DI PADOVA

Sede Amministrativa: Università degli Studi di Padova

Dipartimento di Principi e Impianti di Ingegneria Chimica

SCUOLA DI DOTTORATO DI RICERCA IN INGEGNERIA INDUSTRIALE
INDIRIZZO: INGEGNERIA CHIMICA
CICLO XX

TITOLO TESI

ADVANCED TECHNOLOGIES FOR CARDIAC TISSUE ENGINEERING

Direttore della Scuola : Ch.mo Prof. Paolo Bariani
Supervisore :Ch.mo Prof. Nicola Elvassore

Dottoranda : Ing. Elisa Figallo

DATA CONSEGNA TESI
31 gennaio 2008

Table of contents

Sommario

L'ingegneria dei tessuti e le terapie a basate sull'impiego di cellule staminali sono state recentemente proposte come metodi di cura per malattie legate all'infarto del miocardio. Lo scopo di questa tesi è stato quello di fornire metodologie e tecnologie innovative per un più razionale sviluppo della ricerca in questo ambito. In questa prospettiva, sono stati sviluppati sistemi avanzati per la coltura e differenziamento di cellule staminali. In particolare la ricerca è stata focalizzata su cellule staminali umane, quali ad esempio cellule derivate dal liquido amniotico o embrionali. Nell'intento di voler ottenere un tessuto biomimetico contrattile, queste tecnologie sono state applicate a colture bidimensionali e tridimensionali, studiando in dettaglio quei parametri per più influenzano la stimolazione biofisica cellulare, come ad esempio la stimolazione elettrica. Una valutazione quantitativa della funzionalità cardiaca è stata ottenuta a livello cellulare, con un modello matematico, e a livello di tessuto con sensori ad alta sensibilità o analisi ottiche. Questi risultati sembrano promettenti per lo sviluppo di tecnologie high-throughput che permettano lo screening preclinico *in vitro* di nuovi farmaci per la cura delle cardiopatie, o per la definizione di nuovi metodi clinici per la rigenerazione del tessuto cardiaco.

Introduzione

Le malattie legate all'infarto sono una comune causa di morte nei paesi sviluppati. In seguito ad un attacco di cuore, il miocardio subisce un danno più o meno esteso che porta alla perdita di funzionalità del muscolo cardiaco e alla formazione di tessuto fibroso non funzionale. Il graduale assottigliamento della parete del muscolo determina la formazione di un'insufficienza cardiaca cronica, che attualmente può essere curata in modo efficace solo da un trapianto di cuore. Sfortunatamente questa terapia è resa poco praticabile da una grave carenza di donatori di organi e da problemi legati al rigetto del cuore trapiantato da parte del paziente. Farmaci innovativi per l'insufficienza cardiaca sono ancora uno dei più importanti bisogni clinici. In questo contesto l'ingegneria dei tessuti e terapie basate sull'iniezione locale di cellule sono state recentemente proposte come promettenti alternative.

In questa prospettiva, le cellule, il biomateriale, gli stimoli biochimici e biofisici sono certamente i fattori chiave per la realizzazione efficace di un miocardio funzionale ingegnerizzato. Anche se i risultati in questa direzione sono molto promettenti, il raggiungimento in breve periodo di una terapia efficace è rallentato dalla mancanza di metodi quantitativi d'indagine e d'analisi. La maggior parte delle attuali tecnologie impiegate nella ricerca biologica dimostrano una mancanza di conoscenza dei signaling specifici e di fattori di trascrizione che regolano i processi di differenziamento cellulare e la loro organizzazione in tessuti. Inoltre, poca attenzione è di solito rivolta alla caratterizzazione e al controllo dell'ambiente di coltura a livello cellulare. Recenti progressi nell'ingegneria dei tessuti hanno chiarito la necessità di una comprensione della biologia a livello di sistema. Solo la conoscenza dei valori critici, dell'interazione e dell'evoluzione spazio-temporale dei fattori specifici, che influenzano il processo di formazione del tessuto, permetterà di raggiungere con successo in tempi brevi l'obiettivo finale desiderato.

In una prospettiva ingegneristica, queste limitazioni offrono la possibilità di applicare le conoscenze dell'ingegneria allo sviluppo di nuovi strumenti per rendere la ricerca più veloce, più sensibile e più efficiente, aumentando il tipo e il numero di dati raccolti in

un esperimento. Lo scopo di questa tesi di dottorato è stato quello di fornire metodi razionali per la ricerca nel campo dell'ingegneria dei tessuti cardiaci. Obiettivi specifici sono stati: 1) lo sviluppo di nuovi strumenti e di nuove tecnologie per studiare il differenziamento cardiaca di cellule staminali pluripotenti, come quelle derivate dal liquido amniotico o le cellule staminali embrionali umane, controllando il microambiente cellulare durante la stimolazione biochimica o biofisica, 2) l'individuazione di metodi quantitativi per la valutazione *in vitro* della funzionalità di cellule o tessuti, 3) la valutazione della fattibilità di strategie per la rigenerazione del miocardio correlate al delivery locale di cellule *in vivo.*

La tesi si basa su 6 articoli che sono inclusi in Appendice, secondo la lista di pubblicazioni, che costituiscono il principale risultato della Ph.D. L'elevata complessità della ricerca nel campo dell'ingegneria dei tessuti cardiaca giustifica la focalizzazione del lavoro progetti di ricerca specifici molto diversi ma tutti relativi alle principali fasi di sviluppo dei tessuti funzionali (Figura 1). Alcuni di questi progetti hanno affrontato la progettazione di soluzioni avanzate di sistema cultura, altri la definizione di nuovi metodi di analisi.
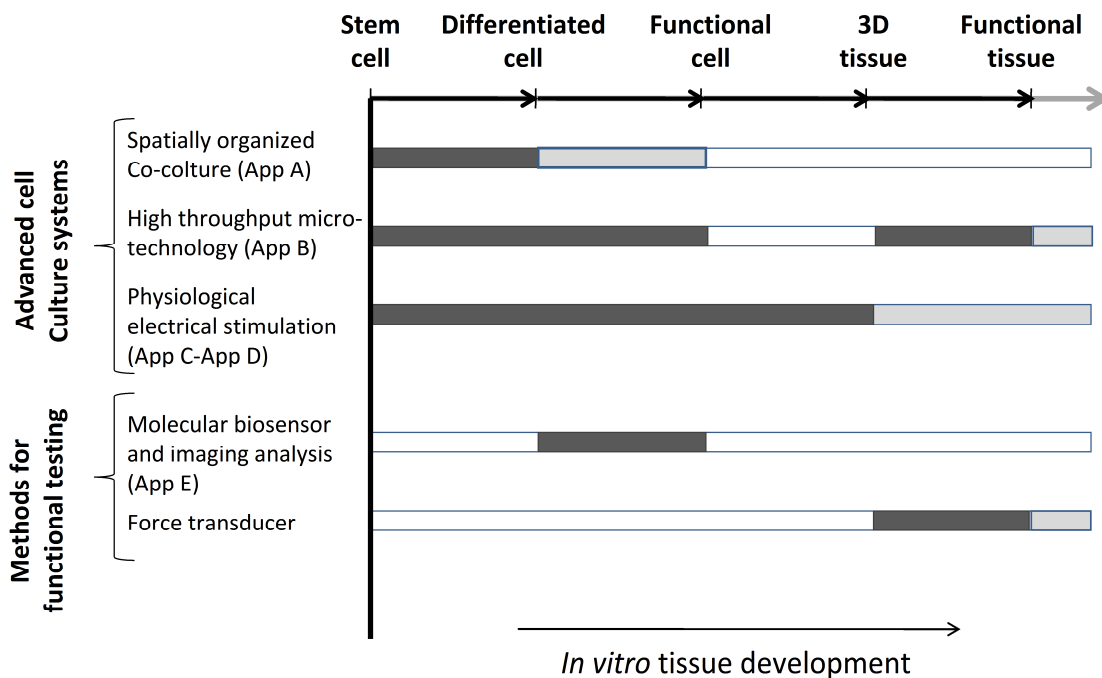
Figure 1 *Rappresentazione schematica della struttura della tesi. In grigio scuro sono segnalate le effettive influenze di un progetto specifico per una fase di sviluppo di un tessuto cardiaco funzionale. Con il grigio chiaro si segnalano invece le prospettive future individuate da tali progetti.*

In accordo con quanto detto sopra, questa tesi di dottorato è organizzata come segue:

1. Il Capitolo 1 descrive i progressi recenti nel campo dell'ingegneria del tessuto cardiaco, focalizzando l'attenzione sui fattori critici che definiscono un tessuto cardiaco funzionale e le limitazioni maggiori date dall'approccio corrente.

1. Il Capitolo 2 è incentrato sul processo di differenziamento delle cellule staminali, dando una visione generale del background della ricerca. Vengono dunque proposti un breve riassunto delle motivazioni e i risultati di tre progetti inerenti a questo argomento. I testi dettagliati delle corrispettive pubblicazioni sono riportati nelle Appendici A-C.

2. Il Capitolo 3 presenta lo stato dell'arte dei metodi di valutazione della fisiologia di una singola cellula. In questo contesto, le conclusioni sono dedicate alla descrizione delle ipotesi, dei risultati e delle prospettive future del modello matematico sviluppato qui per descrivere lo sviluppo spazio-temporale del cAMP intracellulare. Il lavoro completo è riportato in Appendice D.

3. Il Capitolo 4 tratta lo sviluppo di un tessuto tridimensionale cardiaco fornendo una descrizione generale dei requisiti e presentando brevemente un metodo efficace per la produzione di un tessuto funzionale. La descrizione estesa di tale metodologia è riportata in Appendice E. Il capitolo si conclude con la descrizione dei risultati preliminari ottenuti nello sviluppo di due tecnologie per la misura della contrattilità del tessuto ingegnerizzato.

4. Il Capitolo 5 presenta l'effettiva applicabilità di due diverse strategie per la rigenerazione del miocardio *in vivo,* che impiegano un delivery localizzato di cellule. In particolare, vengono riportati i risultati preliminari ottenuti *in vivo* sull'integrazione e vascolarizzazione di uno scaffold in collagene e la caratterizzazione chimico-fisica di un hydrogel fotopolimerizzabile. L'Appendice F descrive in dettaglio tali risultati.

5. Il Capitolo 6 riassume le conclusioni e delinea le prospettive di sviluppo della ricerca evidenziandone le potenzialità sia tecnologiche che scientifiche e le sfide più importanti per la comunità dell'ingegneria chimica in questo settore di frontiera.

Summary

Tissue engineering and cell-based therapies have been recently proposed as promising cure of diseases related to myocardium infarction. Aim of this thesis was to provide methods for rational approach the research in this field. We developed advanced systems for stem cell (SC) culture and differentiation. In particular, we focused on human stem cell, such as fetal amniotic or embryonic. To obtain biomimetic contractile tissue, these technologies have been applied to 2D and 3D cell cultures, studying in depth the parameters which influence significant biophysical stimulations, such as the electrical one. A quantitative evaluation of cardiac functionality was then performed at the cellular level, with a mathematical model, or at the tissue level, with high sensitive sensors and imaging analysis. These results seem promising for the development of high-throughput technologies for preclinical *in vitro* screening of cardiac drugs or for the definition of clinical method for cardiac regeneration.

Foreword

I believe that the most interesting advantage of being a chemical engineer resides in the possibility of applying the chemical engineering principles to a great variety of problems with extreme flexibility. I would like to thank here my supervisor, Nicola Elvassore, for giving me the opportunity of working on a spearhead and challenging field, such as the cardiac tissue engineering.

The work of this PhD program was performed at the Department of Principi e Impianti di Ingegneria Chimica of the Università di Padova. Part of the experimental section of the thesis was carried out at MIT under the supervision of the Prof. Gordana Vunjak Novakovic.

Due to high interdiscipinariety of the topic of the thesis the most relevant collaborators to achieve the final results were:

- Prof. Paolo de Coppi (Department of Pediatrics, University of London)
- Angelo Cenedese (Department of Technique and Management of Industrial Systems, Università di Vicenza)
- Saverio Sartore (Department of Biomedical Science, Università di Padova)

During of the period of the PhD program the following publications have been produced:

1. Elisa Figallo, Sharon Gerecht-Nir, Chris Cannizzaro, Robert Langer, Nicola Elvassore, Gordana Vunjak-Novakovic, "Micro Bioreactor Array for controlling cellular microenviroments", <u>Lab on the Chip</u>, Special Issue, (7) 710 – 719, July 2007, hot article.

2. Nina Tandon, Chris Cannizzaro, Elisa Figallo, Joel Voldman, Gordana Vunjak-Novakovic, "Characterization of Electrical Stimulation Electrodes for Cardiac Tissue Engineering", <u>IEEE Proceedings</u>, Aug. 2006: 845 – 848.

3. Elisa Figallo, Marina Flaibani, Barbara Zavan, Giovanni Abatangelo, Nicola Elvassore, "Micro-patterned biopolymer 3D scaffold for static and dynamic culture of human fibroblasts", <u>Biotechnology Progress</u>, 23 (1): 210 – 6, 2007.

4. W. Grayson, Ph-G Chao, D. Marolt, M. Radisic, C. Cannizzaro, E. Figallo and G. Vunjak-Novakovic, "Bioreactors for tissue engineering and regenerative medicine", <u>Translational Approaches in Tissue Engineering and Regenerative Medicine</u>, Editors: Mao JJ, Vunjak-Novakovic G, Mikos A and Atala A. Artech House, October 2007.

5. Christopher Cannizzaro, Nina Tandon, Elisa Figallo, Hyoungshin Park, Sharon Gerecht, Milica Radisic, Nicola Elvassore, and Gordana Vunjak-Novakovic, "Practical aspects of cardiac tissue engineering with electrical stimulation", <u>Methods in Molecular Medicine: Tissue Engineering</u>, Second Edition, June 2007.

6. Elisa Figallo, Christopher Cannizzaro, Sharon Gerecht-Nir, Nina Tandon, Nicola Elvassore, Gordana Vunjak-Novakovic, "Effect of electrode material on ROS expression of human embryonic stem cell", <u>Journal of Biophysical Chemistry</u> (to be submitted).

7. Elisa Figallo, Andrea Dal Cin, Cristina Longinotti, Nicola Elvassore, "Synthesis and characterization of injectable hyaluronic acid-photoinitiator conjugate hydrogel for biomedical application", <u>J. Biomed. Mater. Res. Part A</u> (to be submitted).

8. Elisa Figallo, Denj Camposilvan, Anna Terrin, Giulietta di Benedetto, Manuela Zaccolo, Nicola Elvassore, "Local diffusivity and intracellular

organization synergy in spatio-temporal cAMP signal transduction in HEK293" (to be submitted).

9. Elisa Figallo, Sveva Bollini, Elisa Bertacco, Paolo De Coppi, Nicola Elvassore, "Micro-grooved Silicone Membrane for In Vitro Co-culture of Human Amniotic Fluid Stem Cell and cardiomyocyte", <u>J. Biomed. Mater. Res. Part B</u> (to be submitted).

During of the period of the PhD program I have submitted abstracts to several international conferences, including: The American Institute of Chemical Engineers (AICHE), Biomedical Engineering Society (BMES), Tissue & Cell Engineering Society (TERMIS-EU), International Society for Stem Cell Research (ISSCR).

Introduction

Diseases related to myocardium infarction are a common cause of death in developed countries. When myocardium is damaged by injury, such as a heart attack, the functional contracting heart muscle dies and is replaced with nonfunctional scar tissue. Heart transplantation is currently the last resort for end-stage heart failure, but is hampered by a severe shortage of donor organs and rejection. Tissue engineering and cell-based therapies have been recently proposed as promising alternative; by the other side, innovative drugs for heart failure is still a major unmet clinical need.

In this perspective, cells, biomaterial and scaffold, control of biochemical and biophysical signaling regulation are certainly the key factors for a efficient engineering of functional myocardium. Even if exciting progresses have been made in this direction, they are hindered and slowed down by the lack of quantitative methods of investigation and analysis. Most of the current technologies for biological research show a lack of specific knowledge of the signaling pathways and nuclear transcription factors that regulate the processes of cell differentiation and tissue assembly. Moreover, no attention is usually given to the characterization and control of the culture environment at the cellular level. Recent progress in tissue engineering clarify the need of understand biology at the system level, knowing the interaction of single cues on the cellular organization and differentiation. Only the understanding of the threshold, the interaction and the spatio-temporal evolution of the specific factors will open the possibility of shortening the effort required to successfully replace a tissue, and direct cellular activity and phenotype toward a desired end goal.

From an engineering perspective, these limitations offer the possibility of applying the knowledge of the engineering on the development of new tools to make the investigation faster, more sensitive, or more efficient increasing the type and the number of data collected in an experiment. Aim of this PhD thesis was to provide methods for rational approach the cardiac tissue engineering research. Specific objectives were to: 1) develop new tools to study the differentiation toward cardiac

lineage of pluripotent stem cell, such as amniotic stem cell or human embryonic stem cell, controlling the cellular microenvironment during biochemical or biophysical stimulation, 2) develop quantitative methods to evaluate the *in vitro* cell or tissue functionality, 3) characterize the feasibility of strategies for myocardium regeneration correlated with localized *in vivo* delivery of cells.

The thesis is based on 6 included papers, according to the list of publications, which constitute the main outcome of the Ph.D. study and are reported in Appendix. The high complexity of the cardiac tissue engineering justifies the focus of the work on more specific research projects related to the main step of tissue functional development (Figure 1). Some of the projects were focused on the design of advanced culture system, other on the definition of new methods of analysis.
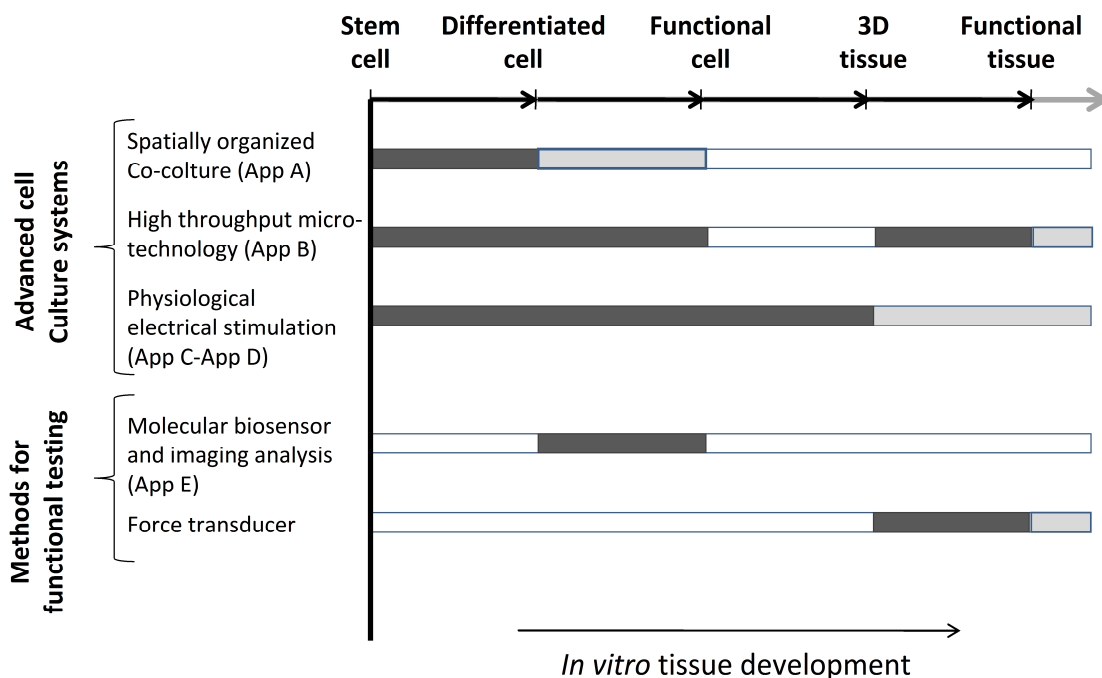
Figure 1 *Schematic representation of the thesis template. The dark grey bars show the actual influence of the specific project on the development of functional cardiac tissue, whereas the light grey gives the future perspectives.*

According to this, the PhD thesis is organized as follows:

1. Chapter 1 reviews the recent progress in cardiac tissue engineering, describing the general requirements for a functional cardiac tissue and the main limitation of the current approach.

2. Chapter 2 deals with stem cell differentiation process giving a general overview of the research background. The motivation and results of three projects, which were developed on this field, are briefly summarized, even if the manuscripts are reported in Appendix (A-C).

3. Chapter 3 presents the state of art of the evaluation of cardiac physiology at the cellular level. In this context, the chapter ends with the description of hypothesis, results and future perspective of a mathematical model for a quantitative evaluation of the intracellular cAMP signaling. The manuscript is reported in Appendix D.

4. Chapter 4 deals with the development of the 3D cardiac tissue giving a general overview of the requirements and presenting briefly an effective method for the functional tissue fabrication. The extensive version of it is reported in Appendix E. The chapter ends with the description of the development and the preliminary results of two methods for cardiac functionality assessment.

5. Chapter 5 reports the evaluation of two different *in vivo* strategies for myocardium regeneration correlated with localized delivery of cells. In particular it summarizes the preliminary results on *in vivo* integration and vascularization of the collagen scaffold and the chemical-physical characterization of a promising photocrosslinkable hydrogel. The Appendix F shows the complete description of these last results.

6. Chapter 6 draws the conclusions of the thesis project and discusses the future perspective of the cardiac tissue engineering underlining the most promising source for scientific and technological innovation and the challenges for the chemical engineering community in this border-line field.

Chapter 1

Cardiac disease and tissue engineering

This chapter reviews the recent progress in cardiac tissue engineering, outlining on the clinical and scientific justification to the present work, the general requirements and the main areas of research involved on the development of an *in vitro* cardiac functional tissue. The chapter concludes describing briefly the main processes for the functional tissue fabrication, focusing on those where a chemical engineer could give a better contribution.

1.1 Heart disease: clinical need and regenerative medicine approach

Heart failure (HF) developed from ischemic heart disease, hypertension, and myocardial infarction is a common cause of death in developed countries. In Europe, the estimated frequency of HF patients is 0.4–2%, and the incidence increases with age, reaching a range between 6–10% in the population >65 years of age (Kaye and Krum 2007). HF is responsible for a large number of prolonged and recurrent hospitalizations, representing 1–2% of global health care costs (Roman-Sanchez, Conthe et al. 2005).

The initiation and evolution of cardiac failure depends on the accumulation of old, poorly contracting cells and the formation of scar tissue. Heart failure after a myocardial infarction (MI) is often progressive. When heart muscle is damaged by injury such as a

heart attack, heart muscle cells, known as cardiomyocytes, die. Macrophages, monocytes, and neutrophils migrate into the infarct area, initiating the inflammatory response (Christman and Lee 2006). Infarct expansion then begins to occur because of the activation of matrix metalloproteases (MMPs), which degrade the extracellular matrix and result in myocyte slippage. This weakening of the collagen scaffold results in wall thinning and ventricular dilation. After the initial inflammatory phase, there is an increase in fibrillar, cross-linked collagen deposition, which resists deformation and rupture (Sun and Weber 2000). Thus, during this process of ventricular remodeling, functional contracting tissue is replaced with nonfunctional scar tissues diminishing heart pumping ability.

Current therapeutic strategies to treat heart failure are limited to pharmacological therapies (Goldstein 2000), surgical transplantation (Miniati and Robbins 2002) and mechanical cardiac support (Stevenson and Kormos 2001). The pharmacological therapies with diuretics, inotropes, vasolidators, ACE inhibitors, β-blockers, and antiarhythmic drugs have demonstrated to reduce the patients mortality, relieving and stabilizing symptoms and preventing the progression of myocardial dysfunction (Zimmermann and Eschenhagen 2003). However, poor prognosis and shorter life expectancy of heart disease patients clearly indicate the need for alternative techniques to complement the present therapies. Mechanical circulatory support devices, such as left ventricular assist devices (LVADs), are currently used as a bridge to cardiac transplantation. Current limitations of these support devices include thromobogenicity, infections, device size and weight, and power transmission. (Stevenson and Kormos 2001). Currently, heart transplantation is the only successful and definitive treatment for heart failure, however it is hampered by a severe shortage of organs donors and rejection (Stevenson, Warner et al. 1994).

In this context, cellular transplantation and tissue engineering approaches have emerged as promising alternatives to heart transplantation. The concept of myocardial regeneration may be divided into four different approaches (Giraud, Armbruster et al. 2007). The first one is the induction or stimulation of endogenous repair mechanisms, such as progenitor cells. Recent works have shown the evidences of their existence in the heart (Garry and Martin 2004; Laugwitz, Moretti et al. 2005; Parmacek and Epstein

2005). However, the triggers, as well as the exact factors or mediators involved in the tissue repair process, remain only partially identified (Virag and Murry 2003).

The second approach involves the transplantation of isolated cells directly in the injury. Various types of cells have been considered for the repair of damaged myocardial tissue such as fetal cardiomyocytes, embryonic stem cells, bone marrow derived stromal and mesenchymal stem cells, skeletal myoblasts, and endothelial precursor stem cells (Laflamme and Murry 2005; Dimmeler, Burchfield et al. 2007). However, cell transplantation has several disadvantages, including substantial cell death soon after the injection of cells. In addition, cell orientation and electromechanical connections after cell engraftment are only partially controllable.

A third approach to cardiac regeneration could be the myocardial implantation of tissue created *in vitro* (Eschenhagen, Fink et al. 1997; Radisic, Park et al. 2004). The aim of an engineered cardiac graft is to provide a large source of viable donor cells to repopulate the myocardium or to provide directly a contracting tissue to replace an injured myocardial area. However, the high mechanical stress represented by the permanent cardiac contraction/relaxation cycle, as well as the electric integration of the tissue within the native cardiac muscle, add to the complexity of myocardial tissue engineering. These *in vitro* 3D models of the cardiac muscle could be applied also as *in vitro* model for cardiac research or drug testing, representing a more physiological organization of cells in a complex 3-D lattice.

Finally, the fourth approach focuses on the design of smart biomaterials. Such method function for example, by organizing nanoscale assemblies of nanofibers, controlling space and orientation of specific cell-adhesive ligands on the biomaterials, and allowing release of proteins or gene delivery (Davis, Hsieh et al. 2005).

1.2   Physiology of myocardium (cardiac muscle)

The essential function of the heart, as muscular organ, is to pump blood to various parts of the body. The mammalian heart has four chambers: right and left atria (upper) and right and left ventricles (lower). The two atria act as collecting reservoirs for blood returning to the heart while the two ventricles act as pumps to eject the blood to the

body. The heart muscle is a "syncytium," meaning a network of muscle cells, called cardiac myocytes, interconnected by contiguous cytoplasmic bridges (connection disc). Under normal circumstances, a wave of electrical excitation is originated by the pacemaker cells and spread to neighboring cells causing a coordinated atrial-ventricular rhythmic contraction. This process does not necessitate of nerve stimulation.

The intact myocardium is composed of a complex array of muscle cells that are distributed in a series of discrete, overlapping cellular layers. Within each layer of cell, the cardiac myocyte are roughly cylindrical and distributed in parallel along a common axis. The biochemical basis of muscle activity is related to the enzymatic and physical properties of actin, myosin, and the accessory proteins (troponin and tropomyosin) that constitute the thin and thick filaments in the cardiomyocyte cytoplasm. Adjacent cell layers are interconnected by an elaborate network of collagen fibrils. Endothelial cells (ECs) and fibroblasts (Fs) complete the 3D muscle structure with a total cell concentration of approximately 100 million cells/cm^3. Due to this extremely high cell density, and high respiration rates of the cells, the cardiac muscle consumes large amounts of oxygen and is characterized by a rich vasculature. However ECs and Fs cells are not only necessary for nutrition and oxygen transportation, constituting the main cell type in a blood vessel, but secrete also growth factors and cytokines that are important for heart function (Shu 2007).

The ventricular wall of rat heart, range from 1-3 mm and contains a rich vasculature. In a rested, non-contracting muscle, a myocardial cell has a negative membrane potential. When the muscles is excited above a threshold value, the voltage-gated ion channels opens with a flood of cations into the cell [depolarization]. When the cytosolic calcium increases, the myosin binding sites on actin become available, an actomyosin complex is formed, followed by the sequential dissociation of Pi and ADP with conversion of myosin to its low-energy conformational state. These events are accompanied by simultaneous translocation of the attached thin filament toward the sarcomere, that gives the contraction. After a delay (the absolute refractory period), potassium channels reopen and the resulting flow of K+ out of the cell causes repolarization to the resting state.

1.3   Cardiac tissue engineering

Tissue engineering has been defined first as ''an interdisciplinary field that applies the principles of engineering and the life sciences toward the development of biological substitutes that restore, maintain, or improve tissue function'' (Langer and Vacanti 1993). In the 2001 the European Commission on Health and Consumer Protection defined tissue engineering as ''the persuasion of the body to heal itself through the delivery, to the appropriate site, independently or in synergy, of cells, biomolecules and supporting structures'' (European, Commission et al. 2001).

Cardiac tissue engineering focuses on the in vitro reconstruction of heart muscle, developing three main areas of research: cell sourcing, scaffold design and functional tissue development (Hecker and Birla 2007).

1.3.1 Cardiac related cell source

Selecting the type of cells and creating a suitable environment in which cells can grow and organize themselves in a functional way are technically and biologically important problems. Numerous studies have experimentally addressed the potential of different types of stem cells to differentiate in contractile cells. Stem cells are self-renewing and undifferentiated primitive cells that develop into functional, differentiated cells. After differentiation, these cells should integrate both functionally and structurally into the surrounding viable myocardium and develop a network of capillaries and larger size blood vessels for supply of oxygen and nutrients to the injured region.

The most promising cell sources for regenerative medicine are human stem cells (hSCs) capable of differentiation toward cardiac lineage, such as: (1) human embryonic stem cells (hES), (2) Cardiac Stem Cell (3), Bone Marrow Stem Cells (BMCs); (4) Skeletal myoblasts (SMs); 5) Fetal Amniotic Stem Cell and (5) Stem Cell derived from adipose (fat) tissue (Fukuda and Yuasa 2006).

MSCs seem to be an exciting source for cell therapy, because they can differentiate *in vitro* into nerve cells, skeletal muscle cells, vascular endothelial cells (Jiang, Jahagirdar et al. 2002), and into cells with cardiomyocyte features (Makino, Fukuda et al. 1999;

Rangappa, Entwistle et al. 2003). Furthermore, after differentiation, these cells are positive for specific cardiac protein, such as β-myosin heavy chain, cardiac troponin T, α-cardiac actin and desmin, they prove functionality with Ca^{2+} transients, several types of action potentials (Orlic, Kajstura et al. 2001; Pittenger and Martin 2004; Xu, Wani et al. 2004), and respond to α and β adrenergic stimulation with an increase in contractility, phosphorylation of ERK1/2 and an increase in cAMP (Li, Yu et al. 2007). Although studies have shown some improvement in cardiac performance after cell transplantation in patients, the cardiomyogenic efficiency of these cells is still very limited (0.02%) (Haider and Ashraf 2005).

In general, Embryonic stem (ES) cells, derived from the inner cell mass of the blastocyst, (Kehat, Kenyagin-Karsenti et al. 2001; Anne E. Bishop, Buttery et al. 2002) and Cardiac Stem Cell, harvested from endomyocardial biopsy of patients (Messina, De Angelis et al. 2004), seem to be the best promising sources for cardiac regeneration therapy because they differentiate into beating cells with a cardiomyocyte phenotype and they can also be expanded *in vitro* to generate large quantities of cells. In particular, Embryonic stem (ES) cells can spontaneously organize, after differentiation, a functional syncitium with action potential propagation. (Margaret V. Westfall, Pasyk et al. 1997; Kehat, Gepstein et al. 2002; Wah Siu, Moore et al. 2007).

1.3.2 Biomaterials and scaffold

Biomaterials are used to provide structural support during the initial stages of tissue formation. The cells utilize the biomaterial as a support for initial attachment and remodeling, but then slowly begin to generate their own ECM components. Production of new ECM is often concurrent with controlled degradation of the biomaterial; the rate of formation of the new ECM and the degradation of the old ECM being equal. Several strategies have been described by the literature for engineering 3-D cardiac tissue *in vitro*: (1) utilizing polymeric scaffolding material as a support matrix (Rebecca L. Carrier, Papadaki et al. 1999; Papadaki, Bursac et al. 2001), (2) incorporating cardiac myocytes within biodegradable gels (Eschenhagen, Fink et al. 1997; Guo, Zhao et al. 2006), or (3) utilizing overlapping of cellular contractile sheets (Shimizu, Yamato et al.

2002; Ishii, Shin et al. 2005). In all these methods, the choice of the most appropriate biomaterial is a key issue.

Natural and synthetic scaffolds have both been used for myocardial tissue engineering. Due to the contraction/relaxation cycle, typical of the muscle tissue, the governing factors for the choice of a scaffold are not only the biodegradability and biocompatibility of matrices, but also the mechanical properties, above all elasticity and strength. The key advantages of synthetic materials include the possibility of designing their mechanical properties, controlling the chemical properties without variations inherent to the production of biomaterials, defining the size and morphology of pores (Zimmermann and Eschenhagen 2003) . In addition, chemical functional groups that induce tissue growth can be added to the polymers (Martina and Hutmacher 2007). Major classes of polymers, such as polyester polyglicolic and polylactic acid (PGA, PLA), and their copolymers and polycaprolactone (PCL) have been tested in clinical applications as synthetic biodegradable materials. However the biodegradation of synthetic polymers can induce inflammatory responses to the original material or byproducts of its degradation (Babensee, Anderson et al. 1998).

In this perspective natural materials, such as hyaluronic acid, collagen and gelatin matrices, are preferred because they provide good mechanical support during tissue growth, a compliant environment allowing proliferation and migration of cells, the integration with the native tissue, and finally they provide the incorporation of growth factors. In addition to its structural role, the cell-biomaterial interaction plays a physiological role by influencing the expression or regulation of the cellular phenotype. In line with this, a natural material will mimic better the properties of the extracellular matrix (Christman and Lee 2006).

The main advantage given by the use of a polymeric scaffold is to provide a stable mechanical support to the tissue formation with a controlled structure, pore size, and polymer fiber orientations. An alternative technique to preformed matrices is the utilization of solubilized scaffold material. Gel-type structures of natural scaffold, like injectable polymers, have been considered because they provide good bonding to tissues and can be more easily shaped or cast to a complex geometry than porous scaffolds and foams. In particular liquid mixture of collagen I and matrigel, has been mixed to the

cells, which are quickly trapped in the 3D space during the gelification process. The environment is then rapidly remodeled by the cardiac cells.

An alternative strategy based on the production of 3D tissue by the overlapping of contractile sheets of cells has also been explored. Cell-culture dishes have been coated with temperature- responsive polymer or with mixture of fibrinogen monomers and thrombin. The culture of cardiomyocyte provides a sheet of contractile cells that are detached from the dish surface by reducing the temperature to less than 20°C (Sekiya, Shimizu et al. 2006) or using intrinsic protease digestion of the fibrin layer. (Itabashi, Miyoshi et al. 2005). The overlapping of these sheets established intercellular gap junctions; the cells were also able to beat synchronously and to integrate with the host animal *in vivo* (Furuta, Miyoshi et al. 2006).

1.3.3 Functional tissue development

The choice of the right cells and biocompatible materials highlights the need of physical conditioning of the cells or the engineered tissue, in order to ensure its physiological compatibility and function.

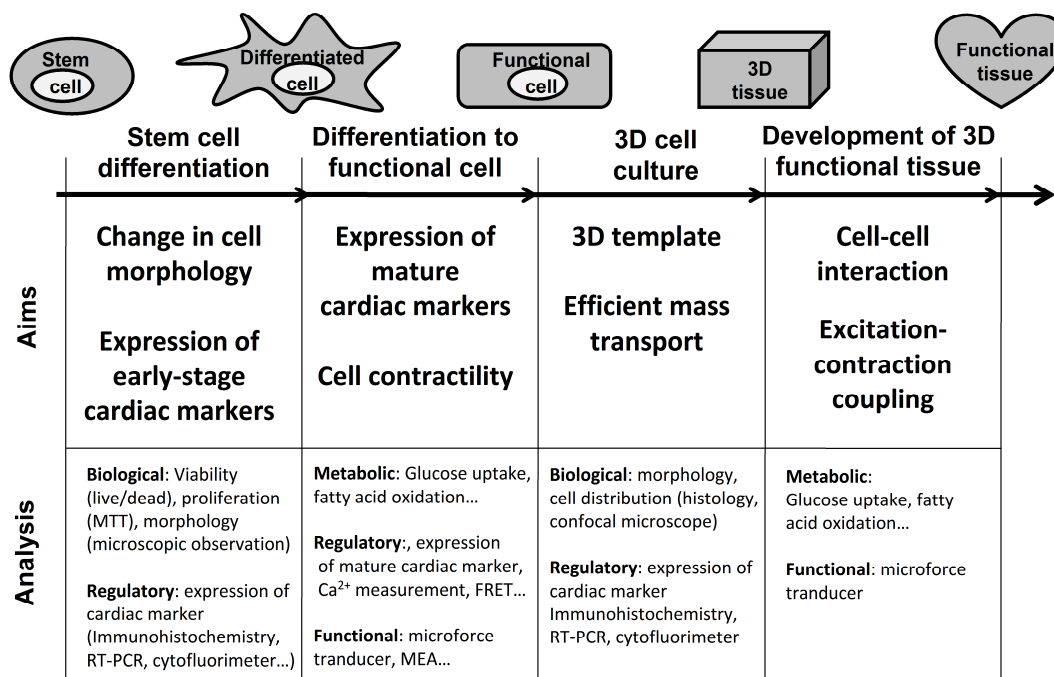|	Stem cell differentiation	Differentiation to functional cell	3D cell culture	Development of 3D functional tissue
Aims	**Change in cell morphology** **Expression of early-stage cardiac markers**	**Expression of mature cardiac markers** **Cell contractility**	**3D template** **Efficient mass transport**	**Cell-cell interaction** **Excitation-contraction coupling**
Analysis	**Biological**: Viability (live/dead), proliferation (MTT), morphology (microscopic observation) **Regulatory**: expression of cardiac marker (Immunohistochemistry, RT-PCR, cytofluorimeter…)	**Metabolic**: Glucose uptake, fatty acid oxidation… **Regulatory**:, expression of mature cardiac marker, Ca^{2+} measurement, FRET… **Functional**: microforce tranducer, MEA…	**Biological**: morphology, cell distribution (histology, confocal microscope) **Regulatory**: expression of cardiac marker Immunohistochemistry, RT-PCR, cytofluorimeter	**Metabolic**: Glucose uptake, fatty acid oxidation… **Functional**: microforce tranducer

Figure 1 *Development of a functional cardiac engineered tissue: main phases.*

Figure 1 summarizes the intermediate processes necessary to a functional tissue fabrication. At the cell level, that mainly includes the differentiation of stem cell toward cardiac lineage and the control of its maturation up to expression of mature cardiac markers and cell functionality. At the tissue level, the process continues with the culture of cell in three dimensional scaffold and its maturation to functional tissue through physical and electrical stimulation. The following section reviews the most common methods to assess these phases and the main limitations.

1.4 Engineering issues from 3D culture to functional tissue

The growing a functional heart tissue is related to several critical issues, some of which apply to all complex tissues and some which are more specific to the heart. The generic issues focus on the problem of growing a 3D construct with multiple cell types, which should homogenously populate the scaffold, be viable and keep the proper phenotype for a long period. Connected to those aims, we can individuate the problem of supplying cells deep within the construct with nutrients and set the culture parameters to permit the cell-cell communication.

Moreover we need to add problems related to the functional requirements. First of all it is necessary to obtain large quantity of mature cardiomyocytes, which should reproduce the physiological functionality of native muscle cell. In addition, it's necessary to control cell function in three-dimensional engineered tissues. This is a requirement in order to promote appropriate tissue development *in vitro* toward a physiological functionality.

In the 3D template, the cells need then to form intercellular connections and matrix arrangements to functionally coordinate and direct the beating. The alignment of myocytes and the proper formation of distinctive biological structures between myocytes (such as the intercalated disks) are also critical in enabling electrical pulses and force transmission between myocytes. The tissue requires an uniform and well-coordinated contraction that generates the required power. In addition, the heart contains specialized cells that participate in the electrical conduction routes found

throughout the heart (e.g., the sino-atrial (SA) node, the atrio-ventricular (AV) node, and Purkinje fibers). These specialized cells are crucial to the coordination of the heart's contractile effort, and substituting their function *in vitro* during the biosynthetic tissue culture may be critical. Thus key issues to a critical feature of a heart is both its morphology and the complexity of the electrical conduction pathways.

A variety of strategies have been developed to achieve these ends, including the use of bioreactors to enhance the mass transport, as well as the application of biochemical and mechanical stimulation to control and improve the cell function. However, there is still a long way to go from the small number of cardiomyocyte-like cells beating in 3D scaffold to the complex architecture of the myocardium and the duplication of its nonlinear viscoelastic properties.

1.5 Current limitations: needs for new advanced technologies

Despite of the good perspective of the cardiac tissue engineering, several issue still need to be addressed to reach a safe clinical technique. Biomedical scientists have recognized that living systems can be studied not only in terms of their mechanistic, molecular-level components but also in terms of many of them simultaneously. In addition, the biologic progress show a lack of specific knowledge of the signaling pathways and nuclear transcription factors that regulate the processes of cell differentiation and tissue assembly. However the collaboration between these two science fields is often complicated by the lack of a common methodology and language and the ability to generate novel technology requires training in multiple disciplines.

In order to understand biology at the system level, we must examine the structure and dynamics of cellular and tissue function, rather than the characteristics of isolated parts of a cell or tissue. New high-throughput technology development is therefore a crucial need to predict the quantitative behavior of a biological process, including the knowledge and control of process components, their interactions, realistic values of their concentrations and time-spatial evolution. For example it is well known that electrical stimulation is an important modulator of cell physiology, and there is

significant evidence that physical factors may be used to improve or accelerate tissue regeneration and repair *in vitro*. However, more needs to be clarified about how the electrical stimulation acts on cell and tissue level within native and artificial extracellular matrices. Knowing the signals which are activate by electrical stimulation may shorten the iterations required to successfully replace a tissue, besides directing cellular activity and phenotype toward a desired end goal.

Once implanted, tissue-engineered constructs will be subjected to significant loads and deformations *in vivo*. Moreover, given the variety of electrical conduction-related diseases in a normal myocardium, there is good reason to suspect that slight un-match with heart muscle properties will determine the failure of the cure. Standards must be set when evaluating the electrophysiological and biomechanical properties of native tissues, and new and improved technology must also be developed for collection of data on physiological function of tissue. This technology should combine high-throughput assay techniques to tissue physiology in vitro, using functional engineered tissues for basic biology as well as pharmacology/toxicology purposes. Continued development of novel molecular imaging technologies, such as fluorescence resonance energy transfer (FRET), increases speed of data acquisition and spatial resolution defining intracellular mapping of small molecules and protein. Coupling this experimental data with computational description of specific process could help on the development and application of quantitative models of physiological function.

1.6 References

Anne E. Bishop, L. D. K. Buttery, et al. (2002). "Embryonic stem cells." <u>The Journal of Pathology</u> **197**(4): 424-429.

Babensee, J. E., J. M. Anderson, et al. (1998). "Host response to tissue engineered devices." <u>Advanced Drug Delivery Reviews</u> **33**: 111-139.

Christman, K. L. and R. J. Lee (2006). "Biomaterials for the Treatment of Myocardial Infarction." <u>Journal of the American College of Cardiology</u> **48**(5): 907-913.

Davis, M. E., P. C. H. Hsieh, et al. (2005). "Custom Design of the Cardiac Microenvironment With Biomaterials." <u>Circ Res</u> **97**(1): 8-15.

Dimmeler, S., J. Burchfield, et al. (2007). "Cell-Based Therapy of Myocardial Infarction." <u>Arterioscler Thromb Vasc Biol</u>.

Eschenhagen, T., C. Fink, et al. (1997). "Three-dimensional reconstitution of embryonic cardiomyocytes in a collagen matrix: a new heart muscle model system." <u>FASEB J.</u> **11**(8): 683-694.

European, Commission, et al. (2001). Opinion on State of the Art Concerning Tissue Engineering.

Fukuda, K. and S. Yuasa (2006). "Stem Cells as a Source of Regenerative Cardiomyocytes." <u>Circ Res</u> **98**(8): 1002-1013.

Furuta, A., S. Miyoshi, et al. (2006). "Pulsatile Cardiac Tissue Grafts Using a Novel Three-Dimensional Cell Sheet Manipulation Technique Functionally Integrates With the Host Heart, In Vivo." <u>Circ Res</u> **98**(5): 705-712.

Garry, D. J. and C. M. Martin (2004). "Cardiac Regeneration: Self-Service at the Pump." <u>Circ Res</u> **95**(9): 852-854.

Giraud, M.-N., C. Armbruster, et al. (2007). "Current State of the Art in Myocardial Tissue Engineering." <u>Tissue Engineering</u> **13**(8): 1825-1836.

Goldstein, M. S. (2000). "Heart Failure Therapy at the Turn of the Century." <u>Heart Failure Reviews</u> **6**: 7-14.

Guo, X.-M., Y.-S. Zhao, et al. (2006). "Creation of Engineered Cardiac Tissue In Vitro From Mouse Embryonic Stem Cells." <u>Circulation</u> **113**(18): 2229-2237.

Haider, H. K. and M. Ashraf (2005). "Bone marrow stem cell transplantation for cardiac repair." <u>Am J Physiol Heart Circ Physiol</u> **288**(6): H2557-2567.

Hecker, L. and R. K. Birla (2007). "Engineering the heart piece by piece: state of the art in cardiac tissue engineering." <u>Regenerative Medicine</u> **2**: 125-144.

Ishii, O., M. Shin, et al. (2005). "In vitro tissue engineering of a cardiac graft using a degradable scaffold with an extracellular matrix-like topography." <u>Journal of Thoracic and Cardiovascular Surgery</u> **130**(5): 1358-1363.

Itabashi, Y., S. Miyoshi, et al. (2005). "A New Method for Manufacturing Cardiac Cell Sheets Using Fibrin-Coated Dishes and Its Electrophysiological Studies by Optical Mapping." <u>Artificial Organs</u> **29**(2): 95-103.

Jiang, Y., B. N. Jahagirdar, et al. (2002). "Pluripotency of mesenchymal stem cells derived from adult marrow." <u>Nature</u> **418**(6893): 41-49.

Kaye, D. M. and H. Krum (2007). "Drug discovery for heart failure: a new era or the end of the pipeline?" <u>Nat Rev Drug Discov</u> **6**(2): 127-139.

Kehat, I., A. Gepstein, et al. (2002). "High-Resolution Electrophysiological Assessment of Human Embryonic Stem Cell-Derived Cardiomyocytes. A Novel In Vitro Model for the Study of Conduction." <u>Circ Res</u>.

Kehat, I., D. Kenyagin-Karsenti, et al. (2001). "Human embryonic stem cells can differentiate into myocytes with structural and functional properties of cardiomyocytes." J. Clin. Invest. **108**(3): 407-414.

Laflamme, M. A. and C. E. Murry (2005). "Regenerating the heart." Nat Biotech **23**(7): 845-856.

Langer, R. and J. P. Vacanti (1993). "Tissue engineering." Science **260**(5110): 920-926.

Laugwitz, K.-L., A. Moretti, et al. (2005). "Postnatal isl1+ cardioblasts enter fully differentiated cardiomyocyte lineages." Nature **433**(7026): 647-653.

Li, X., X. Yu, et al. (2007). "Bone marrow mesenchymal stem cells differentiate into functional cardiac phenotypes by cardiac microenvironment." Journal of Molecular and Cellular Cardiology **42**(2): 295-303.

Makino, S., K. Fukuda, et al. (1999). "Cardiomyocytes can be generated from marrow stromal cells in vitro." J. Clin. Invest. **103**(5): 697-705.

Margaret V. Westfall, K. A. Pasyk, et al. (1997). "Ultrastructure and cell-cell coupling of cardiac myocytes differentiating in embryonic stem cell cultures." Cell Motility and the Cytoskeleton **36**(1): 43-54.

Martina, M. and D. W. Hutmacher (2007). "Biodegradable polymers applied in tissue engineering research: a review." Polymer International **56**: 145-157.

Messina, E., L. De Angelis, et al. (2004). "Isolation and Expansion of Adult Cardiac Stem Cells From Human and Murine Heart." Circ Res **95**(9): 911-921.

Miniati, D. N. and R. C. Robbins (2002). "Heart Transplantation: A Thirty-Year Perspective." Annual Review of Medicine **53**(1): 189-205.

Orlic, D., J. Kajstura, et al. (2001). "Mobilized bone marrow cells repair the infarcted heart, improving function and survival." Proceedings of the National Academy of Sciences **98**(18): 10344-10349.

Papadaki, M., N. Bursac, et al. (2001). "Tissue engineering of functional cardiac muscle: molecular, structural, and electrophysiological studies." Am J Physiol Heart Circ Physiol **280**(1): H168-178.

Parmacek, M. S. and J. A. Epstein (2005). "Pursuing Cardiac Progenitors: Regeneration Redux." Cell **120**(3): 295-298.

Pittenger, M. F. and B. J. Martin (2004). "Mesenchymal Stem Cells and Their Potential as Cardiac Therapeutics." Circ Res **95**(1): 9-20.

Radisic, M., H. Park, et al. (2004). "From the Cover: Functional assembly of engineered myocardium by electrical stimulation of cardiac myocytes cultured on scaffolds." Proceedings of the National Academy of Sciences **101**(52): 18129-18134.

Rangappa, S., J. W. C. Entwistle, et al. (2003). "Cardiomyocyte-mediated contact programs human mesenchymal stem cells to express cardiogenic phenotype." J Thorac Cardiovasc Surg **126**(1): 124-132.

Rebecca L. Carrier, M. Papadaki, et al. (1999). "Cardiac tissue engineering: Cell seeding, cultivation parameters, and tissue construct characterization." Biotechnology and Bioengineering **64**(5): 580-589.

Roman-Sanchez, P., P. Conthe, et al. (2005). "Factors influencing medical treatment of heart failure patients in Spanish internal medicine departments: a national survey." QJM **98**(2): 127-138.

Sekiya, S., T. Shimizu, et al. (2006). "Bioengineered cardiac cell sheet grafts have intrinsic angiogenic potential." Biochemical and Biophysical Research Communications **341**(2): 573-582.

Shimizu, T., M. Yamato, et al. (2002). "Fabrication of Pulsatile Cardiac Tissue Grafts Using a Novel 3-Dimensional Cell Sheet Manipulation Technique and Temperature-Responsive Cell Culture Surfaces." <u>Circ Res</u> **90**(3): e40-48.

Shu, Q. L. (2007). Cardiac Regenerative Engineering. <u>Bioregenerative Engineering: Principles and Applications</u>**:** 584-658.

Stevenson, L. W. and R. L. Kormos (2001). "Mechanical Cardiac Support 2000: Current applications and future trial designJune 15-16, 2000, Bethesda, Maryland." <u>J Thorac Cardiovasc Surg</u> **121**(3): 418-424.

Stevenson, L. W., S. L. Warner, et al. (1994). "The impending crisis awaiting cardiac transplantation. Modeling a solution based on selection." <u>Circulation</u> **89**(1): 450-457.

Sun, Y. and K. T. Weber (2000). "Infarct scar: a dynamic tissue." <u>Cardiovascular Research</u> **46**(2): 250-256.

Virag, J. I. and C. E. Murry (2003). "Myofibroblast and Endothelial Cell Proliferation during Murine Myocardial Infarct Repair." <u>Am J Pathol</u> **163**(6): 2433-2440.

Wah Siu, C., J. C. Moore, et al. (2007). "Human Embryonic Stem Cell-Derived Cardiomyocytes for Heart Therapies." <u>Cardiovascular Haematological Disorders - Drug Targets</u> **7**: 145-152.

Xu, M., M. Wani, et al. (2004). "Differentiation of Bone Marrow Stromal Cells Into the Cardiac Phenotype Requires Intercellular Communication With Myocytes." <u>Circulation</u> **110**(17): 2658-2665.

Zimmermann, W. H. and T. Eschenhagen (2003). "Cardiac Tissue Engineering for Replacement Therapy." <u>Heart Failure Reviews</u> **8**: 259-269.

Chapter 2

Stem cell differentiation

This Chapter focuses on methods for studying stem cell differentiation and presents the relevant parameters that influence most this process. Three different aspects have been investigated in term of: 1) approaching the *in vivo* cardiac microenvironment to study the amniotic stem cell differentiation during co-culture, 2) controlling the cellular microenvironment during culture in a high throughput manner and 3) verifying the effect of electrical stimulation on human embryonic stem cell differentiation. The brief description of each aspect is followed by a discussion of results.

2.1 Background

A stem cell is a cell that can self-renew as well as give rise to daughter cells with more specialized function. To identify stem cells, several specific phenotypic markers are usually used, such as cell surface proteins, transcriptional factors, and cytoplasmatic proteins. For example human Embryonic Stem Cells (hESCs) have enhanced telomerase activity and express a variety of markers for self renewal, such as transcription factor Oct-3/4, the protein Nanog, and the surface marker (SSEA)-3/4 (Hwang, Ryu et al. 2004; Stewart, Stojkovic et al. 2006; Biswas and Hutchins 2007). The stem cell differentiation toward cardiac lineage is a complex process. In an early stage it is proved by the expression of cardiac-related proteins (e.g. cytoskeletal protein β-myosin heavy chain, cardiac troponin-T) and transcription factors (e.g. Nkx2.5, GATA4) (Lev, Kehat et al. 2005). The physiological activity is evaluated by functional assays, including extracellular and intracellular electrophysiological recordings of second messengers,

biochemical species involved in the signal transduction of functional activity, and cell response to pharmacological stimulation (Gepstein 2006).

Stem cell differentiation is influenced by three main categories of factors: 1) cell-cell interactions, 2) biochemical cues and 3) biophysical stimulations. All these act conditioning the cellular microenvironment and triggering the specific biochemical signal transduction pathways (Huang, Lee et al. 2007).

The following sections will be organized with a brief description of the state of the art of each method followed by the summary of the developed research. Extensive description of the research activities are reported in Appendix (Table 1).

Table 1. *Summary of the three relevant categories of factors which influence the stem cell differentiation and the aim research activity developed during this Ph:D. thesis.*

Categories of stimulation	Aim of the research activity
Cell-cell interaction	Development of new tools and methodology for perfoming co-culture of stem cell on aligned cardiomyocytes (Appendix A)
Biochemical cues	Development of new method of high-throughput cell culture on microscale to study and control growth and differentiation of different cell type (Appendix B)
Biophysical stimulation	Developing of a standard method for electrical stimulation of stem cells (Appendix C)

2.2   Cell-cell interactions

Extracellular matrix and cell-cell interaction seems to play an important role in myocardium remodeling during growth and development, as well as upon ischemic injury during myocardial infarction (Matsushita, Oyamada et al. 1999; Goldsmith and Borg 2002). This suggests that the introduction of an appropriate extracellular matrix molecules within *in vitro* culture could enhance the directed differentiation of stem cells into the cardiomyogenic lineage. For example hESCs maintain pluripotency on MEF feeder layer, whereas, when cultured on matrix substrates in absence of MEF, they loose self-renewal and begin to differentiate (Thomson, Itskovitz-Eldor et al. 1998). The

optimal substrate for stem cell attachment, proliferation, and differentiation may differ between various types of stem cells.

Not only the biochemical composition but also the matrix topography and mechanical properties of the substrate direct cell organization and differentiation (Nygren, Jovinge et al. 2004; Ying J. Li, Chung et al. 2006). The stiffness of ECM has been shown to regulate many aspects of cellular functions (Geiger, Bershadsky et al. 2001). For example, cells tend to migrate toward more-rigid surfaces, and cells on soft matrix have a low rate of deoxyribonucleic acid synthesis and growth. Engler et al. (2004) examined the effect of substrate stiffness on myoblast behavior, but recent studies suggest that nano-scale and microscale matrix topography will also affect the differentiation of stem cells. If the stem cell are culture with a different cell population, this cellular organization could influence the cell-cell talking modulating the differentiation process.

Differentiation of ES cells into the cardiomyogenic lineage was enhanced by coculture with visceral endoderm-like cells (Mummery, Ward-van Oostwaard et al. 2003). A number of studies have also reported transdifferentiation of adult stem cell into the cardiomyogenic lineage when coculture with primary cardiomyocytes (Badorff, Brandes et al. 2003; Heng, Haider et al. 2004).

The aim of this study is to investigate the effect on *in vitro* differentiation toward cardiac lineage of human and rat amniotic fluid stem (AFS) cells co-culture with aligned rat neonatal cardiomyocytes (rCM). The main advantage of the co-culture systems resides in the direct biophysical and biochemical contact between the two cellular types; in particular stem cell - cardiomyocytes interactions are mediate by cellular transduction process and electromechanical junctions with neighboring cardiomyocytes (Iijima, Nagai et al. 2003). In contractile tissues such as myocardium, the cardiomyocytes orientation and elongation is critical for the proper electromechanical coupling of cells, and for stimulating the transmission of contraction over the cell length scale (Nianzhen Li, Anna Tourovskaia et al. 2003). The structural template of aligned cells seem a critical condition to optimizing the cell differentiation *in vitro*.

The following work aims to integrate these concepts with the differentiation study of human amniotic fluid stem (hAFS) cells toward the cardiac lineage. The objective of

this part of the thesis was the development of new tools and methodology for performing co-culture of stem cell with aligned and functional differentiated cardiomyocytes. A specific aim was to design a simple and reproducible method to provide topographical stimulation with micrometric resolution promoting cardiomyocytes alignment. The hypothesis was to enhance with structural tissue-like template the cell-cell interaction and cross-talking (i.e. biochemical and biophysical signal transduction). The system was designed to allow the identification of each individual cell with common optical method of analysis.

2.2.1 Micro-grooved Silicone Membrane for In Vitro Co-culture of Human Amniotic Fluid Stem Cell and cardiomyocytes

Amniotic fluid stem cells are a subpopulation of amniotic fluid cells isolated by immunosorting for the expression of c-kit antigen. Recent study has shown that AFS cells could represent a new source for cellular therapy applications, since they demonstrate the capability of differentiating to multiple lineages (De Coppi, Bartsch et al. 2007).

Recently soft-lithographic methods and micro-contact printing approach have been proposed to create a micro-patterned supports to spatially organized layers of cardiomyocytes (Todd C. McDevitt, Angello et al. 2002; Todd C. McDevitt, Woodhouse et al. 2003; Elisa Cimetta, Sara Pizzato et al. submitted). It has been previously demonstrated that monolayer cultures of patterned cardiomyocytes can mimic morphologic features of mature ventricular tissue when cultured on micro-contact-printed protein patterns. All these techniques guarantee the accurate and micrometric reproduction of the selected design; however biomaterials deformation or degradation often produce undesirable effects that limit the practice of these methods and the duration of the experiment. In order to overcome this limitations, two different approaches have been tested to obtain cell pattern monolayer during the co-culture: micro-structured non-biodegradable biopolymer (poly-lactide acid) or polydimethylsiloxane (PDMS) membranes.
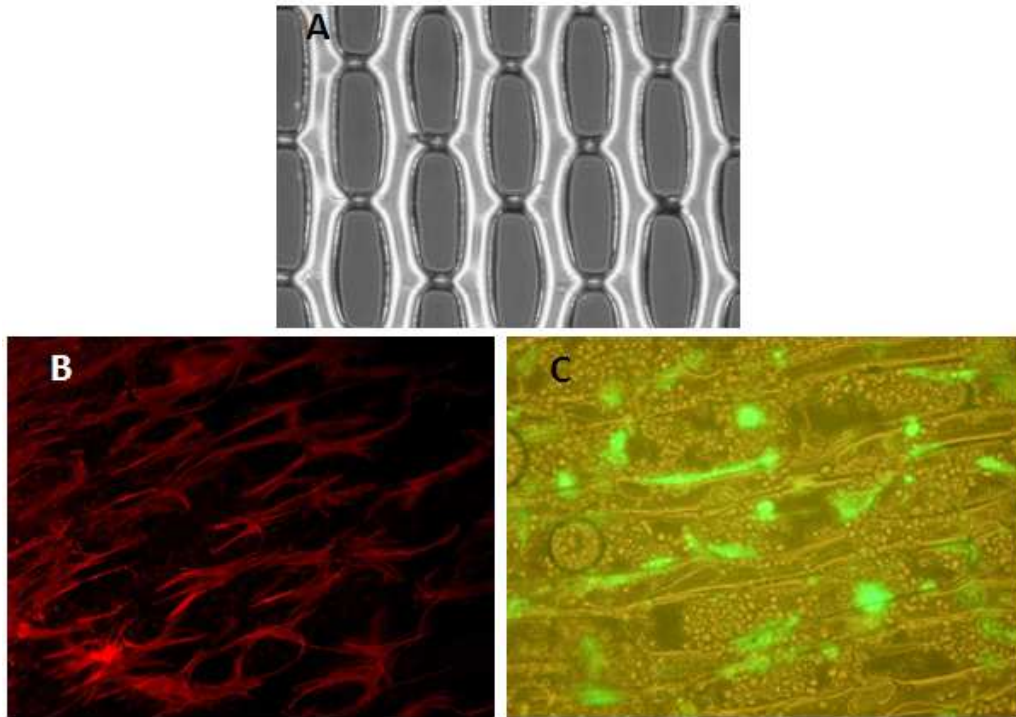
Figure 1 *GFP positive rat AFS cells and cardiomyocyte co-culture on PLA membrane. (A) Bright field picture of the micro-patterned membrane (20x) (B) Fuorescence image (20x) of troponin I staining (in red) after 4 days of co-culture. Positive cells present a macroscopic alignment on stripes. (C) Overlapping of bright field and fluorescence image (20x) after 4 days of co-culture. In the picture are clearly visible round cells, characteristic of non adhesive cells, and rat AFS cells in green homogenously distributed.*

The co-culture was performed on 30 μm PLA membranes, which were developed through a soft-lithographic method, as reported in literature (Elisa Figallo , Marina Flaibani et al. 2007; Luisa Boldrin , Nicola Elvassore et al. 2007). The micropattern on the membrane, shown in Figure 1A, consisted of 50 μm wide polymeric stripes connected every 200 μm by 10 μm lateral bridges. As visible in Figure 1B some rCM attached to the polymer and aligned following stripes. Nevertheless, most the cell present after 4 days of culture still present a round shape, suggesting a low affinity of these cells with the polymeric surface (Figure 1C).

These results proved the significant influence of surface topography on rCM and AFS cells alignment and suggested the idea of repeating the same experiment with a more appropriate substrate material. The use of stiff substrate micro-grooved surface, such as glass, as cell seeding support was proved to drive elongation and organization of

cardiomyocytes (Bursac, Parker et al. 2002; Ting H Au Hoi , Cheng et al. 2007). PDMS is a non-toxic elastomer that was already tested with different cell cultures (Desai, Deutsch et al. 1999; Motlagh, Senyo et al. 2003). For this propose we designed a simple method to create micro-patterned PDMS membrane as suitable environment for the AFS-rCM co-culture. Due to fluid-like gas diffusivity (oxygen diffusion coefficient of 3.55 cm^2/s) and rubber elastic modulus (Young's module of 750 kPa) of PDMS, these membranes could be used as cell culture growth substrate for specific studies that requires the application of mechanical stretch or controlled oxygen concentration. Micro-grooved surface of a 2 cm length polycarbonate cube and we used as template for PDMS mold fabrication. The fabricated frame fits in the commercially available multiwells dish and presents a 50μm thickness membrane on the middle.

Both rCM alone and rCM together with AFS were seeded on silicon membranes. The response of a rCM culture to the PDMS substrate was analyzed investigating: 1) the morphology, 2) the expression of specific cardiac markers and 3) the metabolic response. The most common substrate for cell culture, Petri dish, was used as control. The percentage of differentiation was evaluated by immunofluorescence after 6 and 12 days by the expression of the structural cardiac sarcomeric protein, troponin T. Further details about the material and methods used in this project can be found in Appendix A.

Results and discussion

Two different lapping papers, with grain size of 80 and 200 μm respectively, have been used in the preliminary experiments to produce the micro-grooves onto the surface of different templates and optimize the cell alignment. The PDMS surfaces with 17±9 μm micro-grooves exhibited the strongest effect on neonatal rat cardiomyocyte elongation and orientation, whereas the other micro-groove dimensions still allow the formation of cell colonies (Figure 2). The metabolic response of rCM on silicone surface is comparable with the result obtained on substrate of conventional Petri dish (poly-styrene). This method allows the formation of a more physiological arrangement of cardiac myocytes, which are aligned and contract synchronously up to 15 days, whereas on the common Petri dish surface the cells form colonies with random orientation.
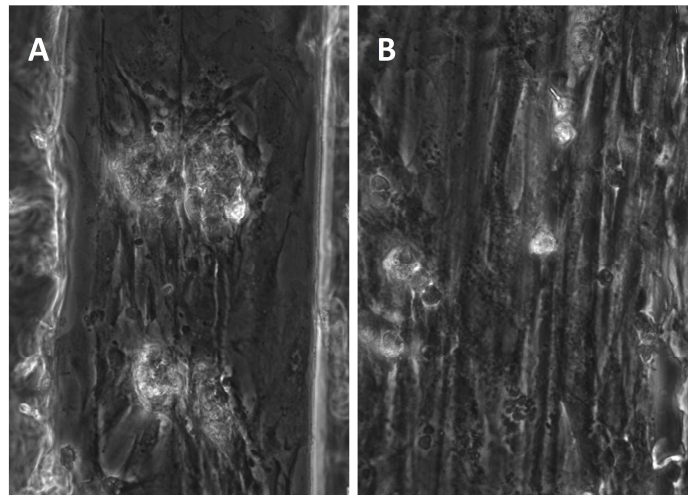
Figure 2 *rCM culture on silicone micro-patterned membrane obtained by micro-grooved polycarbonate templates with characteristic dimension of: (A) 200 μm and (B) 80 μm.*

The culture on micro-grooved PDMS membranes improved both rCM and AFS seeding and alignment *in vitro,* allowing to achieve better spatial organization of the AFS co-culture respect to the Petri dish. These findings suggest that the topographic stimulation improves close interactions between the two cellular population and intracellular cross-talk (Figure 3). The use of cardiomyocytes, tagged with green fluorescent protein (GFP), allows the immediate individuation of the cardiac cell in the culture mixture. Immunohistochemical analysis after 6 days revealed some hAFS, seeded on PDMS membrane positive for the expression of the cardiomyocyte marker troponin T. A complete and detailed description of the results is reported in Appendix A.

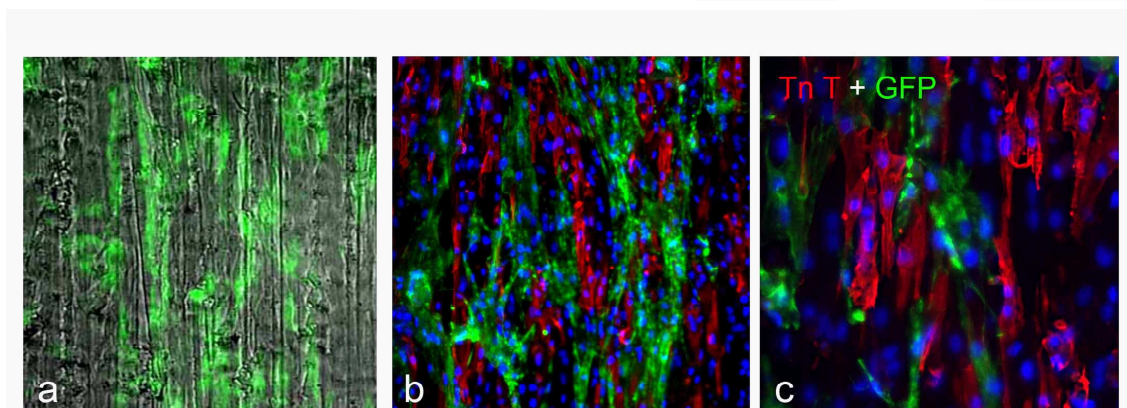**Figure 3** *rCm and gfp positive rAFS co-culture on 2D silicone micro-grooved membrane. (a) merge of bright field and GFP signal of the co-cultured cells, rAFS in green, magnification 20X; (b) and (c): immunostaining at 6 days of culture for cardiac troponin T (TnT, in red) and for GFP (in green), TnT-positive rat cardiomyocyte in red and GFP-positive rat AFS in green, magnification 20 and 40X.*

Conclusions and future perspectives

In this paper we present a simple method to obtain micro-grooved PDMS membranes for cell culture. Compared with the culture on conventional Petri dish, the topographical cues given by the PDMS membranes pattern significantly affect the cardiac myocyte architecture and attachment, influencing the cellular microenvironment. The improvements on cell-cell interaction obtained with this method were tested with a co-culture of hAFS cells and cardiomyocytes. The results seem promising to assess the capability of differentiating in cardiac myocyte even if more efforts are needed to analyze AFS cardiomyocyte differentiating potential.

2.3   Soluble chemical factors

Several works in literature report the increase on yield of the cardiovascular cell types, after the addition of soluble chemical cues directing toward cardiac lineage (Czyz and Wobus 2001; Huang, Lee et al. 2007). Following the example of embryonic development stimulation, signaling molecules such as cytokines and growth factors, have been shown interacting with specific intracellular pathways and modulating the *in vitro* and *in vivo* differentiation of embryonic and adult stem cell toward cardiovascular lineage (Boheler, Czyz et al. 2002; Agapios, Bernd et al. 2003). These chemicals include TGF-β1 family, insulin-like growth factor I, platelet-derived growth factor, fibroblast growth factor, oxytocin and erythropoietin (Schuldiner, Yanuka et al. 2000). Furthermore a number of synthetic chemical compounds such as 5-azacytidine, ascorbic acid, retinoic acid, dimethyl sulfoxide (DMSO) and dynorphin B have also been shown to promote cardiomyogenic differentiation *in vitro* (Boon Chin, Husnain Kh et al. 2004). The advantage on using synthetic chemicals instead of protein-based cytokines and growth factors is in their longer active half-life in solution and better structural and chemical definition. The main limitations of the standard culture system for the determination of optimal protocols to direct the differentiation into a specific cell type can be assesses on: 1) the capability of controlling the cellular microenvironment, also termed a "cell niche", which regulates stem cell fate, 2) the dimensions of standard culture system which allow the study of only few culture conditions each time.

The objective of the following study was to overcome these current limitations developing a new system for 2D-3D cell culture in microscale to study and control growth and differentiation of different cell type, included hESCs. The general advantages of small scale technology is clear: low volumes reduce consumption of samples and reagents and can be handled more easily. Moreover more samples can be processed per time unit in parallel. For a more engineering approach, the aim of the following work was to integrate the advantages introduced by high-throughput technologies with quantitative methods of analysis in order to improve the knowledge and the control of the process.

2.3.1 Micro Bioreactor Array for controlling cellular microenviroments

Stem cell biology is increasingly relying on advanced technologies that provide better cell culture microenvironments and enable control over multiple molecular and physical regulatory signals. These technologies are of particular interest to hESCs, because of the complexity of their regulatory pathways, and uncontrolled variables associated with traditional culture methods. Human embryonic stem cells (hESCs) hold vast promise in science and medicine because of their potential to replicate indefinitely and their capability to differentiate to any cell type found in the adult. Due to the high sensitivity of stem cells, in particular of embryonic stem cell, the determination of optimal protocols to direct the differentiation into a specific cell type requires a better control of cell culture microenvironment and the testing of a very large number of combinations of cell culture conditions, which is reason of a huge amount of time and money consumption. Soft lithography techniques have been recently applied to the development of high-throughput technology to perform in microfluidic systems biological assays (Tokuyama, Fujii et al. 2005; Situma, Hashimoto et al. 2006), cell culture array (Bhatia, Yarmush et al. 1997; Schuldiner, Yanuka et al. 2000; Chin, Taupin et al. 2004) and biomaterials testing (Anderson, Levenberg et al. 2004; Flaim, Chien et al. 2005).

In this work we propose a Micro Bioreactor Array (MBA) designed to perform the simultaneous cell culture in 12 small (3.5 mm of diameter) independent chambers, combining the advantages of microarrays with those of bioreactors.
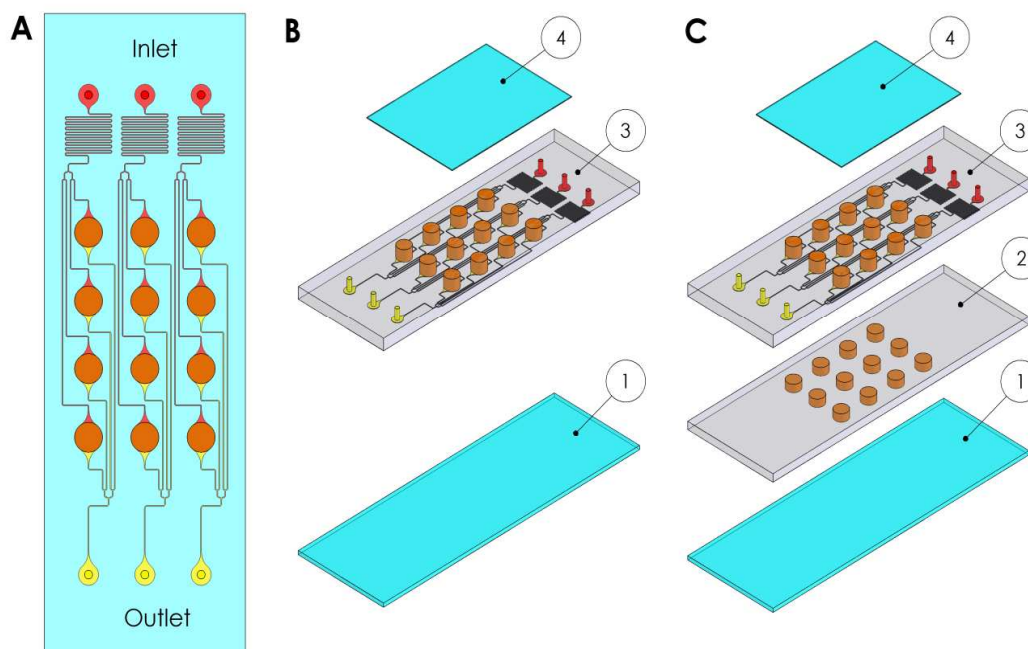

Figure 4 *Micro Bioreactor Array (MBA) design. (**A**) The micro-bioreactor wells (3.5 mm in diameter) are arranged in a 4×3 array (8 mm vertical and 7 mm horizontal center-to-center spacing). The microfluidic channels are 100 µm wide by 100 µm high and deliver between 0.1 - 2.0 ml of medium per day per bioreactor well. Each of three inlets delivers medium (red) through the flow transducers to four wells (orange) via microfluidic channels. Waste medium exits each bioreactor via a separate set of channels (yellow). The devices are assembled from layers of PDMS and glass, attached via plasma treatment of both surfaces. (**B,**) Two configurations were used. A bottom inlet/outlet (BIO) configuration (left) consists of a glass slide, a microfluidic layer, and a gas permeable membrane cover. A middle inlet/outlet (MIO) configuration (right) has an additional layer of PDMS with an array of wells inserted between the microfluidic layer and the slide. The BIO and MIO configuration accommodate the 2d cultivation of cells attached to a substrate (glass with or without additional coating); a thin layer of a photopolymerizable hydrogel in the base of MIO configuration wells allows 3D cultivation.*

The design requirements for the MBA were: (1) high-throughput experimentation with independent conditions for each bioreactor well, and low consumption of reagents and cells; (2) cultivation of cells in both the 2D setting (attached to a substrate) and three dimensional (3D) setting (encapsulated in hydrogel); (3) reproducible steady-state conditions in terms of cell density, medium composition, levels of oxygen and pH, flow regime, hydrodynamic shear and transport rates; (4)

accurate spatial-temporal control of the cell environment; (5) *in situ* quantitative analysis of cell proliferation and differentiation, by automated image analysis of differentiation markers. Further design constraints connected with those included: the ability to precisely control flow rate through the microchannels, a cheap disposable surface for irreversible cell adhesion, and an optical transparency for the observation an microscope.

To validate the utility of the MBA for controlled studies of cell growth and differentiation, we selected three model systems that are representative of the envisioned applications of this device: C2C12 myoblast cell line (middle inlet/outlet (MIO), bottom inlet/outlet (BIO)), primary cardiac myocytes derived from neonatal rat hearts (MIO, BIO), and hESCs (MIO, BIO).

Results and discussion

The devices are fabricated in a multilayer fashion, and the size is that of a microscope slide (26 x 76 mm). Two different configurations of the MBA were developed based on computational fluid dynamic modeling and analysis of mass transport in order to compare the effect on differentiation of a regime controlled by diffusion with a regime controlled by convection (Figure 4). In order to develop reliable and flexible MBA, the design was optimized to solve specific issues linked to the propose of this work and to the micro scale of the process, such those summarized in the following list (See Appendix B for details).

1. *Integrate elements such as pumps and reservoirs for liquid handling*
   The Tygon tubing (0.8 mm ID) was connected to the syringe needle through a commercial Luer lock, which fit onto the end of a filled syringe. Small lengths of stainless steel tubing (21 gauge, 10 mm length) were used to connect MBA ports to atoxic soft Tygon tubing (0.8 mm ID), which keep the flexibility after thermal treatment in autoclave.

2. *Guarantee the physiological pH during the culture*
   A gas exchanger was added after the inlet port The length of the exchanger was calculated comparing the retention time of medium with the time necessary to reach the equilibrium.

3. *Assure the sterility in the chambers during the culture*

An aluminum frame was used to close the culture system by compression. All the materials used were autoclavable.

4. *Solve the problems arising from air bubbles formations*

A gas permeable membrane seals each of the MBA chambers, which are kept in slight depression.

5. *Define the optimal well shape to obtain a more homogenous velocity profile in the chamber*

The flow rate of culture medium in the micro-bioreactors was controlled through a syringe pump, with an accuracy of 0.1 μL/min. The hydrodynamic shear and mass transport was characterized by computational methods.

6. *Solve the problems arising from small particles clogging microchannels*

The bioreactor channels were tested and washed with water before the experiment.

7. *Assure the independent and equal culture conditions in the wells of a same column*

Because of the small size of microchannels, flow is almost always laminar The flow rate within a microchannel is given by $Q = \Delta P/R$, where Q is the flow rate, ΔP is the pressure drop across the channel, and R is the channel resistance. For a rectangular microchannel with a low aspect ratio (i.e., $w \approx h$), the resistance is proportional to the channel length L (Beebe, Mensing et al. 2002). In order to guarantee the same pressure drop in all the channels, their length was designed identical.

8. *Improve the homogeneity on surface coating and cell seeding in the chambers*

The culture chambers can be directly accessed with pipette to apply coatings and uniformly seed the cells. In order to improve the homogeneity of the collagen coating he glass surface of each MBA chamber was treated with a solution of 4% of 3-aminopropyltrimethoxysilane (Sigma-Aldrich, St. Louis, MO) in acetone for 15 min.

9. *Avoid the growth factors degradation during the culture*

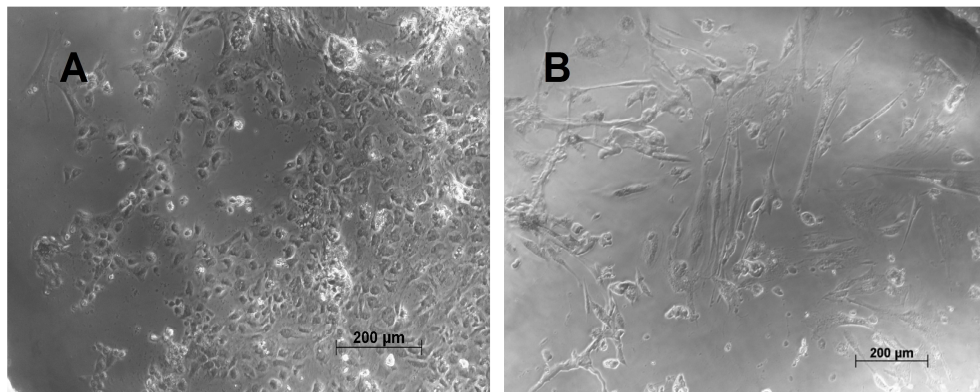The culture medium was kept at 4 °C before fluxing in the bioreactor.

Figure 5 *Phase contrast images showing the influence of MBA fluid-dynamic regime on hESC morphology configuration after 4 days culture in (**A**) middle inlet/outlet (MIO) or (**B**) bottom inlet/outlet (BIO).*

Through simple manipulation of flow rate, chamber height, and inlet/outlet configuration, a wide range of mass transport regimes are attainable and significant effect is determined on the cell morphology (Figure 5) and differentiation. The fluid dynamic simulations show that both configurations operate at very low-shear, but with clear differences (two orders of magnitude) in the values of fluid velocity and hydrodynamic shear.

A system for automated *in situ* image analysis of the expression of cell differentiation markers was developed and used to investigate the effects of cell density and flow regime on vascular differentiation of hESCs (see Appendix B for further details).

Conclusions and future perspectives

This work presents a new technology for 2D and 3D high throughput culture of cells, that we called Micro Bioreactor Array (MBA). To demonstrate operation of the MBA, we cultured C2C12 cells, rat cardiac myocytes and hESCs within the system. Taken together, these studies demonstrated that both MBA configurations (BIO, MIO, Figure 1) support the growth and differentiation of healthy and viable cells. Changing slightly the design of the bioreactor, it's possible to control the mass transport regimes in the well and the cellular reaction. This device hold the potential to be used as a tool for studying hESCs in the context of their environment.

2.4 Physical stimulation

The literature shows that physical stimuli, in the form of electrical pulses or mechanical stretch, could play an important role in cardiomyogenesis, mimicking the *in vivo* stimulation of cells in the heart (Kenneth R. Robinson 2003; Heng, Haider et al. 2004). Application of contractile stretch stimulation to neonatal cardiomyocytes up-regulates myosin heavy chain expression and induced cardiomyocyte organization into parallel arrays. However, the effect on stem cell differentiation into cardiovascular lineages of uniaxial strain has only recently been explored, particularly with SMCs and hESC. Strained Embryoid Bodies, for example, significantly increase the number of spontaneously contracting cardiac foci and areas covered with cardiac muscle (Li, Stouffs et al. 2006; Schmelter, Ateghang et al. 2006).

In line with the propose of mimicking the in situ stimulation, electrical stimulation also need to be taken in account. Since the muscle heart is rhythmically excited by ion transfer, it is likely that electrical stimulation could play an important role in cardiomyogenic differentiation in vivo. Electrical stimulation has already been reported to be beneficial to primary cardiomyocytes cultured in vitro and to enhance the differentiation toward cardiac lineage of mouse ESC (Sauer, Rahimi et al. 2000).

When a metallic electrode is placed inside a physiological culture medium the central process that occurs at the electrode/electrolyte interface is a transduction of charge carriers from electrons in the metal electrode to ions in the electrolyte. This transduction is due to two primary mechanisms of charge transfer at the electrode/electrolyte interface: Faradaic and non-Faradaic reactions.

Non-Faradaic reactions include the polarization of electrolyte due to a redistribution of charged chemical species. Due to this phenomena, the initial linear decay of electrical potential changes quickly profile up to the equilibrium. The stable condition is characterized by the complete shielding of charges on the electrodes surface and by the decay of the electrical potential in a very narrow interphase region, called Debye length.

The second mechanism is a Faradaic reaction, in which electrons are transferred between the electrode and electrolyte, resulting in reduction or oxidation of chemical species in the electrolyte. The presence of Faradaic reactions, the steady state is characterized by constant current in the electrolyte. During current flow, a potential

gradient exists in the electrolyte, generally many orders of magnitude smaller than at the interface.

From a biological point of view it will be really interesting to understand if and how the exogenous electrical stimulation influences the cell differentiation. However uncertainties about the type and magnitude of field make difficult the individuation of the biophysical and biochemical mechanisms activated on the considered biological system. For the engineering perspective, it is still unclear which parameters of the system are more critical for enhancing the stem cell differentiation.

The objective of this study was to describe a rational method to provide an efficient electrophysiological stimulation to stem cell culture. Clearly, stimulation efficiency is determined by the ability to attain a desired physiological response with minimal damage to the biological element. However the interpretation of the cellular response to such fields is usually complicated by inadequate characterization of the system used for stimulation. In particular this work wants to show the effect of electrode material on specific cellular response, such as production reactive oxygen species (ROS) or stem cell differentiation.

2.4.1 Effect of electrode material on ROS expression of human embryonic stem cell

The presence of endogenous electric field during the embryonic development and the effects of exogenous one for different kind of cells have been already reported in several studies (Jaffe and Nuccitelli 1977; Nuccitelli 2003). However uncertainties about the type and magnitude of field make difficult the individuation of the biophysical and biochemical mechanisms activated on the considered biological system. The mechanisms of electrical stimulation are strongly dependent on the electrode geometry and material properties. In biological applications, the material selection for electrodes is a complex issue. The ideal material for use as a stimulating electrode must be biocompatible, have stable characteristics during the stimulation and acceptable electrode degradation or harmful byproducts.

In this work we aim to develop a new technology and methodology to test the effectiveness of the electrode material has been evaluated through the expression of intracellular ROS in hESCs of different developmental stage.

EBs were electrically stimulated within bioreactor characterized by 4 indipendent rows of 4 wells built in poly(dimethylsiloxane) (PDMS) and glass. A stereolithographic method was used to develop the mold for the bioreactor. Electrodes of 2 mm of diameter can be inserted in both sides of each row. Independent stimulation is guaranteed by the PDMS insulation between different rows.

The electrode-electrolyte interface has been modeled by Randle-type equivalent circuit, evaluating from electrochemical impedance spectroscopy (EIS) the capacitance and polarization resistance of Titanium, Titanium Nitride and Stainless Steel electrodes. The EIS results were useful to evaluate the correlation between duration of a stimulation and ROS expression on human EBs, which was evaluated monitoring the expression of DCF fluorescence for 20 min. The evolution of the stimulation has been monitored measuring current in the system.

Results and discussion

The EIS data show mainly differences between electrodes on polarization resistance (R_p) value, which is much lower for Stainless Steel. In agreement with this result, the potential-time plot for stainless steel is kept to constant value of 0.4 mA by the presence of reactions on its surface during the stimulation. For titanium and titanium nitride we have instead an initial increasing of the potential followed by a rapid decrease up to a value close to zero due to the polarization of the medium and the shielding of charges on the electrode.

The applied electric field lead to generation of intracellular ROS in human embryonic stem cells. In agreement with these results, the use Stainless Steel electrodes and the increasing of stimulation duration enhance the intracellular ROS expression. This value was higher in EB of 4 days old respect 6 or 8 days old. The decay ROS generation may suggest the higher predisposition of the hESC to a cardiac differentiation and a more efficacious electrical stimulation at earlier stage of development

This hypothesis is confirmed by the measure of the percentage of beating 19 days-old EBs. EB start beating with higher percentage if seeded at earlier stage of differentiation and if stimulated at 5 V/cm for 90 s. The complete manuscript is reported in Appendix C.

Conclusions and future perspective

The dependence of the biological response from the electrode material proves the extreme importance of a complete characterization of the system before performing a electrophysiological stimulation. Even if the role of ROS in the cardiac lineage differentiation in human embryonic stem cell has still not been investigated, these results seems promising in the final propose of enhancing the number of differentiated human embryonic stem cell through electric stimulation. From the engineering perspective, the knowledge of the system at the cellular level suggests the opportunity of understand and explaining with a mathematical model the mechanism of stem cell differentiation.

2.5 References

Agapios, S., K. F. Bernd, et al. (2003). "Cardiac specific differentiation of mouse embryonic stem cells." Cardiovascular Research **58**(2): 278-291.

Anderson, D. G., S. Levenberg, et al. (2004). "Nanoliter-scale synthesis of arrayed biomaterials and application to human embryonic stem cells." Nat Biotech **22**(7): 863-866.

Badorff, C., R. P. Brandes, et al. (2003). "Transdifferentiation of Blood-Derived Human Adult Endothelial Progenitor Cells Into Functionally Active Cardiomyocytes." Circulation: 01.CIR.0000051460.85800.BB.

Beebe, D. J., G. A. Mensing, et al. (2002). "Physics and applications of microfluidics in biology." Annual Review of Biomedical Engineering **4**(1): 261-286.

Bhatia, S. N., M. L. Yarmush, et al. (1997). "Controlling cell interactions by micropatterning in co-cultures: Hepatocytes and 3T3 fibroblasts." Journal of Biomedical Materials Research **34**(2): 189-199.

Biswas, A. and R. Hutchins (2007). "Embryonic Stem Cells." Stem Cells and Development **16**(2): 213-222.

Boheler, K. R., J. Czyz, et al. (2002). "Differentiation of Pluripotent Embryonic Stem Cells Into Cardiomyocytes." Circ Res **91**(3): 189-201.

Boon Chin, H., H. Husnain Kh, et al. (2004). "Strategies for directing the differentiation of stem cells into the cardiomyogenic lineage in vitro." Cardiovascular Research **62**(1): 34-42.

Bursac, N., K. K. Parker, et al. (2002). "Cardiomyocyte Cultures With Controlled Macroscopic Anisotropy: A Model for Functional Electrophysiological Studies of Cardiac Muscle." Circ Res **91**(12): e45-54.

Chin, V., P. Taupin, et al. (2004). "Microfabricated platform for studying stem cell fates." Biotechnology and Bioengineering **88**(3): 399-415.

Czyz, J. and A. M. Wobus (2001). "Embryonic stem cell differentiation: The role of extracellular factors." Differentiation **68**(4-5): 167-174.

De Coppi, P., G. Bartsch, et al. (2007). "Isolation of amniotic stem cell lines with potential for therapy." Nat Biotech **25**(1): 100-106.

Desai, T. A., J. Deutsch, et al. (1999). "Microtextured Cell Culture Platforms: Biomimetic Substrates for the Growth of Cardiac Myocytes and Fibroblasts." Biomedical Microdevices **2**(2): 123-129.

Elisa Cimetta, Sara Pizzato, et al. (submitted). "Production of arrays of cardiac and skeletal muscle myofibers by micropatterning techniques on a soft substrate." Biomedical Microdevices.

Elisa Figallo , Marina Flaibani , et al. (2007). "Micropatterned Biopolymer 3D Scaffold for Static and Dynamic Culture of Human Fibroblasts." Biotechnol Prog **23**(1): 210-6.

Engler, A. J., M. A. Griffin, et al. (2004). "Myotubes differentiate optimally on substrates with tissue-like stiffness: pathological implications for soft or stiff microenvironments." J. Cell Biol. **166**(6): 877-887.

Flaim, C. J., S. Chien, et al. (2005). "An extracellular matrix microarray for probing cellular differentiation." Nat Meth **2**(2): 119-125.

Geiger, B., A. Bershadsky, et al. (2001). "Transmembrane crosstalk between the extracellular matrix and the cytoskeleton." Nat Rev Mol Cell Biol **2**(11): 793-805.

Gepstein, L. (2006). "Cardiovascular Therapeutic Aspects of Cell Therapy and Stem Cells." Annals of the New York Academy of Sciences **1080**(1): 415-425.

Goldsmith, E. C. and T. K. Borg (2002). "The dynamic interaction of the extracellular matrix in cardiac remodeling." Journal of Cardiac Failure **8**(6, Part 2): S314-S318.

Heng, B. C., H. K. Haider, et al. (2004). "Strategies for directing the differentiation of stem cells into the cardiomyogenic lineage in vitro." Cardiovascular Research **62**(1): 34-42.

Huang, N. F., R. J. Lee, et al. (2007). "Chemical and Physical Regulation of Stem Cells and Progenitor Cells: Potential for Cardiovascular Tissue Engineering." Tissue Engineering **13**(8): 1809-1823.

Hwang, W. S., Y. J. Ryu, et al. (2004). "Evidence of a Pluripotent Human Embryonic Stem Cell Line Derived from a Cloned Blastocyst." Science **303**(5664): 1669-1674.

Iijima, Y., T. Nagai, et al. (2003). "Beating is necessary for transdifferentiation of skeletal muscle-derived cells into cardiomyocytes." FASEB J.: 02-1048fje.

Jaffe, L. F. and R. Nuccitelli (1977). "Electrical Controls of Development." Annual Review of Biophysics and Bioengineering **6**(1): 445-476.

Kenneth R. Robinson, M. A. M. (2003). "Left/right, up/down: The role of endogenous electrical fields as directional signals in development, repair and invasion." BioEssays **25**(8): 759-766.

Lev, S., I. Kehat, et al. (2005). "Differentiation Pathways in Human Embryonic Stem Cell-Derived Cardiomyocytes." Ann NY Acad Sci **1047**(1): 50-65.

Li, J., M. Stouffs, et al. (2006). "The NADPH Oxidase NOX4 Drives Cardiac Differentiation: Role in Regulating Cardiac Transcription Factors and MAP Kinase Activation." Mol. Biol. Cell: E05-06-0532.

Luisa Boldrin , Nicola Elvassore , et al. (2007). "Satellite cells delivered by micro-patterned scaffolds: a new strategy for cell transplantation in muscle diseases." Tissue Eng **13**(2): 253-62.

Matsushita, T., M. Oyamada, et al. (1999). "Remodeling of Cell-Cell and Cell-Extracellular Matrix Interactions at the Border Zone of Rat Myocardial Infarcts." Circ Res **85**(11): 1046-1055.

Motlagh, D., S. E. Senyo, et al. (2003). "Microtextured substrata alter gene expression, protein localization and the shape of cardiac myocytes." Biomaterials **24**(14): 2463-2476.

Mummery, C., D. Ward-van Oostwaard, et al. (2003). "Differentiation of Human Embryonic Stem Cells to Cardiomyocytes: Role of Coculture With Visceral Endoderm-Like Cells." Circulation **107**(21): 2733-2740.

Nianzhen Li, Anna Tourovskaia, et al. (2003). "Biology on a Chip: Microfabrication for Studying the Behavior of Cultured Cells." Critical Reviews in Biomedical Engineering **31**(5&6): 423–488.

Nuccitelli, R. (2003). "Endogenous electric fields in embryos during development, regeneration and wound healing." Radiat Prot Dosimetry **106**(4): 375-383.

Nygren, J. M., S. Jovinge, et al. (2004). "Bone marrow-derived hematopoietic cells generate cardiomyocytes at a low frequency through cell fusion, but not transdifferentiation." Nat Med **10**(5): 494-501.

Sauer, H., G. Rahimi, et al. (2000). "Role of reactive oxygen species and phosphatidylinositol 3-kinase in cardiomyocyte differentiation of embryonic stem cells." FEBS Letters **476**(3): 218-223.

Schmelter, M., B. Ateghang, et al. (2006). "Embryonic stem cells utilize reactive oxygen species as transducers of mechanical strain-induced cardiovascular differentiation." FASEB J. **20**(8): 1182-1184.

Schuldiner, M., O. Yanuka, et al. (2000). "From the Cover: Effects of eight growth factors on the differentiation of cells derived from human embryonic stem cells." PNAS **97**(21): 11307-11312.

Situma, C., M. Hashimoto, et al. (2006). "Merging microfluidics with microarray-based bioassays." Biomolecular Engineering **23**(5): 213-231.

Stewart, R., M. Stojkovic, et al. (2006). "Mechanisms of self-renewal in human embryonic stem cells." European Journal of Cancer **42**(9): 1257-1272.

Thomson, J. A., J. Itskovitz-Eldor, et al. (1998). "Embryonic Stem Cell Lines Derived from Human Blastocysts." Science **282**(5391): 1145-1147.

Ting H Au Hoi , I. Cheng, et al. (2007). "Interactive effects of surface topography and pulsatile electrical field stimulation on orientation and elongation of fibroblasts and cardiomyocytes." Biomaterials **28**(29): 4277-4293.

Todd C. McDevitt, J. C. Angello, et al. (2002). "*In vitro* generation of differentiated cardiac myofibers on micropatterned laminin surfaces." Journal of Biomedical Materials Research **60**(3): 472-479.

Todd C. McDevitt, K. A. Woodhouse, et al. (2003). "Spatially organized layers of cardiomyocytes on biodegradable polyurethane films for myocardial repair." Journal of Biomedical Materials Research Part A **66A**(3): 586-595.

Tokuyama, T., S. i. Fujii, et al. (2005). "Microbioassay System for Antiallergic Drug Screening Using Suspension Cells Retaining in a Poly(dimethylsiloxane) Microfluidic Device." Anal. Chem. **77**(10): 3309-3314.

Ying J. Li, E. H. Chung, et al. (2006). "Hydrogels as artificial matrices for human embryonic stem cell self-renewal." Journal of Biomedical Materials Research Part A **79A**(1): 1-5.

Chapter 3

Development of functional cardiomyocyte: single cell analysis

This chapter deals with the methods for *in vitro* characterization of single cell physiology, in order to evaluate the mature differentiation of stem cell toward cardiac lineage and to investigate the cellular response to biochemical or biophysical stimulation. In this prospective, a mathematical model has been developed to describe the spatio-temporal dynamic of an important secondary messanger, the cAMP, involved on the cardiac contraction. The chapter presents the idea and main results of this work.

3.1 Stem cell functional differentiation and analysis

During the early stage of differentiation, only a small fraction of the total stem cells become functional cardiomyocytes. The complete differentiation to cardiomyocyte is characterized not only by the expression of mature cardiac markers, such as MHC, actinin, desmin, ANP, troponin but also by the exhibition of spontaneous and rhythmic contractions. Moreover, they should show the molecular and ultrastructural characteristics of cardiac myocytes with a normal adult sarcomeric structure, intercalated discs with desmosomes, and gap junctions. Several assays have been developed to measure the cell functionality, including: i) extracellular and intracellular electrophysiological recordings (patch clamp or multi-electrodes array); ii) single cell force transducer; iii) intracellular optical imaging (voltage or calcium imaging, molecular probe FRET) of biochemical and pharmacological response.

3.1.1 Electrophysiological recordings

The classical electrophysiology technique traditionally uses a glass pipette with an open tip diameter of about one micrometer, known as a "patch clamp electrode" (Sakmann and Neher 1984; Hamill OP, Marty A et al. 1981). This electrodes is pressed against a cell membrane and sealed to it. The electrical recording is accessed filling the interior of the pipette with different isotonic solutions compared to the intracellular fluid. A metal electrode in contact with this solution conducts the electrical changes to a voltage clamp amplifier. The composition of the filling solution can be changed or drugs can be added to study the ion channels under different conditions. Even if this method offers high information on the specificity of drug action, its main disadvantage is on the possibility of measuring only the response of a single cell. Only recently, promising results have shown an automation of this technique toward more high throughput analysis (Falconer, Smith et al. 2002; Klauke, Smith et al. 2006). However, the research is still far from totally replacing manual patch clamp with automated patch clamp systems. Presently available patch clamp robots do not support, for example, all variants of the method, and recording from native cells and from single channels is not routinely implemented yet (Meyer, Sartipy et al. 2007).

In addition to the patch clamp technique, a microelectrode array (MEA) has been developed to allow the stimulation of tissues or multiple cells in parallel and record simultaneously the single electrical activities in an arrangement of several (typically 60) electrodes (A. Stett, U. Egert et al. 2003). Once that cells are plated onto an MEA, the recorded waveform depends on the signal source, the geometry of the extracellular space, and the distance of the signal source to the electrode. The advantage respect to patch clamp experiments is on its capacity of examining the activities of whole cells rather than single receptors and in the possibility of comparing the activities of multiple cells under similar experimental conditions, increasing the throughput of the experiment (Natarajan, Molnar et al. 2006). This techniques has been used to demonstrate the presence of a functional syncytium with stable spontaneous pacemaking activity and synchronous action-potential propagation in contracting areas dissected from the EBs (Schwanke, Wunderlich et al. 2006).

3.1.2 Single cell force transducer

Mechanical measurements on single cardiac myocyte's contractile force have been carried out with a variety of transducer designs, mostly optical, which showed a maximal isometric forces of about 12 µN (Tarr, Trank et al. 1983; Vannier, Chevassus et al. 1996). The first approach is based on the bending of cantilevers such as optical fibers (Tung L. 1986), suction pipettes (Cecchi, Colomo et al. 1992), glass needles (Canaday and Fay 1976), steel foil and microfabricated polysilicone beams (MEMS) (Yi Zhao, Lim et al. 2007; Lin, Palmer et al. 2001). MEMS technology offers the ability to shrink the force transducer down to a size comparable to that of a cardiac myocyte. The cantilevers are calibrated with a sensitive optical methods to determine a correlation between the degree and direction of the bending and the magnitude and direction of the force. The technique to detect the deflection of the cantilever is the key element of this type of force transducer. Some authors have used strain gauges; others have measured the displacement of the cantilever tip by video analysis, optoelectronically, or with a laser beam that projected the image of a slit or the blackened glass needle onto a differential photodiode (Tasche, Meyhofer et al. 1999). Moreover, this technical approaches involve cell manipulations with probes, gluing, and clamping, which may have some unknown effect on the cell ends and their function (Brady 1991).

A different optical technique for force measurements has been developed attaching magnetic beads on one end of the myocyte and positioning them between two electromagnets in a magnetic field (Yin, Zhang et al. 2005). Video microscopy and edge detection are used to monitor small movements of the microsphere under generation of magnetic force. An automatic control system adjusts the current through the electromagnets to keep the microsphere in controlled position. The magnitude of specimen-generated force equals to the magnitude of magnetic force on the microsphere. Thus, the specimen-generated force can be derived by calculating the magnetic force on the microsphere via the magnetic field intensity and properties of magnetic microsphere. This method could measure the stationary force generated by specimen, similar to isometric muscle contraction. However, to study physiological contractile properties (isometric and isotonic) of cardiac myocytes, one would need to know the contractile force during the myocyte contraction and relaxation processes.

Due to the movement of specimen (i.e., cardiac myocyte), this method cannot be applied.

Viscous loading has been studied to investigate contractile properties of cells immersed in liquids of different viscosity (Kent, Mann et al. 1989). Different viscous loading can be realized also by changing the concentrations of microspheres added to the liquid. The major advantages of this approach are: 1) it is a noninvasive/minimal invasive approach due to the soft contact between the cell and surrounding liquid medium; 2) the control of the external loading force by changing the viscous loading. However, due to the sophisticated nature of fluid movement, it is very difficult to calculate the exact value of viscous loading force. This method may provide qualitative relationships between the contractile properties and viscous loadings (such as the relationship between the velocity of shortening and relative resistive load). However it is difficult to provide exact value of contractile force (Yin, Zhang et al. 2005).

Finally, a force measurement of cardiac myocyte can be obtained using atomic force microscopy (AFM) (Wojcikiewicz EP, Zhang X et al. 2004). Most AFM sensors utilize small rugged steel and tungsten cantilever beams with dimensions in the range of several micrometers. With the appropriate detection system (i.e., laser beam deflection, tunneling current, interferometer), these sensors can reach nanoNewton resolution. Despite these excellent properties, a complex transmit-receive setup is required and in aqueous medium where cells survive, the reflection and refraction of the transmitted light make the accuracy of cellular force measurement problematic.

3.1.3 Optical methods through intracellular molecular probes

Since the contractility is related to a high-density inward current via voltage-activated channels, calcium ions or membrane-potential-sensitive fluorescent dyes have been used as basis for another group of electrophysiological assays (Waggoner 1979; Baxter, Kirk et al. 2002). The most preferred method for imaging the intracellular calcium spikes and quantify its concentration involves the use of a ratiometric fluorescent dye (Fura-2) which binds to free intracellular calcium (Takahashi, Camacho et al. 1999). Fura-2 is excited at 340 nm and 380 nm of light, and the ratio of the emissions at those wavelengths is directly correlated to the amount of intracellular calcium. The

ratiometric analysis are demonstrated to be independent from a myriad of experimental parameters, such as dye concentration, autofluorescent background, focus drift and ambient light.

A indirect measure of the membrane potential can be obtained with a fluorescent voltage-sensitive dyes (ANEP) (Fast VG 2000; Efimov, Nikolski et al. 2004). The dyes are essentially nonfluorescent in water and become quite strongly fluorescent upon binding to membranes. Furthermore, these dyes couple changes in membrane voltage to a conformational change displaying a potential-dependent shift in their excitation spectra. The optical response is sufficiently fast to detect transient potential changes, which can be quantified using excitation ratio measurements. High throughput and low costs per data point are the main advantages of this assay. However, the correlation to the traditional standard (manual patch clamp) is limited.

An indirect quantitative measure of the local intracellular concentration of a selected molecule can be optically obtained through Fluorescence Resonance Energy Transfer (FRET) technique. The benefit of FRET technology is on its excellent resolution (van Rheenen, Langeslag et al. 2004). This method is an useful tool to quantify the time and space molecular dynamics of a biochemical processes, which produce local changes on protein conformation or molecular composition. This technique measures the changing on energy emission due the reducing of the reciprocal distance between two different fluorescent molecules (fluorophores), which are fused to proteins of interest. When the donor and acceptor fluorophores are in proximity (1-10 nm), the donor transfers some of its energy to the acceptor due to the interaction of the two molecules. The result is that the donor emits less energy than it normally would and this difference can be measured.

This technique was used for a fast and sensitive measure of the membrane voltage changes. The mechanism is based on hydrophobic fluorescent anions that rapidly redistribute from one face of the plasma membrane to the other according to the Nernst equation, reducing the probability of energy transfer (Gonzalez and Tsien 1995). The regulatory mechanisms correlated to the cardiac contraction have been investigated by other FRET-based biosensors, which allow the observation of intracellular cAMP. The fluorescence ratio imaging of cAMP in living cells is obtain by the reaction of this

secondary messenger with a fluorescent dye-tagged enzyme, such as PKA or Epac (Mongillo, McSorley et al. 2004).

3.2 Functional cardiomyocyte analysis through cAMP signalling

The mechanism of decoding external signals, such as cardioactive hormones and drugs, is a crucial and open question for cardiac cell biology. The literature suggests the central role of cAMP signaling compartmentation on cardiac functional regulation, attributing the specificity of the response to spatial and temporal control of signaling molecules. After hormone stimulation, β-AR could be activated and couples with Gs, which activates adenylyl cyclase. The consequent increase in cAMP concentration may activate, in cardiac cells, PKA (cAMP-dependent protein kinase or protein kinase A). PKA phosphorylates a many proteins important for cardiac function including: metabolic enzymes (McCullough and Walsh 1979), transcription factors of the CREB family (Müller, Neumann et al. 2000), and key components of cardiac excitation–contraction coupling (L-type Ca^{2+} channels (Kamp and Hell 2000), ryanodine receptors (Marx, Reiken et al. 2000), phospholamban (Simmerman and Jones 1998), troponin I (Sulakhe and Vo 1995) and myosin-binding protein C (Kunst, Kress et al. 2000). The consequent regulation of calcium-related proteins by PKA leads to increased Ca^{2+} transient and increased contractility in response to the stimulation. At the other end, cAMP actions are counterbalanced by PDEs (phosphodiesterases), which catalyse the hydrolysis of the phosphodiester bond in cyclic nucleotides cAMP or cGMP. PDEs constitute a highly diversified class of enzymes, subdivided into 11 families (Lugnier 2006), and at least four are expressed in the heart.

The mechanisms that create highly specialized cAMP signaling compartments is still unclear. Experimental evidences suggest an implication of caveolae, cholesterol-rich invaginations as regulators in GPCR signaling, creating a local environment that can bring receptors, G proteins, AC and kinase anchoring proteins (AKAPs) in close proximity. Furthermore, AKAP can assemble signaling complexes including PKA and PDE. However, a better understanding of cAMP signaling in the heart could lead to more effective therapeutics for cardiac failure. The mathematical modeling offers the

opportunity to analyze efficiently several hypotheses on the cAMP signaling dynamics and isolate the relative influence of different factors such as structural organization of enzymes, protein kinase A (PKA) and phosphodiesterase (PDE), or non-homogenous intracellular diffusivity.

The aim of this part of the thesis is to develop a diffusion-reaction mathematical model to describe the intracellular dynamic of the cAMP signaling to be used for:

1) validation of biological hypothesis about the functional development, the physiology and the physio-pathology of the cardiac stem cell derived myocytes;

2) designing of experiment and investigation of molecular mechanisms in the physiology of healthy cardiomyocytes and diseases;

3) tools to rationally assist the screening of new pharmaceutical compounds and their effect on the functional activity of cardiac stem cell derived myocytes.

3.2.1 Local diffusivity and intracellular organization synergy in spatio-temporal cAMP signal transduction in HEK293

The biochemistry of cAMP signaling has been partially elucidated with several analytical models developed on different types of cell. However most of these models consider only the time course of cAMP close to the membrane: 1) describing the cAMP production and degradation, and the opening of membrane channel as effect of the high concentration of cAMP (Goldbeter 1996), 2) integrating cAMP production and degradation in different signaling pathways (Bhalla and Ravi Iyengar 1999; Saucerman, Brunton et al. 2003) 3) underlining the role of PKA e PDE activation on cAMP degradation (Golbunova Y.V. 2002; Gorbunova and Spitzer 2002; Rich, Xin et al. 2007). Even though these models were kinetically complete, no attention has been given to cAMP intracellular spatial distribution, fundamental for the activation of specific targets. Rich et al. (2001) tried to combined the biochemical description of the process with a physical compartmentalization of the space. The cell was modeled assuming the existence of two compartments separated by a membrane: the membrane-localized microdomain and the bulk cytosol. The diffusion was significantly impeded between the

two domains, whereas inside each compartment it was assumed so rapid that any spatial difference was abolished.

Huang et al. (1991) shows the importance of the diffusion and the rate of hydrolysis on the kinetic of Na^+ current dependent by the intracellular concentration of cAMP. However the model simulates a simplified system with free and isotropical cAMP diffusion in an infinite cytosol and incomplete chemical description of the signaling. The activation of PDE or the binding with PKA are in fact not considered. In this direction the models developed by Bhalla (2004) e Kholodenko et al. (2003) are particularly interesting because they describe the effect of diffusion limited regime on the signal intracellular distribution, even if the specific description of cAMP spatio-temporal distribution is not investigated.

A quantitative diffusion-reaction model has been implemented in this work to simulate the spatio-temporal evolution of the cAMP signalling, assuming that the intracellular organization of cell, in proximity to the cAMP targets, directs and amplifies the biological effects of the highly diffusible secondary messenger, localizing its concentration. The mathematical model was validate comparing the simulation results with experimental variation of FRET measured with H30 probe on HEK 293 after stimulation with PGE1.
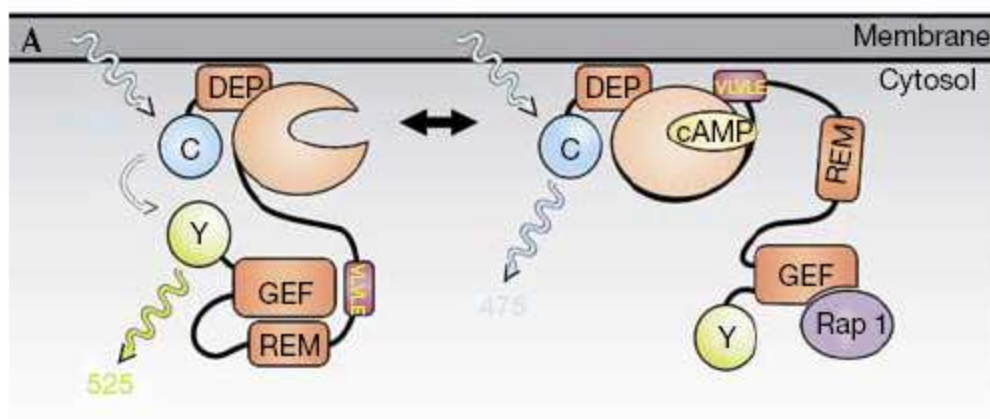

Figure 1 *Schematic representation of the H30 conformational change phenomena due to the cAMP reaction.*

The H30 probes are based on genetically modified Guanine nucleotide Exchange Factor (GEF), Epac1, which are directly triggered by cAMP. Epac1 is characterized by two domains with catalytic and regulatory function. The second domain contains the binding site for cAMP and is linked to the membrane. The probe was developed modifying these domains with two fluorophores, cyan (CFP) and yellow (YFP), which generate FRET at low concentration of cAMP. When the concentration of cAMP increases, the secondary messanger reacts with the regulatory subunit-CFP determining a conformational change of Epac 1 and the dissociation of C-YFP, which abolishes the FRET (Figure 1).

Model framework

When a stimulus binds at the cell surface to a receptor, a sequence of events begins near the membrane determining a spike of cAMP concentration limited in space and time. The arising cAMP concentration into the cell promotes its cleavage through the activation of protein kinase A (PKA) and phosphodierestase isoforms (PDE). Thus, the intracellular concentration of cAMP is regulated by the antagonist actions of AC and PDE (Alberts, Johnson et al. 2002), which determine time-dependent spikes of the secondary messenger inside the cell. The cellular volume is assumed to be divided in three subdomains with characteristic dimensions: the submembrane volume (SM, 10% of the total volume) (Peters R. 1984), the cytosol (C, 70% of the total volume) and nucleus (N, 20% of the total volume) (Kozer N. 2004).

Even if the reactions occurring in sub-membrane and cytosol domain, are the same, the values of free diffusivity could be really different (Figure 2). We give here a brief description of the reactions involved in the cellular domains.
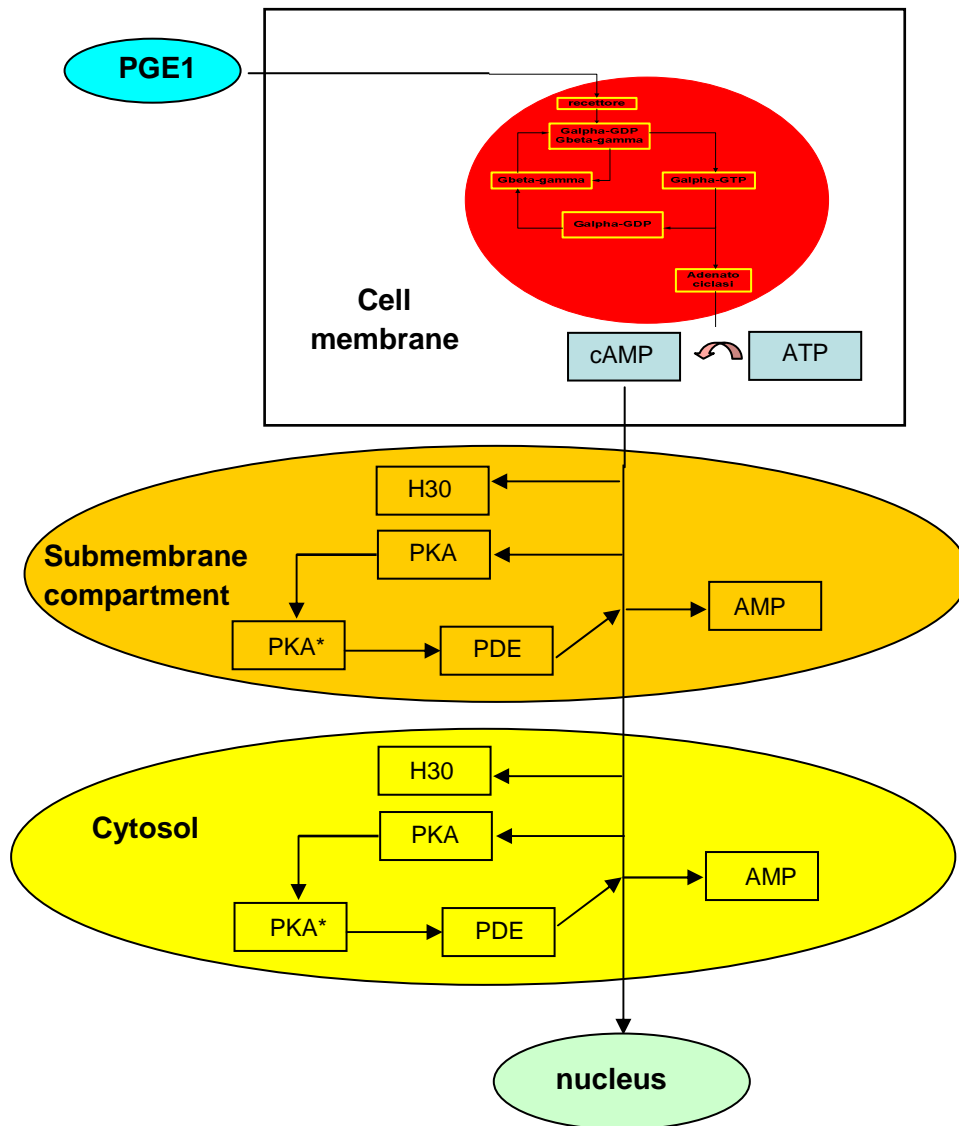
Figure 2 *Schematic representation of the three intracellular domains and of the chemical reactions occurring in each of them.*

At the membrane, the receptor (*R*) binds to the ligand (*L*) (R 3.1) and reacts with G protein (Reaction 3.2). This process activates the adenylate cyclase increasing the production of cAMP (Reaction 3.3). The network of reactions that describes this system is well represented by the following reactions:

$$L + R \Longleftrightarrow LR \tag{3.1.}$$

$$LR + G_{\alpha\beta\gamma} \Longleftrightarrow G_{\alpha-GTP} + G_{\beta\gamma} \tag{3.2.}$$

$$G_{\alpha-GTP} \xleftarrow[ATP]{AC} cAMP + G_{\alpha-GDP} \tag{3.3.}$$

As shown in Figure 3, the receptor stimulation determines a sharp increasing on the cAMP production rate up to reaching a plateau in 1-2 seconds. Increasing the concentration of ligand over does not cause significant changes in the cAMP production rate.

Figure 3 *cAMP production rate profiles as function of time and ligand concentration [L].*

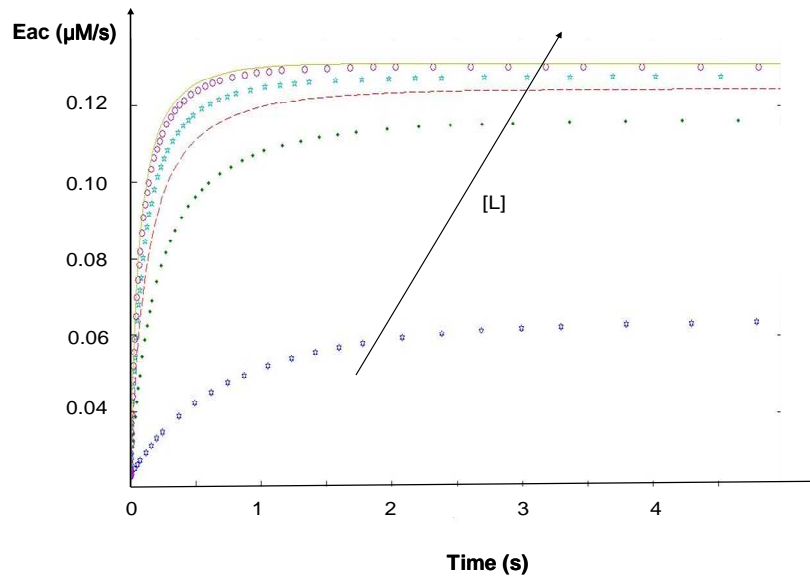Since over 100 nM, there is not significant influence of *L* concentration on the production rate at plateau, its value set for these simulations was always of 1 μM, which was the most frequently used in the experimental work.

Two are the chemical species that influence most cAMP space-time dynamics: PKA and PDE. The PKA has the ability to bind to their two regulatory subunits four cAMP units (Reactions 3.4 - 3.7) and catalyze the PDE activation through two catalytic subunits (Reaction 3.10). The activated PDE hydrolyses cAMP (Reaction 3.11). Since cAMP signalling mainly involves three PDE isoforms: PDE4D, PDE4B and PDE3 (Alberts, Johnson et al. 2002), and reactions 3.10 and 3.11 need to be specifically written for each of this form. Assuming that the H30 probe, which is used to measure the concentration of experimental cAMP, is uniformly distributed in the cell, the reaction 3.12 describes its binding with one cAMP molecule.

$$R_2C_2 + cAMP \rightleftharpoons cAMPR_2C_2 \tag{3.4.}$$

$$cAMPR_2C_2 + cAMP \rightleftharpoons cAMP_2R_2C_2 \tag{3.5.}$$

$$cAMP_2R_2C_2 + cAMP \rightleftharpoons cAMP_3R_2C_2 \tag{3.6.}$$

$$cAMP_3R_2C_2 + cAMP \rightleftharpoons cAMP_4R_2C_2 \tag{3.7.}$$

$$cAMP_4R_2C_2 \rightleftharpoons cAMP_4R_2C + C \tag{3.8.}$$

$$cAMP_4R_2C \rightleftharpoons cAMP_4R_2 + C \tag{3.9.}$$

$$C + PDE_i \rightleftharpoons PDE^* \tag{3.10.}$$

$$cAMP + PDE^* \rightleftharpoons AMP + PP_i \tag{3.11.}$$

$$H30 + cAMP \rightleftharpoons H30 - cAMP \tag{3.12.}$$

Although all the compartments include the same reactions, in the nucleus the concentration of PKA and PDE are assumed negligible.

Results

Figure 4 shows a representative profile of FRET changes due to variation on cAMP concentration. Point A identifies the baseline signal when the stimulus is added. Point B defines the point where the maximum FRET is reached while C shows the value measured just after the peak, when the signal reaches a stationary value.

Point D identifies the baseline signal when the inhibitor is added and E is the FRET value reached at steady state. The time-course of the signal at the membrane was evaluated defining two reference parameters:

1) the time, T_{max}, when the signal reaches its maximum variation,

2) the ratio, *Peak Depth*, between variation of cAMP concentration at T_{max} and during the steady state after the peak (Equation 1).

$$Peak\ Dept = \frac{(B - A) - (C - A)}{(B - A)} \tag{3.13}$$

The compartmentalization is quantified by the ratio of the variation of cAMP concentration at Tmax between the membrane and the nucleus (Compart Ratio).

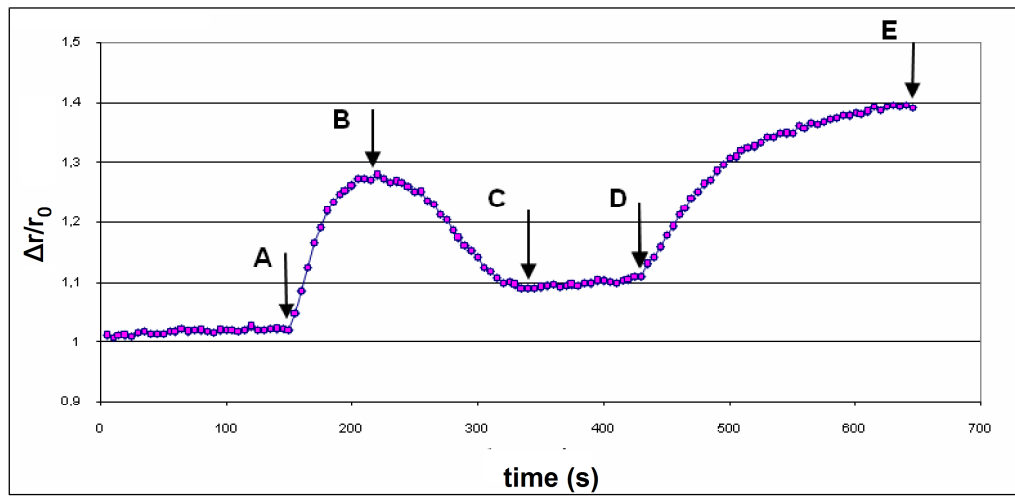$$Compart\ Ratio = \frac{(B - A)_{membr} - (B - A)_{nucleus}}{(B - A)_{membr}} \tag{3.14}$$

Figure 4 *Representative profile of FRET intensity changes after PGE1 stimulation followed by inhibition.*

Sensitivity analysis is commonly used method to characterize the effects of parameter perturbations on model output. Thus, the parameters that influence most the cAMP signalling dynamic were determined by local sensitivity analysis (Saltelli et al., 2000). The study of local sensitivity was assessed for each parameter of the model. Each simulation was conducted by altering 1 parameter at a time and fixing all remaining parameter values. The partial derivative of model output (y) with respect to the perturbed parameter (x_i) provides a measure of the model sensitivity to each parameter.

$$S_i = \frac{x_i}{y}\frac{\partial y}{\partial x_i} \tag{3.15}$$

An approximation of the previous value can obtained by the following equation:

$$\hat{S}_i = \frac{\ln y - \ln y_b}{\ln x_i - \ln x_{ib}} \tag{3.16}$$

Where *b* indicate the reference value. This approach is feasible when changes around the reference are enough small to assume a linear correlation between input and output. Sometimes the percentage of perturbation can be the same for all variables ($\pm$ 5% for Falls et al., 1989). In this work a 1% perturbation was used. All simulations were performed using Matlab.

Qualitatively, assuming homogenous intracellular concentrations of PKA and PDE and ubiquitous cAMP diffusivity of $130\mu m^2/s$, the simulations agree with the experimental results showing a transient peak of cAMP after the PGE1 stimulation. However to deeper quantitative analysis, under these hypotheses no one of the reference experimental parameters are reproduced by the simulated profiles, either T_{max} or *Peak Depth*, that are significantly higher, either *Compart Ratio*, that is much lower (Figure 5).

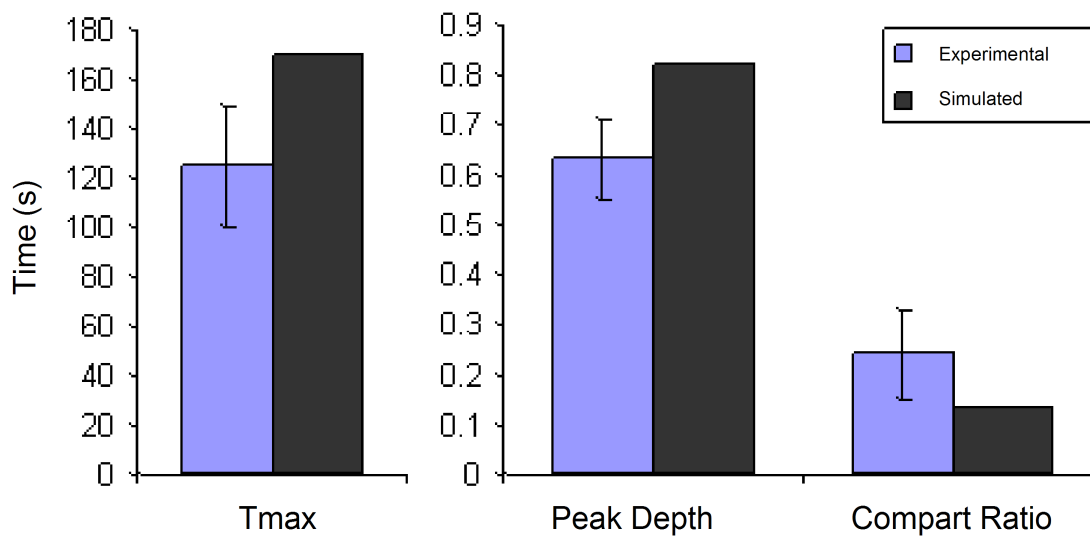
Figure 5 *Comparison of T_{max}, Peak Depth, and Compart Ratio between the experimental reference and the cAMP profile simulated assuming homogenous intracellular concentrations of PKA and PDE and ubiquitous cAMP diffusivity of 130μm²/s.*

Figure 6 shows the results of the local sensitivity for the 32 parameters of the model as function of time. The parameters of investigation were selected according to the range of values available in the literature. These results emphasize the great influence of the coefficient of diffusion of cAMP, whose action extends throughout the time interval examined. Quite sensitive are also the kinetics of PDE and PKA.
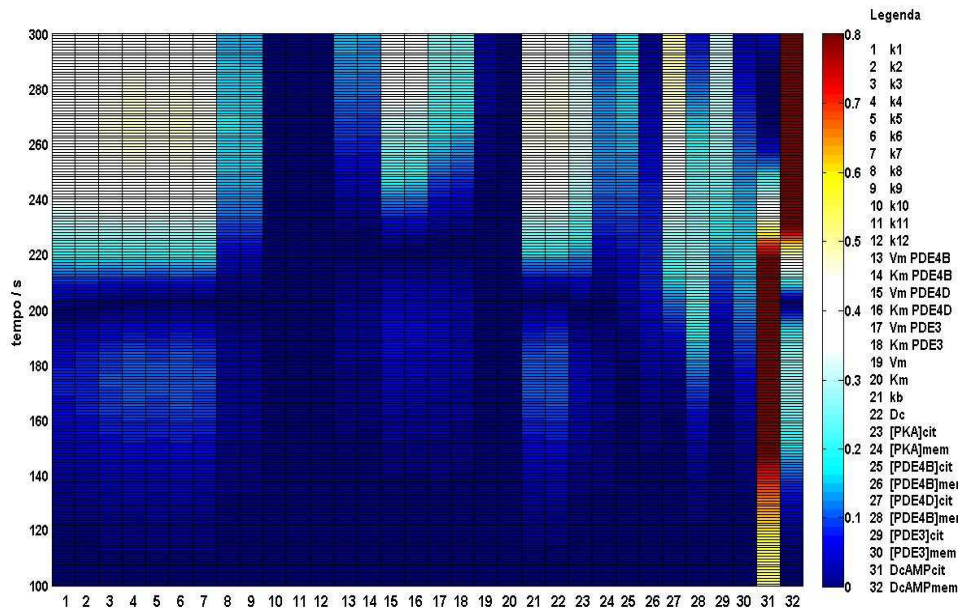

Figure 6 *Results of the sensitivity analysis. The value of sensitivity of the studied parameters, which are listed in the x axis, is reported as function of time (y axis). The colours close to blue represent low influence of the parameter on the model in a particular moment, whereas the a relevant influence on compartmentalisation is expressed by red colours.*

According to that, the reduction of the local diffusivity of cAMP of one order of magnitude has a terrific effect in term of concentration profile development enhancing the compartimentalization and decreasing the peak depth. Our results show that the simple competition between reactions and diffusion, is enough to justify the presence of self-organized dissipative spatio-temporal structures. Even if the localization of specific enzymes doesn't influence significantly the profile expression of secondary messangers, value of diffusivity of $60\mu m^2/s$ is enough to show a relevant effect on the intracellular structural order. These simulations agrees with the experimental observations demonstrating the biological importance of maintaining precise control of PDE4D distribution within the cell whatever is the cAMP diffusivity at the submembrane domain. A complete description of the results is reported in Appendix D.

Conclusion and future perspective

This paper shows how self-organized dissipative spatio-temporal structures, such those related to the cAMP signalling, can be explained assuming chemical reactions and diffusion competition. A quantitative diffusion-reaction model has been implemented here, proving the active role of the intracellular organization on directing and amplifying the biological response of the highly diffusible secondary messenger. The simulated results quantitatively reproduce the experimental data from literature and giving a rational explanation to biological evidences. In a future perspective, it would be interesting to use this new tool for the design of new experiment or for the definition of innovative cardiac drugs.

3.3 References

A. Stett, U. Egert, et al. (2003). "Biological application of microelectrode arrays in drug discovery and basic research." Anal. Bioanal. Chem. **377**(3): 486–495.

Alberts, B., A. Johnson, et al. (2002). Molecular Biology of the Cell, Garland Science.

Baxter, D. F., M. Kirk, et al. (2002). "A Novel Membrane Potential-Sensitive Fluorescent Dye Improves Cell-Based Assays for Ion Channels." J Biomol Screen **7**(1): 79-85.

Bhalla and Ravi Iyengar, U. S. (1999). "Emergent Properties of Networks of Biological Signaling Pathways." Science **283**(5400): 381-387.

Brady, A. J. (1991). "Mechanical properties of isolated cardiac myocytes." Physiol. Rev. **71**(2): 413-428.

Canaday, P. G. and F. S. Fay (1976). "An ultrasensitive isometric force transducer for single smooth muscle cell mechanics." J Appl Physiol **40**(2): 243-246.

Cecchi, G., F. Colomo, et al. (1992). "The stimulus interval-tension relation in enzymatically isolated single myocytes of the frog heart." J Physiol **448**(1): 275-291.

Efimov, I. R., V. P. Nikolski, et al. (2004). "Optical Imaging of the Heart." Circ Res **95**(1): 21-33.

Falconer, M., F. Smith, et al. (2002). "High-Throughput Screening for Ion Channel Modulators." J Biomol Screen **7**(5): 460-465.

Fast VG, I. R. (2000). "Simultaneous optical mapping of transmembrane potential and intracellular calcium in myocyte cultures." J Cardiovasc Electrophysiol. **11**(5): 547-56.

Golbunova Y.V., S. N. C. (2002). "Dynamic interactions of cyclic cAMP transient and spontaneous Ca2+ spikes." Nature **418**: 93-96.

Goldbeter (1996). Biochemical oscillations and cellular rhythms: the molecular bases of periodical and chaotic behaviour.

Gonzalez, J. E. and R. Y. Tsien (1995). "Voltage sensing by fluorescence resonance energy transfer in single cells." Biophys. J. **69**(4): 1272-1280.

Gorbunova, Y. V. and N. C. Spitzer (2002). "Dynamic interactions of cyclic AMP transients and spontaneous Ca2+ spikes." Nature **418**(6893): 93-96.

Hamill OP, Marty A, et al. (1981). "Improved patch-clamp techniques for high-resolution current recording from cells and cell-free membrane patches." Pflugers Arch. **391**(2): 85-100.

Huang R.-C., G. R. (1991). "Kinetic analysis of cAMP-activated Na+ current in the molluscan neuron." J. Gen. Physiol **98**: 835-848.

Kamp, T. J. and J. W. Hell (2000). "Regulation of Cardiac L-Type Calcium Channels by Protein Kinase A and Protein Kinase C." Circ Res **87**(12): 1095-1102.

Kent, R. L., D. L. Mann, et al. (1989). "Contractile function of isolated feline cardiocytes in response to viscous loading." Am J Physiol Heart Circ Physiol **257**(5): H1717-1727.

Klauke, N., G. L. Smith, et al. (2006). "Extracellular Recordings of Field Potentials from Single Cardiomyocytes." Biophys. J. **91**(7): 2543-2551.

Kozer N., S. G. (2004). "Effect of Crowding on Protein–Protein Association Rates: Fundamental Differences between Low and High Mass crowding Agents." J. Mol. Biol. **336**: 763–774.

Kunst, G., K. R. Kress, et al. (2000). "Myosin Binding Protein C, a Phosphorylation-Dependent Force Regulator in Muscle That Controls the Attachment of Myosin Heads by Its Interaction With Myosin S2." Circ Res **86**(1): 51-58.

Lin, G., R. E. Palmer, et al. (2001). " Miniature heart cell force transducer system implemented in MEMS technology." IEEE Transactions on Biomedical Engineering. **48**(9): 996-1006.

Lugnier, C. (2006). "Cyclic nucleotide phosphodiesterase (PDE) superfamily: A new target for the development of specific therapeutic agents." Pharmacology & Therapeutics **109**(3): 366-398.

Marx, S. O., S. Reiken, et al. (2000). "PKA Phosphorylation Dissociates FKBP12.6 from the Calcium Release Channel (Ryanodine Receptor): Defective Regulation in Failing Hearts." Cell **101**(4): 365-376.

McCullough, T. E. and D. A. Walsh (1979). "Phosphorylation and dephosphorylation of phosphorylase kinase in the perfused rat heart." J. Biol. Chem. **254**(15): 7345-7352.

Meyer, T., P. Sartipy, et al. (2007). "New cell models and assays in cardiac safety profiling." Expert Opinion on Drug Metabolism & Toxicology **3**(4): 507-517.

Mongillo, M., T. McSorley, et al. (2004). "Fluorescence Resonance Energy Transfer-Based Analysis of cAMP Dynamics in Live Neonatal Rat Cardiac Myocytes Reveals Distinct Functions of Compartmentalized Phosphodiesterases." Circ Res **95**(1): 67-75.

Müller, F. U., J. Neumann, et al. (2000). "Transcriptional regulation by cAMP in the heart." Molecular and Cellular Biochemistry **212**(1): 11-17.

Natarajan, A., P. Molnar, et al. (2006). "Microelectrode array recordings of cardiac action potentials as a high throughput method to evaluate pesticide toxicity." Toxicology in Vitro **20**(3): 375-381.

Peters R. (1984). "Nucleo-cytoplasmic flux and intracellular mobility in single hepatocytes measured by fluorescence microphotolysis." The EMBO Journal **3**(8): 1831-1836.

Rich T., F. K. A., Tse T. E., Schaack J., Cooper D. M., Karpen J. W. (2001). "A uniform extracellular stimulus triggers distinct cAMP signals in different compartments of a simple cell." PNAS **98**: 13049-13054.

Rich, T. C., W. Xin, et al. (2007). "Cellular mechanisms underlying prostaglandin-induced transient cAMP signals near the plasma membrane of HEK-293 cells." Am J Physiol Cell Physiol **292**(1): C319-331.

Sakmann, B. and E. Neher (1984). "Patch Clamp Techniques for Studying Ionic Channels in Excitable Membranes." Annual Review of Physiology **46**(1): 455-472.

Saucerman, J. J., L. L. Brunton, et al. (2003). "Modeling {beta}-Adrenergic Control of Cardiac Myocyte Contractility in Silico." J. Biol. Chem. **278**(48): 47997-48003.

Schwanke, K., S. Wunderlich, et al. (2006). "Generation and Characterization of Functional Cardiomyocytes from Rhesus Monkey Embryonic Stem Cells." Stem Cells **24**(6): 1423-1432.

Simmerman, H. K. B. and L. R. Jones (1998). "Phospholamban: Protein Structure, Mechanism of Action, and Role in Cardiac Function." Physiol. Rev. **78**(4): 921-947.

Sulakhe, P. V. and X. T. Vo (1995). "Regulation of phospholamban and troponin-I phosphorylation in the intact rat cardiomyocytes by adrenergic and cholinergic

stimuli: roles of cyclic nucleotides, calcium, protein kinases and phosphatases and depolarization." <u>Molecular and Cellular Biochemistry</u> **149**(1): 103-126.

Takahashi, A., P. Camacho, et al. (1999). "Measurement of Intracellular Calcium." <u>Physiol. Rev.</u> **79**(4): 1089-1125.

Tarr, M., J. W. Trank, et al. (1983). "Effect of external force on relaxation kinetics in single frog atrial cardiac cells." <u>Circ Res</u> **52**(2): 161-169.

Tasche, C., E. Meyhofer, et al. (1999). "A force transducer for measuring mechanical properties of single cardiac myocytes." <u>Am J Physiol Heart Circ Physiol</u> **277**(6): H2400-2408.

Tung L. (1986). "An ultrasensitive transducer for measurement of isometric contractile force from single heart cells." <u>Pflugers Arch.</u> **407**(1): 109-15.

van Rheenen, J., M. Langeslag, et al. (2004). "Correcting Confocal Acquisition to Optimize Imaging of Fluorescence Resonance Energy Transfer by Sensitized Emission." <u>Biophys. J.</u> **86**(4): 2517-2529.

Vannier, C., H. Chevassus, et al. (1996). "Ca-dependence of isometric force kinetics in single skinned ventricular cardiomyocytes from rats." <u>Cardiovascular research</u> **32**(3): 580-586.

Waggoner, A. S. (1979). "Dye Indicators of Membrane Potential." <u>Annual Review of Biophysics and Bioengineering</u> **8**(1): 47-68.

Wojcikiewicz EP, Zhang X, et al. (2004). "Force and Compliance Measurements on Living Cells Using Atomic Force Microscopy (AFM)." <u>Biol Proced Online</u> **6**(1-9.).

Yi Zhao, C. C. Lim, et al. (2007). "Simultaneous orientation and cellular force measurements in adult cardiac myocytes using three-dimensional polymeric microstructures." <u>Cell Motility and the Cytoskeleton</u> **64**(9): 718-725.

Yin, S., X. Zhang, et al. (2005). "Measuring Single Cardiac Myocyte Contractile Force via Moving a Magnetic Bead." <u>Biophys. J.</u> **88**(2): 1489-1495.

Chapter 4

3D cardiac tissue development

This Chapter discusses the methods for achieving a culture of cardiomyocytes organized in a 3D cardiac functional tissue. At this propose, the requirements and the most common issues connected with this goal will be highlighted and discussed. Particular attention has been given to the effect of exogenous electric filed as strong physiological stimuli leading to functional tissue differentiation. The chapter ends presenting two methods designed and developed for the evaluation of the cardiac tissue functionality: a) mechanical measurement of strength contraction; b) imaging analysis of optical observation of tissue contractions.

4.1 Engineering issues in 3D cardiac functional tissue development

Even if two-dimensional culture can be very useful for studying and monitoring the cell behavior in a specific environment, in such conditions the cells may lose relevant morphological characteristics and specialized functions. Culturing cells in 3D versus 2D environments dramatically affects (i) *in vivo*-like cell shape, (ii) intercellular crosstalk and (iii) development of a complex extracellular matrix mimicking the native specific microenvironment, integrin/ligand, cell contraction and associated intracellular signaling (Roskelley, Desprez et al. 1994; Knight 2000). The 3D matrix both affects solute diffusion and binds many effector proteins, such as growth factors and enzymes, thereby establishing solute concentration gradients, preserving the natural cellular microenvironment, the specific function and phenotypes (Griffith and Swartz 2006).

Even if the cell seeding and culture condition appeared to be dependent on the type of scaffold used, static culture usually determines unstable and inhomogeneous cellular microenvironment, allowing the viability of cells only for about 100 μm thick outer layer of a tissue construct (Rebecca L. Carrier, Rupnick et al. 2002). On the other hand, the interior remains relatively acellularized or becomes necrotic due to hypoxia, lack of nutrients or poor waste removal. Thus, seeding homogeneity and appropriate cell density in 3D scaffolds play an important role for subsequent tissue development (Ayelet Dar, Leor et al. 2002).

In this perspective, the next stage toward a viable tissue deals with general requirements for a 3D culture: 1) the homogeneous colonization of the scaffold within the entire 3D domain; 2) the viability of the cells within the scaffold during the culture process; 3) the ability of the cells to functionally interact with the biomaterial and maintain differentiated phenotype; 4) the control of medium composition, pH and oxygen levels via gas and medium exchange. These issues can be assessed only implementing the culture in new specialized devices, called bioreactors, designed to culture cells under strictly controlled conditions.

Compared to static cell cultivation, recent studies have evidenced the positive impact of dynamic cell culture conditions in a bioreactor on growth and survival of cells due to better transfer of nutrients and gasses by continuous medium convection (Figallo, Flaibani et al. 2007). Different types of bioreactors have been developed in this sense, such as scaffold floating bioreactors or fixed-wall bioreactors, which are characterized by different level of shear stress on cell (Bilodeau and Mantovani 2006). This feature is really important because shear stresses as low as 0.1 Pa are sufficient to harm cardiac myocytes, so it is necessary to obtain stresses around 0.001 Pa, which is possible only with a laminar flow (Cynthia M. Begley 2000).

The efficient mass transport during the culture is however only necessary but not sufficient condition to obtain a functional tissue. In order to guide the development of cardiac engineered tissue toward the expression of mechanical and electrical properties similar to those of the native myocardium, the bioreactor need to be designed to solve some critical issues related to its functionality: 1) the promotion of a uniform and high density cellularization of porous biomaterials to obtain compact tissue and promote cell-

cell interactions, 2) the assessment of controlled electro–mechanical stimulation to guide cell phenotype to promote excitation-contraction cell coupling.

In either case, it is essential that the cells become electromechanically coupled and capable of synchronously responding to electrical pacing signals, rather than contracting spontaneously. Recent works have shown the effects of strain or electrical stimulation on cell organization and physiology (Ralf Sodian, Lemke et al. 2001; Zimmermann, Schneiderbanger et al. 2002). Stretched cells, for example, align in the direction of the applied strain, and express a longer and wider morphology with a more uniform distribution in the scaffold. By the other side regular electrical stimulation of cardiomyocytes enhances cellular organization, mechanical properties and calcium transients when compared to quiescent myocytes (Radisic, Park et al. 2004).

These evidences of the electrical stimulation positive effects on tissue organization, motivated the interests for a deeper investigation on this field. Since the methodology reported in literature, for functional cardiac tissue fabrication by electrophysiological stimulation, was often imprecise and hardly reproducible, the objective of this thesis work was to clarify the critical aspect of this process, developing a detailed and efficient method. The full description of the resulting manuscript is reported in Appendix E.

4.1.1 Practical aspects of cardiac tissue engineering with electrical stimulation

To induce synchronous contractions of cultured cardiac constructs, we applied electrical stimulation to collagen scaffolds of cardiomyocytes seeded with Matrigel. The electrical signals were designed to mimic those orchestrating the synchronous contractions of cells in native heart. In this work, the protocol of cardiac functional tissue production was optimized considering the following critical issues: 1) cells seeding composition and density, 2) electrical stimulation and 3) scaffold functional characterization.

1) Cells seeding composition and density

Heart cells are obtained from 2-day old neonatal Sprague Dawley rats, using a protocol approved by our Committee on Animal Care. The protocol was optimized to obtained almost 80% of viable cell with high percentage of cardiomyocytes. The cell mixture was seeded with high density (1.35×10^8 cells/cm^3), with a drop by drop technique which enhances the cell attachment on the scaffold.

2) Electrical Stimulation

To perform a reproducible stimulation, it is desirable to maintain the scaffolds in a stable position with respect to the direction of the electric field gradient, without at the same time restricting the contractions of the tissue construct or the ability to observe the constructs with a microscope. We accomplish this task using stainless-steel pins, held in place by a thin layer of PDMS at the bottom of a Petri dish.

The objective of electrical stimulation is to deliver enough current to cells to depolarize membrane and elicit an action potential. Since the stimulation efficiency is influenced by the geometry and material of electrodes, determinant to attain a desired charge-transfer at the electrode-electrolyte interface physiological with minimal damage to the surrounding tissue, a complete characterization of the electrodes was performed using electrochemical impedance spectroscopy (EIS). This method allows the assessment of the relative influence of three different charge transfer mechanisms: (i) non-faradaic charging/discharging of the electrochemical double layer, (ii) reversible faradaic reactions, and (iii) non-reversible faradaic reactions. The optimal material should show high constant phase element (*CPE*) to increase charge injection, and high polarization resistance (R_p) to reduce harmful reactions.

3) Functional characterization of the tissue

The functionality of engineered cardiac constructs was evaluated by measuring contractile activity in response to electrical field stimulation. Electric field stimulation may be delivered from a commercially-available stimulator or through custom-designed hardware controlled by a computer. Although computer-controlled stimulation allows additional flexibility, it requires some expertise in circuit design and software programming. Since the cardiac contractility is significantly influenced by temperature (Giovangrandi, Gilchrist et al. 2006), the temperature of the Petri dish was kept at 37 °C using heating tape fixed to the bottom of the Petri dish and connected to a temperature

controller. Two parameters have been chosen to evaluate the contractile behavior in response to electrical stimulation: excitation threshold, *ET* (the minimum voltage of electrical stimulation required to elicit sustained synchronous contractions of tissue constructs at a frequency of 60 bpm) and maximum capture rate, *MCR* (maximum frequency of sustained synchronous contractions that can be achieved at a stimulation voltage corresponding to 1.5 *ET*). However this method is still very limited by the need of constant observation of the sample during the experiment by a user, which introduces an error on the resulting data.

Conclusion and perspective

In this paper we presented a detailed methodology for the fabrication of a functional 3D cardiac engineered tissue through efficient electrophysiological stimulation. The resulting tissue is characterized by significant contractility and good cellular organization. However more need to be done to improve the tissue homogeneity and the next step in this sense requires the integration of these findings on electrical stimulation in a dynamic system for tissue culture. Better analytical tools need to be designed to evaluate automatically the response to the electrical impulses.

4.2 Cardiac functional tissue characterization

Functional tests often require *in vitro* assessment of electromechanical and histological/biological (gene/protein expression and distribution) properties. The measure of a single cell behavior in certain condition could be useful tool for cardiac pharmacology (Hillier and Bunton 2007). However, to properly assess the functionality of engineered muscle is necessary to measure the physiological performance of the 3D construct contractility, where cell organization and interaction play an important role. Since the twitching tension in an engineered tissue amounted to 0.34±0.03 mN (Zimmermann, Didie et al. 2002), the measure of the cardiac functional response requires very sensitive sensors. Three types of transducers (Bérangère, Philippe et al. 2004) can be defined according to physical principles on which they are based: 1) strain gauges based on changing on electrical resistance (Park, Ryu et al. 2005; Kubo, Shimizu et al. 2007), 2) transducer measuring the variation of magnetic field for Hall

effect (Peterson and Otis 1983; Bérangère, Philippe et al. 2004) 3) optical strain-measuring system (Kazusuke Yamane 1997).

In this scenario, the objective of this thesis work was to design and develop different methodologies for the automatic *in vitro* measure of the muscle contractility. In particular, two approaches were followed considering the use of: 1) a piezoresistive sensor, 2) an automated system of imaging analysis. The following sections summarized the hypotheses, the design and the preliminary results coming out from these two research activities.

4.2.1 Design of 3D culture system for electrophysiological stimulation of cardiac force contractility

In order to assess the functionality of the engineered cardiac tissue, it is necessary to measure the force and amplitude of contractility and the response to a pharmacological stimulation. Our previous work (Appendix E) has already clarified the need of an automatic methodology for an on line definition of the cardiac contractility evaluation.

Aim of this study was to design a small device that integrates the culture of a three-dimensional electrically stimulated cardiac tissues with the online measure of contractile force during culture. The possibility of decoupling the observation of the sample from the measure of contractility is reached using a piezoelectric sensor (AE801, MemsCap), which registers the changing electrical resistance of a material due to applied mechanical stress. This type of sensor has been proposed for ex-vivo studies on muscle strips with sensitivity between 25 and 100 mV/mN (0.25-1.0 mV/mg) (Hanley and Loiselle 1998; Wu, Haystead et al. 1998; Baker, Redfern et al. 2001; Shimizu, Yamato et al. 2002). Although moderately fragile, these sensing elements are small and relatively inexpensive. The output of the sensing element may be recorded automatically by and amplified by a small amplifier mounted on a support block with the element.

Force transducer system design

The device was fabricated curing poly(dimethylsiloxane) (PDMS) in a polycarbonate mold (Figure 2). The 10:1 mixture of PDMS and initiator (Dow Corning, MI) was

poured in the mold where the plastic cube of 16x8 area and 20 mm height was already inserted in specific holes.

The sensor elements (Figure 1A) consist of two main parts, the silicon cantilever beam itself and the header to which the beam is mounted. The beam is made of single crystal N-type silicon and has one ion-implanted P-type resistor on each side. The surface of the beam is passivated with thermally grown silicon dioxide. In order to obtain a creep free mounting of the beam, an alloying technique has been developed for joining the four pins of the header to contact areas on the beam. Thus the four pins of the header serve both as mechanical mount as well as electrical connections for the resistors.
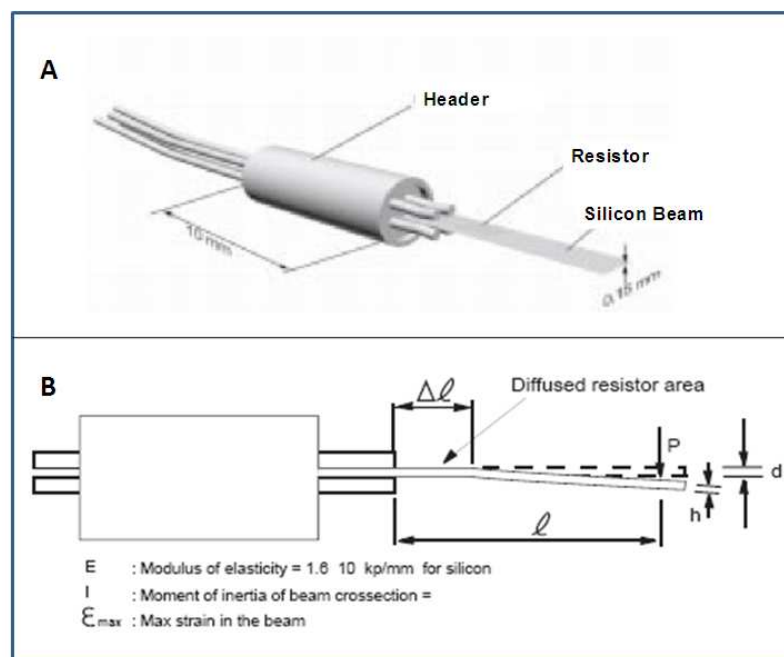

Figure 1 *Sensor element (A) Magnification showing the main parts and dimensions (B) Schematic representation of the cantilever beam deflection, after single force loading.*

The sensor element has two resistors, one on each side of the beam. When the tip of the beam is deflected, the areas where the resistors are located will be set under mechanical stress. Because of the piezoresistive effect in silicon, the resistors will hereby change in value. The resistor on the compressed side will decrease in value, and the resistor on the other side will increase. The change in resistance is determined by various parameters such as deflection and beam dimensions.

Loading of the sensor element by adding a force (P) at the tip. The deflection d is calculated as:

$$d = \frac{P}{EI}\frac{l^3}{3} = \frac{2}{3}\varepsilon_{max}\frac{l^2}{h} \qquad (4.1)$$

Where l and h are given in the Figure 1B. The average strain can be calculated by the following equation:

$$\varepsilon_m = \varepsilon_{max}\frac{l - \Delta l/2}{l} \qquad (4.2)$$

And the relative resistance is given by:

$$\frac{\Delta R}{R} = \lambda\varepsilon_m \qquad (4.3)$$

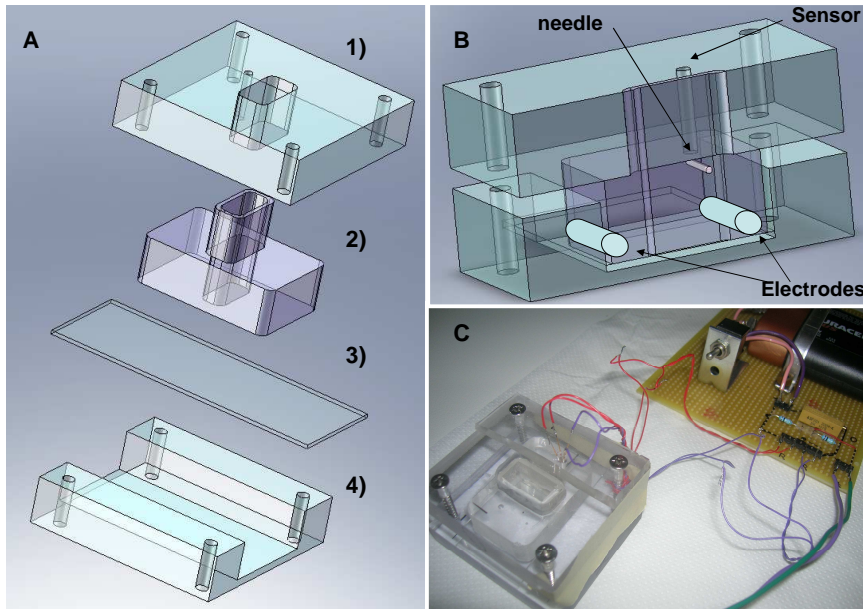where λ is the gauge-factor of the resistors.

Figure 2 *Force transducer bioreactor. (**A**) Schematic 3D view of bioreactor. The bioreactor is constituted by a frame in polycarbonate (**A1**,**A4**) and by a central part in PDMS A2 (well 8x16 mm 20mm height) and glass A3. The devices are assembled from layers of PDMS and glass, attached via plasma treatment of both surfaces. (**B**) Side view of the bioreactor. The electrical stimulation is guarantee during the culture by 2 carbon rods (8mm length, 2mm diameter) set in the central well. The sensor is inserted in the 2mm diameter hole made in the top part of the polycarbonate frame. (**C**) Image of the assembled bioreactor.*

When the active resistors are made part of a Wheatstone bridge, the unbalance potential (ΔV) of the bridge due to a deflection d is given by:

$$\Delta V = V\frac{\Delta R}{2R} \qquad (4.4)$$

The mold has been designed to couple the strain gauge with the sample during the culture and keep always the header dry and stable.

The bioreactor is characterized by a well of 16x8mm and 20mm high, where the tissue is cultured, as showed in Figure 2. The PDMS well is irreversibly bonded to glass slide after treatment with vacuum gas plasma for 45 s (at 0.5 mbar and 50 W) (Harrick Scientific, Pleasantville NY). The central PDMS/glass well is held in place by mechanical compression via a frame consisting of two polycarbonate slides, and four thumbscrews. The top one is characterized by a hole (2mm diameter) where the sensor is introduced. The beam is coupled to the tissue by the introduction of the beam in the eye of a needle (0.8mm diameter). A really thin silicone membrane keeps apart the sensor to the culture medium.

Carbon rods of 2 mm diameter and 8mm length can be inserted in both sides of the well in order to guarantee a stable electrical stimulation. In this way heart tissue can be electrically stimulated within bioreactor while they contractility is measured. A Labview program has been implemented in order to record automatically the sensors signals during the experimentation and generate square wave stimulation.

Conclusions and future perspectives

The preliminary research activities ended with the successfully realization of device prototype (Figure 2C) which was responding to the system specifications such as:

> ➢ easy manipulation and sterilization of the culture system;
> ➢ electrical stimulation of sample during the culture;
> ➢ small dimensions;
> ➢ high sensitivity of the measure and sensor stability;
> ➢ isolation of the sensor from the culture medium;
> ➢ easy coupling of the sensor with the tissue;
> ➢ easy connection to the labview board.

Preliminary experiments on cardiac artificial tissues, produced accordingly to the method previous described (Appendix E) or provided by the research lab of Eschenhagen, give a quite convincing proof of concept of the device. On the other hand,

to fully optimize the device and characterize the heart tissue behavior, more work needs to be done on: 1) calibration of the transducer signals through application of increasing external force while the transducer output is recorded; 2) evaluating the contractility of heart muscle strips in normal medium and in medium conditioned with insulin; 3) coupling this sensor with engineered tissue to understand the influence of electrical stimulation or seeding protocol on tissue contractility. The high potential of the proposed device is in the possibility of scale up the number of simultaneous experiments through an automated analysis of several samples during the culture. From an engineering perspective, this could help on a more rational experimental design for the definition of the physiological response to pharmacological stimulation.

4.2.2 Imaging analysis of 3D cardiac tissue functionality

The possibility of extrapolating automatically relevant physiological information about the cell or tissue contraction from optical analysis, offers an interesting and sensitive tool to measure online the cardiac functionality. Shape extraction or segmentation from images is one of the most challenging task in Computer Vision.

Previous works showed the limitation of a shape recognition technique based only on low level features, such as gradients and edge detectors, neglecting the *a priori* knowledge of the system. The Active Contours technique was developed to support the visual interpretation of shape through the influence of *a priori* shape expectation (Kass, Witkin et al. 1987). Active Contour techniques, alternatively called Snake, is a technique extensively used by Computer Vision and Image Processing to detects and tracks object boundaries in single frames or over time. The seminal paper on Snakes was written by Kass et al. in 1987 (Kass, Witkin et al. 1987). Many variations and extensions of the method have been proposed by the literature including the use of Fourier parameterisation (Scott 1987), the incorporation of hard constraints (Amini, Tehrani et al. 1988) or explicit dynamics (Terzopoulos and Waters 1990; Terzopoulos and Szeliski 1992), the realisation of snakes using B-splines (Blake and Cipolla 1990; Menet, Saint-Marc et al. 1990) combined with Lagrangian dynamics (Curwen, Blake et al. 1991). B-splines used in this way are a form of "finite element", a standard technique for the numerical solution of differential equations (Zinkiewicz and Morgan 1983). In 1995, Black and Yacoob used the visual motion field over a region to track and identify

movement. Particularly oriented to biological images, Patrick Brigger and co-workers (Patrick Brigger, Jeff Hoeg et al. 2000) showed that a B-Spline Cubic Interpolation can be used as a tool for fast and intuitive contour outlining without any loss of generality. Applying this tool to brain scan images (PET), they proved that this kind of interpolation provides robustness and fast algorithmical performance time. Chenyang Xu and Jerry L. Prince (1997) developed a new force, Gradient Vector Flow (GVF), to deal with noisy images. In order to recognize the left ventricle, they applied Gradient Vector Flow-Active Contour to magnetic resonance images of the human heart. The model was further improved by Chenyang Xu and Jerry L. Prince (1998) to overcome some of the difficulties with GVF, namely very tight region of the image and very high noise areas.

The objective of this research work was to develop a tool based on imaging analysis of optical observation, to evaluate and characterize the functional activity of artificial cardiac tissues. In particular we provided an unified framework to obtain complete set of functional data in term of contraction displacement and frequency associated with external electrical stimulation. At the core base of this idea there is an Active Contour based tracking algorithm. This project was developed in collaboration with Alberto Silletti and Angelo Cenedese (Department of Engineering and Information, Università di Padova). This part of the thesis deals with the preliminary evaluation of the feasibility of the proposed technique, which is briefly described in what follows.

Methodology Definition

A Snake can be thought as an elastic ribbon which aims to detect the shapes of interest in an image. The nature of its elastic energy is more or less strongly attracted to certain preferred configurations. The final rest shape of the elastic ribbon depends thus not only on the intensity of the image data, but also on the expected shape configurations.

Formally an Active Contours is a curve $C(s)$ $s \in [0,1]$, closed or not, whose internal energy can be calculated by the following equation:

$$\varepsilon(s) = S(s) + P(s) \tag{4.5}$$

Where ε is the Total Energy of the curve (more generally of the *n*-dimensional hypersurface) while $S(s)$ and $P(s)$ are respectively the Internal and External Energy. $C(s)$ evolves in time in order to minimize the energy functional, stopping its evolution at local minimum. The energy profile $\varepsilon(s)$ determines the evolution of the shape and its steady position. As general guideline we can say that $S(s)$ imposed the smoothness conditions to the Active Contours, while $P(s)$ gives higher level information on the shape. Human beings are particularly able to exploit and to use these kind of informations during common visual and pattern recognition processes.

Internal and External energy have the form:

$$S(s) = \oint_{\Omega} \alpha(s) \left| \frac{\partial C}{\partial s} \right|^2 + \beta(s) \left| \frac{\partial^2 C}{\partial s^2} \right|^2 ds \qquad (4.6)$$

$$P(s) = \oint_{\Omega} F(I(C(s))) \, ds \qquad (4.7)$$

respectively, where α and β are scalar values, function of the curve parameterization, that describe the smoothness and stiffness of the curve. A high value of α encourages smooth curves, without spikes or peaks, while a high value of β enforces a straight curve. In literature most authors use $\alpha = 1$ and $\beta = 0.1$.

$I(C(s))$ represents data from image sensor evaluated at Contour location, while $F(I)$ is a function of the image I describing the response of the Contour to data. $F(I)$ is tightly application dependent and its formulation is an implementation detail: it could reflect image edges, gray values, texture energy, correlation with a pattern and so on. A common general base is to take a feature map $F(r)$ like an edge detector and to treat $-F(r)$ as a "landscape" on which the snake can slither (Figure 3).
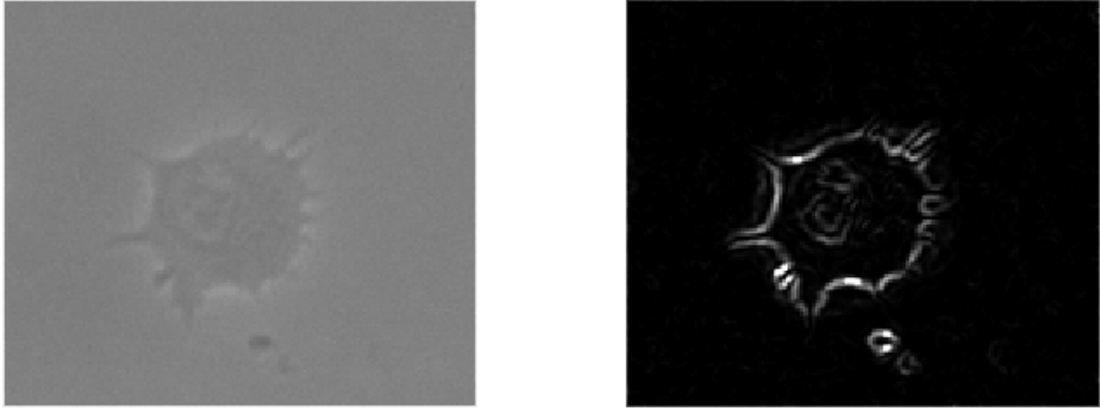
Figure 3 *Process of edge detection starting from a still frame of a video sequence (left picture). The processed image is shown at the right.*

According to the variational principles, the minimum of a functional is equal to the zeros of the derivative, hence:

$$-\nabla F(I(C(s))) + 2\frac{\partial}{\partial s}\left(\alpha(s)\frac{\partial C}{\partial s}\right) - 2\frac{\partial^2}{\partial s^2}\left(\beta(s)\frac{\partial^2 C}{\partial s^2}\right) = 0 \tag{4.8}$$

If one assume $\alpha(s)$ and $\beta(s)$ constant over the entire Contour, the minimum get the form

$$-\nabla F(I(C(s))) + 2\alpha\frac{\partial^2 C}{\partial s^2} - 2\beta\frac{\partial^4 C}{\partial s^2} = 0 \tag{4.9}$$

$\varepsilon(s)$ is generally a function with a high dimensional domain, $s \in R^d, d \gg 1$. For a well-designed functional $\varepsilon(s)$ the same local minima will be reached with several methods, depending on the descending algorithm.

Initialization is provided giving a loose fitting, which surrounds the structure of interest. The reaching of a rest position, by means of a Gradient Vector Flow (GVF) Contour in a pseudo-time, provides us a good starting point for the successive video tracking. As reference frame we used the first frame of the video sequence. The designed $\varepsilon(s)$ showed to be robust, proving the ability of recovering from bad initialization or bad video condition, such as blur or defocus. This aspect is particularly important in long video sequence, in which the probability of losing track grows geometrically with video length.
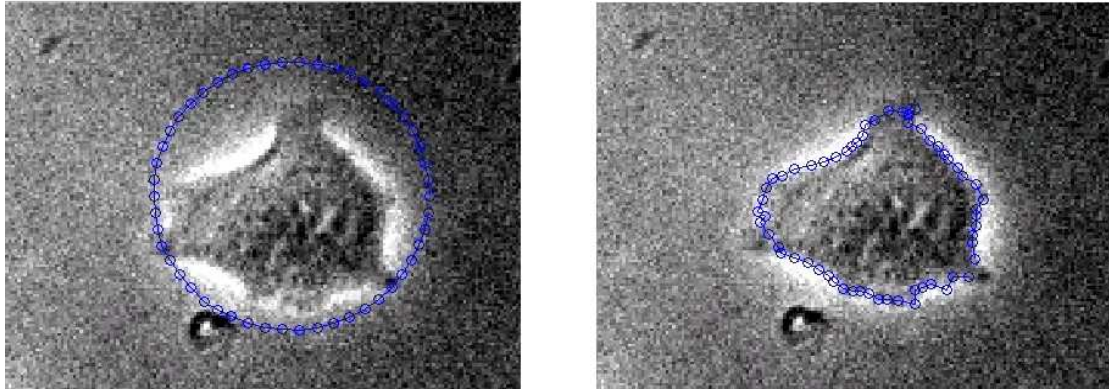
Figure 4 *Cell segmentation process: prove of ε(s) effectiveness. The algorithm showed the ε(s) ability recovering from bad initialization. The left picture shows the initial fitting of a single cell whereas the right picture presents the final rest snake position.*

Video Tracking

In order to obtain a tracking of the biological sample in the video sequence, the segmentation problem was iterated multiple times thought frames. Due to the temporal coherence of the images, each frame is similar to the previous one and the movement of the structure of interest is in general bounded by some physical constraints. Thus, the rest position of a each frame was considered as the starting position of the successive one. The same methodology was used to track single cell motion (Figure 4) and 3D cardiac tissue contraction (Figure 5).

Figure 5 shows a representative image of the output profiles obtained by the analysis of a 3D tissue contraction video. The output data can be processed to calculate geometrical and biological parameters related to the shape, such as mean curvature, area, perimeter, central moments, frequency and amplitude of pulsation. Our framework can provide any kind of information regarding the variation on cell or tissue area. All the information extracted from videos can be treated as signal, applying a vast literature of filtering and manipulation techniques, such us median filters to suppress noise or low pass filters.
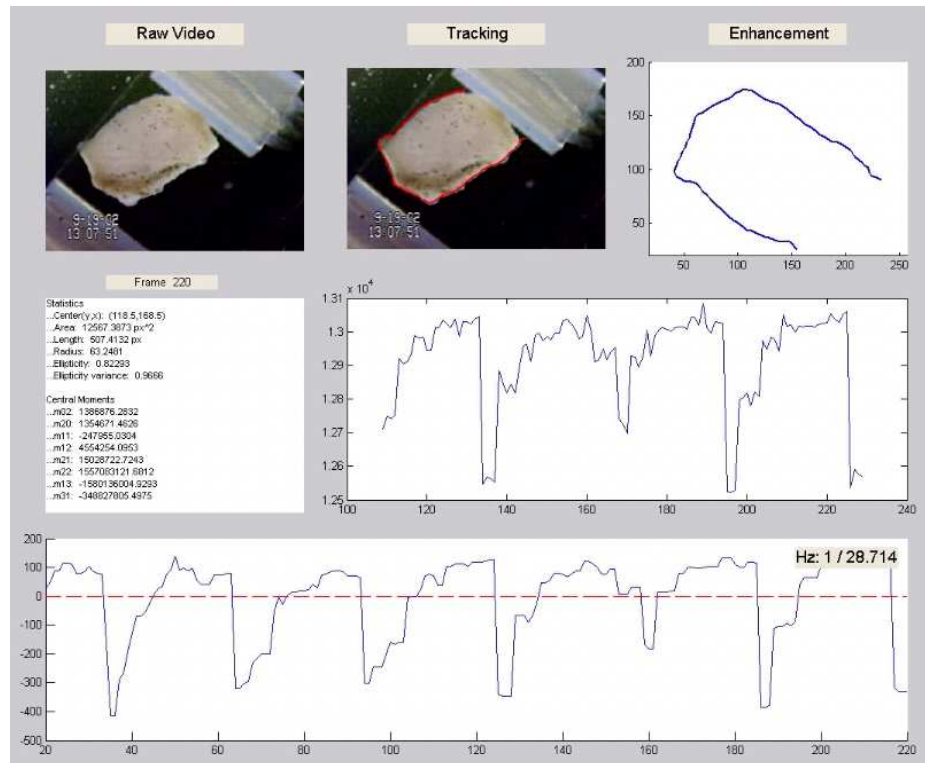
Figure 5 *Output profile given by the application of Active Contour based tracking algorithm for the elaboration of video sequence. The figure represents the final data set obtained by the analysis of an in vitro cardiac engineered patch contraction.*

The graphic user interface is ideally subdivided into three layers, corresponding to different level of abstraction of the achieved data (Figure 6). The first row represent the stream video and the shape extracted from it, the second row shows geometrical statistics while the bottom line show biological parameters such as heart pulsation and frequency.

Figure 6 *Schematic data layering shown in the grafic user interface.*

Conclusion and future perspectives

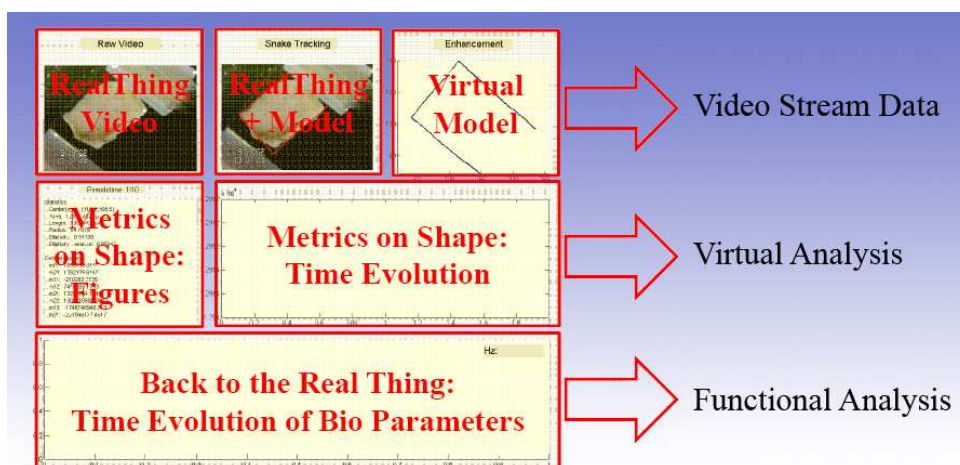In the present work we designed and developed a general, unified framework for segmentation and tracking of biological structures, such as cell or tissue, captured in video sequences. This technique is particularly suitable for the analysis on this field because it minimizes the physical interactions between the sensor and the biological system. This methodology proved to be enough sensitive to follow precisely the cell motion and the contraction of a cardiac engineered tissue. Interesting data on amplitude and frequency of cardiac physiology can be extracted by the analysis of the video sequences, suggesting the idea of combining this tool with a controlled electrophysiological stimulation system. This design will offer the opportunity of defining the quality of the engineered tissue or the optimal setting for each engineered tissue by integrating a feedback system.

4.3 References

Amini, A., S. Tehrani, et al. (1988). Using dynamic programming for minimizing the energy of active contours in the presence of hard constraints. . 2nd Int. Conf. on Computer Vision.

Ayelet Dar, M. S., J. Leor, et al. (2002). "Cardiac tissue engineering Optimization of cardiac cell seeding and distribution in 3D porous alginate scaffolds." Biotechnology and Bioengineering **80**(3): 305-312.

Baker, A. J., C. H. Redfern, et al. (2001). "Abnormal contraction caused by expression of Gi-coupled receptor in transgenic model of dilated cardiomyopathy." Am J Physiol Heart Circ Physiol **280**(4): H1653-1659.

Bérangère, R., P. Philippe, et al. (2004). "Strain and force transducers used in human and veterinary tendon and ligament biomechanical studies." Clinical biomechanics (Bristol, Avon) **19**(5): 433-447.

Bilodeau, K. and D. Mantovani (2006). "Bioreactors for Tissue Engineering: Focus on Mechanical Constraints. A Comparative Review." Tissue Engineering **12**(8): 2367-2383.

Blake, A. and R. Cipolla (1990). Robust estimation of surface curvature from deformation of parent contours. . 1st European Conf. Computer Vision, Springer-Verlag.

Curwen, R., A. Blake, et al. (1991). Parallel implementation of Lagrangian dynamics for real-time snakes. . British Machine Vision Conf.

Cynthia M. Begley, S. J. K. (2000). "The fluid dynamic and shear environment in the NASA/JSC rotating-wall perfused-vessel bioreactor." Biotechnology and Bioengineering **70**(1): 32-40.

Figallo, E., M. Flaibani, et al. (2007). "Micropatterned Biopolymer 3D Scaffold for Static and Dynamic Culture of Human Fibroblasts." Biotechnol. Prog. **23**(1): 210-216.

Giovangrandi, L., K. H. Gilchrist, et al. (2006). "Low-cost microelectrode array with integrated heater for extracellular recording of cardiomyocyte cultures using commercial flexible printed circuit technology." Sensors and Actuators B: Chemical **113**(1): 545-554.

Griffith, L. G. and M. A. Swartz (2006). "Capturing complex 3D tissue physiology in vitro." Nat Rev Mol Cell Biol **7**(3): 211-224.

Hanley, P. J. and D. S. Loiselle (1998). "Mechanisms of force inhibition by halothane and isoflurane in intact rat cardiac muscle." J Physiol **506**(1): 231-244.

Hillier, C. and D. Bunton (2007). "Functional human tissue assays." Drug Discovery Today **12**(9-10): 382-388.

Kass, M., A. Witkin, et al. (1987). Snakes: Active contour models. 1st Int. Conf. on Computer Vision.

Kazusuke Yamane, F. M. (1997). "Optical isometric force transducer for measurement of rat skeletal muscle contraction in the NMR spectrometer." NMR in Biomedicine **10**(6): 292-295.

Knight, B. (2000). "Visualizing muscle cell migration in situ." Curr. Biol. **10**: 576-585.

Kubo, H., T. Shimizu, et al. (2007). "Creation of myocardial tubes using cardiomyocyte sheets and an in vitro cell sheet-wrapping device." Biomaterials **28**(24): 3508-3516.

Menet, S., P. Saint-Marc, et al. (1990). B-snakes: Implementation and application to stereo. DARPA.

Park, J., J. Ryu, et al. (2005). "Real-Time Measurement of the Contractile Forces of Self-Organized Cardiomyocytes on Hybrid Biopolymer Microcantilevers." Anal. Chem. **77**(20): 6571-6580.

Patrick Brigger, Jeff Hoeg, et al. (2000). B-Spline Snakes: A Flexible Tool for Parametric Contour Detection. IEEE Transaction on Image Processing.

Peterson, C. V., Jr. and A. B. Otis (1983). "A Hall effect transducer for measuring length changes in mammalian diaphragm." J Appl Physiol **55**(2): 635-641.

Radisic, M., H. Park, et al. (2004). "From the Cover: Functional assembly of engineered myocardium by electrical stimulation of cardiac myocytes cultured on scaffolds." Proceedings of the National Academy of Sciences **101**(52): 18129-18134.

Ralf Sodian, T. Lemke, et al. (2001). "New pulsatile bioreactor for fabrication of tissue-engineered patches." Journal of Biomedical Materials Research **58**(4): 401-405.

Rebecca L. Carrier, M. Rupnick, et al. (2002). "Effects of oxygen on engineered cardiac muscle." Biotechnology and Bioengineering **78**(6): 617-625.

Roskelley, C. D., P. Y. Desprez, et al. (1994). "Extracellular matrix-dependent tissue-specific gene expression in mammary epithelial cells requires both physical and biochemical signal transduction." Proc. Natl Acad. Sci. USA **91**: 12378-12382.

Scott, G. (1987). The alternative snake — and other animals. . 3rd Alvey Vision Conference.

Shimizu, T., M. Yamato, et al. (2002). "Fabrication of Pulsatile Cardiac Tissue Grafts Using a Novel 3-Dimensional Cell Sheet Manipulation Technique and Temperature-Responsive Cell Culture Surfaces." Circ Res **90**(3): e40-48.

Terzopoulos, D. and R. Szeliski (1992). Tracking with Kalman snakes. , Blake, A. and Yuille, A., editors,Active Vision, MIT.

Terzopoulos, D. and K. Waters (1990). Analysis of facial images using physical and anatomical models. In , . 3rd Int. Conf. on Computer Vision.

Wu, X., T. A. J. Haystead, et al. (1998). "Acceleration of Myosin Light Chain Dephosphorylation and Relaxation of Smooth Muscle by Telokin. SYNERGISM WITH CYCLIC NUCLEOTIDE-ACTIVATED KINASE." J. Biol. Chem. **273**(18): 11362-11369.

Xu, C. and J. L. Prince (1997). Gradient Vector Flow: A New External Force for Snakes IEEE Proceding Conference on Computer Vision and Pattern Recognition.

Xu, C. and J. L. Prince (1998). "Generalized gradient vector flow external forces for active contours." Signal Processing(71): 131-139.

Zimmermann, W.-H., M. Didie, et al. (2002). "Cardiac Grafting of Engineered Heart Tissue in Syngenic Rats." Circulation **106**(90121): I-151-157.

Zimmermann, W. H., K. Schneiderbanger, et al. (2002). "Tissue Engineering of a Differentiated Cardiac Muscle Construct." Circ Res **90**(2): 223-230.

Zinkiewicz, O. and K. Morgan (1983). Finite elements and approximation. , Wiley,New York.

Chapter 5

Cardiac tissue engineering: future perspectives

This Chapter deals with the evaluation of two different *in vivo* strategies for myocardium regeneration correlated with localized delivery of cells. In this perspective, we proved of the effective integration and vascularization of the collagen scaffold, which have been previously used for the *in vitro* fabrication of cardiac functional tissue. The Chapter ends presenting the chemical-physical characterization of a new photocrosslinkable hydrogel to be used as cell carrier for cell based therapy.

5.1 *In vivo* cardiac tissue engineering

Even if the advances on treating myocardial ischemia by injection of exogenous non cardiac-committed stem cells and/or activation of endogenous cardiogenic stem cells have shown promising results, the main limitations for the development of stem cell based clinical therapies are still given by the lack of *in situ* large supply of stem cell and stable cardiomyocytes (Gage 1998; Semsarian 2002; Gu Y, Yu J et al. 2007). Thus, in order to guarantee the quick and efficacious application of these techniques, it is necessary to study and address all the clinical requirements and perform an appropriate selection of the cell source and matrix composition, which should match with the patho-physiological profile of the ischemic region. Moreover, the structure and composition of the matrix should be able to support the growth and differentiation of both neo-vessels and cardiomyocytes (CM) (Kofidis T, Müller-Stahl K et al. 2007).

In particular two strategies have been pursued in this sense: 1) the use of a three dimensional scaffold as cell reservoir, 2) the injection of an efficacious biomaterial, such as an hydrogel, used as cell carrier. The present work aimed to test the feasibility of these two approaches.

The aim of the first study was to develop a methodology to test the effective capability of a collagen patch of promoting a myocardial revascularization adequate to the cardiomyocytes growth. The following sections describe the preliminary *in vivo* results obtained implanting a three dimensional collagen scaffold, which was surgically attached on the external wall of a rat cryoinjured heart muscle.

The second study aimed to develop a promising material to regenerate the ischemic region through a hydrogel injection. This approach could give the advantage of reach the inner part of the muscle where the necrosis starts. The section will summarize briefly the concept and the results obtained by *in vitro* physical-chemical characterization of a new photo-crosslinkable hydrogel. A full detailed description of the results is reported in Appendix F.

5.1.1 *In Vivo* Application of Collagen scaffold in a Cryoinjury Rat Heart Model

In the perspective of using a three dimensional scaffold as cell reservoir for cell delivery in acute or chronic ischemia, the first step is the *in vivo* evaluation biocompatibility, immune acceptance/tolerance and integration with the damaged tissue of the bioengineered constructs. However for a bioactive action of the biomaterial is necessary to demonstrate that the material implant stimulates new blood vessel formation and myocardial regeneration. This neovascularization should support the viability of the cardiomyocytes, which populates the tissue. In this context, we focused on a type I collagen sponge, provided by Davol (Cranston, RI, USA), previously used as a 3D scaffold for engineering cardiac tissue (Radisic, Park et al. 2004). This scaffold has already demonstrated the capability of evoke a powerful angiogenetic and arteriogenetic response in the intact and cryoinjured left ventricle of rats. After 60 days from the implant in the heart, the collagen scaffolds were almost completely adsorbed and became populated by new arterioles and capillaries (Callegari, Bollini et al. 2007).

Aim of this study was to demonstrate the ability of the material to provide an adequate bloody supply for supporting the viability and the growth of cardiomyocytes. In this work we analyzed rat cardiomyocyte gfp positive injection into the patch implanted into Nude Immunodeficient Rat (rNu) with cryoinjured heart plus patch implantation and inoculation of the injection medium.

All surgical and pharmacological procedures used in this study were performed in accordance with regulations expressed in the Guide for Care and Use of Laboratory Animals prepared by the Institute of Laboratory Animal Resources, National Research Council, published by the National Academy Press, revised 1996 (NIH Publication No. 85-23) and the Italian Health Minister Guidelines for Animal Research. The protocol was approved by the University of Padua Animal Care Committee. The surgical procedures were carried out as previously set in literature (Callegari, Bollini et al. 2007). rNu rats were anesthetised by i.m. injection of Zoletil (4 mg/100 g body weight) along with atropin (s.c.; 5 uL/100g) and xylazin (i.p.; 0.4 mg/ 100 g).

Cardiomyocytes wild type (wt) and gfp positive (gfp+ rCM) were isolated from neonatal rats as described in Appendix E and then 5×10^6 cells/animal gfp+ rCM were injected in 90ul of DMEM high glucose medium with hepes (Gibco) and rNU rats serum 1:100 solution (injection medium) in the collagen patch 15 days after its in vivo application on the heart cryoinjury. Animals were sacrificed at 24 hours, 15 and 30 days (this last time point only for the stem cells not for rCM) after the cells injection.
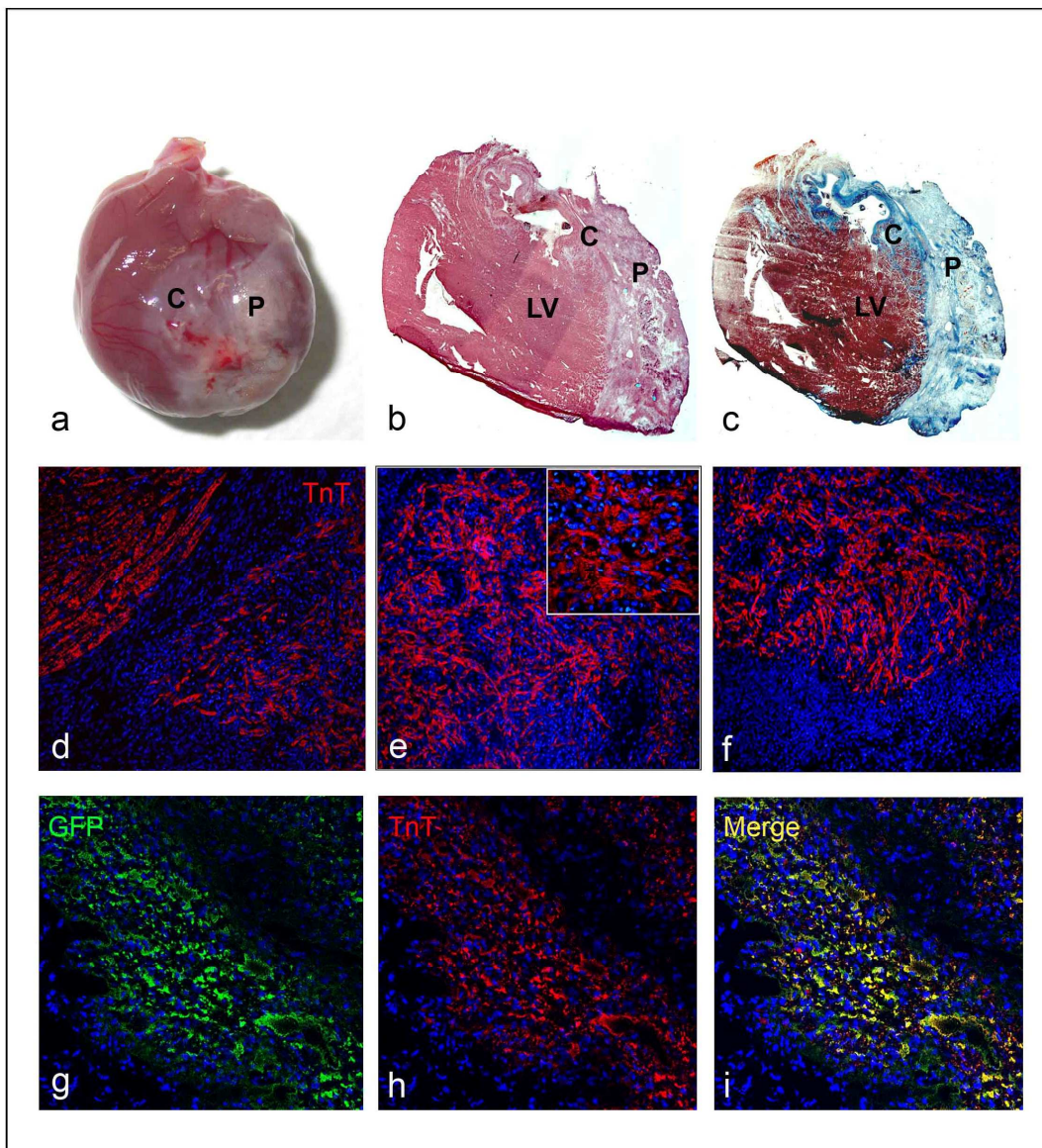
Figure 1 *Gross appearance, histological and immunofluorescence staining of rNU cryoinjured hearts with wt rCM and gfp+ rCM injection 15 days after patch implantation. (**a**) gross appearance of rNu hearts with wt rCM injection: C = cryoinjury area, P = collagen patch; (**b**) hematoxilin and eosin staining of rNu hearts, magnification 2,5x : LV = left ventricule; (**c**) Masson's trichrome staining of rNu hearts with wt rCM injection, magnification 2,5x: in blue the collagen patch and the cryoinjury area, in brown-red intact myocardium. In (**d**, **e**, **f**) immunostaining for cardiac troponin T (in red) on heart slides in the patchcryoinjury area with wt rCM injection: intact myocardium and wt rCM stained in red; magnification 20x and 40x in the inlet in e. In (**g**, **h**, **i**) immunostaining for GFP (in green, **g**) and cardiac troponin T (in red, **h**) and the merged picture (in yellow, **i**) on hearts slides in the patch-cryoinjury area with gfp+ rCM: rCm are both green and red for for GFP and TnT expression as seen in merge in I; magnification 20X and 2X zoom. Both wt or gfp+ rCM (respectively in **e**, **f** and on the right in **d** and in **g**, **h**, **i**), injected in the patch on the cryoinjury, were found as disorganized clusters of cells with no orientation 15 days after the inoculation.*

Eight-micron thick frozen sections were cut from hearts of animals and stained with hematoxylin-eosin and Masson's trichrome staining. Other cryosections were processed by immunofluorescence protocol for cardiac, immune response and inflammatory markers such as anti-cardiac troponin T (TnT mouse IgG, 1:500, Abcam). Briefly, tissue slides were fixed in PFA 4% for 5 minute at room temperature, and incubated at 37°C for 25 minutes with the appropriate dilution of the primary antibody in PBS+1% bovine serum albumin (Gibco and Sigma). Cells were then reincubated at 37°C for 25 minutes with the appropriate dilution of the secondary antibody (goat anti-mouse IgG coniugated with Alexa Fluorescence 564 IgG 1:150, Molecular Probes) PBS+1% bovine serum albumin with human and rat serum (1:100). Cell nuclei were stained with a Hoescht solution diluited 1:5000 in PBS 1X for 5 minutes at room temperature. Observations were made using a Zeiss Axioplan epifluorescence microscope (Zeiss, Oberkochen, Germany), a Leica TCS SP5 confocal microscope and images were obtained using a Leica DC300F digital videocamera. Optical images were acquired by a Leica DMR microscope connected to a Leica DC300 videocamera.

Results and discussion

By gross observation, the cardiac patch was firmly attached to the epicardial surface independently from the previous cryoinjury (Figure 1a-c). Both wt and gfp+ rCM injected into the collagen patch on the cryoinjured left ventricle of rNu rats showed to survive 15 days after the inoculation. rCM were found as big round of not structured or integrated with the host counterpart cell clusters, both in the patch and the area between the patch and the cryoinjury zone. This cellular distribution seemed to be in accord with the original position achieved through the injection, that is the rCM demonstrated to remain exactly where they have been grafted, showing no capacity of migration or homing in response of the factors released by the damaged area (Figure 1d-i).

Conclusions

The *in vivo* implantation of a collagen scaffold in the external wall of the ischemic muscle gave interesting and promising results. The polymeric matrix works reducing the wall thinning and promoting a neovascularization. This vasculature system seem to

provide the adequate metabolic condition to guarantee the viability of cardiomyocytes. However what happens *in vivo* at the cellular level is still unknown. The experimental results show that some cells, as the cardiomyocytes, don't migrate from the site of injection, whereas other cell types, such as stem cells, show an opposite behavior. What regulates this mechanism is still unknown and from an engineering perspective it would be interesting to integrate this methodology with a mathematical model that would explain the phenomena and their evolution over time. Moreover since the oxygen concentration is proved to be a determinant factor for the stem cell differentiation, it would be interesting to monitor *in vivo* the punctual values of this parameters the time evolution during the vasculature formation or the cellular metabolism.

5.1.2 Synthesis and characterization of injectable hyaluronic acid-photoinitiator conjugate hydrogel for biomedical application

The importance of hyaluronic acid (HA), a glycosaminoglycan ubiquitous in all tissue, has been shown in various biological processes (West DC and S. 1989; Chen and Abatangelo 1999; Gerecht, Burdick et al. 2007). At the same time, the research on tissue engineering and drug delivery has been recently focused on a class of biomaterials, hydrogels, for their excellent physical-chemical and mechanical properties which are very similar to soft tissues (Anseth, Bowman et al. 1996; Hoffman 2002; Burdick, Chung et al. 2005; Biancamaria 2007; Fedorovich, Alblas et al. 2007). The possibility of promoting the neovascolarization of the ischemic tissue through the integration of natural biomaterials used as drug or cell carrier seem promising for the development of stem cell based clinical therapy (Christman, Fang et al. 2005; Silva and Mooney 2007).

Photopolymerization has several advantages over conventional polymerization techniques, such as increased spatial and temporal control over crosslinking, fast curing rates and injection of fluid-like biomaterial at physiological temperatures (Anseth and Burdick 2002; Nguyen and West 2002). Moreover, a main advantage of photopolymerization is that hydrogels can be created *in situ* in a minimally invasive manner (Biancamaria 2006; Tessmar and Gopferich 2007). Ultraviolet (UV) light can

be used to initiate and propagate the hydrogel polimerization, and it is important to how UV lamp properties affect the hydrogel characteristics.

The aim of this work was to develop a new injectable hydrogel, HYAFF120, based on HA derivatives. The formulation was obtained by esterification of HA with photoinitiator, thus the resulting solution was designed to polymerize under UV exposure. Different concentration of photocrosslinked hydrogel were physico-chemically characterized, calculating the elastic and viscous modulus, the swelling ratio and the degradation rate. In this analysis particular attention was focused on the effect of polymer concentration and UV exposure time.

In order to achieve a better understanding of stability of the hydrogel for a future *in vivo* application, the mechanical properties were investigate by rheological analysis using polymeric solution before UV exposure and after UV curing.

When a viscoelastic material is subjected to a sinusoidal varying stress, the resulting strain is also sinusoidal having the same angular frequency but retarded in phase by an angle δ (Bogdanov, Schacht et al. 1997; Calvet, Wong et al. 2004). The strain γ and stress τ functions can be written as

$$\gamma = \gamma_o \cdot \sin(\omega t) \tag{5.1}$$

$$\tau = \tau_0 \cdot \sin(\omega t + \delta) \tag{5.2}$$

where ω is the angle rate and γ_0 and τ_0 are respectively the maximum strain and stress amplitude. These two parameters are set up at the beginning of the experiment. Writing the stress function as a complex quantity τ^* whose real part τ'_0 is in phase with the strain and whose imaginary part τ''_0 is 90° out of phase with it:

$$\tau^* = \tau'_0 \cos \omega t + i \tau''_0 \sin \omega t \tag{5.3}$$

We can use this complex form of the stress function to define two different dynamic moduli, both being ratios of stress to strain as usual but having very different molecular interpretations and macroscopic consequences. The first of these is the "real," or elastic modulus G', defined as the ratio of the in-phase stress τ' to the strain $\gamma_0.$ The other is the "imaginary," or viscous modulus G'', defined as the ratio of the out-of-phase stress to the strain.

Furthermore, we investigated the effect of UV exposure on HL1 cell line viability and the possibility of using this material drug or cell carrier supporting the cell proliferation and growth. The full description of material, methods and results is reported in Appendix F. In the following part we summarize briefly the methods used to monitor the reaction of HYAFF120 production and the optimized methodology to perform the gel injection in the heart tissue, which are not included in the paper.

Results and discussion

The reaction of HYAFF 120 production was followed by HPLC (Perkin Helmer, column Nucleosil C18) analysis of 2 mL of solution, which were withdrawn at different times from the volume of reaction. Figure 2 shows the concentration profiles of reactant and product as function of time. These values change over time up to the reaching of a *plateau* in about 25-30 hours.

In order to evaluate the adhesion of material to the surface of the heart and feasibility of crosslinking through cardiac tissue, some solutions Hyaff120 ® were prepared at concentrations of 10, 20, 30, 40 and 50 mg/mL and 100 μL of each solution were
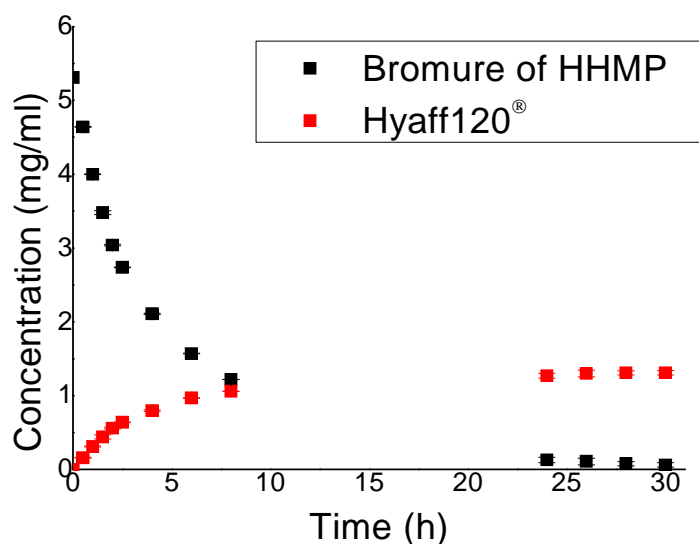

Figure 2 *HYAFF 120 syntesis. Concentration profiles of reactant (Bromure of HHMP) and product (HYAFF120) as function of time.*

deposited on the heart surface and exposed for 10 sec at 2 cm of distance. The results show a significant adherence of solution with concentrations greater than 40 mg/mL.

Since the light is totally absorbed by the tissue, the precursor solution was pre-polymerized in the syringe by 3 sec UV exposure. The hydrogel is then injected in the heart at the desired depth, other three seconds of light exposure (2 cm distant) avoids any possible leakage of not reticulated hydrogel, which forms an adherent clot in the needle hole.
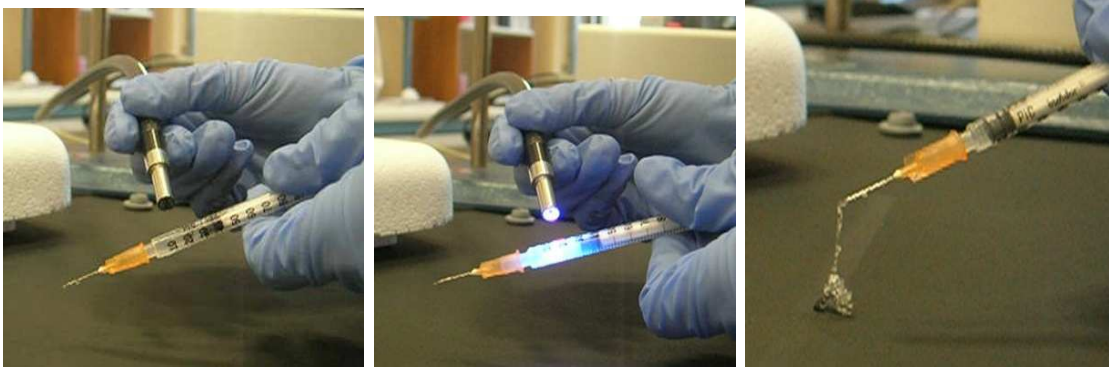
(A)
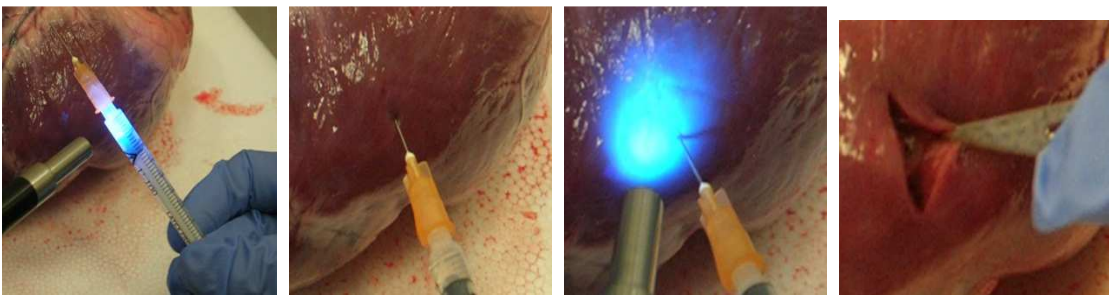
(B)

Figure 3 *Ex vivo test of viability for HYAFF 120 hydrogel injection A) Pre-fotopolymerization in the syringe. After only 3 sec of UV exposure the hydrogel has a more compact appearance B) Injection of HYAFF 120 in the heart*

Conclusions

This study present the development of a new photo-polymerizable hydrogel formulation based on hyaluronic acid derivative, HYAFF120®. Physical/chemical characterization of the Hyaff120® solutions and the Hyaff120® hydrogels have been performed for different polymer concentrations and exposure times. The results, described in detail in the Appendix F, show the gradual enhancing of structural parameters up to the reaching of a plateau. From a clinical perspective, the reaching of a plateau on these values is technically important because it disconnect the hydrogel physico-chemical properties by the in vivo conditions during the polymerization. This characteristic behavior, combined

with the feasibility of polymerization in vivo with a small UV light dose, make this material a good candidate for *in vivo* application as drug or cells carrier. From the engineering perspective it would be interesting to model the delivery of specific drug included in the hydrogel during the polymerization process.

5.2 References

Anseth, K. S., C. N. Bowman, et al. (1996). "Mechanical properties of hydrogels and their experimental determination." Biomaterials **17**(17): 1647-1657.

Anseth, K. S. and J. A. Burdick (2002). " New directions in photopolymerizable biomaterials." MRS Bulletin. **27**(2): 130-136.

Biancamaria, B. (2006). "Photopolymerization of biomaterials: issues and potentialities in drug delivery, tissue engineering, and cell encapsulation applications." Journal of Chemical Technology & Biotechnology **81**(4): 491-499.

Biancamaria, B. (2007). "Hydrogels for tissue engineering and delivery of tissue-inducing substances." Journal of Pharmaceutical Sciences **96**(9): 2197-2223.

Bogdanov, B., E. Schacht, et al. (1997). "Thermal and rheological properties of gelatin-dextran hydrogels." Journal of Thermal Analysis and Calorimetry **49**(2): 847-856.

Burdick, J. A., C. Chung, et al. (2005). "Controlled Degradation and Mechanical Behavior of Photopolymerized Hyaluronic Acid Networks." Biomacromolecules **6**(1): 386-391.

Callegari, A., S. Bollini, et al. (2007). "Neovascularization induced by porous collagen scaffold implanted on intact and cryoinjured rat hearts." Biomaterials **28**(36): 5449-5461.

Calvet, D., J. Y. Wong, et al. (2004). "Rheological Monitoring of Polyacrylamide Gelation: Importance of Cross-Link Density and Temperature." Macromolecules **37**(20): 7762-7771.

Chen, W. Y. J. and G. Abatangelo (1999). "Functions of hyaluronan in wound repair." Wound Repair and Regeneration **7**(2): 79-89.

Christman, K. L., Q. Fang, et al. (2005). "Enhanced neovasculature formation in ischemic myocardium following delivery of pleiotrophin plasmid in a biopolymer." Biomaterials **26**(10): 1139-1144.

Fedorovich, N. E., J. Alblas, et al. (2007). "Hydrogels as Extracellular Matrices for Skeletal Tissue Engineering: State-of-the-Art and Novel Application in Organ Printing." Tissue Engineering **13**(8): 1905-1925.

Gage, F. H. (1998). "Cell therapy." Nature **392**(6679): 18-24.

Gerecht, S., J. A. Burdick, et al. (2007). "Hyaluronic acid hydrogel for controlled self-renewal and differentiation of human embryonic stem cells." Proceedings of the National Academy of Sciences **104**(27): 11298-11303.

Gu Y, Yu J, et al. (2007). " Tissue engineering and stem cell therapy for myocardial repair." Front Biosci. **12**: 5157-65.

Hoffman, A. S. (2002). "Hydrogels for biomedical applications." Advanced Drug Delivery Reviews **54**(1): 3-12.

Kofidis T, Müller-Stahl K, et al. (2007). "Myocardial restoration and tissue engineering of heart structures." Methods Mol Med(140): 273-90.

Nguyen, K. T. and J. L. West (2002). "Photopolymerizable hydrogels for tissue engineering applications." Biomaterials **23**(22): 4307-4314.

Radisic, M., H. Park, et al. (2004). "From the Cover: Functional assembly of engineered myocardium by electrical stimulation of cardiac myocytes cultured on scaffolds." Proceedings of the National Academy of Sciences **101**(52): 18129-18134.

Semsarian, C. (2002). "Stem cells in cardiovascular disease: from cell biology to clinical therapy." Internal Medicine Journal **32**(5-6): 259-265.

Silva, E. A. and D. J. Mooney (2007). "Spatiotemporal control of vascular endothelial growth factor delivery from injectable hydrogels enhances angiogenesis." Journal of Thrombosis and Haemostasis **5**(3): 590-598.

Tessmar, J. K. and A. M. Gopferich (2007). "Matrices and scaffolds for protein delivery in tissue engineering." Advanced Drug Delivery Reviews **59**(4-5): 274-291.

West DC and K. S. (1989). "The effect of hyaluronate and its oligosaccharides on endothelial cell proliferation and monolayer integrity." Exp Cell Res **183**(1): 179-96.

Chapter 6

Conclusions

The social and economical impact of cardiac disease on the western world motivated the research of new therapies alternative to heart transplantation surgery. Cardiac tissue engineering aims to address this objective and the propose of this PhD study was to handle, by an engineering point of view, some of the technological issues related to this research field.

Despite of promising progress in this direction, four relevant limitations can be still identified by a critical analysis of the state of the art, defining specifically a lack of: 1) information and quantitative knowledge on the critical phenomena of the biological system, such as cellular differentiation or organization in the 3D template; 2) technology to get accurate and repeatable control on experimental conditions at the large scale; 3) advanced methodology and technology to address an accurate analysis of the cellular and tissue functionality; 4) non invasive methodology to meet the clinical requirements for *in vivo* cardiac regeneration.

This thesis work was guided by a coherent and rational approach to the cardiac tissue engineering, explicated by the design and development of innovative systems and technical methods, leading to a more rational progress of the research. Within the general issues that belong to cardiac tissue engineering, we focused on fundamental aspects related to *in vitro* production and analysis of a functional tissue: the development of technology to control the differentiation (Chapter 2), the production and physiological evaluation at cell (Chapter 3) and tissue level (Chapter 4) and the definition of the feasibility of clinical approaches for the cardiac tissue in vivo regeneration by stem cell delivery (Chapter 5).

Regarding to the process of stem cell differentiation, we identified the need of high-throughput technology, in order to study simultaneously different conditions and individuate interactions between several factors, reducing time and money consumption for our research. The lack of such technology was one of the main limitation of a work developed with AFS cells and cardiomyocytes co-culture on micro-grooved PDMS membranes. Despite of the promising results on cell organization, interaction and differentiation, we were not able to individuate a optimal condition which would give a high yields of contractile cells for cardiac applications as cell source.

 From a biological and clinical point of view, more interesting results have been obtained through the electrical stimulation of hESCs, which shows contractile properties after few days of cultures. With a proper designed bioreactor, we studied the effect of different electrode materials on the biological response after the stimulation.

However, cell differentiation is only the first step towards a functional tissue production. The evaluation of the engineered tissue quality requires analysis of functionality at the cell and tissue level, especially in the perspective of considering the contractile response as discriminatory parameter during innovative drug screening investigation. Biology does not often meet this need of knowledge of systems, describing the intracellular kinetic by a qualitative point of view without any sensitivity on characteristic time and length scale of the process.

In this thesis, we tested the hypotheses of using an intracellular molecular probes as tool for quantitative analysis of cellular physiology. In this sense, a kinetic-diffusive mathematical model was developed to describe the spatio-temporal evolution of the cAMP. It is useful to emphasize here the importance of cAMP as intermediates for cardiac function evaluation and for the investigation of the physio-pathology of myocardial and the response to drug therapies. The obtained results are very promising because they quantitatively reproduce the experimental data from literature and give a rational explanation to biological evidences. We strongly believe that a rational approach to the molecular biology through mathematical modeling are relevant for the design of experiments and development of new pharmaceutical principle for cardiac related diseases.

The main limitation of this approach is given by the possibility of performing only a single cell observation, which may not be representative of the entire tissue. A better testing

sample in this sense could be given by a three-dimensional tissue, which better reproduces the complex interactions between cardiac cells. Since the literature evidences the importance of the electrical stimulation on the organization of a functional tissue, we focused on the definition of a standard method for the *in vitro* cardiac tissue fabrication. The results show the importance of a deep characterization of the system in order to perform an efficient electrophysiological stimulation, and they suggested the possibility of integrating this knowledge with another important aspect of tissue fabrication, such as the design of a perfusion bioreactor.

The fabrication of an engineered functional tissue moved the interest on the development of methods for a tissue functional evaluation, which was performed in two ways through: 1) the functional measure of contractile strength and 2) the evaluation of area variation amplitude due to contraction. The developed sensors were both designed for the analysis of small tissue samples.

The measurement of the force amplitude associated with the tissue is considered the most important and complete parameter to define the tissue functionality. However, relevant technical difficulties were faced related to the use of small and fragile force transducer, which need to be coupled with the cardiac tissue assuring the sterility in the system. The second approach is more simple because it is based on existing optical technologies, which were adapted to follow the patch contraction. However, it gives incomplete information about the contraction, measuring the variation of a flat two-dimensional volume without a precise knowledge of mechanical resistance given by the scaffold. The main advantage of this technique is given by the possibility of analyzingthe sensor without requiring any contact of the sensor with the sample. This techniques is suitable for functional testing which aims to detect and monitoring contraction frequency rather than the contraction strength or amplitude. What was presented so far suits perfectly with the objectives of developing an *in vitro* artificial tissue to be used as model in the pharmacological research for drug development and drug screening processes. On the other hand, in a clinical perspective, it would be critical to develop biomaterials for an efficient delivery of stem cells in the ischemic region. This propose can be assessed by the use of a scaffold as cell reservoir or of a hydrogel as cell carrier within the muscle. Despite of the promising results on neo-vascularization process promoted by the implant of a collagen scaffold on the

external wall of the ischemic muscle, the hydrogel injection seems particularly interesting because it requires a less invasive surgery procedure. This research was supported by the interest and the important contribution of a well known Italian biomaterials company (Fidia Advanced Biopolymer, FAB, Abano Terme, Italy). The contribution of this thesis work was on the chemical-physical characterization and *in vitro* biocompatibility of a new photocrosslinkable hydrogel.

Looking at these results, because of the high complexity of a biological system, the definition of advanced technologies for the chemical and physical control of system is imperative to speed up the innovation in this area. These results exemplify the possible active role of chemical engineering on the design and development of new tools to support the biological and biomedical research. The main outcomes of this thesis work represent a well-recognized progress on cardiac tissue engineering.

Appendix A

Micro-grooved Silicone Membrane for *In Vitro* Co-culture of Human Amniotic Fluid Stem Cell and cardiomyocytes

Elisa Figallo[1], Sveva Bollini[2], Elisa Bertacco[2], Paolo De Coppi[2], Nicola Elvassore[1§]

[1] Department of Chemical Engineering, University of Padova, Italy

[2] Department of Biomedical Sciences, University of Padova, Italy.

[§] Corresponding authors

Abstract

It has been previously demonstrated that Amniotic Fluid Stem (AFS) Cells could represent a new source for cellular therapy applications. AFS are a subpopulation of amniotic fluid cells isolated by immunosorting for the expression of c-kit antigen. Stem cell differentiation seems to be affected by several factors, related to cell-cell interaction, including matrix topography and rigidity.

In this sense, the aim of the present study was to design an easy and reproducible method to provide topographical stimulation in the micrometrical range and promote in this way the cardiomyocyte alignment. The system was designed to obtain cell pattern monolayer that allows the identification of each individual cell with common optical method of analysis.

Elastic and highly gas-permeable micro-grooved silicone membrane were fabricated, with straight grooves of 17±9 μm width. This experimental set up was useful to verify the synergic effects, on stem cell differentiation toward cardiac lineage, of chemical and mechanical stimulation, due to rCM and human AFS interaction during coculture.

The resulting cardiomyocyte patterns on silicone membrane keep a more synchronous functionality up to 15 days of culture, while this is not visible on polystyrene dishes. Cell metabolism on the silicone membrane was compared to traditional culture on polystyrene dish. Cells were analyzed by immunofluorescence for cardiac markers such as the sarcomeric protein troponin I after 6 and 10 days of culture. Experimental results reveal that tissue engineering approaches using 2D microtextured membranes improve both rCM and AFS alignment and co-culture organization after seeding. The results show an improvement of human AFS differentiation toward cardiac lineage.

A.1 Introduction

Stem cells therapy has been investigated as a novel approach in regenerative medicine for the treatment of degenerative diseases such as myocardial infarction, diabetic mellitus, Parkinson's diseases and skeletal myopathies using several types of stem cells obtained from embryonic or adult tissues (Strauer and Kornowski 2003; Ariff Bongso and Richards 2004; Davani, Deschaseaux et al. 2005). In this perspective the stem cell differentiation process has become one of the most challenging field in cell biology. Amniotic fluid is known to contain multiple cell types derived from the developing fetus. In the past, the cells, which populate the amniotic fluid, were only used for prenatal diagnosis. We have recently described for the first time that it is possible to derive lines of broadly multipotent cells from the amniotic fluid stem cells (AFS cells). These cells meet a commonly accepted criterion for pluripotent stem cells, without implying that they can generate every adult tissue (De Coppi, Bartsch et al. 2007).

Functional properties of contractile tissues, such as myocardium, have been proved to be directly related to the cellular orientation and elongation. Furthermore, many studies have been done on cardiac regenerative medicine showing that stem cells can differentiate *in vitro* and *in vivo* into cardiomyocytes (Mathur and Martin 2004). Concerning to that, different methods have been evaluated, including the use of the metilating agent 5-azacytidine (Fukuda 2003), the employment of cardiomyocyte conditioned media (Rangappa, Fen et al. 2003), of growth, soluble factors and cytokines enriched media (Takahashi, Lord et al. 2003) and, finally, the direct interaction with cardiomyocytes by co-culture (Condorelli, Borello et al. 2001; Mummery, Ward-van Oostwaard et al. 2003; Muller-Borer, Cascio et al. 2004; Nishiyama, Miyoshi et al. 2007). The main advantage of the co-cultivation systems resides in the possibility of reproduce at micro scale the interaction between the two cellular types, which likely stimulate some cellular transduction processes influencing environment molecular signs. Various studies have demonstrated that close contact of two cellular populations is necessary to obtain differentiation in cardiac cells. In particular, recent studies have demonstrated that direct cell-to-cell contact is one of the most important microenvironment factors for trans-differentiation of stem cells by co-colture (Badorff, Brandes et al. 2003; Iijima, Nagai et al. 2003; Rangappa, Entwistle et al. 2003; Xu, Wani et al. 2004; Wang, Xu et al. 2006). Moreover, regarding the tissue engineering

approaches on in vitro cardiac differentiation. The aim of this study was to create in vitro a suitable environment for the AFS-rat neonatal cardiomyocytes co-culture in order to promote the cell organization and alignment.

Literature has demonstrated that monolayer cultures of cardiomyocytes can recapitulate morphologic features of mature ventricular tissue when cultured on microcontact-printed protein patterns. Different methods have been recently described to achieve the cardiomyocyte spatial organization and alignment. In particular soft-lithographic methods and micro-contact printing approach has been proposed to create a micro-patterned supports to spatially organized layers of cardiomyocytes (Todd C. McDevitt, Angello et al. 2002; Todd C. McDevitt, Woodhouse et al. 2003). All these techniques guarantee the precise and micrometrical reproduction of the selected design; however stamp deformation and hydrogel degradation often produce undesirable effects that limit the practice and precision of these techniques. A simple method to drive elongation and organization of cardiomyocytes have been proposed by employment of abraded surface, such as glass or polystyrene, as cell seeding support (Au, Cheng et al. 2007).

In this perspective we describe here a new in vitro method to produce a silicon micro-grooved silicone membrane protocol for structuring cardiac cell cultures. The micro-grooved membranes presented here could be easily suitable as cell culture growth substrate for specific studies that require the application of mechanical stretch or the culture in controlled oxygen concentration.

In this work we analyzed first biocompatibility and the viability of the rCM on the silicone membrane, investigating the cell metabolism up to 6 days of culture. The effect of topographical stimuli of this scaffold was studied on *in vitro* differentiation toward cardiac lineage of GFP-positive rCM (gfp+ rCM) and hAFS co-culture. In this paper we focused on the engineered aspects of the work, whereas the biological significance of this research is reported elsewhere (Sveva Bollini, PhD dissertation).

A.2 Materials and Methods

rCM isolation

GFP-positive rCM (gfp+ rCM) were obtained by enzymatic digestion of 2-3-days old wild type and GFP-positive transgenic Sprague Dawley pup hearts according to Radisic et al. 2004 (Radisic, Park et al. 2004). Briefly hearts were taken by torachotomy, washed in ice cold HBSS buffer, quartered in pieces and digested by an overnight incubation at 4°C with a trypsin (Gibco) solution 0.6 mg/ml in HBBS. The tissue fragments were then processed by several round of digestion at 37°C for 4 minutes in a collagenase Type II solution (Worthington) 1 mg/mL in HBBS. Cells were collected by centrifugation at 1000 rpm for 5 minutes and then non-cardiomyocytes where discarded as the adherent fraction by 1 hour of pre-plating on tissue culture dishes. rCM were then seeded on gelatine and fibronectin coated plastic dishes or on silicone membranes at 100.000 cells/cm^2 in Cardiac Growth Medium (CGM, DMEM high glucose with L-glutamine medium modified with 10% FBS, 1% Hepes Buffer, 1% Penicillin/Streptomycin, all Gibco).

AFS isolation

Human AFS (hAFS) were obtained from healthy discarded back up amniotic fluid samples between 12 and 20th week of gestation, for prenatal diagnosis following informed consent as reported by De Coppi et al. 2007 (De Coppi, Bartsch et al. 2007). AFS were isolated by immunosorting for the stem marker ckit and cultured at 70% confluency on plastic dishes (MEMα Medium modified with 15% FBS, 1% L-glutamine, 1% Penicillin/Streptomycin, from Gibco and 20% Chang B®, 2% Chang C®, Irvine Scientific).

Micro-grooved silicone membrane

Micro-grooved silicone membranes were prepared using polycarbonate cubes, 20 mm high, abraded in one direction using lapping paper with abrasion grain sizes of 80 μm. The mold, with the rough side down, was pressed in the centre of 35 mm well, filled with 3ml of poly(dimethylsiloxane) (PDMS, Sylgard 184 Silicone Elastomer, Ellsworth Adhesives, Germantown, WA). The mold was removed after silicone cross-linking and the frame/membrane device was sterilized in autoclave for 20 min. In order to enhance

cell attachment, the silicone surfaces were incubated at 37°C overnight with 25 mg of fibronectin (Sigma Aldrich) in 2 mL of 0.02% gelatin (Sigma Aldrich) in water. The observation of the membrane at the microscope allowed a rough measure of the groove width.

Cell culture on silicone membrane

Neonatal rat cardiomyocyte (rCM) were seeded on microtextured gelatin and fibronectin-coated silicone membrane at 100.000 cells/cm^2 and analyzed after 6 and 10 days of in vitro culture in Cardiac Growth Medium. Human AFS and gfp positive neonatal rat cardiomyocyte were seeded together on gelatin and fibronectin-coated microgrooved silicone membranes in 6-well dishes at respectively 100.000 and 1000 or 4000 cells/cm^2 density in CGM. As control culture gfp+rCM and hAFS were seeded together on gelatin and fibronectin-coated standard 6-well plastic dishes.

Uptake of 2-deoxyglucose

Uptake of 2-deoxy-[3H]glucose was measured in cells after an overnight serum free medium.Cells were then incubated for an additional hour in the absence or presence of insulin (2 UM). Glucose uptake was determined by 15 min incubations at 37° C with 2-deoxy-[3H]glucose (10 UM) in PBS containing (in mM) 0.1 CaCl2, 0.1 MgCl2, and 10 HEPES, pH = 7.4 .

Uptake was terminated by three rapid washes with ice-cold PBS.

The cell associated radioactivity was determined by solubilization in 0.5 M NaOH. Aliquots of the cell extracts were counted by liquid scintillation counting and used to determine protein concentration.

Immunostaining

rCm seeded on silicone membranes were analyzed by immunofluorescence after 6 and 12 days for the expression of the structural sarcomeric protein troponin T, rCm cocultured with AFS were analyzed after 6 and 12 days of culture for the expression of both troponin T and GFP.

Immunostaining analysis on rCM co-cultured with AFS was made both on cells seeded on silicone membrane and on cellular spots (cytospins) obtained from cells detached

from silicone membranes by trypsinization and then centrifugated on glass coverslips in a Shandon cytocentrifuge at 400 rpm for 5 minutes.

Briefly, cells seeded on silicone membranes and cellular spots were fixed in PFA 4% for 5 minute at room temperature, permeabilized with 0,1% Triton/PBS solution and incubated at 37°C for 25 minutes with the appropriate dilution of the primary antibody in PBS+1% bovine serum albumin (Gibco and Sigma). In order to recognize the cardiac differentiated, we used rabbit polyclonal anti-Cardiac Troponin T (Abcam, rabbit IgG 1:500). Human cells were marked by mouse monoclonal Ab NMF6, which was a kind gift from Dr Saverio Sartore (Department of Biomedical Sciences, University of Padua, Italy). Cells were then re-incubated at 37°C for 25 minutes with the appropriate dilution of the secondary antibody (goat anti-mouse IgG coniugated with Alexa Fluorescence 564 IgG 1:150, Molecular Probes; goat anti-rabbit coniugated with Alexa Fluorescence 488 IgG 1:150, Molecular Probes). PBS+1% bovine serum albumin with human and rat serum (1:100). Cells nuclei were stained with a Hoescht solution diluited 1:5000 in PBS 1X for 5 minutes at room temperature. Observations were made using a Zeiss Axioplan epifluorescence microscope (Zeiss, Oberkochen, Germany), a Leica TCS SP5 confocal microscope and images were obtained using a Leica DC300F digital videocamera. Optical images were acquired by a Leica DMR microscope connected to a Leica DC300 videocamera.

A.3 Results and Discussion

Micro-grooved silicone membrane, of 50 μm thickness and 20x20 mm area, were prepared abrading the bottom surface of polycarbonate mold with a lapping paper. The membrane is surrounded by a PDMS frame, which fits perfectly in the traditional polystyrene multiwell with diameter 3.5cm (Figure 1A). Microscopic analysis of the surface shows abrasions with a preferential direction and straight grooves (Figure 1B). The distribution of groove width is reported in Figure 1C and show an average dimension of 17±9 μm. Although the surface was significantly less uniform than those obtained by microfabrication techniques, the method presented here combine simplicity in the realization and replication of the pattern.
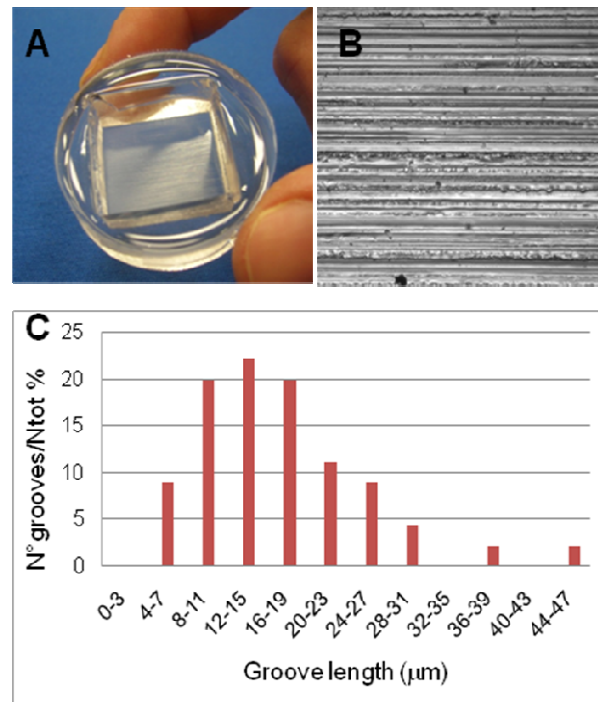
Figure 1 *Micro-grooved silicone membrane. (**A***) Actual picture of the PDMS frame-membrane micro-grooved well. (**B***) Bright field images of the membrane surface (10x magnification). (**C***) Distribution of groove width.*

Due to their high diffusivity (D oxygen= $3.55 \text{cm}^2/\text{s}$) and elastic modulus (Young's module = 750 kPa) of PDMS, these membranes could be used as cell culture growth substrate for specific studies that require the application of mechanical stretch or the culture in controlled oxygen concentration. Moreover the pattern remains stable during the culture, important feature for stem cell differentiation studies, which usually last for long time.

We analyzed the viability and the biocompatibility of the scaffold on the cardiomyocyte culture alone to obtain a more spatially organized *in vitro* culture. The rCm seeded on the 2D silicone membrane express synchronous beating activity up to 15 days of culture. The glucose uptake measured after 6 days of culture showed values comparable with those measured on Petri polystyrene dish culture (Figure 2B). This demonstrates the feasibility of this support as rCm culture.
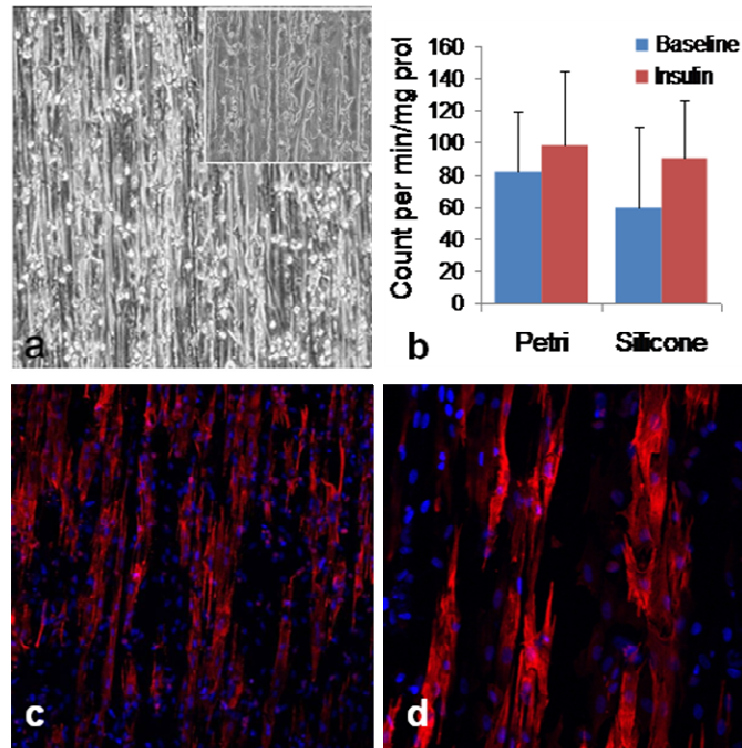
Figure 2 *rCM seeded on 2D microtextured silicone membrane. (**a**): rCM on silicone scaffold, bright field, magnification 200X; inlet 400X; (**c**) and (**d**): immunostaining at 6 days of culture for cardiac troponin T in red revealing aligned rCM, magnification respectively 200X and 400X. (**b**) Comparison between the glucose uptake measured after 6 days of culture on the microgrooved membrane and Petri polystyrene dish culture.*

The *in vitro* results reveal that the topographical cue of the silicone membrane determines the cell alignment with a well defined spatial organization in the direction of the membrane grooves. This is particularly evident with the microscopic observation of the troponin T distribution on the surface. To evaluate our model and to analyze the topological influence of the scaffold on stem cell differentiation. AFS were found growing closely related to rCM on the silicone membrane, following the longitudinal orientation given by the micropattern and, moreover, some stem cells seemed to express a beating activity too. These results suggest that our microtextured silicone surface model can be a good approach to get a better defined spatial organization and orientation of the co-culture in vitro and to improve the mechanical stretch and all the physical and chemical stimulation of cardiomyocytes on the surrounding AFS in respect of the standard conditions using plastic culture dishes.

Thusing 2D scaffold can improve both rCM and AFS seeding and alignment. In particular 2D silicone micro-patterned membrane allows to get a well defined and better cellular organization in *in vitro* co-culture.
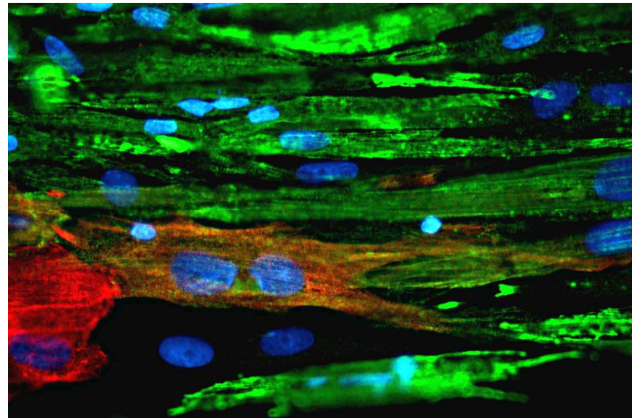
Figure 3 *rCM and hAFS (4000 cells/cm² density) co-cultured on 2D silicone micro-grooved membrane at 6 days. Fluorescence imaging of immunostaining for cardiac troponin T (green) and Ab NMF6 (red), magnification 40X.*

Immunostaining analysis after 6 days of hAFS-rCM co-culture on the 2D micro-grooved membrane (4000 cells/cm^2) revealed the 22.5± 5,7 % of hAFS positive for the expression of the cardiomyocyte marker Troponin T (Figure 3).
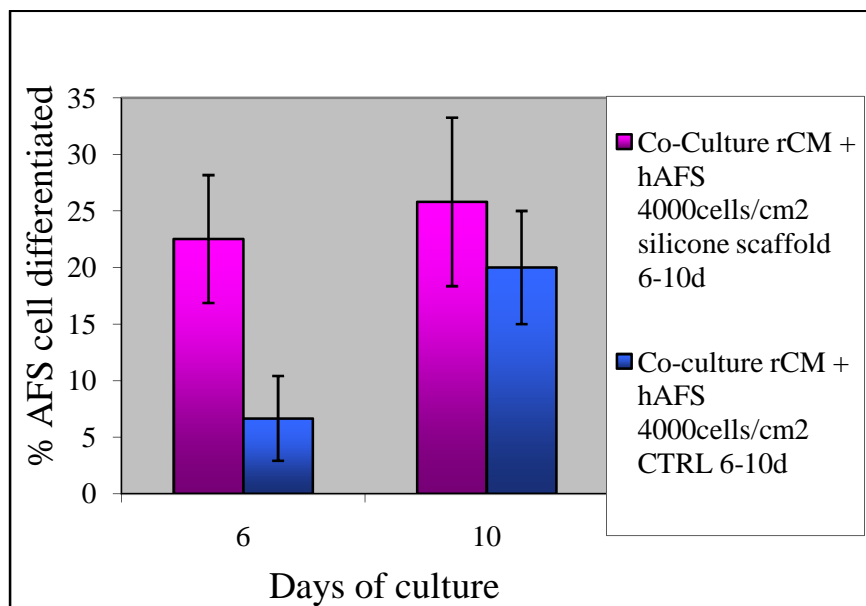
Figure 4 *Percentage of differentiation (troponin expression) of hAFS cells at 6 and 12 days of co-culture. Comparison of the biological response after culture in traditional Petri dish or micro-grooved membrane.*

After 12 days hAFS positive for troponin T were 25.8 ± 7.5% when cultured on microgrooved membrane. In the control co-culture, seeded on standard Petri dishes, the troponin T-positive hAFS were 6,7 ± 3,7 % after 6 days ,whereas the percentage increase to 20,0 ± 5,0 % after 12 days (Figure 4). The effect of a cell alignment and interaction seems more relevant during the early stage of AFS differentiation.

Conclusions

2D scaffold improved both rCM and AFS seeding and orientation in vitro allowing to get a better spatial organization of the AFS co-colture in vitro than on the plastic dishes. Some hAFS expressing the cardiac marker troponin T and a "cardiomyocyte-like" phenotype were also found in co-culture whit rCM on 2D silicone membrane.

These findings suggest that the well defined spatial organization supported by this scaffold also allows to get a better AFS differentiation by co-culture improving the close relation between the two cellular population and their direct intercellular crosstalk and interaction.

A.4 References

Ariff Bongso and M. Richards (2004). "History and perspective of stem cell research." Best Pract Res Clin Obstet Gynaecol **18**(6): 827-42.

Au, H. T. H., I. Cheng, et al. (2007). "Interactive effects of surface topography and pulsatile electrical field stimulation on orientation and elongation of fibroblasts and cardiomyocytes." Biomaterials **28**(29): 4277-4293.

Badorff, C., R. P. Brandes, et al. (2003). "Transdifferentiation of Blood-Derived Human Adult Endothelial Progenitor Cells Into Functionally Active Cardiomyocytes." Circulation: 01.CIR.0000051460.85800.BB.

Condorelli, G., U. Borello, et al. (2001). "Cardiomyocytes induce endothelial cells to trans-differentiate into cardiac muscle: Implications for myocardium regeneration." Proceedings of the National Academy of Sciences: 191217898.

Davani, S., F. Deschaseaux, et al. (2005). "Can stem cells mend a broken heart?" Cardiovascular Research **65**(2): 305-316.

De Coppi, P., G. Bartsch, et al. (2007). "Isolation of amniotic stem cell lines with potential for therapy." Nat Biotech **25**(1): 100-106.

Fukuda, K. (2003). "Regeneration of cardiomyocytes from bone marrow: Use of mesenchymal stem cell for cardiovascular tissue engineering." Cytotechnology **41**(2): 165-175.

Iijima, Y., T. Nagai, et al. (2003). "Beating is necessary for transdifferentiation of skeletal muscle-derived cells into cardiomyocytes." FASEB J.: 02-1048fje.

Mathur, A. and J. F. Martin (2004). "Stem cells and repair of the heart." The Lancet **364**(9429): 183-192.

Muller-Borer, B. J., W. E. Cascio, et al. (2004). "Adult-Derived Liver Stem Cells Acquire a Cardiomyocyte Structural and Functional Phenotype ex Vivo." Am J Pathol **165**(1): 135-145.

Mummery, C., D. Ward-van Oostwaard, et al. (2003). "Differentiation of Human Embryonic Stem Cells to Cardiomyocytes: Role of Coculture With Visceral Endoderm-Like Cells." Circulation **107**(21): 2733-2740.

Nishiyama, N., S. Miyoshi, et al. (2007). "The Significant Cardiomyogenic Potential of Human Umbilical Cord Blood-Derived Mesenchymal Stem Cells In Vitro." Stem Cells **25**(8): 2017-2024.

Radisic, M., H. Park, et al. (2004). "From the Cover: Functional assembly of engineered myocardium by electrical stimulation of cardiac myocytes cultured on scaffolds." Proceedings of the National Academy of Sciences **101**(52): 18129-18134.

Rangappa, S., J. W. C. Entwistle, et al. (2003). "Cardiomyocyte-mediated contact programs human mesenchymal stem cells to express cardiogenic phenotype." J Thorac Cardiovasc Surg **126**(1): 124-132.

Rangappa, S., C. Fen, et al. (2003). "Transformation of adult mesenchymal stem cells isolated from the fatty tissue into cardiomyocytes." Ann Thorac Surg **75**(3): 775-779.

Strauer, B. E. and R. Kornowski (2003). "Stem Cell Therapy in Perspective." Circulation **107**(7): 929-934.

Takahashi, T., B. Lord, et al. (2003). "Ascorbic Acid Enhances Differentiation of Embryonic Stem Cells Into Cardiac Myocytes." Circulation **107**(14): 1912-1916.

Todd C. McDevitt, J. C. Angello, et al. (2002). "*In vitro* generation of differentiated cardiac myofibers on micropatterned laminin surfaces." <u>Journal of Biomedical Materials Research</u> **60**(3): 472-479.

Todd C. McDevitt, K. A. Woodhouse, et al. (2003). "Spatially organized layers of cardiomyocytes on biodegradable polyurethane films for myocardial repair." <u>Journal of Biomedical Materials Research Part A</u> **66A**(3): 586-595.

Wang, T., Z. Xu, et al. (2006). "Cell-to-cell contact induces mesenchymal stem cell to differentiate into cardiomyocyte and smooth muscle cell." <u>International Journal of Cardiology</u> **109**(1): 74-81.

Xu, M., M. Wani, et al. (2004). "Differentiation of Bone Marrow Stromal Cells Into the Cardiac Phenotype Requires Intercellular Communication With Myocytes." <u>Circulation</u> **110**(17): 2658-2665.

Appendix B

Micro Bioreactor Array for controlling cellular microenvironments

Elisa Figallo,[a,¶] **Christopher Cannizzaro,**[b,¶] **Sharon Gerecht,**[b,¶] **Jason A. Burdick,**[c] **Robert Langer,**[b] **Nicola Elvassore,**[a,§] **and Gordana Vunjak-Novakovic,**[d,§]

[a] Department of Chemical Engineering, University of Padova, Italy

E-mail: nicola.elvassore@unipd.it

[b] Harvard – MIT for Health Sciences and Technology, Massachusetts Institute of Technology, Cambridge MA

[c] Department of Bioengineering, University of Pennsylvania, Philadelphia, PA 19104

[d] Department of Biomedical Engineering, Columbia University, 1210 Amsterdam Avenue, MC 8904, New York NY 10027

E-mail: gv2131@columbia.edu

[¶] Equally contributing authors; [§] Corresponding authors

Abstract

High throughput experiments can be used to spatially and temporally investigate the many factors that regulate cell differentiation. We have developed a Micro Bioreactor Array (MBA) that is fabricated using soft lithography and contains twelve independent micro-bioreactors perfused with culture medium. The MBA enables cultivation of cells that are either attached to substrates or encapsulated in hydrogels, at variable levels of hydrodynamic shear, and with automated image analysis of the expression of cell differentiation markers. The flow and mass transport in the MBA were characterized by computational fluid dynamic (CFD) modeling. The representative MBA configurations were validated using the C2C12 cell line, primary rat cardiac myocytes and hESCs (lines H09 and H13). To illustrate the utility of the MBA for controlled studies of hESCs, we established correlations between the expression of smooth muscle actin and cell density for three different flow configurations.

B.1 Introduction

Cellular microenvironment, also termed a "cell niche", controls and regulates stem cell fate (Watt and Hogan 2000; Powell 2005). Historically, the term "niche" was used to describe the stem cell location (Schofield 1983), the components of the microenvironment surrounding the cells, and the biochemical or electrical signals produced by the support cells (Jones 2001; Fuchs, Tumbar et al. 2004). The niche functions as a physical anchor and generates a number of extrinsic factors that control cell fate. From an engineering perspective, we may define the stem cell niche as a microenvironment with multiple regulatory factors, molecular and physical, that change in space and time and govern stem cell behavior. Replicating *in vitro* the "cell niche" normally found *in vivo* would likely help understand and ultimately control the signaling pathways that regulate cell fate, and help utilize the potential of stem cells in regenerative medicine (Griffith and Naughton 2002; Khetani and Bhatia 2006; Polak and Bishop 2006). Each of the standard cell culture methods has advantages but also limitations. Well plates are easy to use, but they are suitable only for studies of molecular factors and cannot provide physical regulatory factors. Also, well plates operate essentially batch-wise, with the composition of medium constantly changing between the two medium replacements. In contrast, cell culture bioreactors can provide perfusion of medium (Koller, Bender et al. 1993; Horner, Miller et al. 1998; Portner, Nagel-Heyer et al. 2005; Vunjak-Novakovic, Meinel et al. 2005; Dvir, Benishti et al. 2006) control medium composition and thereby support the cultivation of high cell densities, including cultures of human embryonic stem cells (hESCs) (Dang, Gerecht-Nir et al. 2004; Fong, Tan et al. 2005) and embryoid bodies(Gerecht-Nir, Cohen et al. 2004). However, the operating volumes of bioreactors are larger than those of well plates, which is a serious limitation in studies involving the use of expensive media components. Microscale approaches can potentially overcome both of these limitations (Dvir, Benishti et al. 2006), (Folch, Jo et al. 2000; Beebe, Mensing et al. 2002; Anderson, Levenberg et al. 2004; Andersson and Van Den Berg 2004; Chin, Taupin et al. 2004; Khademhosseini, Yeh et al. 2005; Albrecht, Underhill et al. 2006; Futai N, Gu W et al. 2006).

Soft lithography techniques, pioneered by Whitesides and colleagues (Whitesides, Ostuni et al. 2001), are inexpensive and relatively facile, and have found widespread application in bioseparation processes (Choi 2005; Zhang, Cooper et al. 2006) micropatterning of cells and biomaterials (Bhatia, Yarmush et al. 1997; Kane, Takayama et al. 1999), cell-based assays (McClain, Culbertson et al. 2003),(El-Ali, Sorger et al. 2006) and cell culture devices (Ales, Zdenka et al. 2004; Kim, Vahey et al. 2006; Whitesides 2006). Early applications of cell culture devices relate to hepatocytes where microscale features provide a reasonable analog for the microstructure of the liver(Jaesung Park, Berthiaume et al. 2005). More recently, microfluidic platforms of interconnected chambers have been proposed as "living cell arrays" for studying gene expression (Thompson, King et al. 2004) and co-culture (Khademhosseini, Yeh et al. 2005).

In the existing microfluidic systems for stem cell differentiation, the individual chambers are not independent, as medium is distributed across one or more columns/rows of array, leading to the cross-talk between the cells. By enclosing each chamber, this problem may be avoided, although it now becomes more difficult to control the individual chambers without resorting to an integrated valving system (Dvir, Benishti et al. 2006). Additionally, direct access to the cell growth surface makes it possible to apply coatings and uniformly seed the cells.

Here we propose Micro-Bioreactor Arrays (MBA) designed to address some of the limitations discussed above. MBAs are a hybrid between a bioreactor (represented by each individual culture well) and a microfluidic device (represented by the system providing independent flow of medium to each individual culture well). The MBA device combines the advantages of multi-well plates (small volume, high throughput, independent culture wells) and perfusion bioreactors (steady-state conditions, enhanced mass transport, application of physical signals). To take advantage of imaging compatibility of this device, we also developed an automated image analysis routine that enables fast and unbiased analysis of nuclear and cytoplasmic differentiation markers.

We use the term "micro-bioreactor" because 12 culture wells, 3.5 mm in diameter x 2 mm deep, are located within a device that is the size of a microscope slide (26 x 76

mm). Two different configurations of the MBA were developed based on computational flow modeling and analysis of mass transport: MBA-bottom inlet/outlet (BIO; medium flows directly over the substrate with attached cells) and MBA- middle inlet/outlet (MIO; medium flows above the plane with the cells in monolayer or encapsulated in hydrogel). These MBA configurations were validated for cultivations of the C2C12 cell line, primary rat cardiac myocytes and hESCs (lines H09 and H13). To illustrate the utility of the MBA for studies of hESCs, we established quantitative correlations between the density of hESCs differentiating into vascular lineages and the expression of smooth muscle actin.

B.2 Micro-Bioreactor Array (MBA) design

The design requirements for the MBA were: (1) high-throughput experimentation with independent conditions for each bioreactor well, and low consumption of reagents and cells; (2) cultivation of cells in both the 2D setting (attached to a substrate) and three dimensional (3D) setting (encapsulated in hydrogel); (3) reproducible steady-state conditions in terms of cell density, medium composition, levels of oxygen and pH, flow regime, hydrodynamic shear and transport rates; (4) accurate spatial-temporal control of the cell environment; (5) *in situ* quantitative analysis of cell proliferation and differentiation, by automated image analysis of differentiation markers.

Figure 1 shows the design of the system. The MBA is fabricated using soft lithography techniques, has the footprint of a standard microscope slide, and contains twelve independent culture wells. The constituent elements are shown in a top view (Figure 1A): inlet (top, shown in red) and outlet (bottom shown in yellow) ports, culture wells (orange), gas exchangers (microfluidic channels between the inlet ports and the culture wells), stream splitters (divide single inlet/outlet streams by four), and the fluidic channels (connecting the inlets, gas exchangers, culture wells and outlets).

The microfluidic channels are 100 μm high by 100 μm wide. Gas exchangers (20 mm total length) are designed to equilibrate the oxygen level and pH in each of the three inlet streams of culture medium. A splitter then divides each of these streams into four

equal parts, resulting in a total of twelve inlet streams leading into the twelve culture wells. In this way, each MBA has three inlet/outlet ports and three four-way splitters directing flow to the 4x3 array of culture wells. The total length of the fluid paths leading into each well is equivalent, and the pressure drop and velocity field are thus also equivalent for each of the culture wells.

The diameter of each culture well (3.5 mm) was selected to provide a small volume of medium (e.g., ~30 µL for BIO configuration) and the surface area (~10 mm^2) large enough for a statistically significant number of cells to adhere (~10^3). With standard soft lithography, the height of the micro-bioreactor chamber would be restricted to the thickness of the photoresist, generally between 50 µm and 200 µm. For our applications, this would result in three constraints: (i) limited access to the cell chamber for surface coating, cell seeding, and analysis, (ii) insufficient medium hold-up within the bioreactor chamber for cell survival without perfusion, and (iii) relatively high shear stresses for medium perfusion. For these reasons, we chose to work with an "open" microfluidic device where each chamber may be individually addressed (i.e., open) and has a height equal to that of device. A removable gas permeable membrane is used to enclose each chamber during experimentation.

Figure 1B shows the two configurations of the MBA device that were used in the present study. Configuration BIO consists of a single layer of poly(dimethylsiloxane) (PDMS) with replica molded microfluidic channels and perforated with an array of culture wells. The microfluidic channels are placed on the glass slide, such that the medium enters and exits the well at the bottom surface and flows directly over the attached cells (Figure 1B, left).
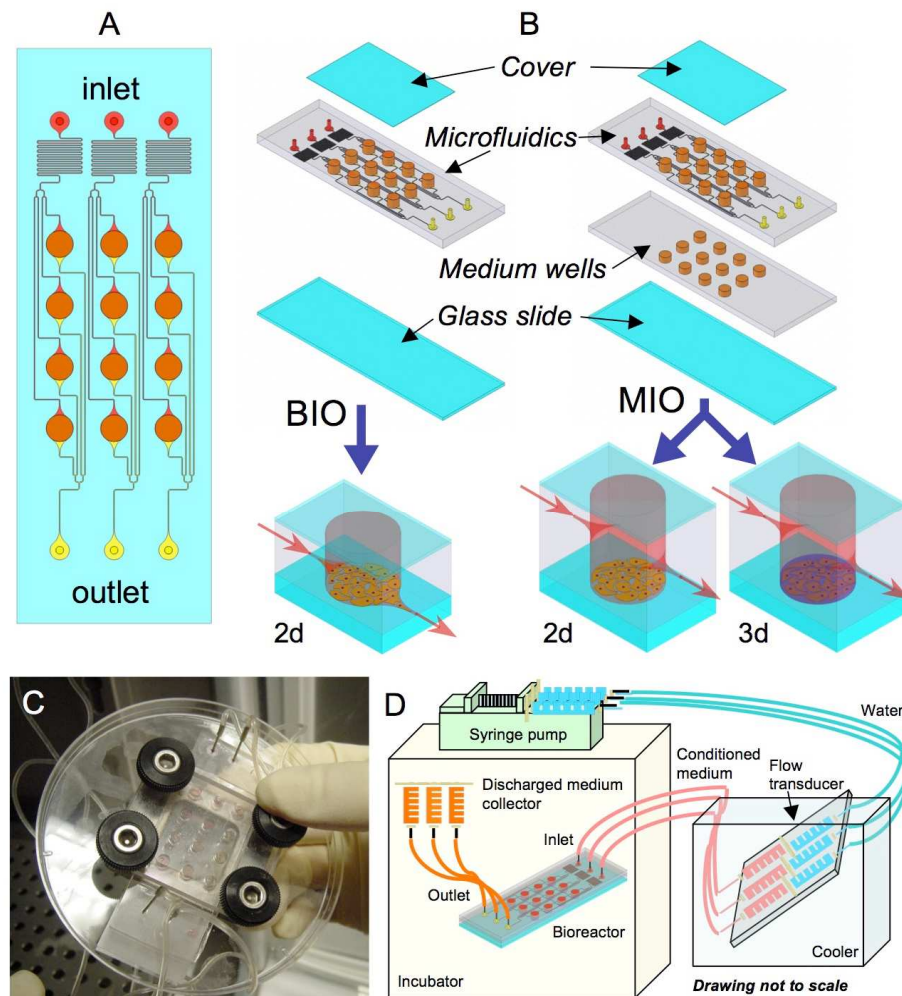
Figure 1 Micro Bioreactor Array (MBA) design. (A) The micro-bioreactor wells (3.5 mm in diameter) are arranged in a 4×3 array (8 mm vertical and 7 mm horizontal center-to-center spacing). The microfluidic channels are 100 μm wide by 100 μm high and deliver between 0.1 - 2.0 ml of medium per day per bioreactor well. Each of three inlets delivers medium (red) through the flow transduces to four wells (orange) via microfluidic channels. Waste medium exits each bioreactor via a separate set of channels (yellow). The devices are assembled from layers of PDMS and glass, attached via plasma treatment of both surfaces. (B) Two configurations were used. A bottom inlet/outlet (BIO) configuration (left) consists of a glass slide, a microfluidic layer, and a gas permeable membrane cover. A middle inlet/outlet (MIO) configuration (right) has an additional layer of PDMS with an array of wells inserted between the microfluidic layer and the slide (C). The BIO and MIO configuration accommodate the 2d cultivation of cells attached to a substrate (glass with or without additional coating); a thin layer of a photopolymerizable hydrogel in the base of MIO configuration wells allows 3d cultivation. (C) Image of a single MBA with compression frame and fluidic connections. (D) Experimental setup. MBAs and medium collectors are placed in an incubator for temperature (37ºC) and gas composition (5% CO_2) control. Medium reservoirs are maintained external to the incubator in an ice bath. The syringes are affixed to a plate that allows a

second set of syringes filled with water to actuate plungers via an external low-flow multi-channel syringe pump.

Configuration MIO (middle inlet/outlet) has an additional layer of PDMS, which (i) increases the depth of the culture well and (ii) presents medium inlet and outlets in the middle plane (Figure 1B, right). As in the BIO configuration, the cells are cultured in a monolayer formed on the glass slide (with or without coating), with the main difference being a substantial reduction in exposure to hydrodynamic shear by culturing the cells outside the main plane of fluid flow. To accommodate the cultivation of hESCs in a 3D setting, a thin layer of photopolymerizing hydrogel may be added to base of wells in this configuration. Since cells *in vivo* are typically surrounded on all sides by extracellular matrix components (Mark J. Powers, Domansky et al. 2002; Albrecht, Underhill et al. 2006; Toh, Zhang et al. 2007), this approach more closely mimics the *in vivo* environment. The compressive stiffness of HA hydrogel can be varied from 0.5 - 50 kPA, by varying the concentration of HA and the level of crosslinking. The hydrogel layer experiences only a small level of shear stress; it is thin enough (typically 200 – 500 µm) to avoid major constraints in mass transfer and changes in flow patterns, yet thick enough for the cells to mimic some aspects of their native 3D environment.

The use of thin hydrogels and medium perfusion provides favorable conditions for encapsulation of hESCs in photopolymerizable hydrogels. First, the high surface to volume ratio of hydrogel in the wells (20–50 cm^2/cm^3) allows for thin film (minimal light attenuation with depth) assumptions to be made. Also, medium perfusion efficiently removes any residual non-polymerized reactants.

The gas permeable membrane that seals each of the MBA chambers is held in place with a compression frame consisting of an aluminum frame, a clear polycarbonate cover, and four thumb screws (Figure 1C). The experimental set-up is designed to assure steady state conditions during the dynamic culture. Each column of wells receives medium from one 10 ml syringe placed on ice (to minimize protein degradation) and is controlled with a syringe pump (Figure 1D). Each outlet tube from MBA was connected to a discharge medium collector placed ~20 cm above the device, all within the incubator.

B.3 Operating conditions: flow and mass transport

To characterize the operating conditions of the MBA, we evaluated the two configurations shown in Figure 2B, in order to establish predictive flow and mass transport correlations for optimizing the conditions in the MBA. The large flow resistance within the 100 μm microfluidic channels ensures equivalence of flow conditions in the twelve individual micro-bioreactor wells of the MBA. At the entrance and exit of each well, the channel width is gradually increased to reach the diameter of the well (1:35 ratio of diameters, 1:20 ratio of heights), and minimize abrupt changes in fluid velocity. With the gradual transient in the effective channel size and the dominance of viscous forces on the microscale, the flow field should remain laminar and uniform. Fluid flow was evaluated by solving the steady-state Navier-Stokes equations for incompressible fluid. The 3D solutions for the BIO and MIO configurations show that the pressure distribution within the chambers is uniform, with > 99% of the pressure drop occurring at the inlet and the outlet to chamber (Figure 2 A-B). The uniformity of flow is further supported by the magnitude of the fluid velocity, which is very low throughout the culture well. In the BIO configuration, the fluid velocity in a plane 50 μm above the cell culture surface is less than 10 μm/s over the entire surface area, and less than 3 μm/s for 75% of the area (Figure 2C). At these low flow rates, the shear stress is < 0.01 dyne/cm^2. In the MIO configuration, the fluid velocity and shear stress are even lower (< 0.01 μm/s, < 0.0001 dyne/cm^2,   Figure 2D).

These simulations show that both configurations operate at very low-shear, but with clear differences (two orders of magnitude) in the values of fluid velocity and hydrodynamic shear.
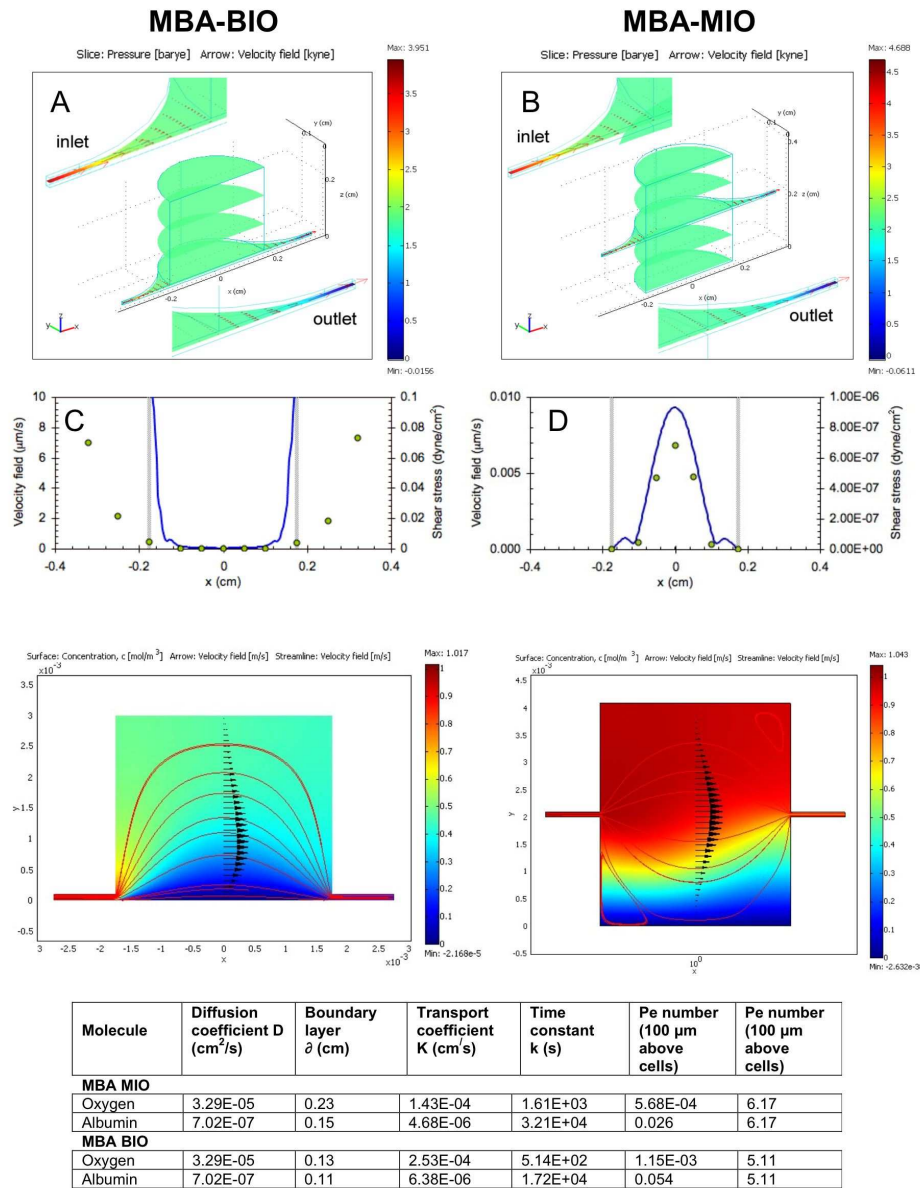
Molecule	Diffusion coefficient D (cm²/s)	Boundary layer ∂ (cm)	Transport coefficient K (cm/s)	Time constant k (s)	Pe number (100 µm above cells)	Pe number (100 µm above cells)
MBA MIO						
Oxygen	3.29E-05	0.23	1.43E-04	1.61E+03	5.68E-04	6.17
Albumin	7.02E-07	0.15	4.68E-06	3.21E+04	0.026	6.17
MBA BIO						
Oxygen	3.29E-05	0.13	2.53E-04	5.14E+02	1.15E-03	5.11
Albumin	7.02E-07	0.11	6.38E-06	1.72E+04	0.054	5.11

Figure 2. *Flow and mass transport conditions in the MBA.* (**A**, **B**) *Pressure distribution (color map) and velocity field (arrows) for BIO and MIO configurations, respectively, obtained by finite element modeling (FEM) of fluid flow.* (**C**, **D**) *Fluid velocity in the plane 50 µm above the cell culture surface (blue line) and shear stress along centerline (circles) for the BIO and MIO configurations, respectively. Gray vertical lines show the boundary of the MBA well.* (**E**, **F**) *Spatial distributions of oxygen concentration (color map), fluid velocity (arrows) and velocity streamlines (lines) for the BIO and MIO configurations, respectively.* (**G**) *Calculated mass transport data for the BIO and MIO configurations, for two representative molecules: oxygen (as a small critical nutrient) and albumin (representative of a large growth factor). Data correspond to images* (**E**, **F**).

A semi-quantitative analysis of mass transport for each of the two flow regimes was performed for two representative molecules: oxygen (the most critical small molecule) and albumin (a molecule representative of large growth factors) (Figure 2E-G). As expected, the thickness of the boundary layer was lower for the BIO configuration, and the mass transport coefficient was higher for oxygen than for albumin and higher for the BIO than for the MIO configuration. The Peclet number (*Pe*) is a measure of the relative contribution of convection with respect to diffusion. At *Pe* > 1, mass transport is dominated by convection, a situation associated with efficient exchange of nutrients and metabolites between the cells and culture media. In contrast, the dominance of diffusion (*Pe* < 1) may be associated with the accumulation of cell-secreted factors, hypoxia and changes in pH. The *Pe* numbers for the MIO configuration strongly suggest that diffusion dominates mass transport, whereas for the BIO configuration, convection plays a much larger role with diffusion only important for small molecules (oxygen) and negligible for large molecules. This analysis demonstrates the flexibility of MBA approach for quantitative experimentation. Through simple regulation of flow rate, chamber height, and inlet/outlet configuration, a wide range of mass transport regimes are attainable.

B.4 Validation of the MBA for representative cell types: C2C12, rat cardiac myocytes and hESC

To validate the utility of the MBA for controlled studies of cell growth and differentiation, we selected three model systems that are representative of the envisioned applications of this device: C2C12 myoblast cell line (MIO, BIO), primary cardiac myocytes derived from neonatal rat hearts (MIO, BIO), and hESCs (MIO). These cell types have well defined differentiation markers, and we have extensive experience in their use in various 2D and 3D configurations (Gerecht-Nir, Ziskind et al.; Radisic, Park et al. 2004; Sharon Gerecht-Nir, Cohen et al. 2004; Vandendriesche D, Parrish J et al. 2004). Figure 3 shows representative growth and differentiation data, at the time points characteristic for each cell type.

C2C12 cells readily adhered to the glass micro-bioreactor surface and formed spatially uniform monolayers with characteristically high cell densities over 7 days of culture (Figure 3A, a-c). Close inspection of the chamber outlet channel shows higher cell density with respect to the inlet channel due to cell migration along the velocity field line (Figure 3Ac). This phenomenon was particularly noticeable within the 100 μm high outlet channel section of the MBA-BIO, where the average velocity and shear stress are high (~100 μm/s and ~0.1 dyne/cm^2 at the flow rate of 10^{-6} ml/s). Within 7-10 days, cells formed multinucleated myotubes that were distributed throughout the culture well (Figure 3A d,e), elongated and expressed smooth muscle actin (Figure 3A e,f). Coating the chamber surfaces with collagen enabled neonatal rat cardiac myocytes to adhere and subsequently form spatially uniform monolayers (Figure 3B a,b). Cell viability, morphology and phenotype were well maintained, as seen by expression of Troponin I. Spontaneous macroscopic contractions demonstrated that the cells were functionally active throughout the culture period.

The cultivation of hESCs turned out to be, as in most other systems, significantly more challenging than that observed for the other cell types. Similar to cardiac myocytes, hESCs required uniform collagen coating of the substrate to obtain even cell distribution (see Methods for details). The hESCs were also cultured encapsulated in a thin layer of hydrogel (hyaluronic acid), a configuration that is 3D for the cells but effectively two dimensional (2D) from the perspective of bioreactor operation.

For cultivation in a 2D setting (MIO), hESCs retained high viability with all conditions (data not shown). For cultivation in a 3D setting medium perfusion affected the viability of all cells studied and most prominently the viability of hESCs (representative data for hESCs shown in Figure 3B c,d), presumably due to the combination of enhanced transport at the hydrogel surface and removal of any residual reagents from hydrogel polymerization. After 4 days of culture, the measured fractions of viable cells were 55 ± 10 % and 67 ± 6 % total cells for the static and perfused culture, respectively. To induce vascular differentiation of the
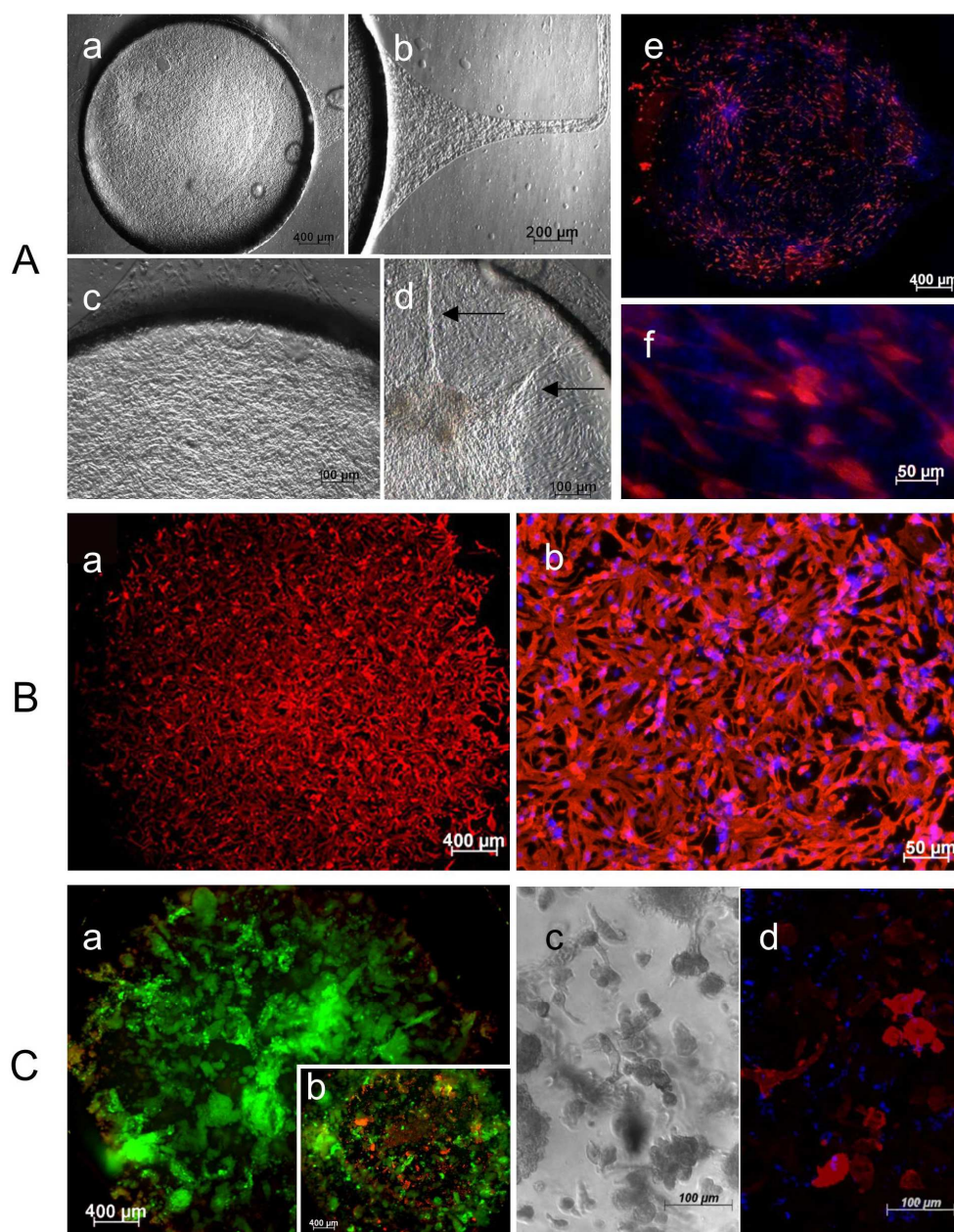
Figure 3 Cultivation of three representative cell types **(A)** System evaluation with C2C12 cell line. **(a)** Phase contrast image showing homogenous distribution of C2C12 over the whole surface area (7 days, MBA-BIO configuration); cells in the outlet channel are shown at the right. **(b)** Enlargement of the outlet channel of chamber showing cell migration in the direction of fluid flow; only few cells are present in the inlet section (not shown). **(c)** Spatially homogeneous cell distribution (higher magnification image). **(d)** Cell differentiation into multinucleated myotubes (arrows). **(e)** Immunostaining of C2C12 for Tropomyosin in the entire well (shown in red; nuclei are shown in blue) in the entire well. **(f)** High magnification of the myotubes (Tropomyosin: red; nuclei: blue). **(B)** System evaluation with primary neonatal rat cardiomyocytes. **(a)** Fluorescent immunostaining for Troponin I showing homogenous cell distribution at 4 days within MBA-MIO configuration. **(b)** Higher magnification of Troponin I and DAPI immunostaining of cardiomyocytes. **(C)** System

evaluation with hESCs. **(a, b)** Representative images of hESCs (3 days, MBA-MIO configuration), **(a)** with and **(b)** without perfusion of culture medium (green: live cells; red: dead cell nuclei). **(c)** Addition of 100ng hVEGF resulted in hESC sprouting and elongation outside the colonies (bright field image). **(d)** Sprouting cells expressed α-SMA, indicative of vascular differentiation (shown in red, confocal microscopy image).

HA-encapsulated hESCs, human vascular growth factor (hVEGF) was added to the culture medium, which resulted in extensive cell sprouting and α-Smooth Muscle Actin (α-SMA) expression (Figure 3B e,f).

Taken together, these studies demonstrated that both MBA configurations (BIO, MIO, Figure 1) support the growth and differentiation of healthy and viable cells.

B.5 Vascular differentiation of hESCs: effects of cell density and flow configuration on SMA expression

The MBA system was designed for live imaging of culture wells with optical and fluorescent microscopy. To take advantage of this option in studies of hESCs, we developed a simple automated system for image analysis that allows fast and unbiased analysis of cell growth and differentiation. Automated and semi-automated routines have been used to measure other biological parameters, such as the spindle length in a Drosophila cell line (Goshima, Wollman et al. 2005). The routine is similar, but not identical (measurements of the length vs. the numbers of positive cells). Figure 4A shows a representative image of hESCs differentiating into vascular lineages and labeled for SMA (red), Oct4 (green) and DAPI (blue). A robust algorithm is used to assess the expression of nuclear and cytoplasmic markers in images of this kind.

To generate quantitative data, the positions of the individual cells stained with DAPI are first determined for a given view field. The expression of intranuclear (e.g., Oct4) and cytoplasmic (e.g., SMA) markers is then tracked for each individual cell, and represented in the form of a histogram or a dot plot in a manner common to flow cytometry. Figure 4B shows a schematic description of the developed imaging routine, which was utilized to probe the effects of cell density and flow regime on hESC differentiation.
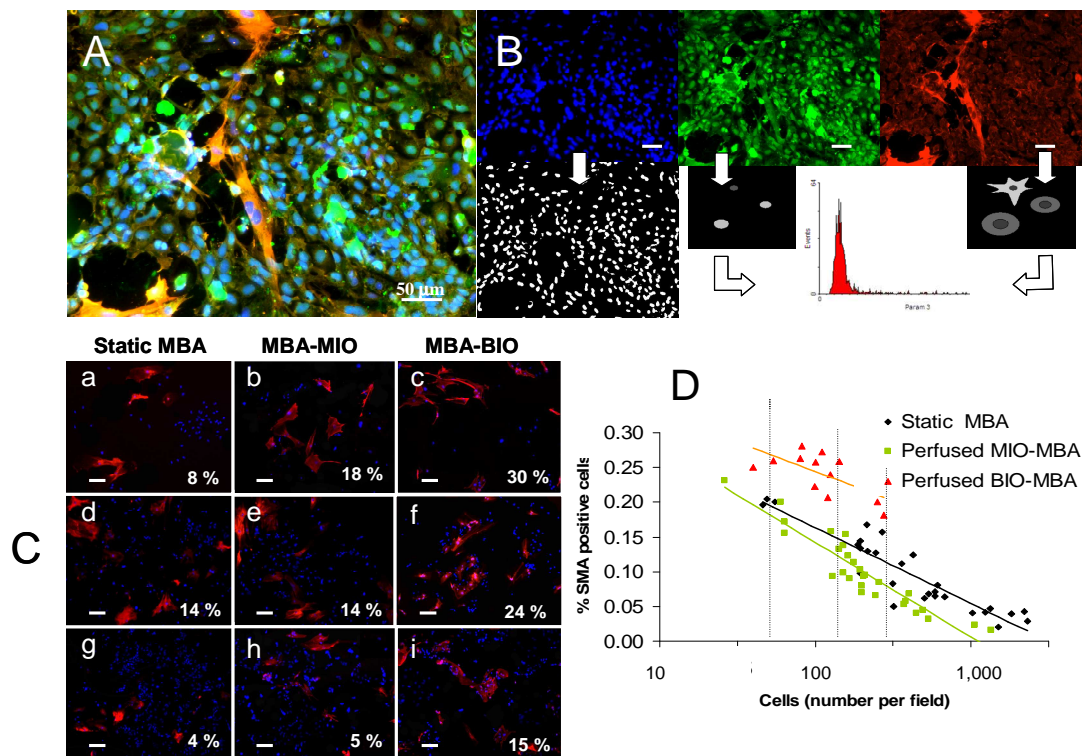
Figure 4 *Effects of cell density and flow configuration on hESC differentiation within the MBA device. (**A**) A representative merged image of cultured hESCs with immunofluorescent labels for SMA (red), Oct4 (green) and DAPI (blue). (**B**) Automated image analysis of cell differentiation. Individual cells are identified by nuclear staining (DAPI) and the coordinates of nuclei are stored in a data matrix. The presence or absence of a nuclear label (Oct4 is shown as an example) and cytoplasmic label (SMA is shown as an example) is identified for each identified cell. Data are processed by a flow cytometer-like analysis, to obtain a dot plot or a histogram representing the intensity of a specific marker within the cell population. (**C**) Examples of the immunofluorescence of SMA (red) and DAPI (Blue) for hESCs cultured in three different flow configurations: static MBA (left column: a, d, g), perfused MBA-MIO (middle column: b, e, h) and MBA-BIO (right column: c, f, i), three different cell densities: 60 ± 6 (top row: a, b, c), 160 ± 4 (middle row: d, e, f) and 314 ± 15 (bottom row: g, h, i). (**D**) The fraction of differentiated cells was determined using the automated image analysis for each flow configuration for a range of cell densities observed over the time of culture. Data are plotted as the fraction of hESCs expressing SMA as a function of the total number of cells in the field (an index of cell density) for each flow configuration. Vertical dotted lines correspond to the conditions in panels (C).*

hESCs were cultured using the MBA-BIO and MBA-MIO configurations, and a non-perfused MBA-BIO to serve as static control. Cell density varied from 3×10^2 to 3×10^4 cells/cm^2, corresponding to ~30 to 3,000 cells per well. Vascular differentiation was evaluated by the expression of SMA, using the imaging routine described above.

Figure 4C shows representative images of cells stained for SMA (red) and DAPI (blue), that were cultured using three different flow configurations (static, BIO and MIO), The

top, middle and bottom rows of panels show images obtained for low, medium and high cell density (60 ± 6, 160 ± 4 and 314 ± 15 cells per well, respectively).

In general, cells cultured in the MBA-BIO configuration (the one with a higher level of shear) exhibited higher levels of differentiation relative to the other two configurations (Figure 4 C,D). This is consistent with the known role of hydrodynamic shear in vascular differentiation (Huang, Y. Nakayama et al. 2005).

In all three configurations, the fraction of hESCs expressing SMA increased as the cell density decreased (Figure 4D). For example, in the MIO configuration, the percent of cells expressing SMA decreased from ~23% to ~2% as the cell density increased from ~200 cells/cm^2 to ~10,000 cells/cm^2. Cells cultured in BIO configuration showed a similar trend, at higher expression levels of SMA for comparable cell densities (Figure 4D). Interestingly, Oct4 was not dependent on cellular density (data not shown). The fractional expression of the SMA in hESC culture decreased linearly with the logarithm of cell density for all three bioreactor configurations. This graph summarizes the results from ~70 individual bioreactors for multiple MBA configurations. The automated assay for quantification of cell differentiation markers, presented here for the case of vascular differentiation of hESCs in 2D culture, could be extended to 3D cultures of cells and a variety of other differentiation markers.

This study demonstrated that the MBA could be used to study the effects of culture parameters on hESC differentiation, in a systematic manner and with only a minimal consumption of cells and reagents. The image processing routine used to assess the fractions of cells expressing differentiation markers (SMA and Oct4 in this case) can be considered an integral part of the proposed method.

B.6 Application of MBA in studies of hESCs

The MBA was designed to culture hESCs in a microarray setting, under controlled conditions, with imaging compatibility, and only minimal consumption of cells and

reagents. hESCs are difficult to grow, require expensive medium and reagents, and from a biological perspective, their complex signaling networks and largely unknown regulatory factors often result in data variability. The use of a system that combines the advantages of microarrays (large numbers of groups and replicates, small volumes) and bioreactors (tight control of environmental conditions) with the automated routines of image processing to assess cell differentiation can largely improve the yield and quality of experimental data.

In general, the MBA shares many properties with other microfluidic-based platforms: low consumption of media, inexpensive fabrication, imaging compatibility, and high throughput. However, MBA also provides close control of culture parameters (including hydrodynamic shear) in each culture well. Additional practical advantages include open access to the cell culture plane in each micro-bioreactor well, to ease surface coating, cell seeding and staining procedures. This allows for an easy translation of the existing biological protocols already established for hESCs to use in MBA formats, and a relatively straightforward use of existing liquid handling/robotic systems and microplate readers.

Notably, each MBA well maintains its own set of steady-state conditions, via perfusion of culture medium in a single-pass mode, and without interaction with other wells within the same array. The medium at the outlet of each well is sent to the waste instead of being recirculated back to the cells (as in most perfused bioreactors). This way, there is no interaction between the wells, and the experiments are not confounded by paracrine signals being transferred downstream. In spite of single-pass flow, the consumption of medium is minimal, because of the miniature size of the device. In studies of vascular differentiation of hESCs, 70 data points were generated over 4 days of culture using only 10 ml of medium.

One of our goals was to provide a uniform and controllable hydrodynamic environment for all cells in the culture chamber. The CFD-assisted design yielded two different configurations - MBA-BIO and MBA-MIO - which exhibit hydrodynamic shear stress that can be as low as <0.1 and <0.001 dyne/cm^2, respectively. Both values are significantly below the threshold levels of shear stress that can affect the cells (1-5 dyne/cm^2), a feature very useful for cultivation of hESCs in a quiescent regime. On the

other hand, if hydrodynamic shear is needed (e.g., to mediate cell differentiation) these levels can be increased by a simple increase of fluid velocity. Also, the BIO and MIO configurations provide different flow environments, and the experiments described above show that the culture of hESCs in a BIO configuration resulted in larger values of α-SMA-positive cells than culture in the MIO configuration.

B.7 Methods

B.7.1 Fabrication of the MBA

The micro-bioreactor array was designed in a standard CAD program (SolidWorks, Concord, MA), and then exported to Adobe Illustrator 9.0 (San Jose, CA) for printing as a transparency mask (5080 dpi, PageWorks, Cambridge, MA). The mask was used to prepare a 4" silicon wafer/SU-8 2100 master of the bioreactor image. The processing guidelines of the photoresist manufacturer were followed to achieve features with a uniform height of 100 μm (MicroChem_Corp. 2006).

The actual bioreactor layers were replica molded (Jackman, Brittain et al. 1998; McDonald and Whitesides 2002) by pouring 35 ml of poly(dimethylsiloxane) (PDMS, Sylgard 184 Silicone Elastomer, Ellsworth Adhesives, Germantown, WA) over a master placed in a 150 mm Petri dish. Prior to this step, a thin layer of hexamethyldisilane (Fluka, Buchs, Switzerland) was vacuum deposited on the wafer surface to prevent adherence of the PDMS. The fluidic connection ports were punched through PDMS with a 21-gauge stainless steel tube (0.635 mm ID, 0.81 mm OD, McMaster-Carr, Atlanta, GA). In a similar manner, the micro-bioreactor wells were cored out using a 3.5 mm punch (Fray Products Corp., Buffalo, NY), resulting in holes that were 3.35 mm in diameter. The layers of PDMS and glass were irreversibly bonded after treatment with vacuum gas plasma for 45 s (at 0.5 mbar and 50 W) (Harrick Scientific, Pleasantville NY). After coating the bottom surface of each well and seeding with cells, the entire bioreactor array was covered with a thin layer (0.2 mm) of PDMS. The MBA layers were held in place by mechanical compression via a frame consisting of an aluminum base, a polycarbonate cover, and four thumbscrews. Small lengths of

stainless steel tubing (21 gauge, 10 mm length) were used to connect MBA ports to soft Tygon tubing (0.8 mm ID, 2.4 mm OD, Cole Palmer, Vernon Hills, IL). The medium flow rate was controlled via a syringe pump, with an accuracy of 0.1 μL/min (PHD, Harvard Apparatus, Holliston, MA). The culture medium was kept at 4 °C, while the entire MBA device was kept in an incubator (NAPCO, Winchester VA) at standard conditions (37 °C, 95% humidity, 5% CO_2).

B.7.2 Hydrodynamic simulation

The Navier-Stokes equations for incompressible fluids were solved using Comsol Multiphysics (Burlington, MA) to obtain a flow field within the micro-bioreactor well for the BIO and MIO configurations. The 3D domain of the micro-bioreactor well was meshed using four-node tetrahedron finite elements with a maximum mesh size of 300 μm. Coarsening and refining of the mesh space grid ensured solutions independent of the spatial discretization.

The inlet boundary condition was set for a fully developed velocity profile (calculated on the basis of flow rate), while a zero pressure condition was imposed on the outlet and non-slip boundary condition set for channel and bioreactor walls. Assumption of longitudinal symmetry allowed solving the equations for only one half of the channel and chamber, thus minimizing computational time.

The medium viscosity and density values for DMEM medium with 5% FCS were taken from the literature (Moreira, Santana et al. 1995). As a check on the validity of the simulation, the shear stress within the uniform rectangular channels was calculated from an approximation of the analytical solution for flow between parallel plates, $\tau = 6\mu Q/bh^2$ where μ is the dynamic viscosity of medium (0.0077 dyne-s/cm^2), Q is the flow rate (5 x 10^{-6} ml/s), b is the channel width (0.01 cm), and h is the channel height (0.01cm). The calculated value of 0.058 dyne/cm^2 compares well to the result obtained by finite element modeling of the flow in the channel (~0.07 dyne/cm^2 at the position 0.32 cm from center of the well, Figure 2C).

B.7.3 Mass transport calculations

To obtain concentration profiles within the micro-bioreactor wells for the BIO and MIO configurations, the mass balance equations for a convective diffusive regime were solved using Comsol Multiphysics software (Burlington, MA). Fluid velocity profiles were obtained from the three dimensional solution. The concentration of 1 mM was used as a boundary condition at the inlet; zero concentration was imposed as a boundary condition at the cell surface. The *Re* and *Pe* numbers were then calculated using standard equations, and literature values of diffusion coefficients for each solute.

B.7.4 Cell culture

C2C12 myoblast cells (murine, American Type Culture Collection) were grown to confluency in growth medium (DMEM with 20% fetal bovine serum, FBS). Cells were trypsinized, counted, and 2,000 cells were added to each MBA well. After 12 h, medium perfusion was initiated at a flow rate of 0.3 µl/min (0.432 ml/day), which corresponds to 0.075 µl/min per bioreactor. Perfusion medium contained low serum levels (2% FBS), to induce myogenic differentiation. Experimental methods with primary cells (cardiomyocytes) were similar to those with C2C12 line except that cells were seeded at 1,000 cells per well and that the culture medium contained 10% FBS. Details on cardiomyocyte isolation from 2-day old neonatal Sprague Dawley rats can be found elsewhere (Cannizzaro, Tandon et al. 2008).

Non-differentiated hESCs (lines H9 and H13; passage 20-35) (WiCell Research Institute, Madison, WI) were grown on inactivated mouse embryonic fibroblasts (Chemicon International, Temecula, CA) in growth medium consisting of 80% KnockOut DMEM, supplemented with 20% KnockOut Serum replacement, 4 ng/ml basic Fibroblast Growth Factor, 1 mM L-glutamine, 0.1 mM β–mercaptoethanol, 1% non-essential amino acid stock (all from Invitrogen Corp., Carlsbad, CA). hESCs were passaged to a new feeder layer using 1mg/ml type IV collagenase (Invitrogen Corp., Carlsbad, CA). For 3D studies, hESCs were removed from the feeder layer by incubation with collagenase for 20-30min. For 2D studies, hESCs were removed from MEFs by incubation with EDTA (Promega) with 5% FCS, for 20min, followed by separation into single cells using a 40µm mesh strainer (Falcon) For 2D studies, the

glass surface of each MBA chamber was treated with a solution of 4% of 3-aminopropyltrimethoxysilane (Sigma-Aldrich, St. Louis, MO) in acetone for 15 min. Each well was then coated with 0.05mg/ml collagen IV (R&D Systems, Minneapolis, MN) for 1 hr in room temp. The cells were seeded at concentrations of 10^3, $3 \cdot 10^3$, $5 \cdot 10^3$, and 10^4 cells per well. Medium perfusion was started 24 h after cell seeding to allow sufficient time for cell attachment.

B.7.5 Hydrogel preparation and hESC microencapsulation

For 3D studies, we utilized previously developed photocrosslinkable methacrylated HA hydrogels (Smeds and Grinstaff 2001; Chung, Mesa et al. 2006; Chung, Mesa et al. 2006). For hydrogel formation, methacrylated HA was dissolved in PBS containing 0.05 wt% 2-methyl-1-[4-(hydroxyethoxy)phenyl]-2-methyl-1-propanone (Irgacure 2959, I2959) and exposed to ultraviolet light (Black Ray, Redding, CA) for 10 minutes. These encapsulation conditions have previously been used for the encapsulation of a variety of mammalian cells (Bryant, Nuttelman et al. 2000).

hESCs were added to the precursor solution at a concentration of $0.5 - 1 \times 10^7$ cells/ml. A volume of 30 µL of the cells/HA mixture was poured into each micro-bioreactor well, and photopolymerized (using ~10 mW/cm^2 UV light, BlackRay, for 10 min). Cell-gel constructs were cultivated in growth medium (for proliferation), and endothelial cell medium (for differentiation) (PromoCell, Heidelberg, Germany). In some studies, medium was supplemented with 100 ng/ml hVEGF (R&D systems, Minneapolis, MN).

B.7.6 Immunofluorescence

Cells were fixed *in situ* with accustain (Sigma-Aldrich, St. Louis, MO) for 25 min at room temperature. Cells were stained for 1 h with the first antibody and then for 30 min with a secondary antibody, at room temperature. The wells were rinsed three times with PBS without calcium and magnesium (Invitrogen Corp., Carlsbad, CA). DAPI (2 µg/mL; Sigma-Aldrich) was added to the last rinse. C2C12 cells were stained for monoclonal Tropomyosin (Sigma-Aldrich). hESCs were stained either for Smooth

Muscle Actin (1:20; Dako, Troy Michigan), or Oct4 (1:50; R&D Systems, Minneapolis, MN). For secondary staining, Cy3 or FITC-conjugated antibody (1:50;.Sigma-Aldrich, St. Louis, MO) were used. Cardiomyocytes were stained for anti-rabbit Troponin I and FITC-conjugated secondary antibody (both from Chemicon International, Temecula, CA). The immuno-labeled cells were examined using a fluorescence microscope (Axiomat, Zeiss, Thornwood, NY).

B.7.7 Data acquisition and analysis

The percent of differentiated and undifferentiated cells were evaluated by an imaging acquisition program written using scripts available in MATLAB, and MATLAB imaging toolbox (The MathWorks, Natick, MA). Images of the entire micro-bioreactor well area (3.5 mm diameter) were acquired as a series of images at $5\times$ magnification for the nuclei (DAPI) and two other markers (cytoplasmic and nuclear intracellular markers). From the DAPI image, the coordinates of the pixel of each nucleus were acquired and stored. The intensity of the pixels corresponding to the DAPI coordinates in the other two images was used to evaluate the existence of nuclear transcription factors. The intensity of the cytoplasmic staining fluorescence was evaluated by considering the intensity of pixels within the ellipsoid corona centered in the nucleus and an area 50% bigger in size. Processed data were then used to count the number of nuclei and evaluate the fraction of cells expressing a specific marker. Graphical representation of data (dot plots, histograms) and statistical evaluation of signal intensities were performed by importing data into a free flow cytometry data analysis program (WinMDI 2.8).

B.8 Conclusions

Stem cell biology is increasingly relying on advanced technologies that provide better cell culture microenvironments and enable control over multiple molecular and physical

regulatory signals. These enabling technologies are of particular interest to hESCs, because of the complexity of their regulatory pathways, and uncontrolled variables associated with traditional culture methods. We have developed a Micro Bioreactor Array (MBA) that combines the advantages of microarrays with those of bioreactors, and provides a means to study the growth and differentiation of hESCs under controlled conditions and in a multiarray setting. The device is the size of a microscope slide and contains twelve independent micro-bioreactors perfused with culture medium. The design is flexible, as it allows 2D and 3D cell culture under variable levels of hydrodynamic shear and mass transport, which were characterized by computational methods. To demonstrate operation of the MBA, we cultured C2C12 cells, rat cardiac myocytes and hESCs within the system. A system for automated *in situ* image analysis of the expression of cell differentiation markers has also been developed and used to investigate the effects of cell density and flow regime on vascular differentiation of hESCs. This device can thus serve as a tool for studying hESCs in the context of their environment.

B.9 Acknowledgments

B.10 References

Albrecht, D. R., G. H. Underhill, et al. (2006). "Probing the role of multicellular organization in three-dimensional microenvironments." Nat Meth **3**(5): 369-375.

Ales, P., P. Zdenka, et al. (2004). "NanoLiterBioReactor: Long-Term Mammalian Cell Culture at Nanofabricated Scale." Biomedical Microdevices **V6**(4): 325-339.

Anderson, D. G., S. Levenberg, et al. (2004). "Nanoliter-scale synthesis of arrayed biomaterials and application to human embryonic stem cells." Nat Biotech **22**(7): 863-866.

Andersson, H. and A. Van Den Berg (2004). "Microfabrication and microfluidics for tissue engineering: State of the art and future opportunities." Lab on a Chip - Miniaturisation for Chemistry and Biology **4**(2): 98-103.

Beebe, D. J., G. A. Mensing, et al. (2002). "Physics and applications of microfluidics in biology." Annual Review of Biomedical Engineering **4**(1): 261-286.

Bhatia, S. N., M. L. Yarmush, et al. (1997). "Controlling cell interactions by micropatterning in co-cultures: Hepatocytes and 3T3 fibroblasts." Journal of Biomedical Materials Research **34**(2): 189-199.

Bryant, S. J., C. R. Nuttelman, et al. (2000). "Cytocompatibility of UV and visible light photoinitiating systems on cultured NIH/3T3 fibroblasts in vitro." Journal of Biomaterials Science, Polymer Edition **11**: 439-457.

Cannizzaro, C., N. Tandon, et al. (2008). Practical aspects of cardiac tissue engineering with electrical stimulation, Humana Press.

Chin, V., P. Taupin, et al. (2004). "Microfabricated platform for studying stem cell fates." Biotechnology and Bioengineering **88**(3): 399-415.

Choi, J.-W. (2005). Fabrication of Micromachined Magnetic Particle Separators for Bioseparation in Microfluidic Systems.

Chung, C., J. Mesa, et al. (2006). "Effects of Auricular Chondrocyte Expansion on Neocartilage Formation in Photocrosslinked Hyaluronic Acid Networks." Tissue Engineering **12**(9): 2665-2673.

Chung, C., J. Mesa, et al. (2006). "Influence of gel properties on neocartilage formation by auricular chondrocytes photoencapsulated in hyaluronic acid networks." Journal of Biomedical Materials Research Part A **77A**(3): 518-525.

Dang, S. M., S. Gerecht-Nir, et al. (2004). "Controlled, scalable embryonic stem cell differentiation culture." Stem Cells **22**(3): 275-82.

Dvir, T., N. Benishti, et al. (2006). "A Novel Perfusion Bioreactor Providing a Homogenous Milieu for Tissue Regeneration." Tissue Engineering **12**(10): 2843-2852.

El-Ali, J., P. K. Sorger, et al. (2006). "Cells on chips." Nature **442**(7101): 403-411.

Folch, A., B. Jo, et al. (2000). "Microfabricated elastomeric stencils for micropatterning cell cultures." Journal of Biomedical Materials Research **52**(2): 346-353.

Fong, W. J., H. L. Tan, et al. (2005). "Perfusion cultures of human embryonic stem cells." Bioprocess Biosyst Eng **27**(6): 381-7.

Fuchs, E., T. Tumbar, et al. (2004). "Socializing with the Neighbors: Stem Cells and Their Niche." Cell **116**(6): 769-778.

Futai N, Gu W, et al. (2006). "Handheld recirculation system and customized media for microfluidic cell culture." Lab Chip **6**(1): 149-154.

Gerecht-Nir, S., S. Cohen, et al. (2004). "Bioreactor cultivation enhances the efficiency of human embryoid body (hEB) formation and differentiation." Biotechnol Bioeng **86**(5): 493-502.

Gerecht-Nir, S., A. Ziskind, et al. "Human Embryonic Stem Cells as an In Vitro Model for Human Vascular Development and the Induction of Vascular Differentiation." Lab Invest **83**(12): 1811-1820.

Goshima, G., R. Wollman, et al. (2005). "Length Control of the Metaphase Spindle." Current Biology **15**(22): 1979-1988.

Griffith, L. G. and G. Naughton (2002). "Tissue engineering--current challenges and expanding opportunities." Science **295**(5557): 1009-14.

Horner, M., W. M. Miller, et al. (1998). "Transport in a grooved perfusion flat-bed bioreactor for cell therapy applications." Biotechnol Prog **14**(5): 689-98.

Huang, H., K. Y. Nakayama, et al. (2005). "Differentiation from embryonic stem cells to vascular wall cells under in vitro pulsatile flow loading." J. Artif. Organs **8**: 110-118.

Jackman, R. J., S. T. Brittain, et al. (1998). "Design and Fabrication of Topologically Complex, Three-Dimensional Microstructures." Science **280**(5372): 2089-2091.

Jaesung Park, F. Berthiaume, et al. (2005). "Microfabricated grooved substrates as platforms for bioartificial liver reactors." Biotechnology and Bioengineering **90**(5): 632-644.

Jones, L. (2001). "Stem cells: So what's in a niche?" Current Biology **11**(12): R484-R486.

Kane, R. S., S. Takayama, et al. (1999). "Patterning proteins and cells using soft lithography." Biomaterials **20**(23-24): 2363-2376.

Khademhosseini, A., J. Yeh, et al. (2005). "Cell docking inside microwells within reversibly sealed microfluidic channels for fabricating multiphenotype cell arrays." Lab on a Chip **5**(12): 1380-1386.

Khetani, S. R. and S. N. Bhatia (2006). "Engineering tissues for in vitro applications." Current Opinion in Biotechnology **17**(5): 524-531.

Kim, L., M. Vahey, et al. (2006). "Microfluidic arrays for logarithmically perfused embryonic stem cell culture." Lab Chip **6**: 394 - 406.

Koller, M. R., J. G. Bender, et al. (1993). "Expansion of primitive human hematopoietic progenitors in a perfusion bioreactor system with IL-3, IL-6, and stem cell factor." Biotechnology (N Y) **11**(3): 358-63.

Mark J. Powers, K. Domansky, et al. (2002). "A microfabricated array bioreactor for perfused 3D liver culture." Biotechnology and Bioengineering **78**(3): 257-269.

McClain, M. A., C. T. Culbertson, et al. (2003). "Microfluidic Devices for the High-Throughput Chemical Analysis of Cells." Anal. Chem. **75**(21): 5646-5655.

McDonald, J. C. and G. M. Whitesides (2002). "Poly(dimethylsiloxane) as a Material for Fabricating Microfluidic Devices." Acc. Chem. Res. **35**(7): 491-499.

MicroChem_Corp. (2006). "Permanent Epoxy Negative Photoresist, Processing Guidelines for: SU-8 2100 and SU-8 2150."

Moreira, J. L., P. C. Santana, et al. (1995). " Effect of viscosity upon hydrodynamically controlled natural aggregates of animal cells grown in stirred vessels." Biotechnol Prog. **11**(5): 575-83.

Polak, J. M. and A. E. Bishop (2006). "Stem Cells and Tissue Engineering: Past, Present, and Future." Annals of the New York Academy of Sciences **1068**(1): 352-366.

Portner, R., S. Nagel-Heyer, et al. (2005). "Bioreactor design for tissue engineering." J Biosci Bioeng. **100**(3): 235-45.

Powell, K. (2005). "Stem-cell niches: it's the ecology, stupid!" Nature. **435**(7040): 268-70.

Radisic, M., H. Park, et al. (2004). "From the Cover: Functional assembly of engineered myocardium by electrical stimulation of cardiac myocytes cultured on scaffolds." PNAS **101**(52): 18129-18134.

Schofield, R. (1983). "The stem cell system." Biomed Pharmacother. **37**(8): 375-80.

Sharon Gerecht-Nir, S. Cohen, et al. (2004). "Three-dimensional porous alginate scaffolds provide a conducive environment for generation of well-vascularized embryoid bodies from human embryonic stem cells." Biotechnology and Bioengineering **88**(3): 313-320.

Smeds, K. and M. Grinstaff (2001). "Photocrosslinkable polysaccharides for *in situ* hydrogel formation." Journal of Biomedical Materials Research **54**(1): 115-121.

Thompson, D. M., K. R. King, et al. (2004). "Dynamic Gene Expression Profiling Using a Microfabricated Living Cell Array." Anal. Chem. **76**(14): 4098-4103.

Toh, Y.-C., C. Zhang, et al. (2007). "A novel 3D mammalian cell perfusion-culture system in microfluidic channels." Lab on a Chip **7**(3): 302-309.

Vandendriesche D, Parrish J, et al. (2004). "Space Station Biological Research Project (SSBRP) Cell Culture Unit (CCU) and incubator for International Space Station (ISS) cell culture experiments." J Gravit Physiol. **11**(1): 93.

Vunjak-Novakovic, G., L. Meinel, et al. (2005). "Bioreactor cultivation of osteochondral grafts." Orthod Craniofac Res **8**(3): 209-18.

Watt, F. M. and B. L. M. Hogan (2000). "Out of Eden: Stem Cells and Their Niches." Science **287**(5457): 1427-1430.

Whitesides, G. M. (2006). "The origins and the future of microfluidics." Nature **442**(7101): 368-373.

Whitesides, G. M., E. Ostuni, et al. (2001). "Soft lithography in biology and biochemistry." Annual Review of Biomedical Engineering **3**(1): 335-373.

Zhang, X., J. M. Cooper, et al. (2006). "Continuous flow separation of particles within an asymmetric microfluidic device." Lab Chip **6**: 561 - 566.

Appendix C

Effect of electrode material on ROS expression of human embryonic stem cell

Elisa Figallo[1,2], Christopher Cannizzaro[1], Sharon Gerecht-Nir[1], Nina Tandon[3],
Nicola Elvassore[2], Gordana Vunjak-Novakovic[3]

[1] Division of Health Sciences and Technology and Bioengineering departments, Massachusetts Institute of Technology, Cambridge MA 02139

[2] Department of Chemical Engineering, University of Padova, Italy

[3] Department of Biomedical Engineering, Columbia University, 1210 Amsterdam Avenue, MC 8904, New York NY 10027;

¶ corresponding author, gv2131@columbia.edu

Abstract

Cardiac tissue engineering and cell transplantation are emerging as alternatives to traditional therapies for cardiac diseases, which are the leading cause of death in Western society. Human embryonic stem cells (hESCs) are considered an ideal cell source for cardiovascular treatments for their greater potency for proliferation and differentiation. When cultured in suspension, hESCs form aggregates termed embryoid bodies (EBs). EBs have the ability to differentiate spontaneously in vitro into beating areas containing cardiomyocytes. Reactive oxygen species (ROS) have been previously shown to be involved in the regulation of murine stem cell differentiation, in particular toward cardiac lineage.

In this study, ROS production in EBs increased significantly after exposure to a 5 V/cm field. The interpretation of the cellular response to such fields needs an adequate characterization of the system used for stimulation. Different electrode materials, such as Stainless Steel, Titanium and Titanium Nitride, were characterized by electrochemical impedance spectroscopy (EIS) and used for electrical stimulation of EBs of 6 days old at different duration stimulation (either 1 s or 90 s). The ROS expression showed a high dependence on electrode material and a higher response for longer stimulation. The magnitude of this increase was correlated with EB age (either 4, 6 or 8 days old) with a maximum occurring at 4 days. In addition, the magnitude of the increase was also dependant on electrode material properties and charge-transfer characteristics at the electrode-electrolyte interface.

An increase in the percentage of beating cells occurred after field stimulation indicating a possible link between ROS expression and cardiac differentiation. The extent of differentiation was highly dependent upon EB age, with the best results observed with 4 day old EBs stimulated for 90 s. This may suggest the higher predisposition of the hESC to a cardiac differentiation and a more efficacious electrical stimulation at earlier stage of development.

C.1 Introduction

The true utility of stem cells (SCs) will only be realized when they can be safely differentiated into cell lines of clinical importance (Lovell and Mathur 2004; Fukuda and Yuasa 2006). Compared to adult SCs embryonic SCs (ESCs) have been shown to have greater potency for proliferation and differentiation (Izhak Kehat 2001; Odorico, Kaufman et al. 2001; Laflamme, Gold et al. 2005; Boyle, Schulman et al. 2006). Numerous studies have demonstrated the importance of chemical and/or mechanical stimulus in directing SC differentiation (Heng, Cao et al. 2004; Heng, Haider et al. 2004; Hong Wei 2005; Passier and Mummery 2005). Other stimuli such as physical ones, are less well understood. In particular, the role of electrical fields and currents during differentiation of SCs, is unclear.

Endogenous electromagnetic fields (EF) are present in developing and regenerating animal tissue, usually in the extracellular space, but sometimes within the cytoplasm of a single cell or a group of cells, and they range in strength from a several to hundreds of mV/mm (Jaffe and Nuccitelli 1977; Robinson 1985). The magnitude of these electrical fields can directly guide cell movement and growth (Joshua Rutenberg 2002). They may also generate chemical gradients of charged macromolecules (Zhao, Pu et al. 2002) that can be present for hours, days, or even weeks during both development and regeneration (McCaig, Rajnicek et al. 2005). At the site of an injured epithelium, for example, a substantial electrical field is instantly generated and may extend over many cell diameters and persist for hours (Song, Zhao et al. 2002; Pullar and Isseroff 2005). Combined with diffusible chemical gradients, electric fields lead to the polarization and the formation of spatial patterns in developing embryo (Richard Nuccitelli 1992; Kenneth R. Robinson 2003; Lodish, Berk et al. 2003) creating directional signals necessary for the proper placement of the components of the organism.

In the laboratory, exogenous electrical fields have been shown to influence cell direction and differentiation (Zhao, Forrester et al. 1999). Several studies have reported galvanotaxis in a variety of cells cultured *in vitro* after stimulation with a constant DC field comparable with those detected *in vivo* (Mycielska and Djamgoz 2004). The cell responds to an externally applied electric fields with specific mechanism, including the passive and active

intracellular influx of ions, such as calcium and sodium (Djamgoz, Mycielska et al. 2001; Donna R. Trollinger 2002), or the localization of lipid and epithelial growth factor (EGF) receptors in the membrane (Zhao, Pu et al. 2002). The equilibrium between these processes determines the reorganization of the cytoskeleton and the migration towards one of the two electrodes.

It has been shown that the exposure to electric fields promote mouse ESC cardiomyogenic (Heinrich Sauer 1999), mESC angiogenic (Zhao, Bai et al. 2004; Sauer, Bekhite et al. 2005), mouse N1E-115 neuroblastoma neuronal (Mie, Endoh et al. 2003) and MG63 osteogenic (C. H. Lohmann, Schwartz et al. 2000; Walter Hong-Shong Chang, Chen et al. 2004) differentiation. The course of action of electrical stimulation on the activation of differentiative pathways is still unclear.

One possible hypothesized mechanism involves the increasing of reactive oxygen species (ROS) within the cell (Heinrich Sauer 1999; Sauer and Wartenberg 2005). Sauer et al (1999) found that electric field stimulation increased intracellular ROS production in mouse EBs. ROS are very small highly reactive molecules generated during the normal metabolism of oxygen by NADPH oxidases or as side products of several enzymatic systems (e.g., cyclooxygenases, nitric oxide (NO) synthases, mitochondrial cytochromes). Although excessive concentration of ROS, such as superoxide anions (O_2^-) and hydrogen peroxide (H_2O_2), are considered destructive and results in inhibition of gene expression (Puceat, Travo et al. 2003; Puceat 2005), small amounts of ROS function as intracellular second messengers and activate signaling cascades involved in growth and differentiation of many cell types (Sun and Oberley 1996; Rhee 1999; Sauer, Rahimi et al. 2000; Shah and Sauer 2006). Sauer et al found that electric field stimulation increased intracellular ROS production in mouse embryoid bodies (EBs). Furthermore, ROS was shown to activate the mitogenactivated protein kinase (MAPK) pathways enhancing the angiogenesis through the activation of ERK1,2 and JNK and the cardiomyogenesis through the phosphorylation of ERK1,2, JNK and p38 (LEV, KEHAT et al. 2005; Li, Stouffs et al. 2006; Schmelter, Ateghang et al. 2006).

These studies introduce the applicability of electrical stimulation as a possible technique to control cell differentiation. However, in a clinical prospective the use of human SCs would be necessary. It's then important to investigate the effects of the electric field on these cell types, in particular human ESCs (hESC) (Lovell and Mathur 2004; Boyle, Schulman et al. 2006).

In order to control the cell behavior through the efficacious application of exogenous electrical fields, it is necessary to characterize the stimulation at the electrical level and understand its mechanisms of action at the biological level.

To enable an efficacious *in vitro* stimulation it is necessary to control the intensity, duration and frequency of the stimulus on the cell. If the stimulation is given applying a constant voltage between the working and counter electrodes, for example, the geometry of the system and the properties of the electrode determine the duration of the cell stimulation. When a couple of electrodes are introduced in an electrolyte and the potential across the electrodes is set, the ions in the medium will be redistributed by the electrostatic forces creating, in a very narrow volume at the interface called electrical double layer, a plane of charge that shields the charges on the electrode surface. The movement of ions determines the transient presence of current in the system. At the steady state, in absence of chemical reactions, the potential drop is concentrated in the double layer and the current in the system is absent. If a cell is placed between the electrodes in a steady condition, it will not be affected by any electrical stimulation because the electric field across it will be negligible (Merrill, Bikson et al. 2005). In presence of reactions, the equilibrium condition is characterized by a small current in the system due to the charge-transfer on the electrode-electrolyte interface (Norlin, Pan et al. 2002).

The time necessary to reach a steady state condition is dependant on the properties of the electrolyte and the amount of charge accumulated on the electrode surface. The amount of charge accumulated on the electrode surface is in turn dependant on the voltage applied between the electrodes and the properties of the electrode material, such as its surface area, capacitance, and chemical properties. For biological applications, additional electrode requirements stem from the requirement that the electrode material be biocompatible and

prove adequate mechanical properties. Herein lies the necessity of characterize accurately the system before performing biological experiments.

In this study the electrical properties of electrodes of same geometry and different material have been evaluated through electrochemical impedance spectroscopy (EIS). The electrode-electrolyte interface has been modeled by Randle-type equivalent circuit, evaluating capacitance and polarization resistance of Titanium, Titanium Nitride and Stainless Steel electrodes. The evolution of the stimulation has been monitored measuring current in the system. The effectiveness of the electrode material has been evaluated through the expression of intracellular ROS in hESCs. Since the EB differentiation stage could influence the intracellular production of ROS, different stages of EB differentiation have been investigated. The percentage of beating EBs in presence of electrical stimulation has also been compared with the basal condition in absence of stimulation.

C.2 Material and methods

C.2.1 Human Embryonic Stem Cells culture

Undifferentiating hESCs (H13.B line WiCell Research Institute, Madison, WI; p19-40) were grown on inactivated mouse embryonic fibroblasts (MEF) in growth medium consisting of 80% KnockOut DMEM, supplemented with 20% KnockOut Serum Replacement, 4 ng/ml basic Fibroblast Growth Factor, 1 mM L-glutamine, 0.1 mM   β– mercaptoethanol, 1% non-essential amino acid stock (Invitrogen Corporation, Carlsbad, CA). hESCs were passaged to new feeder using 1mg/ml type IV collagenase (Invitrogen Corporation, Carlsbad, CA). To induce the formation of human EBs, the undifferentiated hESCs were treated with 1 mg/mL collagenase, and then transferred to low attachment plates containing EB medium: 80% knockout Dulbecco´s modified Eagle medium (Gibco Invitrogen Co.) supplemented either with 20% defined fetal bovine serum (Hyclone), 1mM L-glutamine, and 1% nonessential amino acid stock (all from Gibco-BRL). Human EBs were cultured at 37 ºC, and 5% CO_2 in a humidified atmosphere, with changes of media every 3 days.

For checking the influence of electrical stimulation in cardiac differentiation, 4 and 7 days-old EBs were stimulated in the electrical stimulation system described below, at concentration of 2-4 EBs per well in presence of "pulsing buffer". The EBs were then cultured in EB medium and allowed to attach for 24 h. Media was replaced everyday.

C.2.2 Electrical stimulation system

EBs were electrically stimulated within bioreactor built exclusively for this purpose in poly(dimethylsiloxane) (PDMS). The bioreactor is characterized by an array of 4 by 4 wells as showed in Figure 1. Electrodes of 2 mm of diameter can be inserted in both sides of each row. Independent stimulation is guaranteed by the PDMS insulation between different rows.
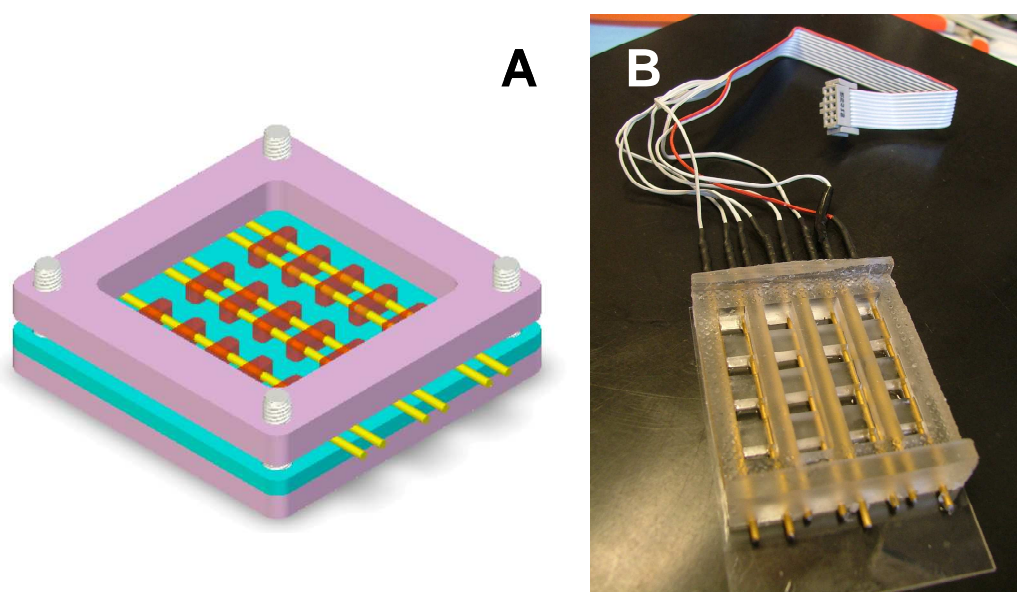

Figure 1 *Bioreactor for electrical stimulation (**A**) Schematic representation of the bioreactor design (**B**) Actual picture.*

The device was fabricated with stereolithographic method curing PDMS in a (material) mold. The mold, fabricated by (QuickParts, GA, USA), reproduces with a precision of 50 μm our specific drawing. The 10:1 mixture of PDMS and initiator (Dow Corning, MI) was poured in the mold where the electrodes were already inserted in specific holes. The inlet

and outlet holes of the electrodes were designed slightly smaller of the electrodes dimension in order to seal them. The PDMS bioreactor is attached directly to a (dimensions) glass slide via plasma treatment of both surfaces. The optical transparency of the glass slide allows the EB observation during the stimulation. EBs were suspended in a bioreactor well in a low ionic content ''pulsing buffer,'' which contained (in mM) sucrose, 255, CaCl2 1, MgCl2 1, and HEPES 5 (pH 7.2) (Sigma-Aldrich, St. Louis, MO) and had a conductivity of 500 μS/cm. The electrodes were connected to electrical stimulator generating square-wave electric pulses (Gras S88X, Astro-Med, Inc., West Warwick, RI). A single electrical field pulse with a field strength of 5 V/cm and duration of 90 s was applied to embryoid bodies.

C.2.3 Electrode material characterization

The electrode/electrolyte interface was characterized through electrochemical impedance spectroscopy (EIS) and charge injected measurements for different electrode materials. Electrodes (10 cm length x 1.6 mm diameter) were fabricated from 304 Stainless Steel and Titanium rods (McMaster-Carr, Atlanta, GA). Some of these Titanium rods were sent Eclat Industries Inc. (Levittown, NY), where they coated with Titanium Nitride. EIS measurements were performed with an electrochemical interface (Solartron 1287) and a frequency response analyzer (FRA, Solartron 1250) controlled by a computer with ZPlot software (Solartron Analytical, Oak Ridge, TN). The system was set up as the equivalent circuit shown in Figure 2A and associated parameters are determined using ZView 2.5b. This program plots the Nyquist and Bode plots for each condition. The EIS spectra were acquired over a frequency range from 1 x 106 to 1 x 10–2 Hz with perturbation amplitude of 10 mV, 100 mV and 1 V.

The current profile in the system during 90 s stimulations was measured by the potential drop profile across a 330 ohm resistor placed in series in the stimulation loop. The current value was calculated by dividing the potential measured across the resistor (with an oscilloscope) by the value of the resistor (Ohm's law). Since the current across the system

was low enough to reach the 10 mV lower limit of the oscilloscope, at least 11 measurements were taken for each material.

C.2.4 Cell Viability

The cell viability after 4 days of continuous electrical stimulation was studied in EBs through live/dead assay (Molecular Probes, Eugene, OR). The 4 days old EBs were stimulated continuously at 5 V/cm for 5 ms at the frequency of 1 Hz. This fluorescence based method detects live and dead cells using 3 mM calcein AM and 3 mM ethidium homodimer-1 (EthD-1) dye. The calcein AM is well retained within live cells and converted enzymatically in green fluorescent calcein (ex/em ~495 nm/~515 nm). EthD-1 enters cells with damaged membranes where it binds to nucleic acids, thereby producing a bright red fluorescence in dead cells (ex/em ~495 nm/~635 nm). Prior to staining, the EBs were washed with PBS to minimize serum esterase activity present in serum-supplemented growth medium. Serum esterases could increase background fluorescence by hydrolyzing calcein AM extracellularly. Each well was covered by 250 μL of the combined LIVE/DEAD dyes solution using concentration of 3 mM for calcein AM and ethidium. The solution was incubated for 90 minutes at room temperature. The labeled cells were analyzed using fluorescence microscope Zeiss inverted microscope.

C.2.6 ROS expression

Generation of intracellular reactive oxygen species was measured using the fluorescent dye dichlorofluorescein diacetate (DCFH-DA) (Sigma Aldrich, St. Louis, MO). DCFH-DA was stored at -20 °C at a concentration of 10 mg/mL in methanol. DCFH-DA is a nonpolar and nonfluorescent compound that can diffuse into the cell where it is deacetylated by cellular esterases into a nonfluorescent polar derivative 2′,7′-dichlorofluoroscein (DCFH) that is impermeable to cell membrane. DCFH is rapidly oxidized to the highly fluorescent dichlorofluorescein (DCF) in the presence of intracellular ROS. Embryoid bodies were incubated in Knockout medium containing 40 μM DCFH-DA for 30 min at room temperature. Embryoid bodies were then washed twice in a low conductivity medium (255 mM sucrose, 1 mM $CaCl2$, 1 mM $MgCl2$, and 5 mM HEPES),

and transferred to the bioreactor for electrical stimulation. Fluorescence images were taken with excitation wavelength of the 488 nm and emission wavelength of 530 nm every 20 s for the first minute and every minute after that. The fluorescence variation was calculated by taking ratio of average of fluorescence intensity at each time point after stimulation (F) to the initial value (F0).

C.2.6 Statistical Analysis

Significance of each data point was determined by Anova test, where a value of $P < 0.05$ was considered significant.

C.3 Results

C.3.1 Bioreactor characterization

In order to evaluate the influence of different electrode materials on effectiveness of embryoid bodies stimulation, the bioreactor was characterized through electrochemical impedance spectroscopy (EIS). Fixing the type of stimulation, the current profile in the system depends on the geometry of the system and properties of electrode materials, such as effective surface area or polarization resistance.

Bode and Nyquist plots, obtained by EIS analysis with a perturbation of 10 mV, are shown in Figure 1 for Stainless Steel (SS), Titanium (Ti) and Titanium Nitride (TiN)-coated (TiN) electrodes, respectively. The equivalent circuit shown in Figure 2A was used to fit the spectra and model the electrode-electrolyte interface. The interfacial capacitance and polarization resistance were obtained by this fitting and are summarized in Figure 2B.

The tested electrodes show similar interfacial capacitance of the order of 10^{-6} F/cm^2 whereas the polarization resistance (R_p) for Titanium and Titanium Nitride is an order of magnitude higher than for the Stainless Steel. This more accentuated curvature in the Nyquist plot gives a visual confirmation of this calculation.
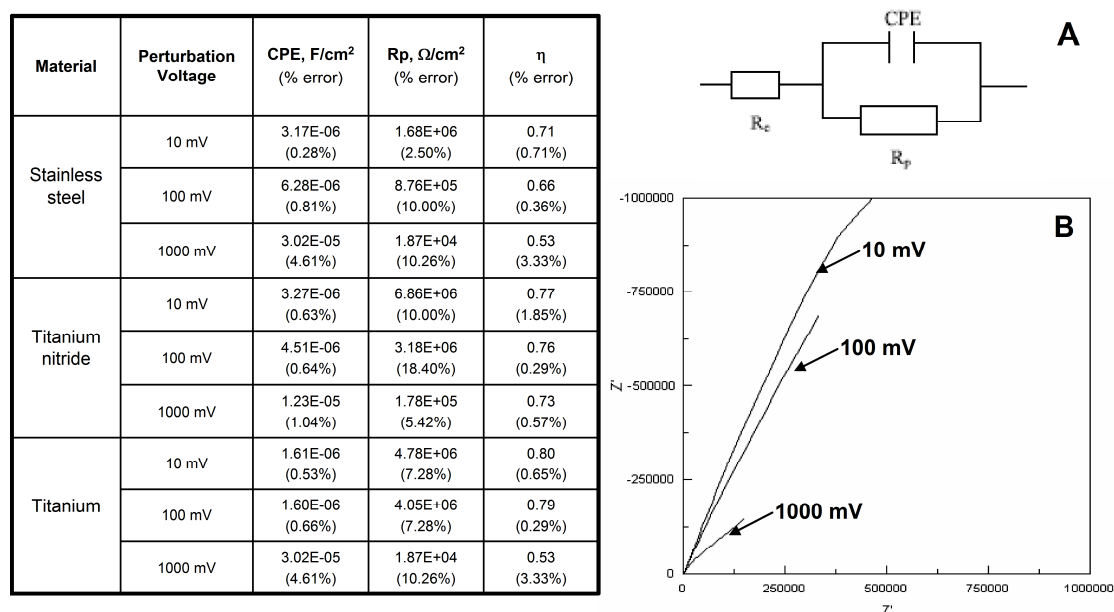
Material	Perturbation Voltage	CPE, F/cm² (% error)	Rp, Ω/cm² (% error)	η (% error)
Stainless steel	10 mV	3.17E-06 (0.28%)	1.68E+06 (2.50%)	0.71 (0.71%)
	100 mV	6.28E-06 (0.81%)	8.76E+05 (10.00%)	0.66 (0.36%)
	1000 mV	3.02E-05 (4.61%)	1.87E+04 (10.26%)	0.53 (3.33%)
Titanium nitride	10 mV	3.27E-06 (0.63%)	6.86E+06 (10.00%)	0.77 (1.85%)
	100 mV	4.51E-06 (0.64%)	3.18E+06 (18.40%)	0.76 (0.29%)
	1000 mV	1.23E-05 (1.04%)	1.78E+05 (5.42%)	0.73 (0.57%)
Titanium	10 mV	1.61E-06 (0.53%)	4.78E+06 (7.28%)	0.80 (0.65%)
	100 mV	1.60E-06 (0.66%)	4.05E+06 (7.28%)	0.79 (0.29%)
	1000 mV	3.02E-05 (4.61%)	1.87E+04 (10.26%)	0.53 (3.33%)

Figure 2 *In the table. Constant phase element (CPE), polarization resistance (Rp) and capacitance dispersion (η) calculated fitting the equivalent circuit of the electrode/electrolyte systems (**A**), where Re is the resistance of the electrolyte. (**B**) Nyquist plot of stainless steel electrodes at increasing perturbation voltage.*

Increasing the amplitude of the stimulus up to 1 V, the capacitance increases whereas the resistance to the reactions becomes up to two orders of magnitude lower, as summarized in Figure 1. These results agree with the changing on the Nyquist plot shape that becomes more and more curved, as shown in Figure 2.

The amount of charge injected was calculated for stimulations of 50 ms, 1 s and 90 s. The potential-time plots show an initial increasing of the potential followed by a rapid decrease due to the polarization of the medium and the shielding of charges on the electrode, as shown in Figure 3.

However the potential reaches values close to zero only for Ti and TiN, whereas for SS electrodes the reactions that occur in the electrode-electrolyte interface keep the potential higher up to saturation around 5 s.
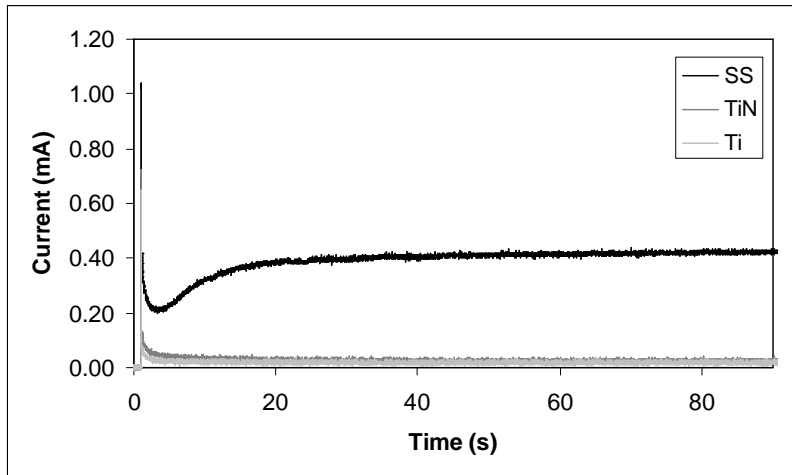
Figure 3 *Effects of electrode material on effectiveness of electrical stimulation (5 V/cm 90 s). Current vs time profile in the system during stimulation with stainless steel, titanium nitride and titanium electrodes.*

C.3.2 Cell viability and ROS expression

Continuous electrical stimulation doesn't compromise the embryoid bodies viability, as shown by the live and dead assay performed after 4 days of stimulation (5 V/cm).
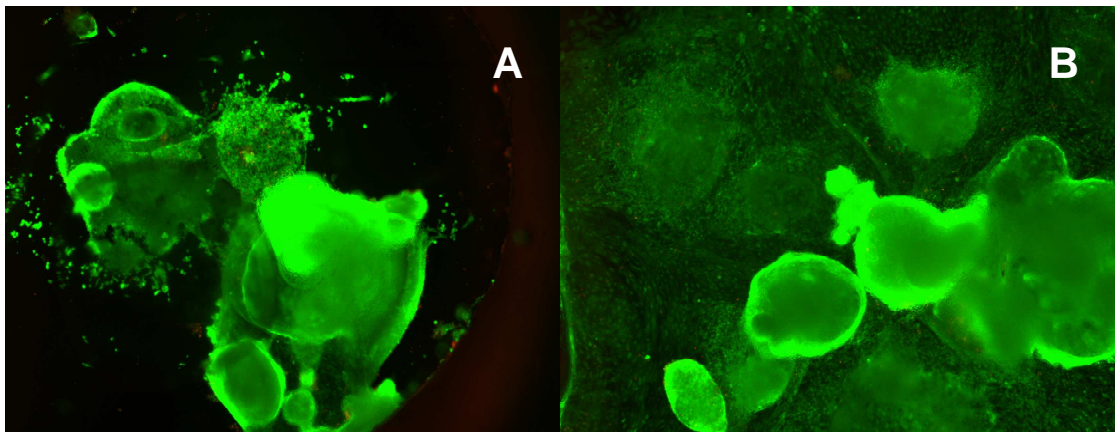

Figure 4 *Effect of electrical stimulation on cell viability. Live/Dead assay of 8 day-old EB non stimulated (**A***) and after 4 days continuous simulation at 5 V/cm (***B***).*

As shown in Figure 4, the presence of dead cells is negligible in stimulated and not stimulated EBs. Moreover the electrical stimulation seems to improve the cell attachment

as shown in Figure 4. This could be due to the passive increasing of intracellular calcium localization and consequent enhancement in the actin production (Mycielska and Djamgoz 2004).

The effect of the electrical stimulation on production of intracellular ROS was determined by the variation on fluorescence of oxidized DCF with 6 days-old embryoid bodies. The stimulation was performed at 5 V/cm and duration of 50 ms, 1 s and 90 s using Ti, TiN and SS rods as electrodes. As shown in Figure 5C, the intracellular ROS continuously increased during and after the field pulse, for up to 20 minutes when it seems to reach a plateau. The variation in fluorescence intensity can be quantified comparing the images collected at the beginning and after 20 min (Figure 5A-B).
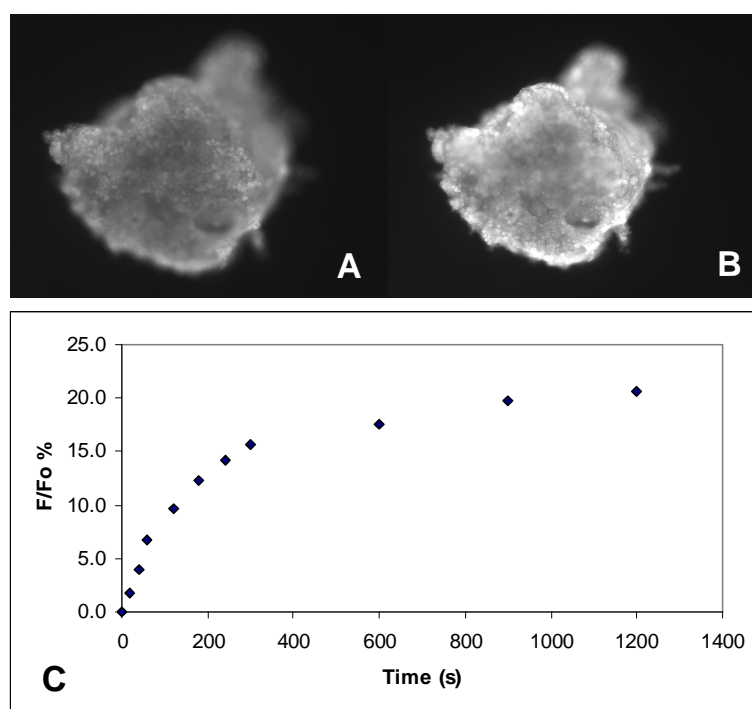

Figure 5. *Example of intracellular ROS due to electrical stimulation (5 V/cm 90 s). Fluorescence image of EB before stimulation (**A**) and after 20 minutes (**B**). (**C**) Time course of normalized dichlorofluorescein (DCF) after stimulation.*

This ratio between the average of fluorescence intensity at the beginning and after 20 min gives the amount of reactive oxygen species produced in the EB by the stimulation, as

summarized in Figure 6A. Considerable changes in ROS expression were observed with increasing durations of stimulation, as shown in Figure 6A.
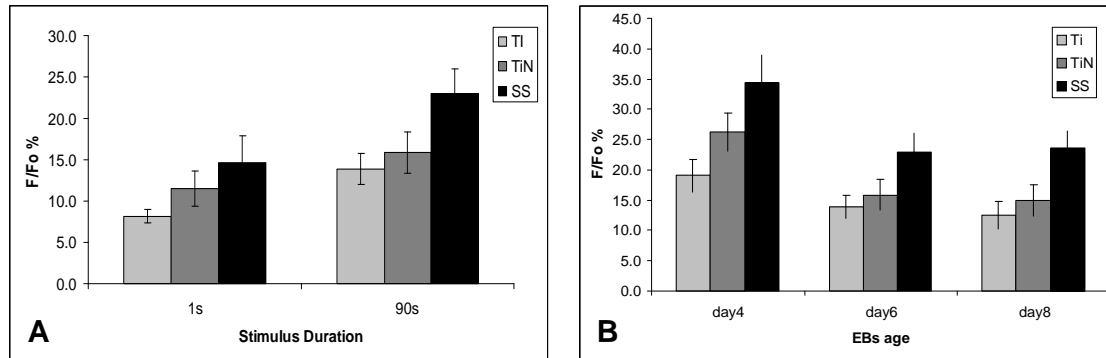

Figure 6 *Generation of reaction species (ROS) in embryoid bodies after electrical stimulation (5 V/cm) with different electrode materials.* (**A**) *Dichlorofluorescein (DCF) fluorescence increasing after 50 ms, 1 s and 90 s of stimulation.* (**B**) *Dichlorofluorescein (DCF) fluorescence increasing of 4, 6 and 8 days-old embryoid bodies after electrical field treatment.*

This concurrent increase suggests the dependence of the ROS production on the duration and strength of the stimulation. In particular, the difference between the electrodes is more significant for 90 s stimulation. The reactions on stainless steel electrodes keep a higher electric field constant for all 90 s stimulation, increasing the final expression of ROS. The difference between electrodes after 50 ms and 1 s stimulation is not significant.

Since human embryonic stem cells have been shown to begin differentiation toward cardiac lineage 4 days after EBs formation (Mummery, Ward et al. 2002) and they may show different reactivity to exogenous electric field at different stage of the development, it seemed interesting to check the ROS expression after electrical stimulation of 5 V/cm for 90 s of 4, 6 and 8 days-old embryoid bodies. The fluorescence variation was calculated as previously described. As shown in Figure 6B, embryoid bodies 4 days old exhibited higher increase of fluorescence than at day 6 or 8.

C.3.3 Cardiac differentiation

To evaluate whether electrical field and intracellular ROS expression enhances cardiomyocyte differentiation of hESC, 4 and 7 day-old EBs were exposed to a single

electrical field pulse with field strength of 5 V/cm and duration of 90 s, and then plated. Titanium Nitride electrodes were used for this stimulation because of its intermediate effect upon the increase of ROS production. After 3 days of culture (after plating), embryoid bodies started to beat spontaneously. The number of beating EBs increases day by day up to age of 19 days-old. The percentage of beating embryoid bodies at this stage is summarized in Figure 7.

Treatment of EBs with a single electrical field pulse of 90 s at 5 V/cm slightly stimulated cardiomyogenesis. In particular higher percentage of beating embryoid bodies was observed in embryoid bodies seeded at day 4. Under these experimental conditions, the number of beating embryoid bodies (in %) was 11.4 and 7.6 for EBs stimulated at 4 and 7 day-old respectively.
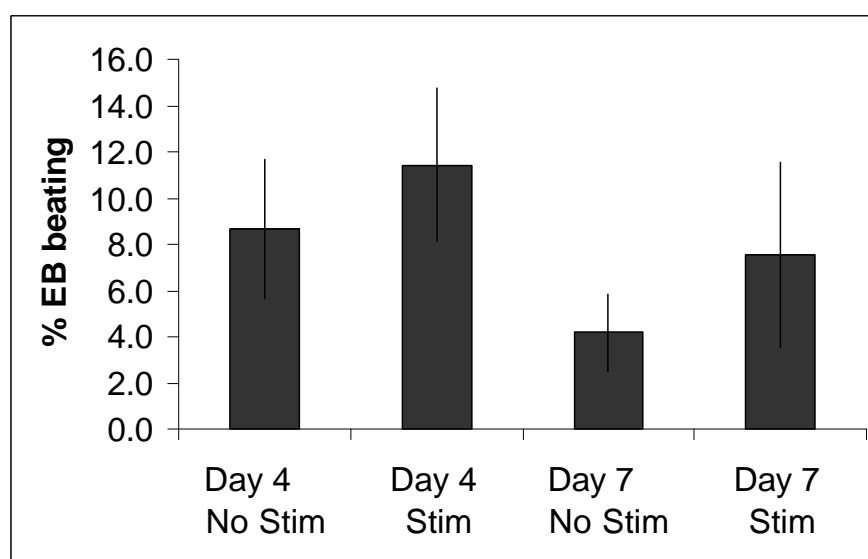

Figure 7 *Effect of electrical stimulation on cardiomyocyte differentiation. 4 and 7 days-old EBs were plated and then stimulated with 5 V/cm 90 s pulse with Titanium Nitride electrodes. Percentage of beating EBs was evaluated in 19 days-old EBs.*

C.4 Discussion

The presences of endogenous electric field during the embryonic development and the effects of exogenous one for different kind of cells have been already reported in several studies (Jaffe and Nuccitelli 1977; Nuccitelli 2003). However the interpretation of the cellular response to such fields is complicated by inadequate characterization of the system used for stimulation. Uncertainties about the type and magnitude of field make difficult the individuation of the biophysical and biochemical mechanisms activated on the considered biological system. Here we report differences in intracellular ROS generation solely due to choice of electrode material.

In biological applications, material selection for electrodes is a complex issue. The ideal material for use as a stimulating electrode must be biocompatible, have stable characteristics during the stimulation and acceptable mechanical properties. The effects of electrical stimulation are strongly dependent on the electrode geometry and material properties. The charge-transfer at the electrode-electrolyte interface happens through three mechanisms: (i) non-faradaic charging/discharging of the electrochemical double layer, (ii) reversible faradaic reactions, and (iii) non-reversible faradaic reactions (Merrill, Bikson et al. 2005; Cannizzaro, Tandon et al. 2006). Electrochemical impedance spectroscopy (EIS) gives information about the relative presence of each mechanism, determining the value of capacitance and resistance to reactions for each specific electrode.

This method was used here to characterize different electrodes in stainless steel, titanium and titanium nitride. The data shows mainly differences on polarization resistance (R_p) value, which is much lower for Stainless Steel. In agreement with this result, the potential-time plot for stainless steel is kept to constant value of 0.4 mA by the presence of reactions on its surface during the stimulation. For titanium and titanium nitride we have instead an initial increasing of the potential followed by a rapid decrease up to a value close to zero due to the polarization of the medium and the shielding of charges on the electrode.

Previous studies have shown the correlation between electrical stimulation and ROS expression in different kind of cells, including murine embryonic stem cells (Wartenberg,

Hescheler et al. 1997; Heinrich Sauer 1999). Here we show that the applied electric field lead to generation of intracellular ROS in human embryonic stem cells. The EIS results were useful to evaluate the correlation between duration of a stimulation and ROS expression on human EBs, which was evaluated monitoring the expression of DCF fluorescence for 20 min. In agreement with these results, the use Stainless Steel electrodes and the increasing of stimulation duration enhance the intracellular ROS expression.

Since mouse embryonic stem cells have shown a reduction of the intracellular ROS production during development (Sauer, Rahimi et al. 2000), it was interesting to check what was the behavior of human cell. EBs of different stages of development (4, 6 and 8 days-old) were stimulated with 5 V/cm and 90 s, showing an maximum expression of ROS at 4 days-old.

The decay ROS generation may be likely due to down regulation of NADPH oxidase activity during the development, as already shown for mESC (Sauer, Rahimi et al. 2000). The active role of NADPH oxidase in differentiation, already shown in other cell type (Li, Stouffs et al. 2006), may suggest the higher predisposition of the hESC to a cardiac differentiation and a more efficacious electrical stimulation at earlier stage of development

This hypothesis is confirmed by the measure of the percentage of beating 19 days-old EBs. EB start beating with higher percentage if seeded at earlier stage of differentiation and if stimulated at 5 V/cm for 90 s.

Even if the role of ROS in the cardiac lineage differentiation in human embryonic stem cell has still not been investigated, these results seems promising in the final propose of enhancing the number of differentiated human embryonic stem cell through electric stimulation.

C.5 References

Boyle, A. J., S. P. Schulman, et al. (2006). "Stem Cell Therapy for Cardiac Repair: Ready for the Next Step." Circulation **114**(4): 339-352.

C. H. Lohmann, Z. Schwartz, et al. (2000). "Pulsed electromagnetic field stimulation of MG63 osteoblast-like cells affects differentiation and local factor production." Journal of Orthopaedic Research **18**(4): 637-646.

Cannizzaro, C., N. Tandon, et al. (2006). "Practical aspects of cardiac tissue engineering with electrical stimulation." Methods in molecular medicine.

Djamgoz, M. B. A., M. Mycielska, et al. (2001). "Directional movement of rat prostate cancer cells in direct-current electric field: involvement of voltagegated Na+ channel activity." J Cell Sci **114**(14): 2697-2705.

Donna R. Trollinger, R. R. I. R. N. (2002). "Calcium channel blockers inhibit galvanotaxis in human keratinocytes." Journal of Cellular Physiology **193**(1): 1-9.

Fukuda, K. and S. Yuasa (2006). "Stem Cells as a Source of Regenerative Cardiomyocytes." Circ Res **98**(8): 1002-1013.

Heinrich Sauer, G. R., Jürgen Hescheler, Maria Wartenberg, (1999). "Effects of electrical fields on cardiomyocyte differentiation of embryonic stem cells." Journal of Cellular Biochemistry **75**(4): 710-723.

Heng, B. C., T. Cao, et al. (2004). "An overview and synopsis of techniques for directing stem cell differentiation in vitro, Cell and Tissue Research." Cell Tissue Res **315**(3): 291-303.

Heng, B. C., H. K. Haider, et al. (2004). "Strategies for directing the differentiation of stem cells into the cardiomyogenic lineage in vitro." Cardiovascular Research **62**(1): 34-42.

Hong Wei, O. J., Jinliang Li, Yelena S. Tarasova, Kenneth R. Boheler (2005). "Embryonic stem cells and cardiomyocyte differentiation: phenotypic and molecular analyses." J. Cell. Mol. Med. **9**(4): 804-817.

Izhak Kehat, D. K.-K., Mirit Snir, Hana Segev, Michal Amit, Amira Gepstein, Erella Livne, Ofer Binah, Joseph Itskovitz-Eldor, Lior Gepstein (2001). "Human embryonic stem cells can differentiate into myocytes with structural and functional properties of cardiomyocytes." J Clin Invest. **108.**(3): 407–414.

Jaffe, L. F. and R. Nuccitelli (1977). "Electrical Controls of Development." Annual Review of Biophysics and Bioengineering **6**(1): 445-476.

Joshua Rutenberg, S.-M. C. M. L. (2002). "Early embryonic expression of ion channels and pumps in chick and <I>Xenopus</I> development." Developmental Dynamics **225**(4): 469-484.

Kenneth R. Robinson, M. A. M. (2003). "Left/right, up/down: The role of endogenous electrical fields as directional signals in development, repair and invasion." BioEssays **25**(8): 759-766.

Laflamme, M. A., J. Gold, et al. (2005). "Formation of Human Myocardium in the Rat Heart from Human Embryonic Stem Cells." Am J Pathol **167**(3): 663-671.

LEV, S., I. KEHAT, et al. (2005). "Differentiation Pathways in Human Embryonic Stem Cell-Derived Cardiomyocytes." Ann NY Acad Sci **1047**(1): 50-65.

Li, J., M. Stouffs, et al. (2006). "The NADPH Oxidase NOX4 Drives Cardiac Differentiation: Role in Regulating Cardiac Transcription Factors and MAP Kinase Activation." Mol. Biol. Cell: E05-06-0532.

Lodish, Berk, et al. (2003). Molecular Cell Biology. New York, W.H Freeman and Company.

Lovell, M. J. and A. Mathur (2004). "The role of stem cells for treatment of cardiovascular disease." Cell Proliferation **37**(1): 67-87.

McCaig, C. D., A. M. Rajnicek, et al. (2005). "Controlling Cell Behavior Electrically: Current Views and Future Potential." Physiol. Rev. **85**(3): 943-978.

Merrill, D. R., M. Bikson, et al. (2005). "Electrical stimulation of excitable tissue: design of efficacious and safe protocols." Journal of Neuroscience Methods **141**(2): 171-198.

Mie, M., T. Endoh, et al. (2003). "Induction of neural differentiation by electrically stimulated gene expression of NeuroD2." Journal of Biotechnology **100**(3): 231-238.

Mummery, C., D. Ward, et al. (2002). "Cardiomyocyte differentiation of mouse and human embryonic stem cells." Journal of Anatomy **200**(3): 233-242.

Mycielska, M. E. and M. B. A. Djamgoz (2004). "Cellular mechanisms of direct-current electric field effects: galvanotaxis and metastatic disease." J Cell Sci **117**(9): 1631-1639.

Norlin, A., J. Pan, et al. (2002). "Investigation of interfacial capacitance of Pt, Ti and TiN coated electrodes by electrochemical impedance spectroscopy." Biomolecular Engineering **19**(2-6): 67-71.

Nuccitelli, R. (2003). "Endogenous electric fields in embryos during development, regeneration and wound healing." Radiat Prot Dosimetry **106**(4): 375-383.

Odorico, J. S., D. S. Kaufman, et al. (2001). "Multilineage Differentiation from Human Embryonic Stem Cell Lines." Stem Cells **19**(3): 193-204.

Passier, R. and C. Mummery (2005). "Cardiomyocyte differentiation from embryonic and adult stem cells." Current Opinion in Biotechnology Tissue and cell engineering/Biochemical engineering **16**(5): 498-502.

Puceat, M. (2005). "Role of Rac-GTPase and Reactive Oxygen Species in Cardiac Differentiation of Stem Cells." Antioxidants & Redox Signaling **7**(11-12): 1435-1439.

Puceat, M., P. Travo, et al. (2003). "A Dual Role of the GTPase Rac in Cardiac Differentiation of Stem Cells." Mol. Biol. Cell **14**(7): 2781-2792.

Pullar, C. E. and R. R. Isseroff (2005). "Cyclic AMP mediates keratinocyte directional migration in an electric field." J Cell Sci **118**(9): 2023-2034.

Rhee, S. G. (1999). "Redox signaling: hydrogen peroxide as intracellular messenger." Experimental and Molecular Medicine **31**(2): 53-59.

Richard Nuccitelli (1992). "Endogenous ionic currents and DC electric fields in multicellular animal tissues." Bioelectromagnetics **13**(S1): 147-157.

Robinson, K. (1985). "The responses of cells to electrical fields: a review." J. Cell Biol. **101**(6): 2023-2027.

Sauer, H., M. M. Bekhite, et al. (2005). "Redox control of angiogenic factors and CD31-positive vessel-like structures in mouse embryonic stem cells after direct current electrical field stimulation." Experimental Cell Research **304**(2): 380-390.

Sauer, H., G. Rahimi, et al. (2000). "Role of reactive oxygen species and phosphatidylinositol 3-kinase in cardiomyocyte differentiation of embryonic stem cells." <u>FEBS Letters</u> **476**(3): 218-223.

Sauer, H. and M. Wartenberg (2005). "Reactive Oxygen Species as Signaling Molecules in Cardiovascular Differentiation of Embryonic Stem Cells and Tumor-Induced Angiogenesis." <u>Antioxidants & Redox Signaling</u> **7**(11-12): 1423-1434.

Schmelter, M., B. Ateghang, et al. (2006). "Embryonic stem cells utilize reactive oxygen species as transducers of mechanical strain-induced cardiovascular differentiation." <u>FASEB J.</u> **20**(8): 1182-1184.

Shah, A. M. and H. Sauer (2006). "Transmitting biological information using oxygen: Reactive oxygen species as signalling molecules in cardiovascular pathophysiology." <u>Cardiovascular Research</u> **71**(2): 191-194.

Song, B., M. Zhao, et al. (2002). "Electrical cues regulate the orientation and frequency of cell division and the rate of wound healing invivo." <u>PNAS</u> **99**(21): 13577-13582.

Sun, Y. and L. W. Oberley (1996). "Redox regulation of transcriptional activators." <u>Free Radical Biology and Medicine</u> **21**(3): 335-348.

Walter Hong-Shong Chang, L.-T. Chen, et al. (2004). "Effect of pulse-burst electromagnetic field stimulation on osteoblast cell activities." <u>Bioelectromagnetics</u> **25**(6): 457-465.

Wartenberg, M., J. Hescheler, et al. (1997). "Electrical fields enhance growth of cancer spheroids by reactive oxygen species and intracellular Ca2+." <u>Am J Physiol Regul Integr Comp Physiol</u> **272**(5): R1677-1683.

Zhao, M., H. Bai, et al. (2004). "Electrical stimulation directly induces pre-angiogenic responses in vascular endothelial cells by signaling through VEGF receptors." <u>J Cell Sci</u> **117**(3): 397-405.

Zhao, M., J. V. Forrester, et al. (1999). "A small, physiological electric field orients cell division." <u>PNAS</u> **96**(9): 4942-4946.

Zhao, M., J. Pu, et al. (2002). "Membrane lipids, EGF receptors, and intracellular signals colocalize and are polarized in epithelial cells moving directionally in a physiological electric field." <u>FASEB J.</u> **16**(8): 857-859.

Appendix D

Practical aspects of cardiac tissue engineering with electrical stimulation

Christopher Cannizzaro[a], **Nina Tandon**[a], **Elisa Figallo**[ab], **Hyoungshin Park**[a],

Sharon Gerecht[a], **Milica Radisic**[c], **Nicola Elvassore**[b], **Gordana Vunjak-Novakovic**[d§]

[a] Harvard – MIT for Health Sciences and Technology, Massachusetts Institute of Technology, Cambridge MA

[b] Department of Chemical Engineering, University of Padova, Italy

[c] Department of Chemical Engineering and Applied Chemistry, University of Toronto, Toronto, Ontario M5S 3E5

[d] Department of Biomedical Engineering, Columbia University, 1210 Amsterdam Avenue, MC 8904, New York NY 10027

[§] Corresponding authors

Abstract

Heart disease is a leading cause of death in Western society. Despite the success of heart transplantation, a chronic shortage of donor organs, along with the associated immunological complications of this approach, demands that alternative treatments be found. One such option is to repair, rather than replace, the heart with engineered cardiac tissue. Multiple studies have shown that in order to attain functional tissue, assembly signaling cues must be recapitulated *in vitro*. In their native environment, cardiomyocytes are directed to beat in synchrony by propagation of pacing current through the tissue. Recently, we have shown that electrical stimulation directs neonatal cardiomyocytes to assemble into native-like tissue *in vitro*. This chapter provides detailed methods we have employed in taking this biomimetic approach. After an initial discussion on how electric field stimulation can influence cell behavior, we examine the practical aspects of cardiac tissue engineering with electrical stimulation such as electrode selection and cell seeding protocols, and conclude with what we feel are the remaining challenges to be overcome.

D.1 Introduction

The overall goal of cardiac tissue engineering is to direct the cells to (re)establish the structure and function of the native tissue being repaired over clinically relevant thicknesses, ~ 1 cm for adult human heart (Zammaretti and Jaconi 2004). The utility of engineered cardiac grafts depends on cell survival, integration, functionality, and electrical coupling (Zimmermann, Didie et al. 2002). To engineer functional myocardium, we used a "biomimetic" approach that involves the cultivation of cardiac cell populations on scaffolds (designed to provide a structural and logistic template for tissue formation), using bioreactors (designed to provide environmental control and biophysical signaling). This approach involves three related aspects: (a) establishment and maintenance of physiologic density of viable cells, (b) convective-diffusive oxygen supply to the cells using channeled scaffolds (to mimic the capillary flow) and oxygen carriers in culture medium (to mimic the role of hemoglobin) and (c) electrical field stimulation (to induce excitation-contraction cell coupling). In this chapter, we focus on the electrical stimulation aspect of cardiac tissue engineering.

Native heart tissue has low resistance pathways for electrical signal propagation due to presence of gap junctions and high cell density. Individual cells are packed tightly together and held in place by tight junctions, such that the myocardium acts as a synctium (Malmivuo and Plonsey 1995; Basser and Roth 2000; Merrill, Bikson et al. 2005). To induce synchronous contractions of cultured cardiac constructs, we apply electrical signals designed to mimic those orchestrating the synchronous contractions of cells in native heart. Over only 8 days *in vitro*, electrical field stimulation can induce cell alignment and coupling, increase the amplitude of synchronous construct contractions and result in a remarkable level of ultrastructural organization. Electrical stimulation can promote cell differentiation and coupling, as evidenced

by the presence of striations and gap junctions, and it results in concurrent development of conductive and contractile properties of cardiac constructs (Figure 1) (Radisic, Park et al. 2004).
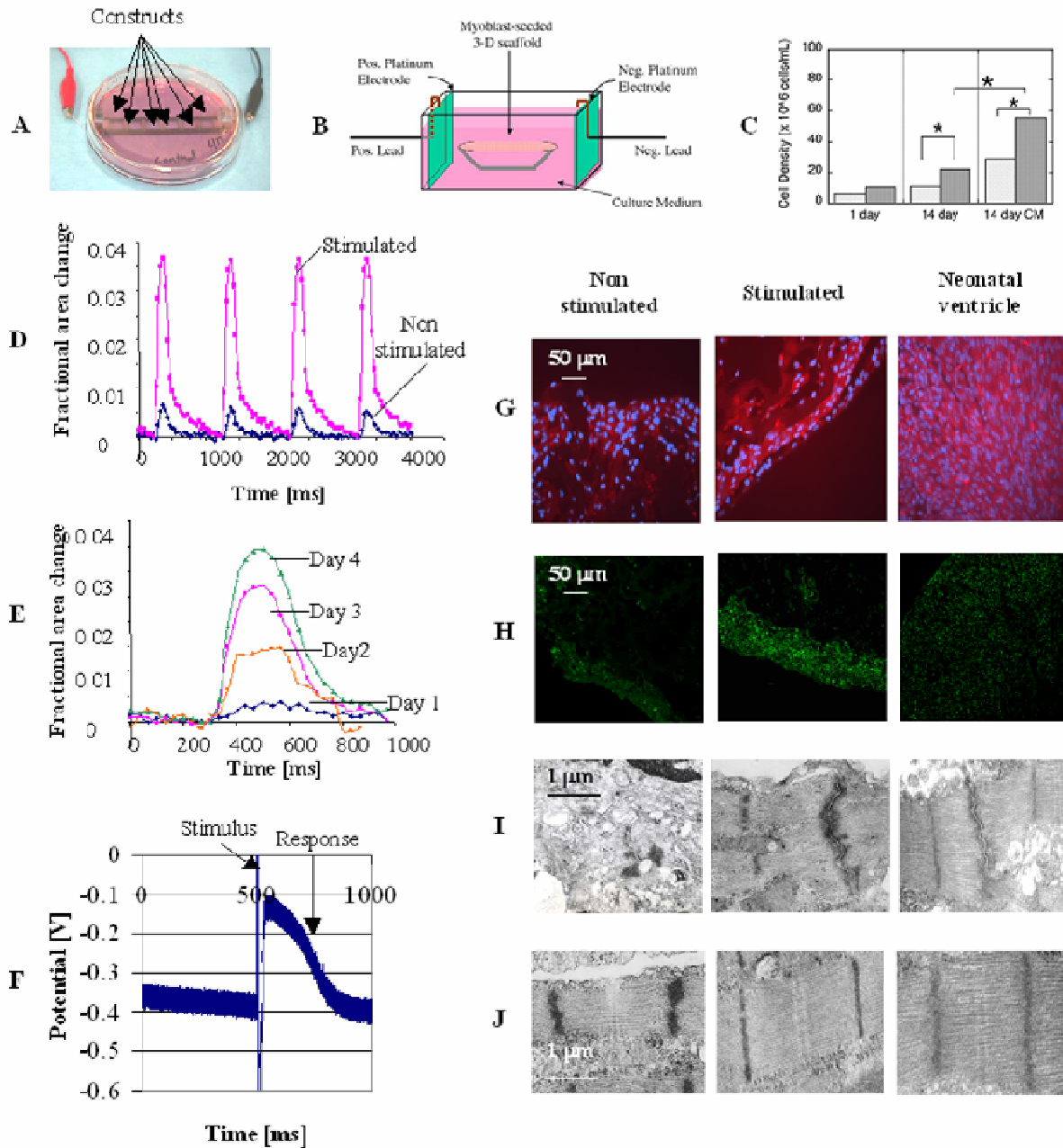

Figure 1 *Electrical stimulation promoted myocyte differentiation and functional.* (**A**) *Experimental setup for supra-threshold stimulation of cardiac myocytes cultured on a elastic, porous scaffold. A Petri dish is*

*fitted with two stimulating electrodes that generate electrical field gradiants with a supra-threshold amplitude; results are shown in D-J. (**B**) Experimental setup for stimulation of endfothelial cells on a polymer scaffold. A chamber is fitted with two platinum electrodes generating electrical field stimuli with a sub-threshold amplitude; results are shown in C. (**C**) Enhanced cell proliferation. (**D**) Contraction amplitude was 7 times higher in stimulated than non-stimulated constructs. (**E**) Contraction amplitude progressively increased with time of stimulation. (**F**) Contractile activity was associated with the propagation of action potential at cell membranes. Expression of a-MHC (**G**) and gap junctional protein connexin-43; immunostains. (**H**) were markedly higher in stimulated group. Stimulated constructs had well developed myofibrills with parallel sarcomeres and intercalated discs placed symmetrically between the Z lines. I. Intercalated discs, J. Sarcomeres.*

D.2 Materials

Bioreactor

1. 60-mm glass Petri dish (VWR, West Chester, PA).

2. 6-well polystyrene plate (NalgeNunc International, Rochester, NY).

3. 3.0-mm biopsy punch (MedExSupply Co., Monsey, NY).

4. Poly-dimethylsiloxane (PDMS, Sylgard 184, Dow Corning, MI).

5. Stainless steel push pins (size 000, Fine Science Tools, N. Vancouver, Canada).

6. Electrodes, all in form of a 1/8" rod:

    a. Carbon (12" x 0.120", Ladd Research, Williston, NY).

    b. Stainless steel, type 303 (McMaster-Carr, Atlanta, GA).

    c. Titanium, grade 2 (McMaster-Carr).

    d. Titanium nitride (TiN) coated titanium, grade 2 (Eclat Industries, Inc., Levittown, NY).

7. Platinum wire (0.005" diameter, Ladd Research).

Electrical characterization of bioreactor

1. Electrochemical impedance spectroscopy: Solartron 1287 and Solartron 1250 FRA (Solartron Analytical, Oak Ridge, TN) interfaced to computer with ZPlot software (Scribner Associates, Southern Pines, NC).

2. Digital oscilloscope with storage capability: TDS3000B (Techtronix, Richardson, TX).

3. Alligator clips and test leads (Mouser, Mansfield, TX).

4. 10 Ω resistors (Mouser).

5. Phosphate-buffered saline (PBS) calcium- and magnesium-free (Gibco/BRL, Bethesda, MD).

Electrical stimulation

1. Dual output square pulse stimulator (Grass S88X, Astro-Med, Inc., West Warwick, RI) *and/or*

2. Custom computer-controlled stimulator consisting of:

   a. Data acquisition and control software: Labview 7.1 (National Instruments, Austin, TX).

   b. Analog output board with 8 independent channels: NI 6713 (National Instruments).

   c. I/O connector block and cable: SCB 68 and R6868 (National Instruments).

   d. Amplifier board and power supply: for each channel, one high current operational amplifier connected in unity-gain mode (TI OPA-551, Digikey, Thief River Falls, MN) and one Elpac 43 W power supply (WM220-1, Digikey) for all channels.

3. Flat ribbon cable (16 wire, 26 AWG) and IDC ribbon cable interconnects (Mouser).

Cell culture

1. Hank's balanced salt solution (HBSS) and PBS with 1 M of HEPES buffer (Gibco/BRL).

2. Trypsin (U.S. Biochemicals, Cleveland, OH).

3. Collagenase type II (Worthington, Freehold, NJ).

4. Matrigel® (Becton Dickinson, Bedford, MA).

5. Ultrafoam hemostat collagen sponge (Davol Inc., Cranston, RI).

6. Cardiac growth medium: Dulbecco's modified Eagle Medium (DMEM), 10% fetal bovine serum (FBS), 1% HEPES and 1% penicillin (10,000 U/ml) / streptomycin (10,000 µg/ml), all from Gibco/BRL.

Histological analysis

1. 10% buffered-formalin (Sigma Diagnostic, St. Louis, MO).

2. Horse serum (Vector Laboratories, Burlingame CA).

3. Tween 20 (Sigma, St. Louis, MO).

4. Avidin–biotin complex agent (Sigma).

5. 3,39-diaminobenzidine (Sigma).

6. Mouse anti-cardiac troponin I (TnI, Biodesign, Saco, ME), 1:150 dilution in PBS containing 0.5% Tween 20 and 1.5% horse serum.

7. Rabbit anti-connexin 43 (Cx43, Chemicon International, Temecula, CA), 1:150 dilution in PBS containing 0.5% Tween 20 and 1.5% horse serum.

8. Horse anti-mouse IgG, Standard Elite ABC kit (Vector Laboratories), 1:200 dilution in PBS containing 0.5% Tween 20 and 1.5% horse serum.

9. Fluorescein-conjugated goat anti-rabbit IgG (Sigma), 1:200 dilution in PBS containing 0.5% Tween 20 and 1.5% horse serum.

Ultrastructure analysis

1. Karnovsky's reagent: 0.1 M sodium cacodylate with 2% paraformaldehyde and 2.5% gluteraldehyde, pH = 7.4.

2. Epoxy embedding kit (Epon 812, SPI Supplies, West Chester, PA).

3. 1% osmium tetroxide in veronal-acetate buffer.

4. Graded ethanol in propylene oxide.

5. Lead citrate.

6. Uranyl acetate.

D.3 Methods

Bioreactor assembly

To assess cell alignment after stimulation, it is desirable to maintain a constant alignment of scaffolds with respect to the direction of the electric field gradient, while at the same time not restricting the contractions of the tissue construct nor the ability to observe the constructs with a microscope. We accomplish this task using stainless-steel pins, held in place by a thin layer of PDMS at the bottom of a Petri dish (see Figure 2). Below is protocol for bioreactor assembly, while scaffold positioning is covered in the following sections.
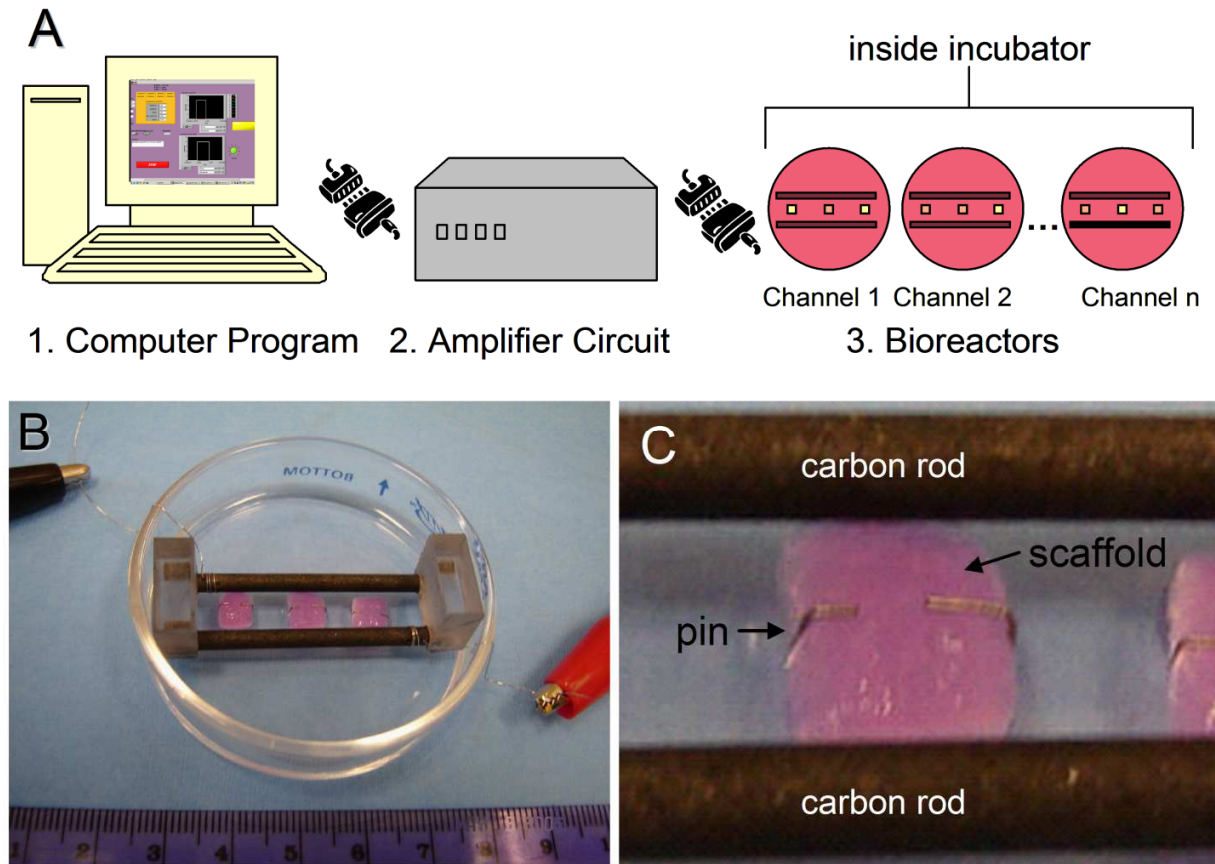
Figure 2 Experimental setup for supra-threshold stimulation of cardiac myocytes**.** (**A**) *Electrical stimulation voltages are set using a computer program, output through 8-channel AO card, amplified, and interfaced to bioreactors.* (**B**) *60 mm Petri dish with carbon rod electrodes, spaced 1 cm apart.* (**C**) *Close up view of scaffold positioned between electrodes and held in place with two stainless steel pins.*

1. Prepare 10 g of the 10:1 mixture of PDMS and initiator. Pour 7 g of mixture into one 60-mm glass Petri dish and de-gas under vacuum for 1 h. Cure in oven at 65 °C for 2 h. The final thickness of PDMS is 0.3 cm, thick enough to hold pins in place, but thin enough to observe scaffolds with an inverted microscope.

2. Prepare an additional 60 g of the 10:1 mixture of PDMS and initiator, add 10 g to each well of a six-well plate, and cure. The final thickness of PDMS in each well will be 1.0 cm.

3. Remove PDMS disks (3.5 cm diameter) from well and cut in half. Use 3.0 mm biopsy punch to make 2 holes along linear surface, 1.0 mm from bottom edge, and spaced 1.0 cm apart.

4. Cut electrode rods to length of 5.0 cm.

5. Wrap wire multiple times around ends of each rod. For carbon rods, drill a small hole in end of rod and insert wire before wrapping. Leave an additional 10 cm of wire attached to each electrode.

6. Insert two rods into punched holes of one PDMS half-disk. On opposing end, insert rods into a second half-disk. Length of electrode exposed to electrolyte is 4.0 cm.

7. Place electrode/PDMS block into center of Petri dish with PDMS base. Electrode supports may need to be trimmed to fit.

Electrical characterization of bioreactor

Stimulation efficiency is determined by the ability to attain a desired physiological response with minimal damage to the surrounding tissue. For each application, electrical stimulation conditions should be optimized by not only choosing appropriate electrode geometry but also by studying electrode material properties and charge-transfer characteristics at the electrode-electrolyte interface. Electrodes must be biocompatible to avoid toxic or immune responses in the adjacent tissue or medium, and they should efficiently transfer charge from the electrode material where it is carried by *free electrons* to the medium or tissue where it is carried by *ions*. Charge transfer can occur through three mechanisms: (i) non-faradaic charging/discharging of the electrochemical double layer, (ii) reversible faradaic reactions, and (iii) non-reversible faradaic reactions. The first two mechanisms are desirable, while the last should be avoided because it is associated with

electrode degradation and harmful byproducts. The relative presence of each mechanism can be assessed using electrochemical impedance spectroscopy (EIS), from which an equivalent circuit of the stimulation system can be constructed.

EIS measurements of bioreactor

In our laboratory, EIS measurements are taken with an electrochemical interface (Solartron 1287) and a frequency response analyzer (FRA, Solartron 1250) controlled by a computer with ZPlot software. Equivalent circuits and associated parameters are determined using ZView 2.5b. Please see (Norlin, Pan et al. 2004; Norlin, Pan et al. 2005; Norlin, Pan et al. 2005) for additional information on EIS measurement of common electrode materials.

1. Take electrochemical impedance spectroscopy (EIS) measurements of electrodes in Petri dish with 20 ml of PBS (see Note 1). Acquire EIS spectra over a frequency range from 1 x 10^6 to 1 x 10^{-2} Hz with a perturbation amplitude of 10 mV.

2. Record for each frequency the real (resistive) and imaginary (capacitive) components of the impedance response, Z' and Z'', respectively.

3. Evaluate data in ZView to generate Nyquist and Bode plots for each condition (see Note 2).

4. Create an "equivalent circuit" of the system using resistors and capacitors in series and in parallel (see Note 3). Calculate the values for *CPE*, R_p and η using instant fit functions in ZView software. An example of EIS analysis of common electrode materials (carbon, stainless steel, titanium, and titanium nitride) is shown in Figure 3 and extended studies on carbon are shown in Figure 4.
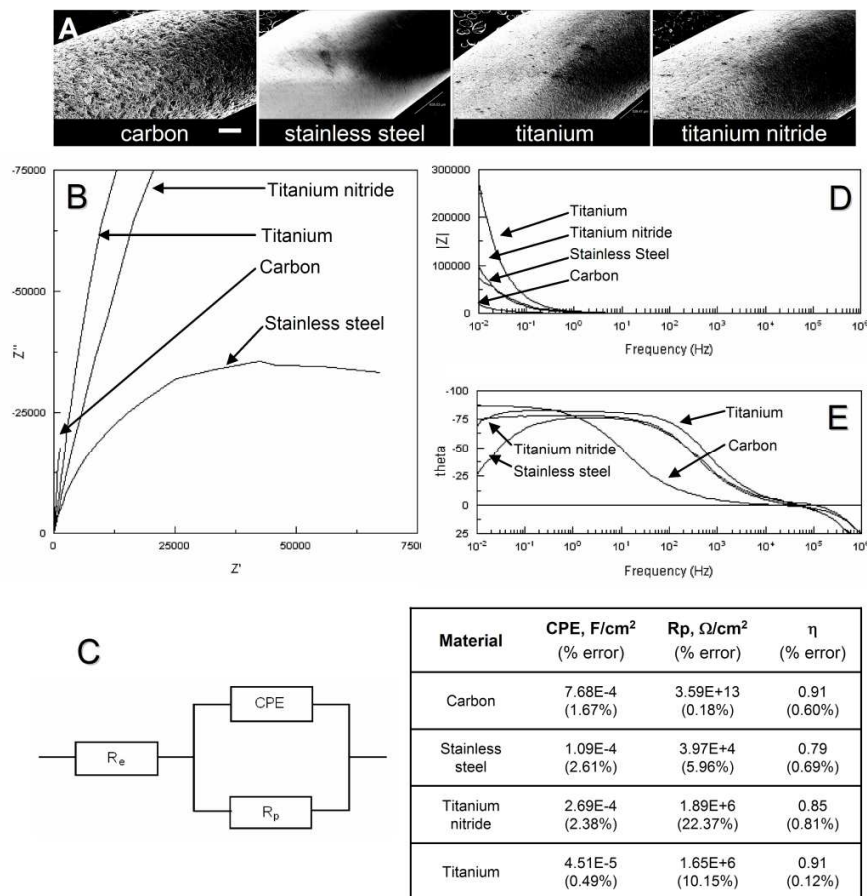
Figure 3 *Electrical characterization of stimulation electrodes with EIS. 30x scanning electron microscopy (SEM) images of electrodes, 1/8" diameter (*A*). White bar corresponds to 500 μm. The semicircular shape of stainless steel in the Nyquist plot (*B*) suggests the presence of reactions, whereas titanium, titanium nitride, and carbon have progressively more linear profiles associated with high polarization resistance. When the electrode/electrolyte interface is modeled with an equivalent circuit (*C*), where R_p is the polarization resistance, CPE a constant phase element, and R_e electrolyte resistance, the relatively low value of R_p for stainless steel confirms that it is more susceptible to faradaic reactions, and hence corrosion. At the other extreme, the carbon electrodes are best suited for electrical stimulation: their very high R_p value minimizes faradaic reactions and the relatively high CPE value indicates that the electrode transfers more charge to electrolyte, and hence tissue construct. Furthermore, as indicated in the Bode plots (*D*,*E*), carbon has the lowest impedance modulus |Z| across all frequencies. Experimental setup was as shown in Figure 2 with 4 cm electrodes and 10 mV perturbation.*

Current measurement in the bioreactor

The amount of injected charge is calculated simply by measuring the potential drop across a resistor placed in series in the stimulation loop.

1. Place 10 Ω resistance in series with the bioreactor in the stimulation loop. The value of this resistance is high enough to allow measurement of a voltage across the electrode, even with small current.

2. Apply the stimulus (e.g., 5 V, 2 ms square wave). Check with oscilloscope that intended waveform is faithfully applied to bioreactor. If not, current limit of stimulator may be exceeded and corrective action must be taken (e.g., electrode area or medium conductivity reduced or current rating of stimulator increased).

3. Record over time the voltage across the resistor with the oscilloscope, and for each time point, calculate the value of current by dividing the voltage across the resistor by the resistance value (Ohm's law).

4. Calculate the total amount of injected charge by integrating the current profile for the duration of the stimulus. Current profiles and calculated injected charge for electrodes of different materials (carbon, stainless steel, titanium, and titanium nitride) are shown in Figure 5.
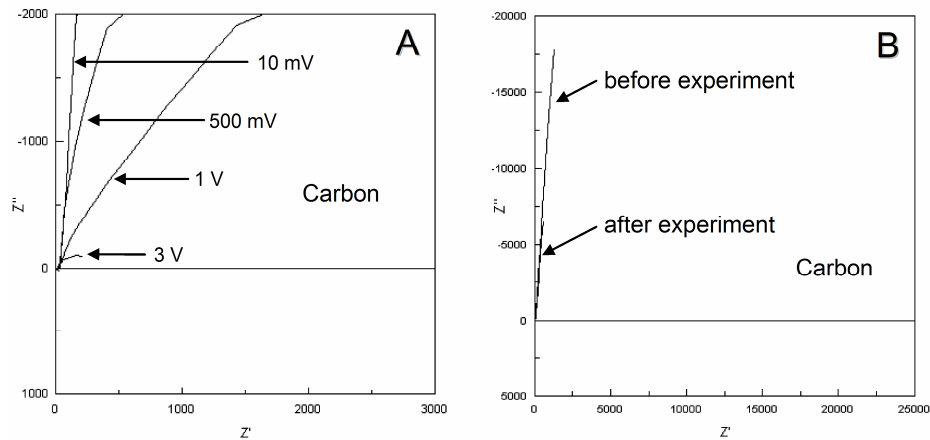
Figure 4 (A) *Nyquist plot of carbon rod electrodes for increasing perturbation voltage. As potential moves further from equilibrium, the plots become curved and faradaic reactions become of increasing importance.* **(B)** *Nyquist plot of carbon rod electrodes measured before an experiment and after 5 days of electrical stimulation (5 V, 2 ms, 1 Hz). While at low frequencies the aged electrode had decreased impedance, its resistance to reactions remained unchanged, i.e. R_p values were equal. Experimental setup was as shown in Figure 2 with 4 cm electrodes.*

Choice of the electrode material

The design considerations required for electrical stimulation of engineered cardiac tissue are many and interdependent. Factors to consider include the duration and shape of the stimulus waveform, the size of the tissue construct in question, the electrical property being exploited (generation of reactive oxygen species versus eliciting action potential, for example), the duration of the experiment, and the mechanical properties required of the electrode in the bioreactor setup. For our work, we started with a desired stimulus waveform, examined the electrical characteristics of that stimulus, and based subsequent design decisions with this in mind.
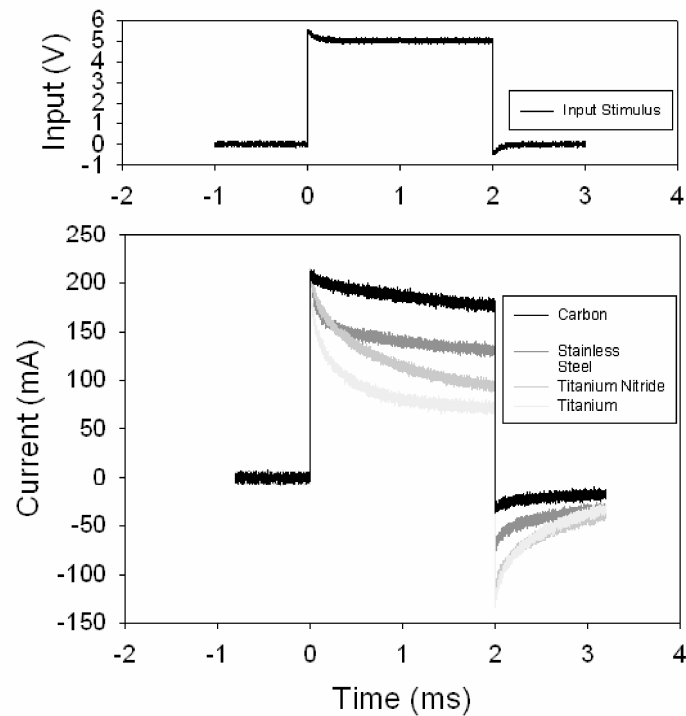
Figure 5 Current measured over 5 V, 2 ms square wave pulse. *The total amount of injected charge in coulombs is equal to area beneath each curve, or 2.3 x 10-4 C for carbon, 1.79 x 10-4 C for stainless steel, 1.63 x 10-4 C for titanium nitride, and 1.20 x 10-4 C for titanium. Experimental setup was as shown in Figure 2 with 4 cm electrodes.*

1. Calculate the power spectral density of the stimulus waveform to determine the frequency band that concentrates most of the energy in the pulse. For 5 V, 2 ms square pulses delivered at 1 Hz it is the frequency band below 1 kHz (see Figure 6 and Note 5).

2. Analyze the Bode plot to determine the behavior of the electrode material within this frequency band. For example, the carbon electrodes we use have a corner frequency of approximately 10 Hz, and so the electrode behaves as both a capacitor below this frequency and a resistor above this frequency. Therefore, we must consider both the electrode's *CPE* and R_p values (see Figure 3).

3. Compare *CPE*, R_p and injected charge values calculated from EIS for different electrodes. Choose electrode material with high *CPE* to increase charge injection, and high R_p to reduce harmful reactions.
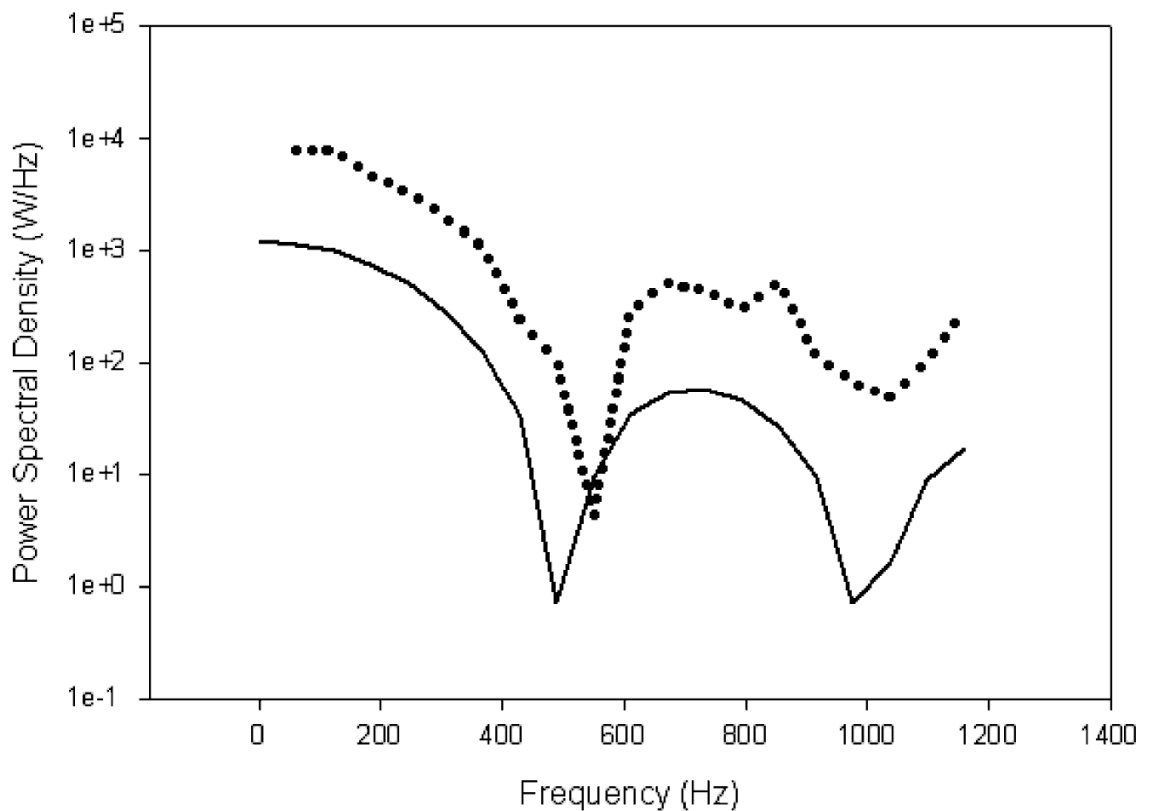

Figure 6 *Power spectral density for 5 V 2 ms square wave pulse. Solid line is theoretical spectrum (see Note 4), dashed line is measured spectrum.*

Cell line and culture

The following protocols are for neonatal rat cardiomyocytes, which are readily available at most institutions. However, the general methods of electrical stimulation described here are applicable to all electrically excitable cells.

Rat cardiomyocyte isolation

Heart cells are obtained from 2-day old neonatal Sprague Dawley rats, using a protocol approved by our Committee on Animal Care (see (Radisic, Park et al. 2004) for additional details).

1. Excise a whole heart from the rat and place it in cold HBSS buffer.

2. Remove the left and right atrium and blood vessels by using small scissors and forceps.

3. Quarter remaining heart ventricles and wash in HBSS buffer.

4. Digest quartered hearts in 25 ml of 0.06% (w/v) trypsin in HBSS buffer by shaking overnight at 4˚C.

5. Stop trypsin digestion by adding 10 ml of cardiac growth medium followed by incubation at 37 ˚C for 4 min with shaking at 150 rpm. After discarding supernatant, add 10 ml of 0.1% (w/v) type II collagenase in HBSS to the tissue and incubate at 37˚C for 4 min with shaking at 150 rpm.

6. Collect the cell suspension from the digestion and wash the pellet with 10 ml of HBSS buffer and collect the supernatant.

7. Repeat steps 6 and 7 until no more tissue remains.

8. Centrifuge at 750 rpm for 10 min the pooled cell suspension from step 8 and then wash the cell pellet with 25 ml of cell culture medium to remove residual collagenase (see Note 5).

9. Resuspend the cells in the cell culture medium and pre-plate for 1 h to enrich cell suspension with cardiomyocytes by removing fibroblasts. In this step, fibroblasts will adhere to the culture dish within 1 h but most of cardiomyocytes will remain in suspension.

10. Harvest cells by centrifugation at 1,000 rpm for 5 min.

11. Determine cell number and viability of cardiomyocytes by hemocytometer counts using trypan blue to exclude dead cells. Twenty neonatal rat hearts will yield 8-12 x 10^7 cells.

Scaffold preparation and seeding

1. Cut the collagen scaffold into squares 5 mm x 5 mm x 1.5 mm.

2. Immediately before use, hydrate each collagen scaffold in culture medium for 2 h in the 37°C at 5% CO_2 incubator.

3. Collect cells by centrifugation at 1,000 rpm for 10 min and resuspend in liquid Matrigel using 5 µl Matrigel per 1 million cells, while working on ice to prevent premature gelation.

4. Gently blot dry pre-wetted collagen scaffolds, and then pipette cell suspension in Matrigel evenly on the top surface of each scaffold. Inoculate each scaffold with freshly isolated heart cells at a density 1.35 x 10^8 cells/cm^3.

5. Gelation is complete within 15 min in a 37 °C incubator, and inoculated scaffolds are then transferred into Petri dish.

Electrical stimulation of constructs

The objective of electrical stimulation is to deliver enough current to cells to depolarize membrane and elicit an action potential. In addition, there is some evidence that electrical stimulation aids in cardiomyocyte alignment. For scaffolds of cardiomyocytes seeded with Matrigel we have previously determined that the optimal time to begin electric field stimulation is 3 days after scaffolds are seeded and to assess contractile function after 8 days (Radisic, Park et al. 2004).

1. Place three scaffolds between electrodes in 60 mm Petri dish. Fix scaffold position with two stainless steel pins bent over scaffold and into PDMS base layer (see Figure 2). These pins

should not touch each other or the electrodes in order to minimally interfere with the electric field.

2. Add 15 ml of cardiac medium to Petri dish and place in incubator (37 °C, 5% CO_2).

3. Make electrical connections with an effort to prevent any undesired electrical connections via metal or electrolyte. Place a layer of autoclave paper beneath all bioreactors to prevent unintentional electrical connections via moisture in the bioreactor or via metal parts within the incubator.

4. Stimulate with 5 V, 2 ms duration square pulses delivered at 1 Hz (see Note 6). Monophasic pulses were chosen for their simplicity and compatibility with carbon electrodes (see Note 7).

5. Start electrical stimulation 3 days after seeding scaffolds with isolated heart cells.

6. Stop electrical stimulation 8 days after seeding scaffolds (5 days of electrical stimulation).

Scaffold characterization

Contractile activity

Contractile function of engineered cardiac constructs is evaluated on-line (during culture) by measuring contractile activity in response to electrical field stimulation.

1. Place each construct between two carbon electrodes connected to a cardiac stimulator (either Grass S88X or custom system) in a 60-mm Petri dish filled with 15 ml cardiac growth medium.

2. Maintain the temperature of the Petri dish at 37 °C using heating tape fixed to the bottom of the Petri dish and connected to a temperature controller (see Note 8).

3. Place the entire setup on an optical microscope, and monitor contractile responses to electrical stimuli (rectangular pulses, 2 ms duration) using 2x magnification.

4. Increase signal amplitude in 0.1 V increments up to 10 V, and the stimulation frequency up to 400 beats-per-minute (bpm).

5. For each combination of voltage and frequency, look for the presence of random, spontaneous contractions (an indicator of immature tissue) versus synchronous contractions in response to electrical pacing (an indicator of more mature tissue containing electromechanically coupled cells).

6. Measure two parameters to evaluate the contractile behavior in response to electrical stimulation: *excitation threshold*, *ET* (the minimum voltage of electrical stimulation required to elicit sustained synchronous contractions of tissue constructs at a frequency of 60 bpm) and *maximum capture rate*, *MCR* (maximum frequency of sustained synchronous contractions that can be achieved at a stimulation voltage corresponding to 1.5*ET*).

Histological analysis

Fix cell-scaffold constructs in 10% buffered formalin for 24 h, dehydrate, embed in paraffin, bisect in cross section through the center, and section to 5 µm thickness. Sections are stained with hematoxylin and eosin for general evaluation and stained with cardiac specific antibodies to assess the distribution of cardiac markers. Use a humidified chamber for all incubation steps. Neonatal rat heart and bovine tendon serve as positive and negative controls, respectively.

1. Deparafinize sections to retrieve antigen by heat treatment for 20 min at 95°C in a decloacking chamber (Biocare Medical, Concord, CA).

2. Subsequently, block sections with 10% horse serum for 30 min at room temperature (RT) in a humidified chamber.

3. Incubate the sections for 1 h at 37 °C with mouse anti-cardiac troponin I and rabbit anti-connexin 43 (Cx43) diluted in PBS containing 0.5% Tween 20 and 1.5% horse serum.

4. For TnI, incubate sections at RT, first for 30 min with the secondary antibody (horse anti-mouse IgG), then for 30 min with an avidin–biotin complex agent for 30 min, and finally for 15 min with 3,39-diaminobenzidine (Sigma).

5. For Cx-43, use fluorescein-conjugated goat anti-rabbit IgG (1:200).

6. Assess construct architecture and cell distribution from the stained sections using fluorescent microscope (Axioplan, Zeiss, Thornwood, NY).

Ultrastructure analysis

Transmission electron microscopy allows observation of gap junction and z-band formation.

1. Fix constructs in Karnovsky's reagent (0.1 M sodium cacodylate with 2% paraformaldehyde and 2.5% gluteraldehyde, pH = 7.4), post-fix in 1% osmium tetroxide in veronal-acetate buffer, dehydrate in graded ethanol in propylene oxide, and embed in Epon 812 (Polysciences).

2. Cut thin sections (70 nm) using a Leica Ultra Cut and a diamond knife.

3. Stain sections with lead citrate and uranyl acetate.

4. Examine sections for ultrastructural properties relevant to cardiac tissue (volume fraction and developmental stage of sarcomeres, Z and M lines, H, I and A bands, gap junctions, T

tubules) using a Philips EM410 transmission electron microscope operated at 80 kV (JEOL-100CX, JEOL).

5. Morphometric analysis was performed on 20-46 randomly taken transmission electron micrographs at magnification of 100,000. A test grid with uniform squares (0.26 cm x 0.26 cm) was superimposed onto the micrographs and the area covered by sarcomeres, mithochondria, nuclei and the overall area of the cells were determined. The volume fraction of each organelle was determined as previously described (Nuccitelli 1992). The frequency of intercalated discs and gap junctions (number per μm^2) was determined by counting. A total of 20 micrographs of non-stimulated constructs, 46 micrographs of stimulated constructs and 42 micrographs of neonatal ventricles were evaluated with respect to each structural parameter by two independent observers.

D.4 Notes

1. Measurements are made in PBS to facilitate comparison with *EIS* data in the literature and from our own laboratory. The conductivity of PBS (15 mS/cm) is similar to that of culture medium with 10% FBS (~14 mS/cm).

2. In a Nyquist plot, the imaginary component of the impedance is plotted against the real part at each frequency. A Bode plot gives the logarithm of impedance, |Z|, and the phase angle versus the logarithm of frequency.

3. The electrode-electrolyte system can be described by a Randles cell that consists of electrolyte resistance R_e, a constant phase element *CPE* and charge transfer or polarization resistance R_p. The constant phase element is a mathematical description of the double-layer

capacitance and accounts for nonideal capacitive behavior of the electrochemical double layer with the non-dimensional η term (Norlin, Pan et al. 2005).

4. For square pulses delivered at 1 Hz, the analytical solution to the power spectral density is given by the following equation: $\sum_{k=-\infty}^{\infty} \frac{2\sin k\omega_o T_1}{k} \delta\left(\omega - \frac{2\pi k}{T}\right)$ where ω is the frequency expressed in radians, δ represents the Dirac-delta function, ω_0 is the fundamental frequency expressed in radians, T is the period, and T_1 is half the length of the pulse.

5. It is important that collagenase removal by washing is complete to prevent degradation of collagen scaffold during cell seeding.

6. Electric field stimulation may be delivered from a commercially-available stimulator or through custom-designed hardware controlled by a computer. Although computer-controlled stimulation allows additional flexibility, it requires some expertise in circuit design and software programming.

7. Waveform selection (e.g., between monophasic, biphasic or other wave shapes) depends on the electrode material characteristics, as biphasic pulses can aid in reversing reversible faradaic reactions, but at the same time may be undesirable since biphasic pulses may inhibit action potential.

8. In a very nice microelectrode array (MEA) study on cardiomyocyte activity, Giovangrandi et al. (2006) clearly show how cardiomyocyte beat rate closely follows imposed temperature profile (beat rate increases as temperature increases and vice versa). In an earlier study by the same group (Gilchrist, Giovangrandi et al. 2005), medium pH and osmolarity were also considered.

9. Looking forward –

   a. Better analytical tools required such as closed-loop feedback systems for capture rate. Off-the-shelf pacemakers may be useful in this regard.

   b. High throughput approaches are needed to determine optimal stimulation parameters.

   c. More advanced bioreactors that integrate electrical stimulation with medium perfusion are needed to engineer tissue of sufficient thickness for clinical applications.

Acknowledgements

D.5 References

Basser, P. J. and B. J. Roth (2000). "New currents in electrical stimulation of excitable tissues." Annual Review of Biomedical Engineering **2**: 377-397.

Gilchrist, K. H., L. Giovangrandi, et al. (2005). "Sensitivity of cell-based biosensors to environmental variables." Biosensors & Bioelectronics **20**(7): 1397-1406.

Giovangrandi, L., K. H. Gilchrist, et al. (2006). "Low-cost microelectrode array with integrated heater for extracellular recording of cardiomyocyte cultures using commercial flexible printed circuit technology." Sensors and Actuators B-Chemical **113**(1): 545-554.

Malmivuo, J. and R. Plonsey (1995). Bioelectromagnetism - Principles and Applications of Bioelectric and Biomagnetic Fields. New York, Oxford University Press.

Merrill, D. R., M. Bikson, et al. (2005). "Electrical stimulation of excitable tissue: design of efficacious and safe protocols." Journal of Neuroscience Methods **141**(2): 171-198.

Norlin, A., J. Pan, et al. (2004). "Investigation of Pt, Ti, TiN, and nano-porous carbon electrodes for implantable cardioverter-defibrillator applications." Electrochimica Acta **49**(22-23): 4011-4020.

Norlin, A., J. Pan, et al. (2005). "Electrochemical behavior of stimulation/sensing materials for pacemaker electrode applications III. Nanoporous and smooth carbon electrodes." Journal of the Electrochemical Society **152**(9): J110-J116.

Norlin, A., J. Pan, et al. (2005). "Investigation of electrochemical behavior of stimulation/sensing materials for pacemaker electrode applications I. Pt, Ti, and TiN coated electrodes." Journal of the Electrochemical Society **152**(2): J7-J15.

Nuccitelli, R. (1992). "Endogenous ionic currents and DC electric fields in multicellular animal tissues." Bioelectromagnetics **Suppl 1**: 147-157.

Radisic, M., H. Park, et al. (2004). "Functional assembly of engineered myocardium by electrical stimulation of cardiac myocytes cultured on scaffolds." Proceedings of the National Academy of Sciences of the United States of America **101**(52): 18129-18134.

Zammaretti, P. and M. Jaconi (2004). "Cardiac tissue engineering: regeneration of the wounded heart." Current Opinion in Biotechnology **15**(5): 430-434.

Zimmermann, W. H., M. Didie, et al. (2002). "Cardiac grafting of engineered heart tissue in syngenic rats." Circulation **106**(13): I151-I157.

Appendix E

Local diffusivity and intracellular organization synergy in spatio-temporal cAMP signal transduction in HEK293

Elisa Figallo[1], Denj Camposilvan[1], Anna Terrin[2], Giulietta di Benedetto[2],

Manuela Zaccolo[2], Nicola Elvassore[1]

[1]Department of Chemical Engineering, University of Padova, via F. Marzolo 9, I-35131 Padova PD, Italy

[2]Dulbecco Telethon Institute, Venetian Institute of Molecular Medicine, via Orus 2, 35129 Padova, Italy

(*)To whom correspondence should be addressed

E-mail: nicola.elvassore@unipd.it

phone: +39 (049) 8275469; fax: +39 (049) 8275461

Abstract

The tremendous importance of cAMP signaling is due to its capability of activating some major biological signal pathways through a dissipative but self-organized spatio-temporal distribution inside the cell. So far, no conclusive answer has been experimentally found to justify the ability of responding to different receptors selectively, by enabling for example metabolic processes, when the secondary messenger is concentrated close to the membrane, or transcription factors, when it reaches the nucleus. The mathematical modeling offers the opportunity to analyze efficiently several hypotheses on the cAMP signaling spatio-temporal dynamics and isolate the relative influence of different factors such as structural organization of enzymes, concentration of protein kinase A (PKA) and phosphodiesterase (PDE), or non-homogenous intracellular cAMP diffusion coefficient.

In particular, we hypothesize that localized competition between diffusion and reaction rate determines the specific spatial organization of cAMP. The model combines the constitutive relationships for signaling reaction rates and Fickian mass transport within the species mass balance. The system of 12 second-order partial differential equations was solved for the concentrations of molecules involved on the signaling.

The results show a good agreement to experimental evidences and the cAMP time course at the membrane is well described by the model. Specific factors due to the intracellular organization, such as PKA over-expression, low diffusivity at membrane compartment and spatial distribution of PDEAD and PDE3, have been found responsible for the cAMP compartmentalization.

These results suggest the molecular basis to the cAMP compartmentalization, without the necessity of strong and unrealistic assumptions, such as the presence of intracellular physical barriers.

E.1 Introduction

The biological evolution often generates variability and complexity in the system, and the formation of steady non-homogeneous microenvironments. One example is given by biological systems, where chemical reactions and diffusion competition determines self-organized dissipative spatio-temporal structures, far from equilibrium (Prigogine 1961). Particularly interesting is the application of this concept to a small and fast diffusing molecule as the cyclic AMP.

The importance of intracellular cAMP, as ubiquitous secondary messenger, is in its ability of modulating selectively, through its spatial organization, the transduction of a wide variety of hormonal signals and biological processes, such as gene expression (Abramovitch, Tavor et al. 2004), metabolism (Dachicourt, Serradas et al. 1996; Claudia, Salvatore et al. 2006), cell division (Dumaz, Hayward et al. 2006) and, in particular, cardiac functional contraction (McConnachie, Langeberg et al. 2006). The molecular mechanism responsible of spatial organization of this secondary messenger is a key task to understand and control the high specificity of this signalling.

When a stimulus binds at the cell surface to a receptor, a sequence of events begins near the membrane determining a spike of cAMP concentration limited in space and time (Figure). The arising cAMP concentration promotes its cleavage through the activation of protein kinase A (PKA) and phosphodierestase isoforms (PDE). Thus, the intracellular concentration of cAMP is regulated by the antagonist actions of AC and PDE (Alberts, Johnson et al. 2002), which determine time-dependent spikes of the secondary messenger inside the cell. Experimental evidences show the compartmentalization of these spikes in specific

intracellular volumes and it is aim of this work to screen the hypotheses behind this behaviour.

Even if the cAMP signaling biochemistry has been studied for a long time, so far no conclusive answer has been identified by the literature about the reasons of cAMP compartmentalization. The introduction of the cAMP-sensitive fluorescence resonance energy transfer (FRET), as accurate experimental method to show the intracellular localization of small molecules (Sato, Ozawa et al. 2002; Zaccolo, Magalhaes et al. 2002; Zaccolo and Pozzan 2002), suggested different hypotheses on cAMP localization *in vivo,* such as: 1) the existence of membrane subdomains called caveolae or lipid raft (Rybin, Xu et al. 2000; Isshiki, Ando et al. 2002; Ostrom, Liu et al. 2002; Steinberg 2004; Nikolaev, Bunemann et al. 2006; Saucerman and McCulloch 2006), 2) the localized production of cAMP in membrane (Zippin, Chen et al. 2002; Feliciello, Gottesman et al. 2005; McConnachie, Langeberg et al. 2006) and 3) the intracellular localization of multi-enzymes complex involved in the signaling, such as PKA and PDE isoforms (Pugh 2000; Rybin, Xu et al. 2000; Kapiloff 2002; Barnes, Livera et al. 2005; McConnachie, Langeberg et al. 2006). In particular, the critical importance of PDE on signal transduction is proved by a reduction in cAMP localization upon PDE inhibition with IBMX of frog heart cells locally stimulated with isoproterenol (Zaccolo, Magalhaes et al. 2002). The selective inhibition of PDE isoforms has shown the increasing relevance of PDE4 action, followed by PDE2 and PDE3, on the sharp cAMP gradient formation in cardiac myocytes (Nikolaev, Bunemann et al. 2006). In this prospective the different signaling dynamic, observed when β1- or β2AR are activated, can be justified by the confined generation of local pools of cAMP and enzymes involved in the signaling, such as A-kinase-anchoring proteins (AKAPs), PKA and PDE isoforms. (Nikolaev, Bunemann et al. 2006).

Even if these experimental results give interesting information about the signaling dynamics, they lack of more appropriate and accurate experimental techniques which can give evidences about the role of cellular anisotropy, of local *in vivo* intracellular diffusivity or about the interaction between structural organization of enzymes and molecular diffusion. The mathematical modeling offers a unique opportunity to bridge this gap giving a rational description of the spatio-temporal complexity and testing quickly and efficiently the synergic effect and the interplay of different phenomena on cAMP spatial distribution.

The literature reports several analytical models to describe the cAMP time course close to the membrane even if no attention is given to cAMP intracellular spatial distribution (Goldbeter 1996), (Bhalla and Ravi Iyengar 1999; Golbunova Y.V. 2002; Gorbunova and Spitzer 2002; Saucerman, Brunton et al. 2003; Rich, Xin et al. 2007). On the other hand those models, which describe the importance of diffusion and cell compartmentalization on cAMP spatial evolution (Huang et al. (1991); Rich 2001), are based on an incomplete or non realistic description of cell structure assuming isotropical diffusion in an infinite cytosol or the existence of hypothetical physical barrier to the diffusion, never found experimentally.

In what follows, we describe first the theoretical framework adopted to define the spatio-temporal dynamics of the intracellular cAMP. The compartmentalization of this small molecule is described by a constitutive diffusion-kinetics model, considering a non homogenous cellular space. The cells are treated as finite volume with cAMP production on the membrane surface. The model consideres the spatio-temporal cAMP dynamics investigating the effect of local lower cAMP diffusivity and PDE and PKA spatial localization. The chemical concentrations of chemical species involved in cAMP signaling, are controlled through 12 partial differential equations. In the definition of the model parameters we put particular attention on choosing value reported from the literature.

Excluding the local diffusivity value and the enzymes localization, only two parameters over 31 have been optimized later to reproduce the experimental behaviour in different conditions. The mathematical model was validate comparing the simulation results with experimental variation of FRET measured with H30 probe on HEK 293 after stimulation with PGE1.

The following section discusses the development of the mathematical model, the simplifications made for simulations and the experimental method used to validate it.

E.2 Material and methods

E.2.1 The theoretical framework

The chemical binding of stimulus to cell surface receptors activates the production of cAMP through the adenylyl cyclase (AC) action. The cAMP concentration arises and promotes the dissociation of the protein kinase A (PKA) in two regulatory and catalytic subunits. Each catalytic subunit catalyzes the phosphorylation of different phosphodierestase isoforms (PDE), which cleave cAMP (Figure1). The cAMP signalling mainly involves three PDE isoforms: PDE4D, PDE4B and PDE3 (Alberts, Johnson et al. 2002). These enzymes differ for concentration and activity, in particular PDE3 and PDE4D show a high affinity for cAMP. The cell membrane is assumed impermeable to the cAMP and characterized by homogeneous distribution of adenylyl cyclase (AC). All simulations were initiated by a step increase cAMP production, simulating the action of PGE1.
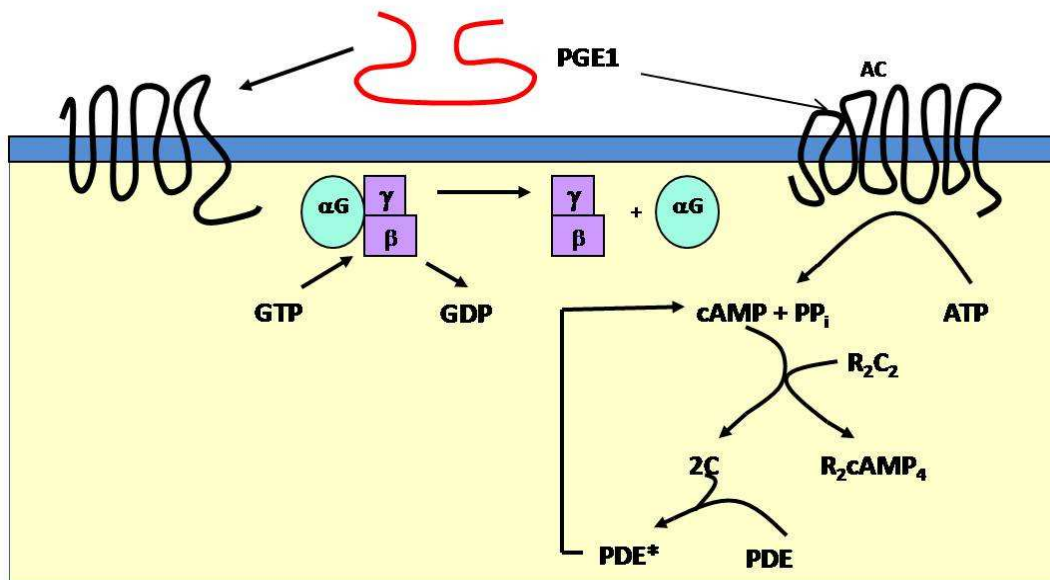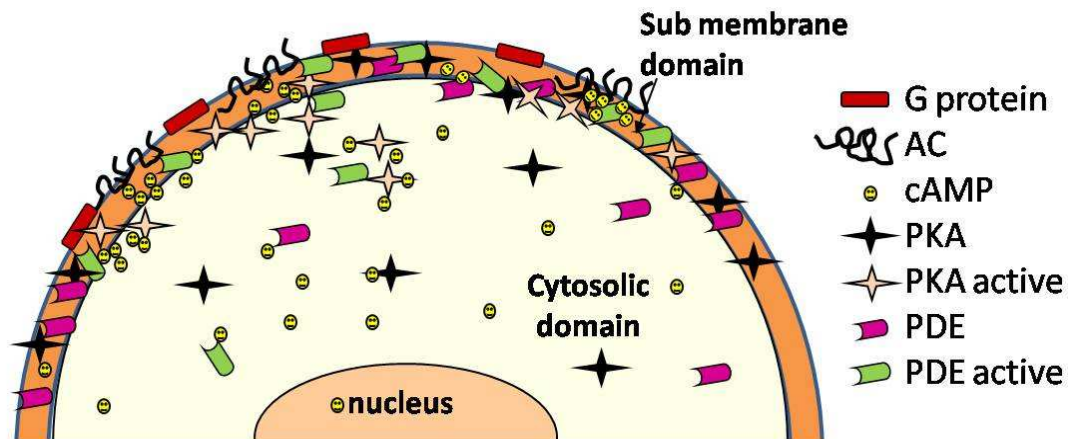
Figure 1 cAMP signaling schematic When an extracellular ligand such as an hormone binds to and activates a seven-transmembrane G-protein-coupled receptor, the signal is passed through the heterotrimeric G protein to adenylyl cyclase. The activated adenylyl cyclase converts ATP into the second messenger cAMP. As the gradient of cAMP concentration diffuses in the cell, various enzymes are activated, including PKA, and several isoform of PDE. Schematic subdivision of the intracellular space, which shows a likely localization of the chemical species involved on cAMP signaling **(top figure).** Schematic diagram of cAMP synthesis and downstream signaling activation **(down figure).**

The model studies the spatio-temporal distribution of the cAMP in HEK 293 cells due to competition between diffusion and reactions rates in the cytoplasm. The cellular volume is

assumed to be divided in three subdomains with characteristic dimensions: the submembrane volume (SM, 10% of the total volume) (Peters R. 1984), the cytosol (C, 70% of the total volume) and nucleus (N, 20% of the total volume) (Kozer N. 2004). Since the experimental set up includes the observation of adherent HEK293, the cell morphology is approximated to semi-sphere with radius R=20μm, as shown in Figure 1.

The cAMP signaling is modelled considering a continuous intracellular concentration of chemical species, guaranteed by the absence of physical barriers. In these assumptions, the cAMP is uniformly produced next to the membrane and diffuses freely only in r direction (Figure 1). Assuming isotropical diffusion of cAMP, the contributions in θ and φ direction can be neglected. All the chemical species diffuse freely in the cytosol, except AC, that is bound to the membrane.

Although all the compartments include the same reactions, the concentrations or the diffusivity of free molecules can be different, as explained in Figure 1. In particular in the nucleus the concentration of PKA and PDE is assumed negligible. For each simulation the diffusivity of a certain chemical species is assumed homogenous in each compartment.

E.2.2 Mathematical model

The mathematical model is defined by a system of partial differential equations obtained by mass balances of all the chemical species involved in the signaling. The spatio-temporal dynamics of the molar concentration, C_i, of species i is related to its molar flux, N_i, and to the kinetics rates of production or destruction of chemical species R_j, by the conservation equation given by (Bird R. 2002):

$$\frac{dC_i}{dt} = -\boldsymbol{\nabla N_i} + \sum \boldsymbol{R_j} \qquad\qquad (E.\,1)$$

The constitutive expressions of flux N_i and reactions rates R_j are summarized as follows.

The flux expression accounts here (E.2) only the diffusive contribution proportional to the

concentration gradients of the species i and is modelled by the Fick's law, where D_i is the

diffusion coefficient of the species i.

$$N_i = -D_i \nabla C_i \qquad\qquad (E.\,2)$$

The diffusivity of cAMP in cytosol is always set at 130 μm^2/s averaging literature

experimental data (Luby-Phelps, 2000; Verkman, 2002; Garcia-Perez et al., 1999; Mastro

and Babich, 1984; Mastro and Keith, 1984). In this work, we simulate the cAMP signaling

with different local diffusivity in the submembrane domain (1-130 μm^2/s). The term Rj can

be formulated by general molecular scheme (E.3):

$$R_j = k_f \cdot [A]^a \cdot [B]^b - k_d \cdot [C_i] \cdot [D]^d \qquad\qquad (E.\,3)$$

or using Michaelis-Menten kinetics (E.4):

$$R_j = \frac{v_m \cdot [C_i]}{K_m + [C_i]} \qquad\qquad (E.\,4)$$

where the concentration of product is specified by the two rate constants v_m and K_m or by

molecolarity coefficients a, b, d, and the rate constants of production and destruction of C_i,

k_f and k_d respectively.

Table 1 List of mass balance equations used to simulate the cAMP signaling

Chemical species		Mass Balance Equation
c_1	[cAMP]free	$\dfrac{\partial[cAMP]}{\partial t}=\dfrac{\partial c_1}{\partial t}=\dfrac{D_1}{r^2}\dfrac{\partial^2\left(r^2c_1\right)}{\partial r^2}-\dfrac{V_{mPDE4D}c_2c_1}{K_{mPDE4D}+c_1}-\dfrac{V_{mPDE4B}c_{10}c_1}{K_{mPDE4B}+c_1}-\dfrac{V_{mPDE3}c_{11}c_1}{K_{mPDE3}+c_1}+$ $-k_1([R_2C_2]_{TOT}-c_3-c_4-c_5-c_6-c_7)c_1-k_2c_3+k_3c_3c_1-k_4c_4+k_5c_4c_1-k_6c_5+$ $+k_7c_5c_1-k_8c_6-k_{11}(H30_{tot}-c_{12}\quad)c_1+k_{12}c_{12}-k_{13}c_{12}c_1\cdot$
c_2	[PDE4D*] active	$\dfrac{\partial\left[PDE4D^*\right]}{\partial t}=\dfrac{\partial c_2}{\partial t}=\dfrac{D_2}{r^2}\dfrac{\partial^2\left(r^2c_2\right)}{\partial r^2}+\dfrac{V_m^*\left([PDE4D]_{TOT}-c_2\right)c_9}{K_m^*+\left([PDE4D]_{TOT}-c_2\right)}-k_bc_2$
c_3	[R$_2$C$_2$cAMP]	$\dfrac{\partial c_3}{\partial t}=\dfrac{\partial[R_2C_2cAMP]}{\partial t}=\dfrac{D_3}{r^2}\dfrac{\partial^2\left(r^2c_3\right)}{\partial r^2}+k_1([R_2C_2]_{TOT}-c_3-c_4-c_5-c_6-c_7)c_1+$ $-k_2c_3-k_3c_3c_1+k_4c_4$
c_4	[R$_2$C$_2$cAMP$_2$]	$\dfrac{\partial c_4}{\partial t}=\dfrac{\partial[R_2C_2cAMP_2]}{\partial t}=\dfrac{D_4}{r^2}\dfrac{\partial^2\left(r^2c_4\right)}{\partial r^2}+k_3c_3c_1-k_4c_4-k_5c_4c_1+k_6c_5$
c_5	[R$_2$C$_2$cAMP$_3$]	$\dfrac{\partial c_5}{\partial t}=\dfrac{\partial[R_2C_2cAMP_3]}{\partial t}=\dfrac{D_5}{r^2}\dfrac{\partial^2\left(r^2c_5\right)}{\partial r^2}+k_5c_4c_1-k_6c_5-k_7c_5c_1+k_8c_6$
c_6	[R$_2$C$_2$cAMP$_4$]	$\dfrac{\partial c_6}{\partial t}=\dfrac{\partial[R_2C_2cAMP_4]}{\partial t}=\dfrac{D_6}{r^2}\dfrac{\partial^2\left(r^2c_6\right)}{\partial r^2}+k_7c_5c_1-k_8c_6-k_9c_6+k_{10}c_7c_9$
c_7	[R$_2$CcAMP$_4$]	$\dfrac{\partial c_7}{\partial t}=\dfrac{\partial[R_2CcAMP_4]}{\partial t}=\dfrac{D_7}{r^2}\dfrac{\partial^2\left(r^2c_7\right)}{\partial r^2}+k_9c_6-k_{10}c_7c_9-k_9c_7+k_{10}c_8c_9$
c_8	[R$_2$cAMP$_4$]	$\dfrac{\partial c_8}{\partial t}=\dfrac{\partial[R_2cAMP_4]}{\partial t}=\dfrac{D_8}{r^2}\dfrac{\partial^2\left(r^2c_8\right)}{\partial r^2}+k_9c_7-k_{10}c_8c_9$
c_9	[C]	$\dfrac{\partial c_9}{\partial t}=\dfrac{\partial[C]}{\partial t}=\dfrac{D_9}{r^2}\dfrac{\partial^2\left(r^2c_9\right)}{\partial r^2}+k_9c_6-k_{10}c_7c_9+k_9c_7-k_{10}c_8c_9$
c_{10}	[PDE4B*] active	$\dfrac{\partial\left[PDE3^*\right]}{\partial t}=\dfrac{\partial c_{10}}{\partial t}=\dfrac{D_{10}}{r^2}\dfrac{\partial^2\left(r^2c_{10}\right)}{\partial r^2}+\dfrac{V_m^*\left([PDE3]_{TOT}-c_{10}\right)c_9}{K_m^*+\left([PDE3]_{TOT}-c_{10}\right)}-k_bc_{10}$
c_{11}	[PDE3*] active	$\dfrac{\partial\left[PDE4B^*\right]}{\partial t}=\dfrac{\partial c_{11}}{\partial t}=\dfrac{D_{11}}{r^2}\dfrac{\partial^2\left(r^2c_{11}\right)}{\partial r^2}+\dfrac{V_m^*\left([PDE4B]_{TOT}-c_{11}\right)c_9}{K_m^*+\left([PDE4B]_{TOT}-c_{11}\right)}-k_bc_{11}$

| c_{12} | [H30-cAMP] | $\dfrac{\partial c_{12}}{\partial t}=\dfrac{\partial[H30-cAMP]}{\partial t}=\dfrac{D_{12}}{r^2}\dfrac{\partial^2\left(r^2 c_{12}\right)}{\partial r^2}+k_{11}(H30_{tot}-c_{12}-\bigcirc)c_1-k_{12}c_{12}-k_{13}c_{12}c_1$ |

The mathematical expression for each R_i was chosen considering experimental parameters available in literature (Table 1). As reported in literature, we assume that at PDE3 compete the 30% of the action of PDE4 whereas at the PDE4B compete the 30% of the action of PDE4D (Lynch, Baillie et al. 2005). The equation used to describe this model are reported in Table 1 whereas the parameters are in Table 2.

Table 2 Parameters used to simulate transient cAMP signals

Parameter	Value	Reference
D_{cAMP}	130μm²/s	(Nikolaev, 2006)
R^m_{cAMP}	$8*10^{-7}$ μmol/(dm²s)	(Rich, 2001)
[PDE]	0.8μM	(Rich, 2006)
[PDE4B]	0.53	(Lynch, Baillie et al. 2005)
[PDE4D]	0.26	(Lynch, Baillie et al. 2005)
[PDE3]	0.01	(Lynch, Baillie et al. 2005)
[PKA]	1.5μM	(Golbunova, 2002)
k_1	54(μMs)⁻¹	(Golbunova et al., 2002)
k_2	33s⁻¹	(Golbunova et al., 2002)
k_3	54(μMs)⁻¹	(Golbunova et al., 2002)
k_4	33s⁻¹	(Golbunova et al., 2002)
k_5	75(μMs)⁻¹	(Golbunova et al., 2002)
k_6	110s⁻¹	(Golbunova et al., 2002)
k_7	75(μMs)⁻¹	(Golbunova et al., 2002)
k_8	32.5s⁻¹	(Golbunova et al., 2002)
k_9	60s⁻¹	(Golbunova Y. V. et al., 2002)
k_{10}	18(μMs)⁻¹	(Golbunova et al., 2002)
Vm	9s⁻¹	(Golbunova et al., 2002)(Balla et al., 1999)

K_m	7.5μM	(Golbunova et al., 2002)(Balla.et al., 1999)
k_b	$0.1s^{-1}$	(Golbunova et al., 2002)
V_{mPDE4B}	$0.552s^{-1}$	Optimized
K_{mPDE4B}	1.5μM	(Bender, 2006)
V_{mPDE4D}	$2.7\ s^{-1}$	(Bender, 2006)
K_{mPDE4D}	1.2μM	(Bender, 2006)
V_{mPDE3}	$17.71\ s^{-1}$	(Bender, 2006)
K_{mPDE3}	0.38μM	(Bender, 2006)

E.2.3 Boundary and initial conditions

The cellular membrane prevents all the chemical species of entering the cell, the entering flux is therefore considered null for all the chemical species except for free cAMP, which is produced at the interface with cytosol. The boundary conditions at the cell membrane can be expressed by E.5 and E.6:

$$N_i = -D_i^{SM} \frac{\partial c_i}{\partial r}\bigg|_{r=R} = 0 \qquad \textit{if } i \neq cAMP \qquad (E.\ 5)$$

$$N_i = -D_i^{SM} \frac{\partial c_i}{\partial r}\bigg|_{r=R} = R_i^m \qquad \textit{if } i = cAMP \qquad (E.\ 6)$$

where R_{cAMP}^m is the cAMP production rate at cell membrane (Table 2).

Considering the spherical symmetry, the flux of any species in the centre of the semi-sphere must vanish. In particular, the radial component of the flux must satisfy:

$$N_i = -D_i^N \frac{\partial c_i}{\partial r}\bigg|_{r=0} = 0 \qquad (E.\ 7)$$

The initial concentration of active PDE was set at 5% of the total. The initial concentration of cAMP and PKA activated was assumed negligible (Alberts B., 2002)

E.2.4 Numerical method

The system of partial differential equations, obtained by the species mass conservation law, was solved numerically using the finite volume method implementing in Matlab a multistep variable order solver based on the numerical differentiation formulas (NDFs). This solver is particularly suitable for a stiff systems (Shampine 1994). The finite volume guarantee a conservative discretization even if the system is characterized by spherical symmetry and not constant diffusivity in all the entire volume. The relative tolerance, RelTol (10^{-4}), and the specified absolute tolerance, AbsTol (10^{-5}) was used. Mesh refinement was performed till the numerical solution provide stable numerical output and comparable with the relative tolerance used.

The local sensitivity analysis is used to determine the most influent parameters in the model and which one contribute the most to the cAMP compartmentalization (Saltelli, Chan et al. 2001). The method tests a variation of 1% of parameters from the value of the literature.

E.2.5 Model validation

For a rigorous validation of the model, the cAMP profile have been analyzed with simple mathematical parameters which describe the time and space course, and correlate the experimental value of FRET with the simulated concentration of H30-cAMP. It's reasonable to assume that the FRET variation is proportional to the cAMP concentration (Sourjik et al., 2001). If the H30 probe is not saturated and reaches a rapid equilibrium with cAMP, we can

define the FRET signal variation as the ratio between the increments of H30-cAMP complex concentrations respect the initial one:

$$H30 + cAMP \leftrightarrow H30cAMP \qquad\qquad K_e = \frac{[H30cAMP]}{[H30][cAMP]}$$

$$\frac{\Delta r}{r_0} = k_1 \frac{\Delta[cAMP]}{[cAMP]_0} = k_2 \frac{\Delta[H30cAMP]}{[H30cAMP]_0}$$

The time-course of the signal at the membrane was evaluated defining two reference parameters: 1) the time, Tmax, when the signal reaches its maximum variation, 2) the ratio, Peak Depth, between variation of cAMP concentration at Tmax and during the steady state after the peak (Figure). The compartmentalization is quantified by the ratio of the variation of cAMP concentration at Tmax between the membrane and the nucleus (Compart Ratio).

E.2.6 Biological experiment

Cell culture and transfection

HEK293 cells were grown in DME containing 10% FBS supplemented with 2 mM L-glutamine, 100 U/ml penicillin, and 100 µg/ml streptomycin in a humidified atmosphere containing 5% CO_2. For transient expression, cells were seeded onto 24-mm diameter round glass coverslips, and transfections were performed at 50–70% confluence with FuGENE-6 transfection reagent according to the manufacturer's instructions using 1–2 µg DNA per coverslip. Imaging experiments were performed after 24–48 h.

To achieve the selective knockdown of PDE4B or PDE4D subfamilies, we used double-stranded 21-mer RNA duplexes (Dharmacon) targeted at regions of sequence that are unique to each of these subfamilies as described previously (Lynch et al., 2005).

FRET imaging

FRET imaging experiments were performed 24–48 h after transfection. Cells were maintained in Hepes-buffered Ringer-modified saline containing 125 mM NaCl, 5 mM KCl, 1 mM Na3PO4, 1 mM MgS04, 5.5 mM glucose, 1 mM CaCl2, and 20 mM Hepes, pH 7.5, at room temperature (20–22°C) and imaged on an inverted microscope (IX50; Olympus) with a 60x NA 1.4 oil immersion objective (Olympus). The microscope was equipped with a CCD camera (Sensicam QE; PCO), a software-controlled monochromator (Polychrome IV; TILL Photonics), and a beam-splitter optical device (Multispec Microimager; Optical Insights). Images were acquired using custom-made software and processed using ImageJ (National Institutes of Health). FRET changes were measured as changes in the background-subtracted 480/545-nm fluorescence emission intensities on excitation at 430 nm and expressed as either $R/R0$, where R is the ratio at time t and R0 is the ratio at time = 0 s, or $\Delta R/R0$, where $\Delta R = R - R0$.

E.3 Results

Most of the existing mathematical models of intracellular signaling approximate often the cell as a continuous stirred tank reactor (CSTR), where the cell is approximated as an unorganized collection of metabolites and enzymes in a defined volume. The proposed model aims here to test how the presence of steady-state structural and functional order in the cellular volume, influences the cAMP spatio-temporal dynamic. The sensitivity analysis identifies the cAMP diffusivity and the kinetic constants of PDE as the most influent parameters on the spatio-temporal course of intracellular cAMP (data not shown).

In line with this data, we checked:

1) the effect of a structural order, where the molecular crowding close to the membrane determines a lower local cAMP diffusivity in the sub-membrane (SM) domain respect to the cytosolic diffusivity (130 μm^2/s).

2) the influence of a functional order expressed by the localization of specific enzymes in distinct microdomain (PDE4D, PDE4B, PDE3) and by the over-expression of PKA.

E.3.1 Structural order: local cAMP diffusivity

Some studies suggest that the molecular crowding can be responsible of the decreasing of the local cAMP diffusivity in the subdomain next to the membrane or in the caveolae (Gershon, Porter et al. 1985; Verkman 2002). In order to evaluate the role of diffusivity on cAMP intracellular distribution, the model was simulated with diffusion coefficient of 1, 30, 60 and 130 μm^2/s in the SM domain and 130 μm^2/s in cytosol. Simulations of the model are shown in Figure 2a-d and they prove the high influence of the cAMP diffusion on spatio-temporal dynamics of the secondary messenger.

A quantitative evaluation of the results can be done comparing reference parameters Tmax, Peak Depth and Compart Ratio for the experimental (Table 3) and simulated cases (Figure 2).

Table 3 Quantitative evaluation Tmax, Peak Depth and Compart Ratio for the experimental cases

Parameters		Experimental value
Tmax	[s]	125 ± 25
Peak Depth		$0.54 \pm 0,09$
Compart Ratio		$0,22 \pm 0,07$

If the diffusivity of cAMP is everywhere set at 130 $\mu m^2/s$, only a small compartmentalization ratio is observable (0.12, Figure 2a) and the time to reach the maximum concentration is too slow (225s), whereas the Peak Depth is closer to the experimental value (0.55).

Decreasing of diffusivity, the concentration of cAMP next to the membrane becomes higher because of the buffering in the SM domain. The peak on the concentration profile appears when rate of cAMP cleaving and production becomes comparable but some PDE are still not active. The peak is much more visible lower is the rate of PDE activation. When the local diffusivity is low, the PDE activation is more faster, changing the Tmax, which is reached earlier, and reducing the width and the depth of the peak shape.

Quantifying these observations, the Figure 2e shows clearly how a slower diffusion in the SM domain determines by itself an increase of the compartmentalization (Compart Ratio) and a decrease of the Peak Depth values. The effect is much sharper for diffusivities lower than 60 $\mu m^2/s$, when the characteristic diffusion time becomes comparable or lower than the reaction times. Reducing the diffusivity of one order of magnitude (10$\mu m^2/s$), the Compart Ratio increases up to 0.3 reaching a value close to the experimental one, whereas the Peak Depth falls to 0.22.
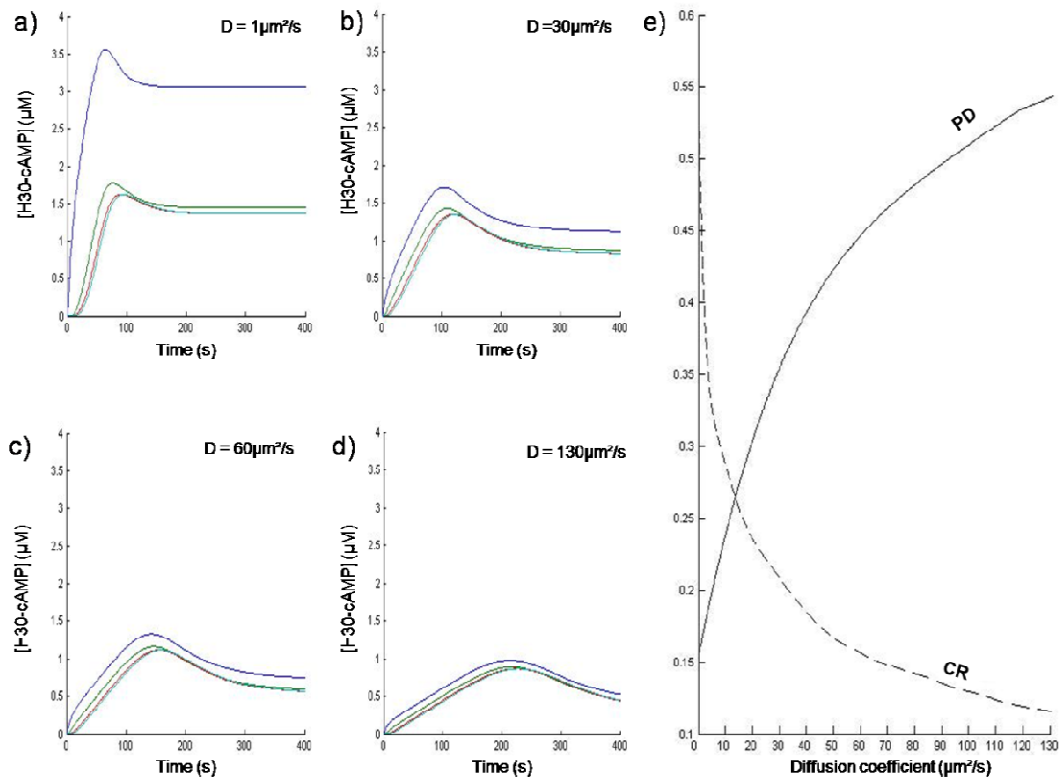
Figure 2 cAMP-H30 profiles for different membrane diffusivity (1, 30, 60, 130µm²/s) near the membrane (blue line) and at 20µm from the membrane (lightblue line) (a,b,c,d respectively). e) Peak depth (continuous line) and compartimetation ratio (dashed line) as function of the membrane diffusivity

Therefore it is clear that the optimal diffusivity should solve the compromise between these two parameter, and 60 μm^2/s seems to respond to this requirement.

E.3.2 Functional order: PDE4B, PDE4D and PDE3 isoforms localization or PKA sovraespression.

Previous studies have demonstrated the predominant role of PDE4 and PDE3 activities in HEK293 cells. In particular, it has been proved a higher influence of PDE4D respect PDE4B on cAMP signaling dynamics in HEK-293 cells stimulated with PGE1 (Terrin, 2006). Here

we sought to investigate the role of localization of each PDE isoforms (PDE4B, PDE4D and PDE3) in either sub-membrane or cytosolic domain. The model was run for different molar percentage of enzyme in the submembrane domain, evaluating the synergy between this phenomena and a lower diffusivity.

In general, due to the bigger dimension and consequent longer residence time in the C domain, the localization of the enzyme in the cytosol determines a more relevant decay of cAMP. This phenomena influences the spatio-temporal evolution of cAMP as shown by reduction of the Peak depth coupled with an increasing of the compartmentalization. However the action of different PDE isoforms is specific.
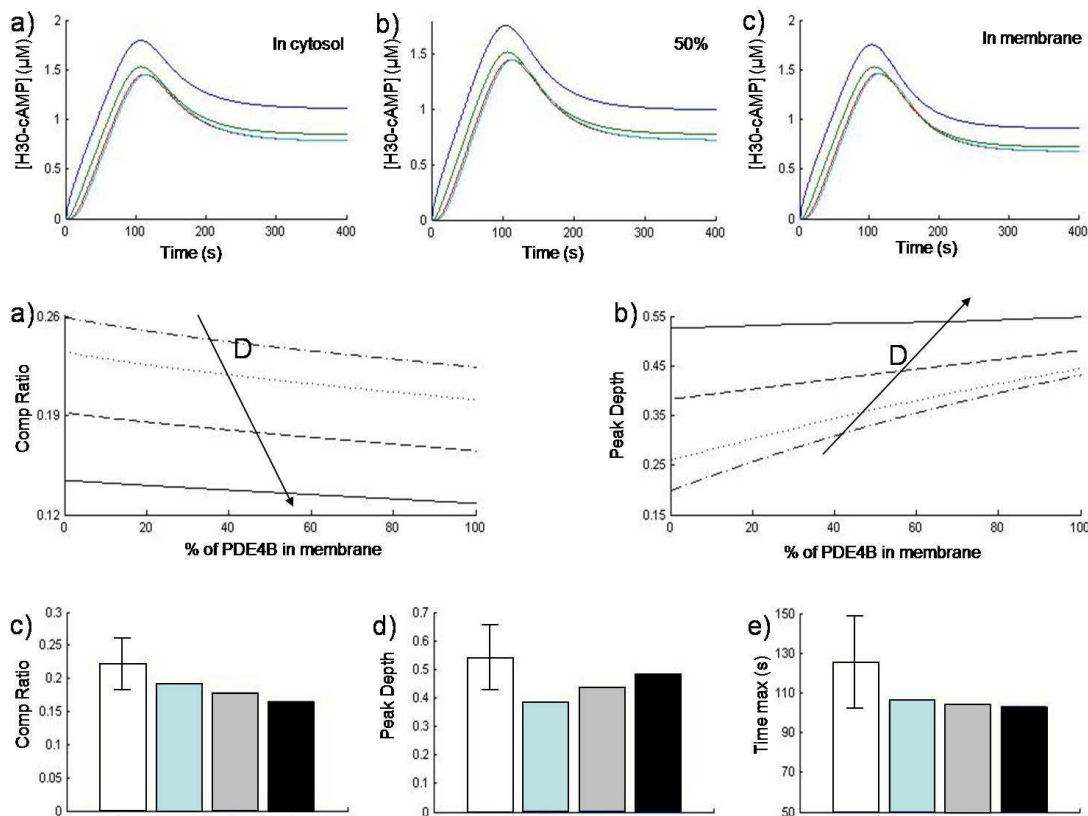

Figure 3 *a) Compartmentalization ratio (b) and peak depth as function of PDE4B concentration in membrane for 4 different membrane diffusivity (130μm²/s (continuous line), 60μm²/s (dashed line), 30μm²/s (dotted line), 1 μm²/s (pricked line)). Comparison between experimental data and simulated data for different percentage of PDE4B in membrane (0, 50 and 100% respectively) in terms of compartmentalization ratio, peak depth and time of maximum concentration for a membrane diffusivity of 60μm²/s (c, d and e) respectively.*

The simulations are consistent with the experimental observations (Terrin, Di Benedetto et al. 2006), showing a low influence on cAMP signaling of PDE4B intacellular distribution (Figure 3c-e). With a local diffusivity of 130 μm^2/s, the localization of PDE4B in the cytosolic compartment determines a changing on Compart Ratio of about 1.5%. As shown in Figure 3a, this parameter changes from a value of 14%, when all the PDE4B are in SM, to the 12.5% when they are located in C. Halving the diffusivity, this difference increases to 2.5%. Similar consideration can be made regarding the Peak Depth profiles, which are almost constant for fast diffusivity (Figure 3b).

A different behavior is underlined by the same analysis performed with PDE4D and PDE3. The simulations (Figure 4-5) show a strong influence of the localization of these enzymes on cAMP spatio-temporal dynamic.

membrane diffusivity of 60μm^2/s (f, g and h) respectively).

Even for very fast diffusion (130μm^2/s), the cAMP compartmentalization is strongly dependant by the PDE4D localization (5% variation, Figure 4a-c). As shown in Figure 4d, this effect is slightly stressed by the lower cAMP diffusivity, obtaining a variation of 8% with a diffusivity of 1μm^2/s. Setting the local diffusivity to 60 μm^2/s, the maximum Compart Ratio is of 21%, reached when all PDE4D is in cytosol.

The diffusivity has also a terrific effect on peak shape, which disappears if the PDE is localized in cytosol for 1 μm^2/s (Figure 4e), evidencing the contribute of this parameter to the activation of PDE.
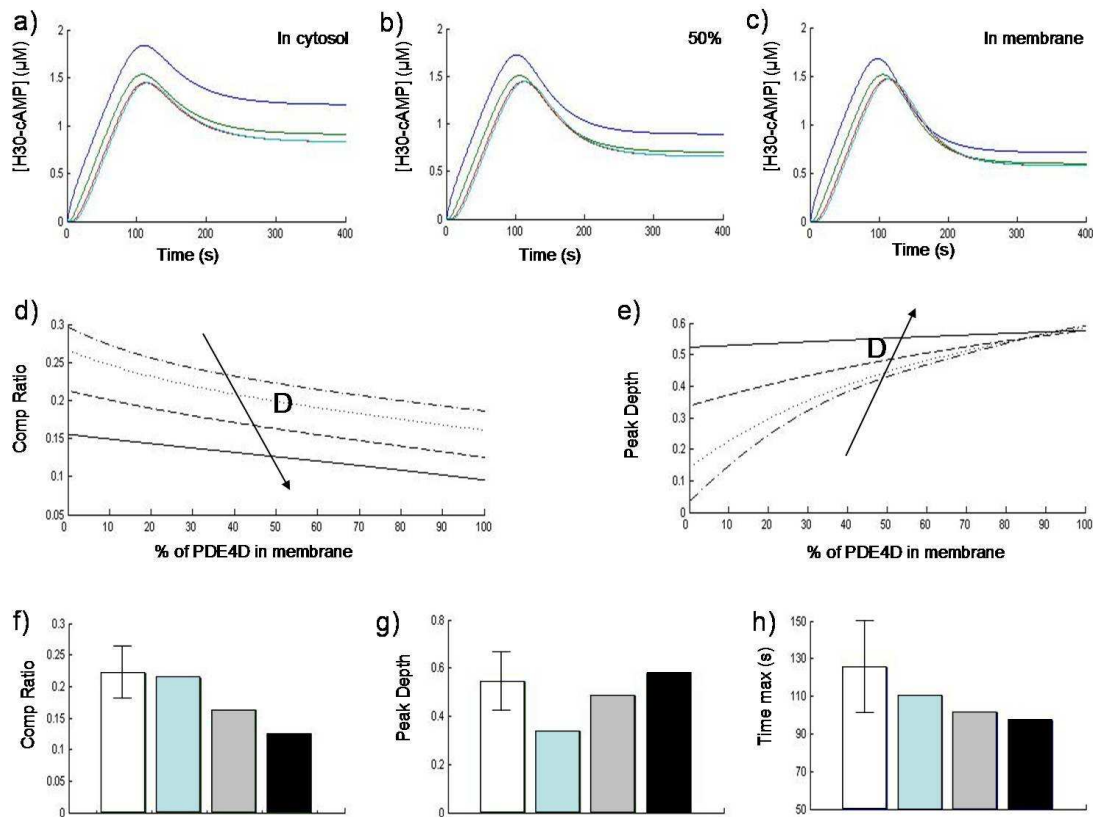
Figure 4 cAMP-H30 profiles for different percentage of PDE4D in submembrane compartment (0, 50%, 100%) near the membrane (blue line) and at 20 μm from the membrane (lightblue line) (a,b,c respectively). Compartmentalization ratio (d) and peak depth (e) as function of PDE4D concentration in membrane for 4 different membrane diffusivity (130μm²/s (continuous line), 60μm²/s (dashed line), 30μm²/s (dotted line), 1 μm²/s (pricked line)). Comparison between experimental data and simulated data for different percentage of PDE4D in membrane (0, 50 and 100% rispectively) in terms of compartmentalization ratio, peak depth and time of maximum concentration for a

The effect of a faster enzymatic action, is proved also by the decreasing of Tmax (Figure 4h) and by the presence of a delay between the membrane and nucleus concentration profiles (10s). When all the enzyme is localized in the SM domain, it is possible to compare the characteristic times of diffusion and reaction and determines the maximus value of diffusivity to obtain a competition between these two phenomena. Therefore the peak shape is much more dependant to the enzyme localization when the diffusivity is lower than 60 μm^2/s.
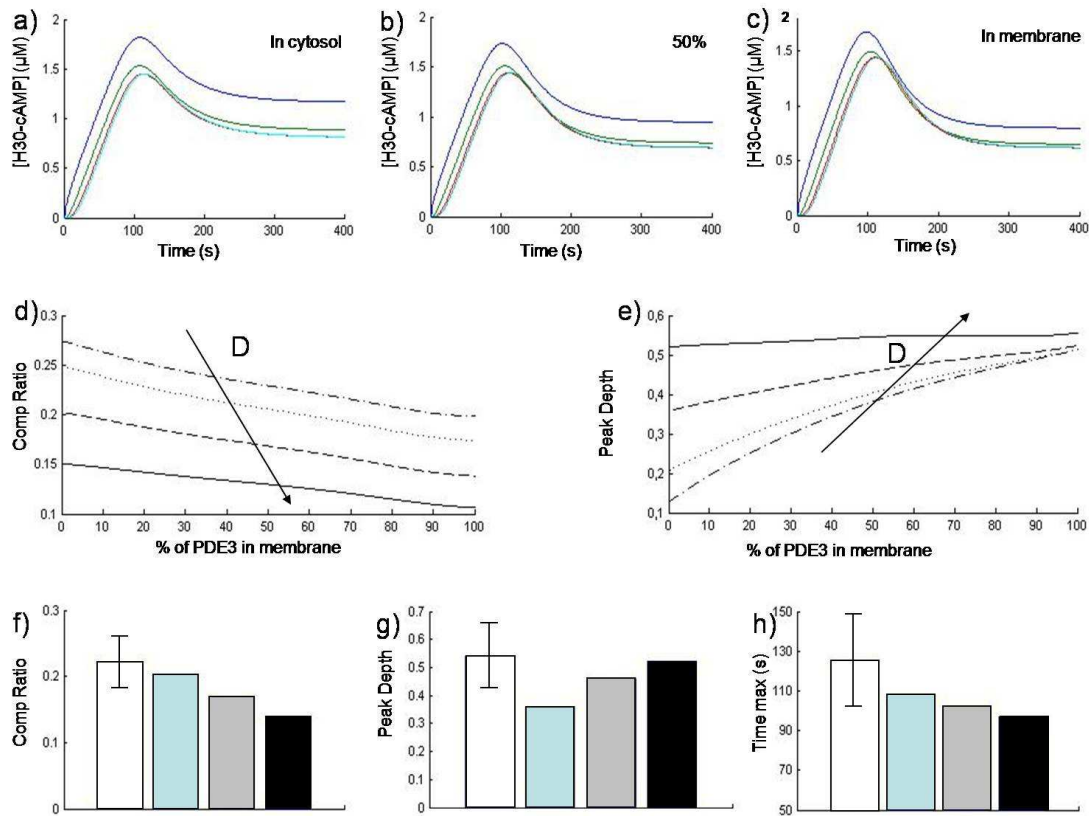
Figure 5 cAMP-H30 profiles for different percentage of PDE3 in submembrane compartment (0, 50%, 100%) near the membrane (blue line) and at 20 μm from the membrane (lightblue line) (a,b,c respectively). Compartmentalization ratio (d) and peak depth (e) as function of PDE3 concentration in membrane for 4 different membrane diffusivity (130μm²/s (continuous line), 60μm²/s (dashed line), 30μm²/s (dotted line), 1 μm²/s (pricked line)). Comparison between experimental data and simulated data for different percentage of PDE3 in membrane (0, 50 and 100% respectively) in terms of compartmentalization ratio, peak depth and time of maximum concentration for a membrane diffusivity of 60μm²/s (f, g and h) respectively.

As shown in Figure, the Peak Depth (PD) profile is also function of the PDE4D localization and cAMP local diffusivity. Lower is the cAMP local diffusivity, more significative is the reaction contribute to the concentration profile. Percentages lower than 50% reproduce the experimental value with a diffusivity of 60 μm^2/s. These results prove the importance of PDE4D close to the membrane, as suggested by the experimental evidences.

Similar observations can be done about the effect of PDE3 compartmentalization (Figure 5). As shown in Figure, assuming a local cAMP diffusivity of 60 μm^2/s, a molar percentage of PDE3 in SM domain of about 50% adequately reproduces all the experimental profiles. In

good agreement with the experimental observations, PDE4D and PDE3 mainly control the cAMP expression, with a predominance of the PDE4D.
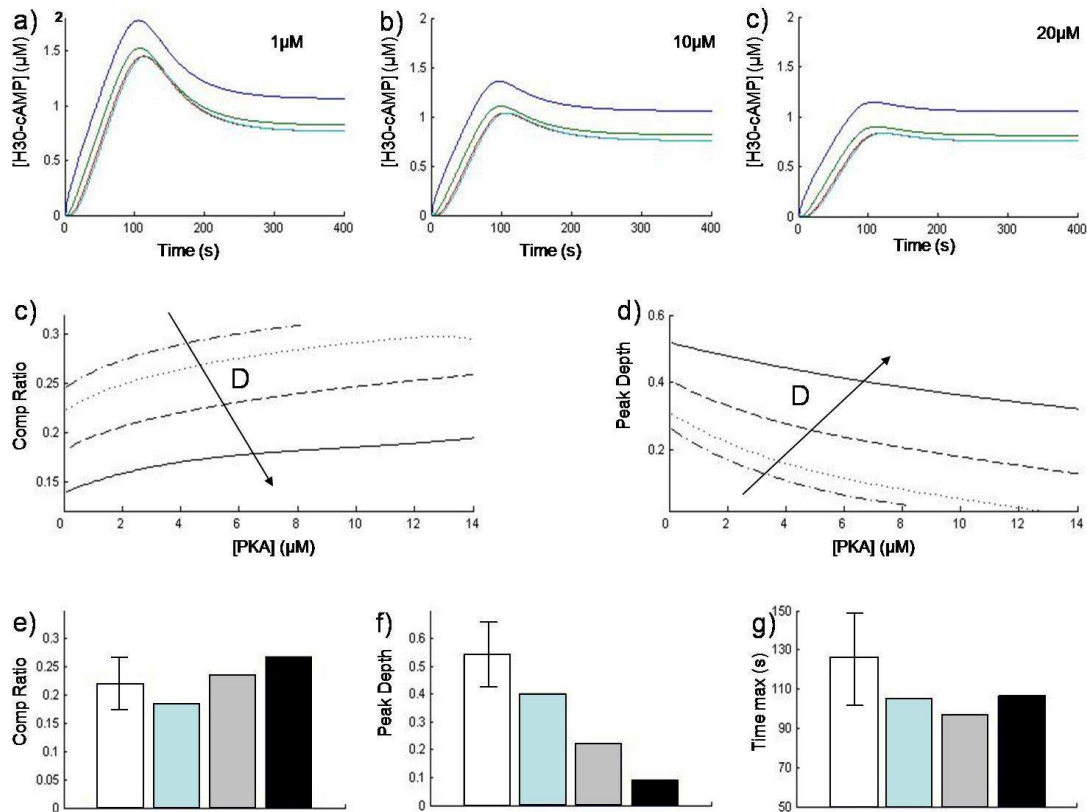

Figure 6 cAMP-H30 profiles for different membrane PKA concentration (1, 10, 20 mM) near the membrane (blue line) and at 20 μm from the membrane (lightblue line) (a,b,c respectively). d) Compartimetation ratio (d) and peak depth (e) as function of PKA concentration for 3 different membrane (130μm²/s (continuous line), 60μm²/s (dashed line), 30μm²/s (dotted line), 1 μm²/s (pricked line)). Comparison between experimental data and simulated data for different PKA concentration (1, 10, 20μM) in of compartimentation ratio, peak depth and time of maximum concentration for a membrane diffusivity of 60μm²/s (e), f) and g) respectively).

Experimental evidences of PKA particular affinity for specific membrane protein (AKAP) have been reported in literature (Kapiloff 2002; McConnachie 2006). The localization of these protein could justify different PKA concentrations in specific intracellular compartments. To further investigate the relative of PKA on cAMP signal modulation, the model was run for different PKA concentration. As shown in Figure, the cAMP spatio-

temporal dynamics is strongly influenced by the PKA concentration determining an increasing of the Compart Ratio of about 10 % if the concentration changes 1 to 20μM. Higher PKA concentration will decrease the free cAMP concentration acting as buffer and enhancing the PDE activity. Particularly significative is also the changing on peak shape, which progressively disappeared increasing the PKA concentration and reducing the local diffusivity.

E.4 Discussion and Conclusion

The fascinating stability of the signal transduction of highly variable and complex extracellular inputs specific response seem to be related to a versatile use of high diffusible signalling molecules, such as cAMP, through spatial-temporal pattering inside the cell.

The biochemistry of cAMP signaling has been partially elucidated with several analytical models developed on different types of cell. However most of these models consider only the time course of cAMP close to the membrane: 1) describing the cAMP production and degradation, and the opening of membrane channel as effect of the high concentration of cAMP(Goldbeter 1996), 2) integrating cAMP production and degradation in different signaling pathways (Bhalla and Ravi Iyengar 1999; Saucerman, Brunton et al. 2003) 3) underlining the role of PKA e PDE activation on cAMP degradation (Golbunova Y.V. 2002; Gorbunova and Spitzer 2002; Rich, Xin et al. 2007). Even though these models were kinetically complete, no attention has been given to cAMP intracellular spatial distribution, fundamental for the activation of specific targets. Rich et al. (2001) tried to combined the biochemical description of the process with a physical compartmentalization of the space. The cell was modeled assuming the existence of two compartments: the membrane-localized microdomain and the bulk cytosol. The diffusion was significantly impeded between the two

domains, whereas inside each compartment it was assumed so rapid that any spatial difference was abolished.

Huang et al. (1991) shows the importance of the diffusion and the rate of hydrolysis on the kinetic of Na^{2+} current dependent by the intracellular concentration of cAMP. However the model simulates a simplified system with free and isotropical cAMP diffusion in an infinite cytosol and incomplete chemical description of the signalling. The activation of PDE or the binding with PKA are in fact not considered. In this direction the models developed by Bhalla (2004) e Kholodenko et al. (2003) are particularly interesting because they describe the effect of diffusion limited regime on the signal intracellular distribution, even if the specific description of cAMP spatio-temporal distribution is not investigated.

A quantitative diffusion-reaction model has been implemented here to simulate the spatio-temporal evolution of the cAMP signalling, hypothezing that the intracellular organization of cell, in proximity to the cAMP targets, directs and amplifies the biological effects of the highly diffusible secondary messenger, localizing its concentration. Qualitatively, assuming homogenous intracellular concentrations of PKA and PDE and ubiquitous cAMP diffusivity of $130\mu m^2/s$, the simulations agree with the experimental results showing a transient peak of cAMP after the PGE1 stimulation. However to deeper quantitative analysis, no one of the reference experimental parameters are reproduced with these hypotheses, either Tmax or Peak Depth, that are significantly higher, either Compart ratio, that is much lower.

The reduction of the local diffusivity of cAMP of one order of magnitude has a terrific effect in term of concentration profile development enhancing the compartimentalization and decreasing the peak depth. The simple competition between reactions and diffusion, is more than enough to justify the presence of self-organized dissipative spatio-temporal structures. The literature report several experimental evidences of a lower local diffusivity in the

cytoplasm than in the water (Luby-Phelps, 2000; Verkman, 2002; Perez et al., 1999; Mastro and Babich, 1984; Mastro and Keith, 1984). It is then reasonable to think that the molecular crowding in these discrete micro-domains will further influence the cAMP local diffusivity. However the *in vivo* determination of this value is really complex to measure because of the high reactivity and diffusivity of this secondary messenger. In this sense this mathematical modeling offer the unique opportunity to test the biological importance of local diffusivity modulation inside the cell. Our data underlines a predominant influence of cAMP diffusivity in the submembrane domain on the cAMP compartmentalization.

The local diffusivity modulation is not the only way to influence the cAMP spatio-temporal evolution. If for fast diffusion time, the localization of specific enzymes doesn't influence significantly the profile expression of secondary messangers, value of diffusivity of $60\mu m^2/s$ is enough to show a relevant effect of an intracellular structural order are enough to localization of specific PDE or PKA in-homogeneity on cell volume features is not expressed only by the decreasing on local diffusivity but also by the specific localization of enzymes, which deternine locally the reducing of reaction time. The effect of an intracellular structural order has been tested considering molecular crowding on the submembrane compartment, or specific enzymes localization, such as PDE4D, PDE4B, PDE3 e PKA. In presence of a low diffusivity the displacement of PDE isoforms in the cytosolic domain determines a decrease on the peak concentration and a higher Peak Depth. These simulations agrees with the experimental observations demonstrating the biological importance of maintaining precise control of PDE4D distribution within the cell whatever is the cAMP diffusivity at the submembrane domain.

E.5 References

Abramovitch, R., E. Tavor, et al. (2004). "A Pivotal Role of Cyclic AMP-Responsive Element Binding Protein in Tumor Progression." Cancer Res **64**(4): 1338-1346.

Alberts, B., A. Johnson, et al. (2002). Molecular Biology of the Cell, Garland Science.

Barnes, A. P., G. Livera, et al. (2005). "Phosphodiesterase 4D Forms a cAMP Diffusion Barrier at the Apical Membrane of the Airway Epithelium." J. Biol. Chem. **280**(9): 7997-8003.

Bhalla and Ravi Iyengar, U. S. (1999). "Emergent Properties of Networks of Biological Signaling Pathways." Science **283**(5400): 381-387.

Bird R., S. W., Lightfoot E., (2002). Transport Phenomena.

Claudia, P., S. Salvatore, et al. (2006). "cAMP controls oxygen metabolism in mammalian cells." FEBS letters **580**(18): 4539-4543.

Dachicourt, N., P. Serradas, et al. (1996). "Decreased glucose-induced cAMP and insulin release in islets of diabetic rats: reversal by IBMX, glucagon, GIP." Am J Physiol Endocrinol Metab **271**(4): E725-732.

Dumaz, N., R. Hayward, et al. (2006). "In Melanoma, RAS Mutations Are Accompanied by Switching Signaling from BRAF to CRAF and Disrupted Cyclic AMP Signaling." Cancer Res **66**(19): 9483-9491.

Feliciello, A., M. E. Gottesman, et al. (2005). "cAMP-PKA signaling to the mitochondria: protein scaffolds, mRNA and phosphatases." Cellular Signalling **17**(3): 279-287.

Gershon, N. D., K. R. Porter, et al. (1985). "The Cytoplasmic Matrix: Its Volume and Surface Area and the Diffusion of Molecules through It." Proceedings of the National Academy of Sciences **82**(15): 5030-5034.

Golbunova Y.V., S. N. C. (2002). "Dynamic interactions of cyclic cAMP transient and spontaneous Ca2+ spikes." Nature **418**: 93-96.

Goldbeter (1996). Biochemical oscillations and cellular rhythms: the molecular bases of periodical and chaotic behaviour.

Gorbunova, Y. V. and N. C. Spitzer (2002). "Dynamic interactions of cyclic AMP transients and spontaneous Ca2+ spikes." Nature **418**(6893): 93-96.

Huang R.-C., G. R. (1991). "Kinetic analysis of cAMP-activated Na+ current in the molluscan neuron." J. Gen. Physiol **98**: 835-848.

Isshiki, M., J. Ando, et al. (2002). "Sites of Ca2+ wave initiation move with caveolae to the trailing edge of migrating cells." J Cell Sci **115**(3): 475-484.

Kapiloff, M. S. (2002). "Contributions of Protein Kinase A Anchoring Proteins to Compartmentation of cAMP Signaling in the Heart." Mol Pharmacol **62**(2): 193-199.

Kozer N., S. G. (2004). "Effect of Crowding on Protein–Protein Association Rates: Fundamental Differences between Low and High Mass crowding Agents." J. Mol. Biol. **336**: 763–774.

Lynch, M. J., G. S. Baillie, et al. (2005). "RNA Silencing Identifies PDE4D5 as the Functionally Relevant cAMP Phosphodiesterase Interacting with {beta}Arrestin to Control the Protein Kinase A/AKAP79-mediated Switching of the {beta}2-Adrenergic Receptor to Activation of ERK in HEK293B2 Cells." J. Biol. Chem. **280**(39): 33178-33189.

McConnachie, G., L. K. Langeberg, et al. (2006). "AKAP signaling complexes: getting to the heart of the matter." Trends in molecular medicine **12**(7): 317-323.

McConnachie, G., L. K. Langeberg, et al. (2006). "AKAP signaling complexes: getting to the heart of the matter." Trends in Molecular Medicine **12**(7): 317-323.

Nikolaev, V. O., M. Bunemann, et al. (2006). "Cyclic AMP Imaging in Adult Cardiac Myocytes Reveals Far-Reaching {beta}1-Adrenergic but Locally Confined {beta}2-Adrenergic Receptor-Mediated Signaling." Circ Res **99**(10): 1084-1091.

Ostrom, R. S., X. Liu, et al. (2002). "Localization of Adenylyl Cyclase Isoforms and G Protein-Coupled Receptors in Vascular Smooth Muscle Cells: Expression in Caveolin-Rich and Noncaveolin Domains." <u>Mol Pharmacol</u> **62**(5): 983-992.

Peters R. (1984). "Nucleo-cytoplasmic flux and intracellular mobility in single hepatocytes measured by fluorescence microphotolysis." <u>The EMBO Journal</u> **3**(8): 1831-1836.

Prigogine (1961). <u>Thermodynamics of Irreversible Processes</u>.

Pugh, E. N., , Jr. (2000). "Transfected Cyclic Nucleotide-gated Channels as Biosensors." <u>J. Gen. Physiol.</u> **116**(2): 143-146.

Rich T., F. K. A., Tse T. E., Schaack J., Cooper D. M., Karpen J. W. (2001). "A uniform extracellular stimulus triggers distinct cAMP signals in different compartments of a simple cell." <u>PNAS</u> **98**: 13049-13054.

Rich, T. C., W. Xin, et al. (2007). "Cellular mechanisms underlying prostaglandin-induced transient cAMP signals near the plasma membrane of HEK-293 cells." <u>Am J Physiol Cell Physiol</u> **292**(1): C319-331.

Rybin, V. O., X. Xu, et al. (2000). "Differential Targeting of beta -Adrenergic Receptor Subtypes and Adenylyl Cyclase to Cardiomyocyte Caveolae. A MECHANISM TO FUNCTIONALLY REGULATE THE cAMP SIGNALING PATHWAY." <u>J. Biol. Chem.</u> **275**(52): 41447-41457.

Saltelli, A., K. Chan, et al. (2001). <u>Sensitivity analisys</u>

Sato, M., T. Ozawa, et al. (2002). "Fluorescent indicators for imaging protein phosphorylation in single living cells." <u>Nat Biotech</u> **20**(3): 287-294.

Saucerman, J. J., L. L. Brunton, et al. (2003). "Modeling {beta}-Adrenergic Control of Cardiac Myocyte Contractility in Silico." <u>J. Biol. Chem.</u> **278**(48): 47997-48003.

Saucerman, J. J. and A. D. McCulloch (2006). "Cardiac beta-Adrenergic Signaling: From Subcellular Microdomains to Heart Failure." <u>Ann NY Acad Sci</u> **1080**(1): 348-361.

Shampine (1994). <u>Numerical solution of ordinary differential equation.</u> New York, Chapmann & Hall.

Steinberg, S. F. (2004). "[beta]2-Adrenergic receptor signaling complexes in cardiomyocyte caveolae/lipid rafts." <u>Journal of Molecular and Cellular Cardiology</u> **37**(2): 407-415.

Terrin, A., G. Di Benedetto, et al. (2006). "PGE1 stimulation of HEK293 cells generates multiple contiguous domains with different [cAMP]: role of compartmentalized phosphodiesterases." <u>J. Cell Biol.</u> **175**(3): 441-451.

Verkman, A. S. (2002). "Solute and macromolecule diffusion in cellular aqueous compartments." <u>TRENDS in Biochemical Sciences</u> **27**: 27-33.

Zaccolo, M., P. Magalhaes, et al. (2002). "Compartmentalisation of cAMP and Ca2+ signals." <u>Current Opinion in Cell Biology</u> **14**(2): 160-166.

Zaccolo, M. and T. Pozzan (2002). "Discrete Microdomains with High Concentration of cAMP in Stimulated Rat Neonatal Cardiac Myocytes." <u>Science</u> **295**(5560): 1711-1715.

Zippin, J. H., Y. Chen, et al. (2002). "Compartmentalization of bicarbonate-sensitive adenylyl cyclase in distinct signaling microdomains." <u>FASEB J.</u>: 02-0598fje.

Appendix F

Synthesis and characterization of injectable hydrogel based on photoinitiator-hyaluronic acid conjugate for biomedical applications

Elisa Figallo[1-2], Andrea dal Cin[1], Cristina Longinotti[2], Nicola Elvassore[1]

[1]Department of Chemical Engineering, University of Padova, via F. Marzolo 9, I-35131 Padova, Italy

[2]Fidia Advanced Biopolymer srl (FAB), Via Ponte della Fabbrica 3/A 35031 Abano Terme (Padova), Italy

([*])To whom correspondence should be addressed

E-mail: nicola.elvassore@unipd.it

phone: +39 (049) 8275469; fax: +39 (049) 8275461

Abstract

The research on tissue engineering and drug delivery has been recently focused on injectable photocrosslikable hydrogels based on hyaluronic acid (HA). In this work, we synthesized a novel pothoinitiator-hyaluronic acid conjugate (HYAF120[®]) which can photopolymerized in absence of a photoinitiator in a crosslinked polymeric network. The objective of this study is to characterized the physical and mechanical properties of this hydrogel and evaluate its feasibility as cell carrier for in vivo cell delivery. In particular, the chemical structure, the mechanical properties, the morphology and the *in vitro* degradation rate of the cross-linked hydrogel was investigated for different HA concentrations and crosslinking exposure energy. Mechanical properties of the hydrogel studied by rheological measurements show a well-developed cross-linked polymer network at short exposure time. The elastic modulus is a range of 1-2 kPa and constantly higher than viscous modulus. The results confirm that these two modulus are increasing with exposure time and HA concentration, up to a plateau around 40mg/ml. The equilibrium swelling theory was used to determine the cross-link density, given by the effective number of cross linked subunit ν_e and the average molecular weight between cross links M_c. The results confirm the rheological observations with a decreasing of the swelling capacity with the increasing of the exposure time and HA concentration up to a plateau. Finally, the effect of light exposure on cell viability was evaluated with HL1 cardiomyocyte cell line. The cells were then encapsulated into hydrogel and remained viable as demonstrated by MTT assay and hystology.

F.1 Introduction

Hydrogels are highly hydrated polymeric networks that have been fabricated from a wide range of hydrophilic polymers (Anna C. Jen 1996; Peppas and Sahlin 1996; Grijpma, Hou et al. 2005). Since they are characterized by good biocompatibility (J.A. Cadée, Luyn et al. 2000), suitable physical properties (Anseth, Bowman et al. 1996) and efficient mass transport (Ingrid Zhang 1996), they have been proposed for controlled release of bioactive macromolecules and for tissue engineering applications (Hennink and van Nostrum 2002; Hoffman 2002). Moreover, because the hydrogel can be used in combination with non-invasive clinical techniques, they have been extensively exploited as promising cell carrier systems for healing and regeneration of damaged tissues (Stocum 1998; Hubbell 1999; Ratner 2002). One of the main limitations for the effective development of stem cell based clinical therapy are: i) the definition and the control of an artificial "in vivo" microenvironment within the 3D hydrogel network which has to be suitable for cell growth and organization; ii) the lack of methods and apparatus for efficient delivering of a confluent population of cells (Penn and Topol 2007).

Among various hydrogels, those based on hyaluronic acid (HA) have captivated the enthusiasm of scientists and clinicians because they are chemically, structurally and mechanically designed to capture some of the features of native extra cellular matrix (ECM) (Jennie Baier Leach, Bivens et al. 2003; Anderson, Burdick et al. 2004; Burdick, Chung et al. 2005; Ali Khademhosseini, Eng et al. 2006). HA is ubiquitously distributed and is known to co-regulate gene expression, signaling, proliferation, motility, adhesion, metastasis, and morphogenesis (Toole 2004). Furthermore, HA plays a prominent role in various wound-healing processes, because it promotes early inflammation, which is a critical steps during

the wound healing, but then moderates later stages of this process, allowing matrix stabilization and reduction of long term inflammation (Chen and Abatangelo 1999). Moreover, several physicochemical aspects of HA are advantageous for biomaterial fabrication and application. For example, HA can be easily and controllably produced in large quantities through microbial fermentation, enabling the scale-up of HA-derived products (Lapcik, De Smedt et al. 1998) and avoiding the risk of animal-derived pathogens. This cumulative evidence suggests that HA is an ideal candidate material for the design of effective biomaterial.

On the other hand, from a clinical perspective, among different cell delivery systems the cell injection represent one of the most promising non-invasive techniques and the use of hydrogel shows a significant improvement over cell injections with saline or culture media.

The ideal injectable material should: i) have controllable and homogenous physico-chemical properties; ii) not affected by the *in vivo* conditions during the polymerization; iii) support attachment and differentiation of injected cells; iv) remain mechanically stable enough to provide temporary scaffolding and structural support. The *in vivo* photopolymerization has several advantages over conventional polymerization techniques, such as increased spatial and temporal control over polymer crosslinking, fast curing rates, injection of fluid-like viscosity material at physiological conditions and, consequently, the formation of in situ hydrogels in a minimally invasive manner (Anseth and Burdick 2002), (Nettles, Vail et al. 2004).

However, *in vivo* photopolymerization cannot lead to reproducible and homogeneous products for difficulty of controlling environmental condition overall hydrogel volume (for example pH, temperature, ionic strength or photo initiator concentration). Moreover, the

photoinitiator activated by at specific light wavelength produce radical initiating species and product which can be toxic if it is not quickly removed.

It seems that the control of the stechiometric ratio between the HA and the photoinitiator, and the homogenous dispersion of the photoinitiator within the HA blend can be considered one of the key aspect in developing clinical grade photocrosslinkable hydrogel.

In this article, we describe the development of a new injectable hydrogel (HYAFF120[®]) based on pothoinitiator-hyaluronic acid conjugate which can be easily crosslinked in homogeneous hydrogel under UV exposure. This formulation is ready to use and does not require any additional mixing of initiators or reagents. It can be sterilized by conventional autoclave, mixed with cells, injected and photopolymerized in vivo.

In order to characterize the hydrogel in the view of clinical application as cell delivery carrier, we studied the physico-chemical properties of several hydrogels, including elastic and viscous modulus, swelling ratio and degradation rate, checking in particular the effect of polymer concentration and UV exposure energy. Furthermore, we investigated the effect of UV exposure energy, required for photocrosslinking, on the viability of HL1 cell line and the possibility of using this material drug or cell carrier supporting the cell proliferation and growth.

F.2 Material and methods

F.2.1   Photoinitiator-HA   conjugate   (HYAFF120)   chemical
synthesis

The photoinitiator-HA conjugate (Hyaff120®) is an esterified derivative of hyaluronic acid
(HA) obtained by chemical reaction between HA with an alcohol bromide, which behaves as
photoinitiator during the hydrogel curing. HA (200 kDa) was provide by Fidia S.p.a (Abano
Terme, Italy) and was produced by fermentative process. The photoinitiator, 1-[4-(2-
Hydroxyethoxy)-phenyl]-2-hydroxy-2-methyl-1-propane-1-one (HHMP, Irgacure 2959) was
purchased from Fluka. The process of bromination of HHMP includes a first stage with 5
hours reaction between HHMP and chloride dimethyl sulfoxide (Fluka) at room temperature
in anhydrous methane dichloride (Carlo Erba, Italy). This is followed by bromination with
lithium bromide (Fluka) in boiling acetone for about 12-18 hours. Once the bromination was
completed, the extraction allowed the separation between inorganic and organic phase, the
latter containing the desired product which was analysed by means of High Pressure Liquid
Cromatography (Perkin Helmer, MA, USA). The purity of the HHMP bromide was 83%.

The HA was salified and freeze-dried to get a greatly hygroscopic ammonium salt (HATBA).
The HATBA esterification was conducted in n-methyl pyrrolidone (NMP, Carlo Erba, Italy)
and HHMP bromide was slowly added up to the exact quantity in order to achieve a degree
of carboxylic groups substitution in HA molecule equal to 50%. The reactor was made of
glass and it was provide with a cooling/heating jacket and a mechanical stirrer (60-80 rpm).
The reaction took 25-30 hours at a temperature of 37° C. To follow the reaction, 2 ml of

solution were withdrawn at different times from the volume of reaction, they were carefully weighted and diluted up to 10 ml in the elution solvent of HPLC(Perkin Helmer, column Nucleosil C18). In this way it was possible to calculate the esterification percentage, monitoring the product quality in real time.

Once the reaction was completed, the temperature was turned down to 10° C and water was added in the reactor. By mixing methane dichloride with the solution, the aqueous phase containing the product was separated from the organic phase containing NMP and methane dichloride. The aqueous extract was collected and slowly mixed with ethanol which was absorbed by the product up to saturation. Once this point was reached, a thin white powder gradually precipitated and it was recovered by filtering. Finally the powder was washed by mixing with a solution of water and ethanol in order to remove reaction residuals as chlorine ions and it was further vacuum-dried.

The chemical structures of both Hyaff120® and HA were compared by means of infrared spectroscopy (Nexus 670 Nicolet).

F.2.2 Hydrogel preparation

The partial esterification guaranteed the product solubility in physiological solution which was subsequently sterilized in autoclave. The hydrogel was formed irradiating the solution with 366 nm UV light. The light exposure allowed the formation of radical species responsible of initiating the cross-link reaction resulting in a wall to wall compact hydrogel. For the physical characterization, the solution was placed in multi-wells (Iwaki, diameter 22 mm) which were irradiated by UV lamp (Triwood 6/36 Helios Italquartz) at a distance of 2 cm ($4mW/cm^2$). As this lamp was too cumbersome, it was not suitable for *in vivo* applications where precision of localization was requested. Thus the biocompatibility

analysis was carried out using a Bluewave50 lamp (Dymax) provided with a water-probe of diameter 0.5 cm which emitted a 366 nm conical beam. The light intensity decreases as function of the sample distance from the probe (427 mW/cm^2 at 2 cm).

F.2.3 Rheological measurements

A rheometer (Rheostress RS150 Haake) was used to evaluate viscoelastic and rheological properties of cross-linked hydrogel. It was equipped with a temperature control (20.0±0.5° C) and a plate-cone sensor (1°) of 60 mm diameter. During measurements the distance between cone and plate was 0.051 mm. Experiments were carried out on different concentrations of Hyaff120$^®$ solutions from 10 up to 75 mg/ml. Higher concentrations gave solutions too viscous and so unlikely workable. The solution rheological behaviour (before irradiation) was evaluated by analyzing the shear stress as function of rising deformation rates (0-5 s^{-1}). Stress sweep measurements on cross-linked hydrogels were performed in order to find its linear viscoelastic region where the complex modulus was independent from the shear stress. Finally, elastic (G') and viscous (G") moduli of cross-linked hydrogels were calculated as function of rising oscillation frequencies (0.1-10 Hz) at constant shear stress ($\tau = 1$ Pa).

For all concentrations hydrogel disks (1.5 ml) were prepared by UV curing for 3 and 5 min at 2 cm distance from the Triwood lamp (4mW/cm^2). The time of exposition had to be long enough to allow the hydrogel formation but also reasonable for a future *in vivo* application.

Elastic and viscous moduli were also measured for hydrogels cured by means of Bluewave50 probe: samples of different concentrations (10, 20 and 30 mg/ml) and exposition times (from 3 s up to 5 min) were prepared at a distance equal to 2 cm from the probe (427±2.5 mW/cm^2).

F.2.4 *In vitro* degradation

The degradation process was studied on samples of different Hyaff120® concentrations ranging from 10 to 75 mg/mll. First, all solutions were cross-linked in multi-well Iwaki of 22 mm diameter at 2 cm distance from the Triwood lamp for 1, 3 and 5 min (4 mW/cm²). Then the disks were weighed , placed in 60×15 mm Petri, dipped under 5 ml of saline buffer (pH = 6.98), closed with parafilm and incubated at 37° C up to 28 days. The solution were analyzed by means of HPLC which allowed the determination of alcohol HHMP and Hyaff120® concentrations as function of incubation time, following the kinetics till complete degradation.

F.2.5 Swelling measurements

One ml of solution ranging from 10 to 75 mg/ml were cross-linked in multi-well (Iwaki) of 22 mm diameter at 2 cm from the Triwood lamp for 1, 3 and 5 min (at 4 mW/cm²). The disks were weighed and gently dried at 37° C for about 24 hours. The samples were reweighed, placed in larger multi-well (36 mm diameter) and dipped under 10 ml of physiological solution at room temperature. The weight swelling ratio (Q_M) was monitored by weighing the disks from 5 min up to 3 days after dipping, when the equilibrium conditions were reached:

$$Q_M = \frac{W_S}{W_D} \times 100, \tag{1}$$

$$W_S = W_D (Q_M - 1). \tag{2}$$

where W_S (g) and W_D (g) are the weights of swelled and dried hydrogels respectively.

F.2.6 Hydrogel morphology

The morphology of cross-linked structure was analyzed by SEM (JSM-6490 Jeol). Two ml of solutions ranging from 10 up to 75 mg/ml were cross-linked in multi-well Iwaki of 22 mm diameter at 2 cm from the Triwood lamp for 5 min (4 mW/cm^2). The samples were freeze-dried, gold sputtered and analyzed (Lyovac GT2 Leybold-Heraeus).

F.2.7 Photo-encapsulation of HL1 cells

The HL-1 cells are a cardiac muscle cell line, derived from the AT-1 mouse, atrial cardiomyocyte tumor lineage and were cultured as reported in literature (Claycomb, Lanson et al. 1998). HL1 cells were added to the precursor solution at a concentration of 10^6 cells/mL. A volume of 100 µL of the cells/HYAFF120 mixture was poured into 96 multi-wells, and photopolymerized. The cultures were incubated (Heraeus BBD 6220) at 37° C and the HL-1 culture medium was substituted daily. As reported in literature, the cells grew, proliferated and express phenotype of adult cardiomyocytes.

F.2.8 Cell viability and proliferation

The effect of UV exposure on cell viability was evaluated by Trypan Blue and Live/dead assay. HL1 cell and culture solution (100 µL) was placed in 96 multi-wells (10^6 cells/mL each) and irradiated for 3 s up to 10 min (at 1.1 W/cm^2). A 50 µl of solution was mixed with equal volume of Trypan Blue and the dead cell fraction was counted in the Burker's room.

The cell viability was assessed through live/dead assay (Molecular Probes, Eugene, OR) after 2 days of culture in hydrogel photo-polymerized for 3 s up to 10 min exposure (at 1.1 W/cm^2). This fluorescence based method detects live and dead cells using 3mM calcein AM

and 3mM ethidium homodimer-1 (EthD-1) dye. The calcein AM is well retained within live cells and converted enzymatically in green fluorescent calcein (ex/em ~495 nm/~515 nm). EthD-1 enters cells with damaged membranes where it binds to nucleic acids, thereby producing a bright red fluorescence in dead cells (ex/em ~495 nm/~635 nm). Each well was covered by 100 µL of the combined live/dead dyes solution using concentration of 3mM for calcein AM and ethidium. The solution was incubated for 90 minutes at room temperature. The labeled cells were observed using fluorescence microscope Zeiss inverted microscope.

F.2.9 Cell proliferation (MTT)

After mixing the culture solution with Hyaff120® previously solubilised in physiological liquid, the 100 µL final solution (30mg/ml) was placed in 96 multi-wells ($2x10^6$ cells/mL) and cross-linked by UV exposure 20 s (at 1.1 W/cm^2). Finally the hydrogels were placed in 24 multi-wells and dipped in 2 mL of culture medium.

The proliferation of HL1 cell line encapsulated in hydrogel was measured by MTT test (Sigma-Aldrich), which evaluate the presence of mitochondrial dehydrogenase activity enzyme from viable cells. The yellow tetrazolium MTT (3-(4, 5-dimethylthiazolyl-2)-2, 5-diphenyltetrazolium bromide) is cleaved during the 4 hours incubation at 37°C to form a dark blue formazan crystals which is largely impermeable to cell membranes. The resulting intracellular purple formazan can be solubilized in isopropanol/dimethyl sulfoxide (90/10% volumetric ratio) solution and quantified by spectrophotometric means (λ=580 nm).

F.2.9 Histological analysis

Histological analysis by means of ematossilin and eosin allowed to evaluate the cell distribution inside the hydrogel. Particularly, the first, acidophil substance, coloured cell

nuclei and hydrogel violet, whereas the second, basophile substance, coloured cell cytoplasm purple. The sample was frozen in liquid nitrogen and sectioned (25 μm). The sections were collected on a glass slide and dipped in ematossilin for 1min and 30 s. After rapid wash in water (2 min), the slide was dipped 8-12 times in acidulous alcohol (400 ml of ethanol 70% with 1 mL of hydrochloric acid 12N) in order to decrease the intense colour of ematossilin. The eosin staining was achieved dipping the slide in eosin for 2 min and quickly washing in water to remove the excess of dye. The staining was fixed dipping the slide in ethanol 50% for 1min, 80% for 4 min, 100% for 5 min and xylole for 5 min in order to dehydrate the sections. The samples were dried and analysed with the optical microscope.

F.3 Results and discussion

F.3.1 Physical-Chemical characterization

The Hyaff120® Hydrogel is easily obtained by solubilising the polymer Hyaff120® in water and by curing the aqueous solution under UV light. The main advantage of this method respect others involving HA, is the elimination of double bonds C=C in the polymer for the photocrosslinking reaction.

The process of Hyaff120® synthesis is schematically illustrated in Figure 1A. During the esterification reaction the carboxylic group of the polysaccharide is substituted by bromide group using ion of an ammonium salt as intermediate of reaction. By increasing the bromide concentration, the percentages of esterification rises determining the increasing of its hydrophobic feature and the reduction of the UV-curing time. Low percentages of esterification (20-30%) allowed good solubility in water but it requires long time for the hydrogel formation (30 min at 4mW/cm^2). Higher degree of substitution (75 % esterification)

allowed a faster cross-link (2-3 min at 4mW/cm^2) even if the concentration of ester is low (15 mg/ml), but the product is no more soluble in water because of its hydrophobic nature. The best compromise was achieved by producing a hydrogel with 50% degree of esterification in term of good water solubility and relatively moderate time in the UV processing of hydrogel preparation.

The Hyaff120$^®$ production was monitored by measuring through HPLC analysis the percentage of esterification up to the reaching of a plateau (data not shown). The chemical structures of HATBA and photoinitiator-HA conjugate (HYAFF120$^®$) were compared by FT-IR spectroscopy. As shown in Figure 1B, the differences between the spectra were visible at 1750 cm^{-1} and a 1250 cm^{-1}. The first peak represents the stretching of the esterified bond. The second peak refers to the oscillation between the aromatic group and the oxygen atom. Both of them prove that the esterification reaction gives the desired product.

In order to evaluate optimal concentration of non-irradiated polymer solutions for clinical application, rheological analysis was performed by frequency sweeping with different concentrations of photoinitiator-HA conjugate (10, 20, 30, 40, 50 e 75 mg/ml) in physiological solution. Applying rising deformation rates, the shear stress was recorded by the rheometer. Since the viscosity decreased with increasing deformation rates, the experimental profiles suggest a pseudoplastic behaviour typical of polymer solutions with high molecular weight. Pseudoplastic fluids approximate at low deformation rates newtonian viscosity limit (η_0). However in a pseudoplastic fluid, as the deformation rates increased, the polymeric chains begin organising in the flow direction and at very high deformation rates, once the complete orientation was gained, the viscosity would reach a new constant value (η_∞). Thus, the results suggest that the polymer solutions may contain effective entanglements over this range of frequencies (0.1-10 Hz).
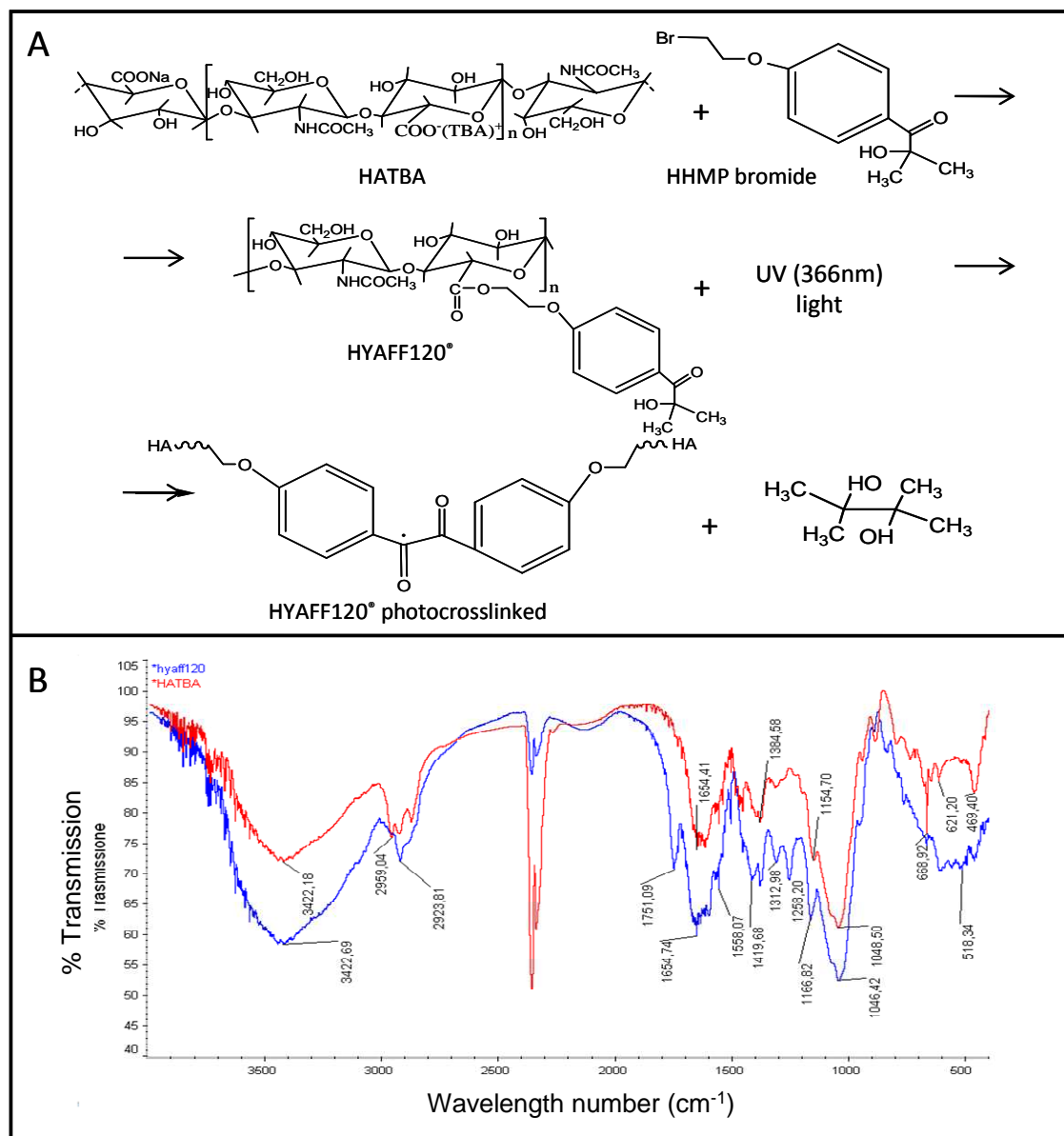
Figure 1 *Photoinitiator-hyaluronic acid conjugate (Hyaff120) synthesis and FT-IR characterization. A) Schematic illustration of Hyaff120 synthesis; B) Comparison of FT-IR spectra of HATBA in red and photoinitiator-hyaluronic acid conjugate in blue.*

The slope values of the flow curves at low deformation rates ($\dot{\gamma} \to 0$) are reported in Table 1 as function of the concentration. By increasing the concentration of photoinitiator-HA

conjugate, η_0 increased rapidly up to 2.5 Pa s in the most concentrated solution. Solutions with a viscosity higher than of 0.4 Pa s, are handled with difficulty with a 27 Gauge needle, which is used for *in vivo* cell injection.

In the frequency range studied, all the polymer solutions show a viscous modulus greater than to the elastic one.

Table 1. *Values of apparent viscosity for different concentration of photoinitiator-HA solution*

Concentration (mg/ml)	Viscosity (Pa s)
10	0.025
20	0.094
30	0.107
40	0.403
50	0.783
75	2.459

By cross-linking the solutions under UV exposure, a wall-to-wall compact and stable hydrogel was achieved with uniform morphological properties. All samples were characterized by dynamic mechanical rheology. Before applying forced oscillation analysis, it was investigate the linear elastic region in which the complex modulus was constant. The shear stress was gradually increased maintaining a constant frequency (1 Hz) and the complex modulus was recorded until the breaking point, when the complex modulus fell down to zero (Figure 2A). The same analysis was repeated for two exposure time, 3 and 5

min, and different polymer concentrations (Figure 2A-B). Since these concentration exhibit a linear response over a wide range of applied stress, we expect these hydrogels will have a uniform and predictable rheological response *in vivo* regardless of the mechanical environment to which they are subjected. For exposure time of 3 min, the maximum stress increases from 50 Pa (10 mg/ml) to about 1500 Pa (75 mg/ml), whereas a longer UV exposure time led to an increasing of the modulus of only the 10-20%. Thus, the concentration value seems to be more critical respect to the exposure time for the reaching of the maximum stress value.

In order to evaluate the elastic and viscous moduli, frequency sweep was performed for different concentrations and cross-linking times. The measure was repeated 3 times for each condition, keeping the shear stress at 1Pa during measurements in order to ensure to be in the linear elastic region. Figure 2 C-D illustrate the elastic and viscous moduli recorded for different polymer concentrations at constant temperature of 20 °C after 3 min of UV exposure. A remarkable difference between hydrogel and precursor solutions can be observed by the rheological experimental profiles. The presence in hydrogels of chemical bonds among the polymeric chains, reduces drastically their mobility and stabilized the network in a semisolid 3D structure. The hydrogel displays a high degree of elasticity, with G' only weakly dependent on frequency and greater than G'' over the entire frequency range. The stability and the relative large value of G' compared to G'' over a range of frequencies is a characteristic feature of a cross-linked hydrogel.
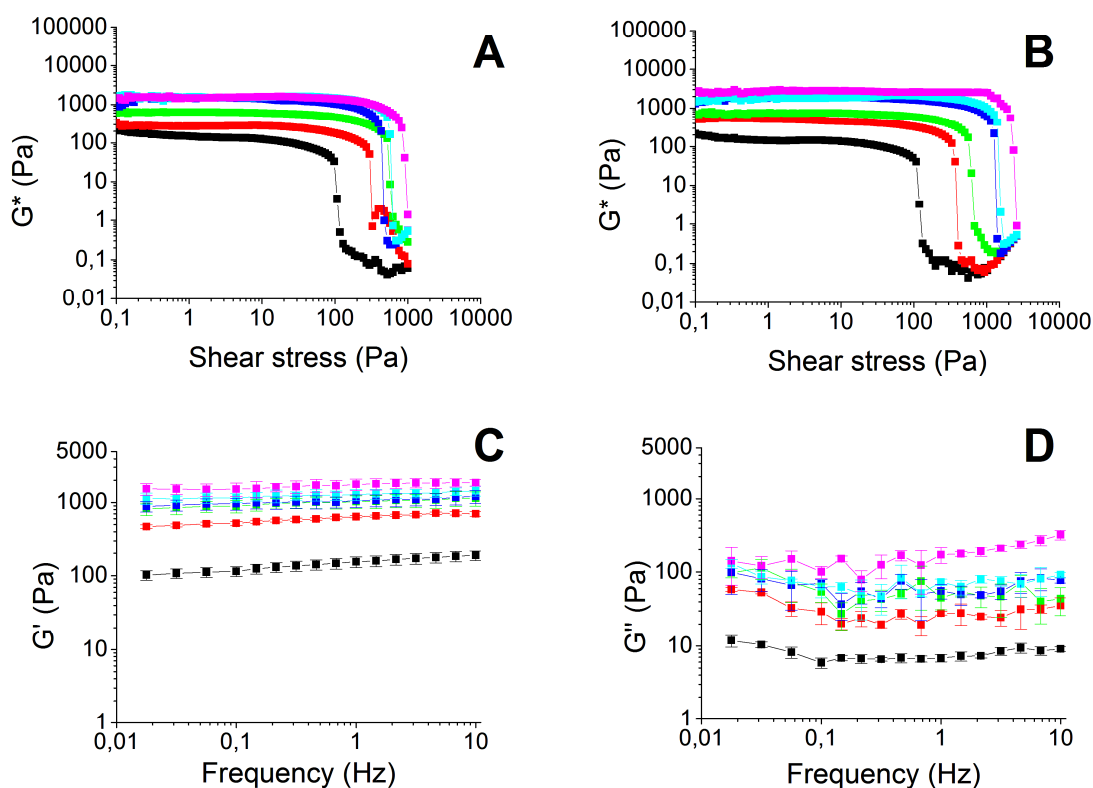
Figure 2 *Rheological analysis of hydrogel with different concentration of HYAFF120. Stress sweeping measurements after curing: 3 min (A) and 5 min (B). Elastic (C) and viscous(D) moduli profiles obtained by frequency sweeping of different concentration of hydrogels cross-linked for 3 min.*

For low concentrations, the increasing of polymer concentration led to a rising of elastic modulus, up to reaching a plateau at 1500-2500 Pa with concentration greater than 40mg/ml (Figure 3A). Similar consideration can be done studying the G' as function of the exposure time. As the irradiation energy increases, the numbers of cross-links formed in the system are expected to increase, giving the formation of more compact hydrogel. The growth of G' was rapidly passing from 3 to 30 s but, as the exposition time rose, elastic modulus stabilized reaching a plateau (Figure 3B). The stabilization of the mechanical properties of hydrogels

over certain experimental conditions assure the use *in vivo* of a material with controlled properties. Table 2 shown the average value of elastic modulus for different concentration and exposure time.

Table 2 *Average elastic modulus as function of concentration and time exposure (Italquarz lamp)*

Elastic modulus (Pa)		
Conc (mg/ml)	3 min	5min
10	144±23	155±15
20	605±29	759±84
30	990±92	1300±162
40	1034±194	1448±89
50	1256±184	1723±291
75	1680±285	1979±434

The slight increase of G' over the frequency could be due a different organization of the polymer chains and entanglements. It is known, from the linear viscoelastic model of Kamphuis et al (1984), that at high frequency, the short time (faster) relaxation is primarily due to elastic relaxation of individual chains whereas longer-time (slower) relaxation modes reflected an rearrangement of the 3D network into more energetically favourable configurations. In order to gain more information about the viscoelastic behaviour of the hydrogels, the elastic modulus was analysed by linear regression as function of frequencies and concentrations (Figure 3C). With the increasing of the polymer concentration the slope of G' progressively decreases up to a plateau, due to the formation of a more rigid structure.
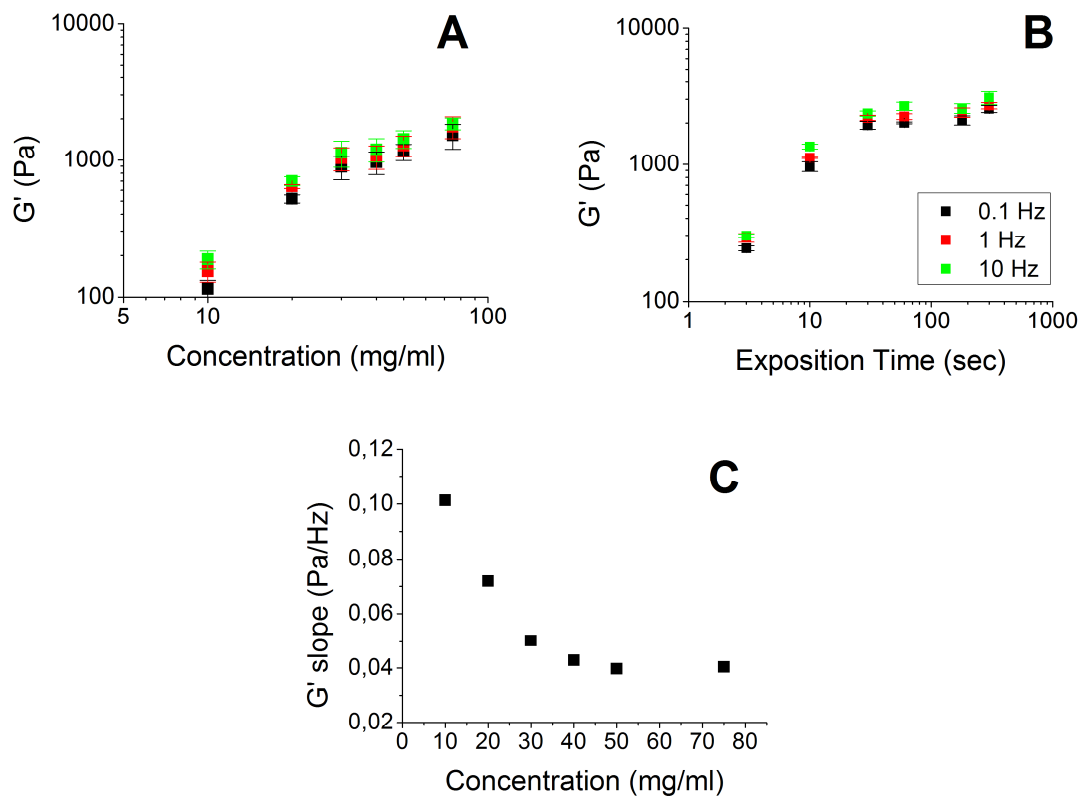
Figure 3 *Elastic modulus profiles. A) G' as function of concentration for different frequencies for hydrogels cross-linked for 3 min B) G' profile as function of the exposure time c) G'slope as function of concentration of hydrogels cross-linked for 3 min*

The phase shift angle δ,

$$\tan(\delta) = G''/G'$$

where δ is an indicator of internal dissipation. For purely elastic solids, the stress is in phase with the strain, that is $\delta = 0$, while for ideally viscous fluids, the stress is 90° out of phase with the strain, that is $\delta = 90$. The phase shift angle of all hydrogels is almost constant for all the concentrations (3°) with a higher value calculated for a concentration of 75 mg/ml (8°).

Since the *in vivo* application require the use of small beam as light source, we compare the performance of two light sources: Italquartz lamp and Dymax. At the same distance from the source (2 cm) Dymax light intensity (427 ± 2.5 mW/cm^2) is two orders of magnitude higher than Italquartz lamp (4 mW/cm^2). Thus, in order to achieve the same crosslinking regime and

elastic response we need a shorter exposure time. In order to compare the performance of two lamps in terms of elastic response of the material, rheological analysis were performed for hydrogel at different concentrations for several exposure times, keeping the same distance from the surface for both light sources.

The results, summarized in Table 3, show that the values obtained with an exposure time of 3-5 minutes at 4 mW/cm2 (source Italquartz, Table 2) are achieved, as expected, in less than 10 seconds using the Dymax lamp.

Table 3. *Average elastic modulus as function of concentration and time exposure (Dymax lamp)*

Elastic modulus (Pa)						
Conc (mg/ml)	3 sec	10 sec	30 sec	1 min	3 min	5 min
10	43±7	162±7	261±24	250±13	251±37	253±19
20	155±42	646±79	1035±73	1117±137	1258±37	1421±182
30	267±13	1113±39	2112±118	2264±92	2315±174	2722±248

F.3.2 Swelling analysis

The swelling behaviour of hydrogels was investigated measuring weight ratio due to water uptake as function of polymer concentration and UV exposition time (Figure 4).

Generally, the maximum water uptake is reached in the first 24 hours. Swelling at equilibrium depend upon the polymer concentration and the UV exposition time. In particular the swelling capacity decreases with the increasing of these two parameters, as already reported by other research groups (Flory 1953; Jennie Baier Leach, Bivens et al. 2003; Zhao 2006). As the cross-linkage density increased the characteristic dimension of the 3D network decreased. Following the Flory-Rehner calculations, the swelling results can be used to calculate some important structural parameters of the hydrogel such as:

a) the average molecular weight between cross-links, M_C (g/mol), defined as the chain average molecular weight between two following cross-links;

b) the cross-linkage density, υ_e (mol/cm^3), expressed by the ratio between the number of moles between two following cross-links and the volume of dry polymer.

c) the mesh size, ξ (nm), defined as the length of the polymer chain between two following cross-links.
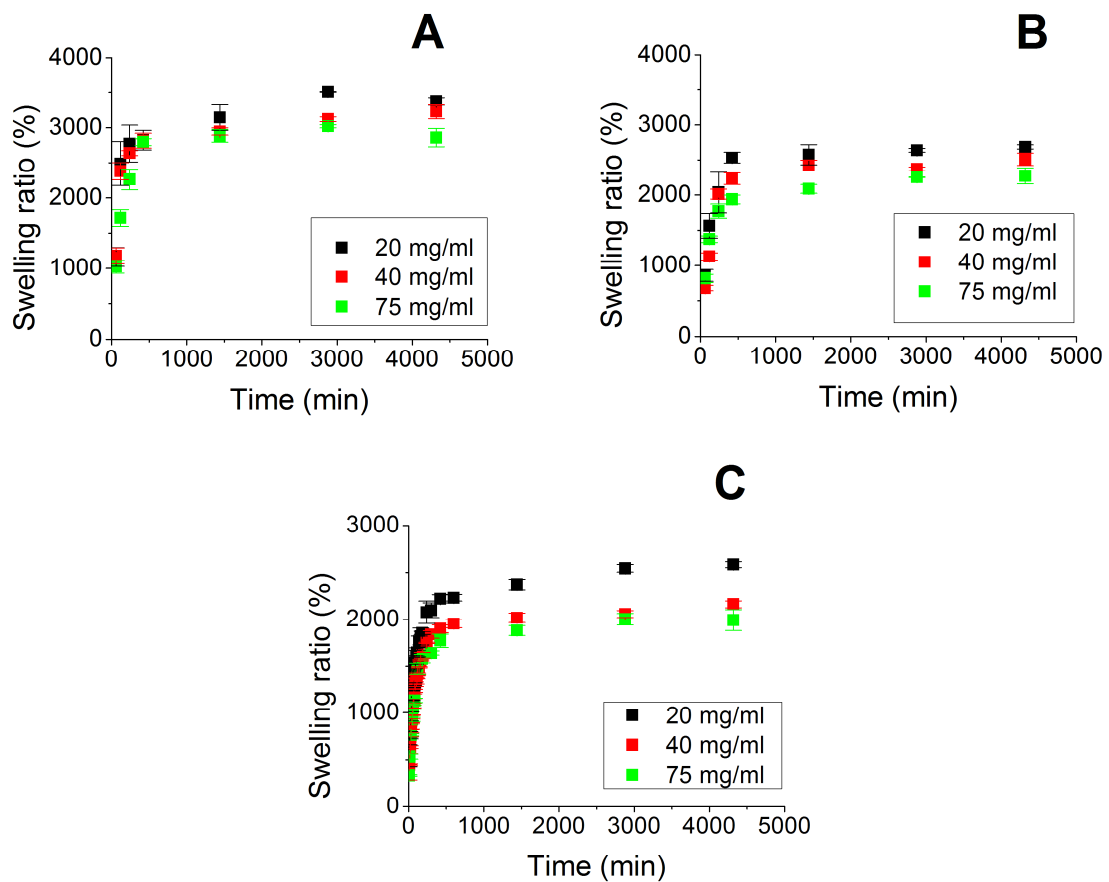

Figure 4. *Swelling ratio as function of analysis time for exposition time equal to 1 min (A), 3 min (B) and 5 min (C).*

When a polymer network was swollen by a particular solvent, the chains are in elongated conformation, but, by increasing the elongation, an elastic force developed in the opposite

direction limiting the process of stretching. On the other hand, the polymer-solvent mixing increased the system entropy favouring the hydrogel swelling towards lower free energy configurations. The action of these opposite forces led up to an equilibrium situation.

The average molecular weight M_C was calculated using a simplification of Flory-Rehner equation (Flory 1953):

$$Q_v^{5/3} = \frac{\upsilon M_c}{V_1}\left(0.5 - \chi\right), \tag{F.1}$$

where Q_V is the volumetric swelling ratio, υ is the specific volume of dry polymer (0.893 cm^3/g), V_1 is the specific volume of solvent (1 cm^3/g) and χ is the Flory interaction parameter between polymer and solvent (0.473).

Q_V was evaluated from the weight swelling ratio Q_M with the following equation (Marsano, Gagliardi et al. 2000):

$$Q_v = 1 + \frac{\rho_p}{\rho_s}\left(Q_M - 1\right), \tag{F.2}$$

where ρ_p is the density of dry polymer (1.12 g/cm^3) and ρ_s is the density of solvent (1 g/cm^3).

The cross-linkage density was determined as follows (Huglin MB, Rehab MM et al. 1986):

$$\upsilon_e = \frac{\rho_p}{M_C}, \tag{F.3}$$

The swollen hydrogel mesh size was calculated with the following equation (De Jong SJ, Van Eenderbrugh B et al. 2001):

$$\zeta = Q_v^{1/3}\sqrt{r_0^2}, \tag{F.4}$$

where $\sqrt{r_0^2}$ is the root-mean square distance between cross-links (nm). For HA, the following value was reported (Cleland 1970):

$$\sqrt{r_0^2} \cong 2.4\sqrt{2n}, \tag{F.5}$$

where n is the number of disaccharide repeat units for HA with a given molecular weight. For HA with the molecular weight (M_n) 178000, n is 450, thus:

$$\sqrt{r_0^2} = 0.1707\sqrt{M_n} \, . \tag{F.6}$$

A combination of Eqs. 9 and 11 and a substitution of M_C for M_n gives

$$\zeta = 0.1707\sqrt{M_C}\,Q_v^{1/3}\,, \tag{F.7}$$

Once Q_M was evaluated experimentally, Q_V was determined from Eq. 2 and M_C, υ_e and ξ were calculated from Eqs. 1, 3 and 7 respectively. The results were plotted as function of Hyaff120$^®$ concentration and different exposition times (Figure 5).
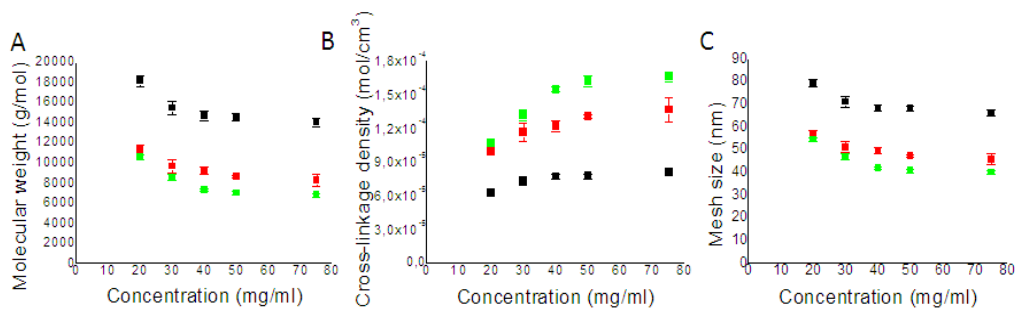

Figure 5 *Molecular weight between cross-links (A), cross-linkage density (B) and mesh size (C) as function of Hyaff120® concentration and exposition time (1min in black, 3 min in red, 5 min in green).*

The results show that both the polymer concentration and the exposition time promotes the formation of a more compact structure by increasing the cross-link number υ_e among the chains. This closer network is characterized by lower molecular weight between cross-links and the mesh size decreased giving a closer network. As expected from the rheological data, the dependence to these parameters results is much stronger for short exposure times. As shown in Figure 5, the results obtain for 3 and 5 min were very similar to each other.

F.3.3 Hydrolytic degradation

Generally the ester is expected to degrade in aqueous solutions. The composition of the solution during the hydrogel degradation was monitored over time by HPLC analysis, which allowed following the kinetics of release of alcohol photoinitiator (HHMP) and ester Hyaff120®. The in vitro degradation rate was tested (5 repetitions) for different Hyaff120® concentrations and different exposition times (Figure 6).

Whereas for 3 and 5 min the hydrogel was compact and wall to wall limited, with an exposition time equal to 1 min the structure was weak and jelly-like. Observing the results at 3 and 5 min for a concentration of 30 mg/ml (Figure 6A-B), the degradation process was characterized by a first phase (7-10 days) where the quantities of alcohol HHMP and ester Hyaff120® were moderate. In this phase the samples, dipped under the buffer solution, swelled, releasing the inner unreacted ester. At the same time this ester degraded under the action of OH⁻ ions in solution and it broke down into its starting reactants, hyaluronic acid and alcohol HHMP. Similar consideration can be made for all concentrations (data not shown).
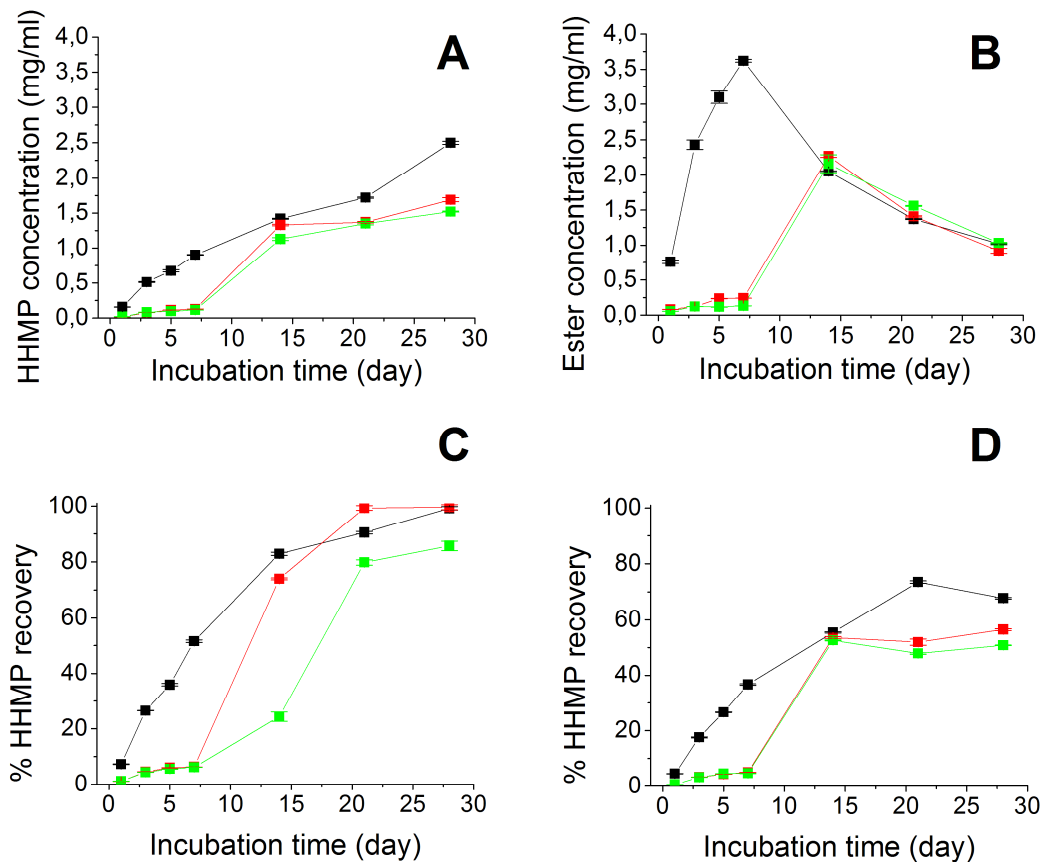
Figure 6. *Degradation in water of hydrogel obtained after UV exposure of 1 min (red), 3min (green), 5 min (blue). HHMP (A) and Hyaff120® (B) concentrations as function of incubation time for a fixed concentration (30 mg/ml). HHMP recovery as function of time for 10 mg/ml (C) and 75 mg/ml (D).*

Nevertheless, the continuous stretching of chemical bonds together with the OH⁻ attack caused the structure breakage up to its solubilisation after about 14 days, demonstrate by a very fast rising in the ester concentration. Since then the quantity of ester decreased as function of time, because of its slow but relentless degradation into HA and HHMP.

In the case of the lowest exposition time (1 min), as a consequence of the weak structure, within 5-7 days the ester concentration reached the peak indicating that these samples were already degraded and solubilised in the buffer solution. This difference is directly related to the hydrogel physical structure: at a fixed concentration, by increasing the exposition time,

i.e. the energy received for unit of time, the cross-linkage density leading to a rigid and compact network which was more resistant to the stretching of chemical bonds and to the attack of OH$^-$.

As the initial quantity of HHMP and the volumes of the samples were known, once the HHMP concentration was calculated as function of incubation time, the quantity of alcohol recovered respect to the initial quantity was calculated as function of incubation time (Figure 6C-D). The diagrams showed the behaviours of two concentrations, 10 mg/ml and 75 mg/ml. In the case of the most diluted sample cross-linked for 1 and 3 min, after 28 days the HHMP recovery was complete, reaching the 99% of the total quantity present at the beginning of the degradation process. By increasing the exposition time up to 5 min, the percentage decreased (85%). The most concentrated hydrogel reached values of about 70%, 60% and 50% for increasing exposition times, 1 min, 3 min and 5 min respectively. At a fixed exposition time, by increasing polymer concentration, the higher resistance of hydrogel to the degradation proves again a rising of the number of cross-links among the chains.

F.3.4 Hydrogel Morphology

The morphology of freeze-dried hydrogels was studied by SEM as function of different concentrations (Figure 7).

The SEM analysis of the surface and interior morphology (data not shown) of the hydrogel clearly showed its three-dimensional sponge structure. Even if the structure observed by SEM give only a qualitative idea of the original morphology because of the shrinkage of the gel volume, the pictures prove an highly homogenous properties through the entire hydrogel volume. As the polymer concentration increasing the characteristic diameter of the pore decreases showing a more compact structures of the sample.
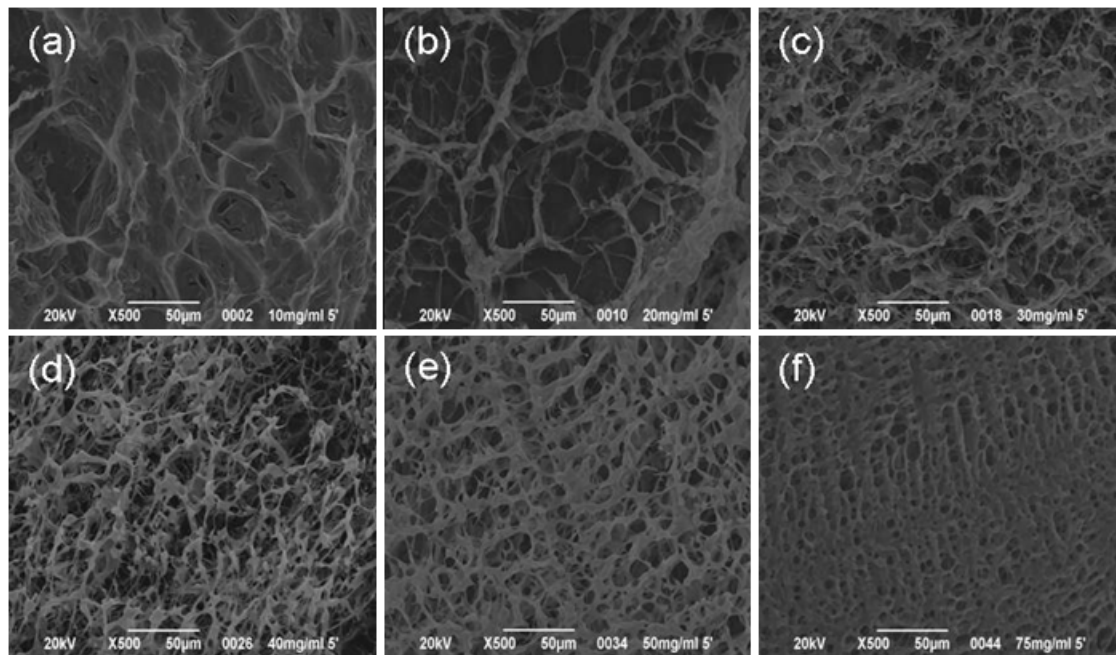
Figure 7 *SEM photographs (500x) of cross-sectional interiors of freeze-dried hydrogels obtained after 5min (4mW/cm²) UV exposure of solution with different polymer concentrations: A) 10mg/ml, B) 20 mg/ml, C) 30 mg/ml, D) 40mg/ml, E) 50mg/ml, F) 75 mg/ml*

F.3.5 Cell-Hydrogel Interaction

In the view of using Hyaff120 hydrogels as cell carrier, it is important to determine the material biocompatibility *in vitro* and the effect of UV exposition on cell-viability. As mentioned previously the clinical applicability of these hydrogels is related to the possibility of using a lamp characterized by a small light beam. Experimental observation of the conical light emitted by the probe led to calculation of the top angle (66°). Thus the light intensity of 1329 ± 0.6 mW/cm^2 assessed at 0.5 cm decreases as the distance from the lamp probe increases, reaching the value of 4.1 ± 0.3 mW/cm^2 to 20 cm. The power absorbed by the material determines an increasing of surface temperature, which was plotted as function of time exposure and distance from the light beam (Figure 8B). The experimental profile show a rapid increasing of temperature with the exposure time up to the reaching of a plateau around

100 sec. The equilibrium temperature is strongly dependant on the distance from the beam, even if similar results are registered for 2 and 3 cm of distance (Figure 8B).

To avoid cell damaging, it is then reasonable to maintain the exposure time as low as possible, though guaranteeing the hydrogel formation. HL1 cardiomyocyte cell line were encapsulated in 30mg/ml solution and their viability was determined both immediately after different UV exposure time (3", 30", 1.5', 3', 6' e 10') at 1.1 W/cm^2 (Figure 8A). A qualitative assessment of the cell viability in polymeric solution was made by Live/Dead dye-staining. By this method, the living and dead cells were, respectively, stained in green and red under fluorescence microscope. The Figure 8 shows indicates that the majority of cells remain viable up to 30 seconds.
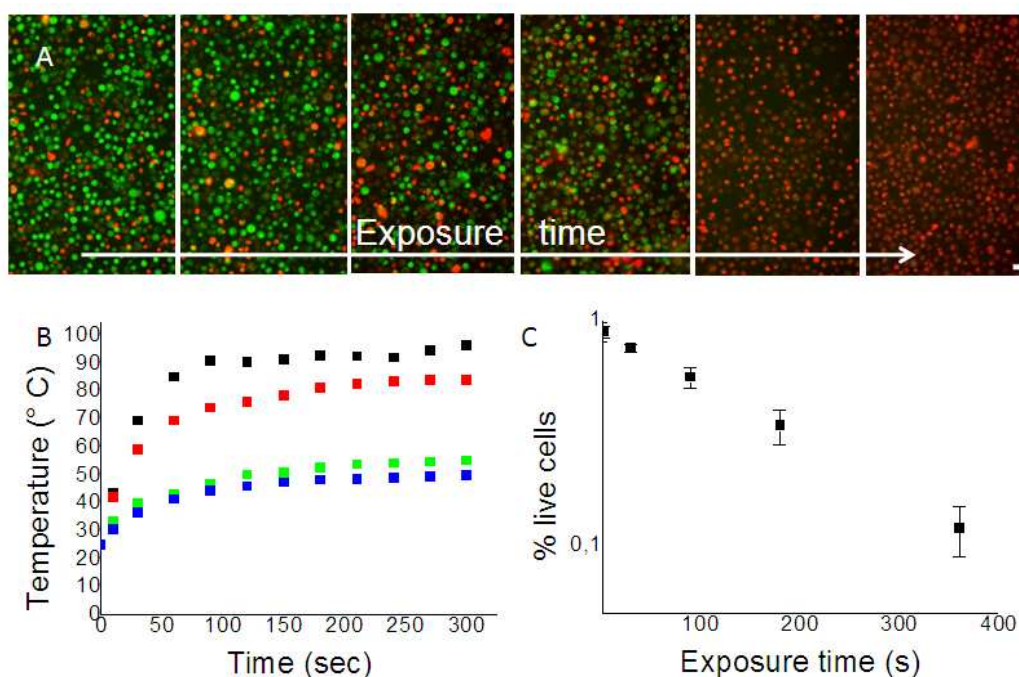

Figure 8. *Effect of UV exposure cell-hydrogel blend during photopolymerization. A) Fluorescence imaging (20x magnification) of hydrogels after 3", 30", 1.5', 3', 6' e 10' UV exposure at 1.1 W/cm²*
(scale bar =10 µm) Viable cell in green, dead cells in red. B) Surface temperature profile as function of the exposure time (0.5 cm black, 1cm red, 2cm green, 3cm blue). C) Percentage of viable cells as function of the exposure time (Trypan blue assay)

In order to quantify this correlation, live and dead cells were counted after UV exposition by Trypan Blue assay. This method measures the percentage of a cell suspension that is viable. The viability test proved the good tolerance of cells to UV for exposure time up to 30 seconds (75% the population is viable). However the percentage of dead cells grows exponentially with the exposure time, halving the cell population approximately in 1.5-2 minutes (Figure 8C).
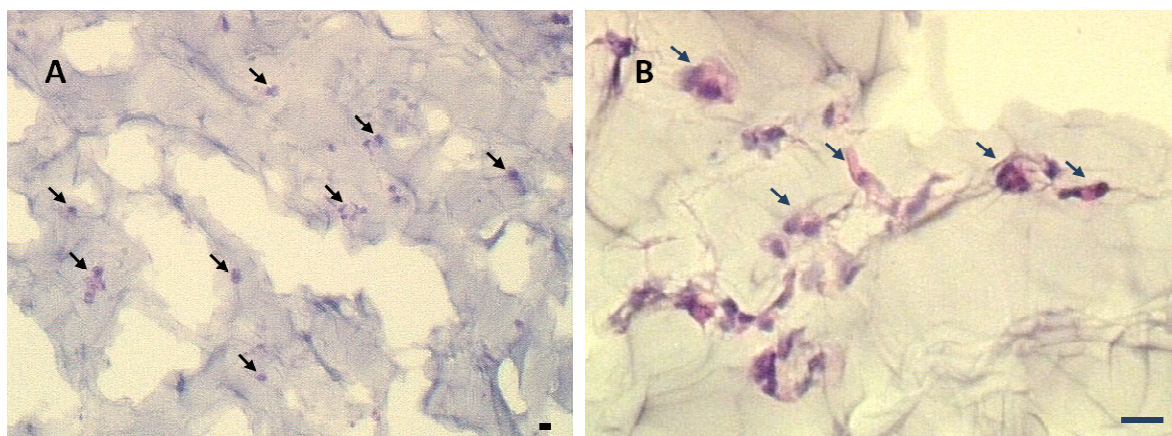

Figure 9. *Representative image of 30mg/ml hydrogel histology after ematossilin-eosin staining. HL1 were cultivated in hydrogel for 2 days after photopolymerization with 10 seconds UV light exposure. Microscopic image of hydrogel sections: HL1 in pink, hydrogel in violet A) 10x magnification B) 20x magnification. Scale bar 10 μm.*

In order to evaluate if the mass transport meets the requirements necessary to the cells survival, the cell viability and proliferation were investigated on HL1 cell-containing hydrogels by MTT assay. The microscopic observation of the hydrogel after MTT staining, indicate good cell proliferation up to 5 days of culture, proving the biocompatibility of material. The MTT absorbance increases from 1 to 4 in the first 24 hours. After that, since the cell encapsulation enhances the hydrogel degradation, the hydrogel swells and completely degrades in 5 days. The morphology of encapsulated cells was investigated by ematossilin and eosin staining after 2 days of culture and some representative images are recorded in

Figure 9. The microscopic observation of the hydrogel sections confirms the MTT results, showing the cytoplasm (pink coloured) of some cells characterized by the typical elongated shape. However most of the cells maintain a round shape, indicating poor adhesion to the hydrogel surface.

F.4 Conclusions

This study present the development of a new photo-polymerizable hydrogel formulation based on hyaluronic acid derivative, HYAFF120$^®$.

Physical/chemical characterization of the Hyaff120$^®$ solutions and the Hyaff120$^®$ hydrogels have been performed for different polymer concentrations and exposure times. The macroscopic effect is the fabrication of a compact hydrogel that presents an elastic response and low degradation rate. As the concentration and/or the exposure time increases, hydrogel structural parameters change, in particular the cross-linking density increases. All the analysis show the gradual enhancing of these properties up to the reaching of a plateau.

The study of the interactions between HL1 cells and hydrogel assessed the biocompatibility of the hydrogel and the best working conditions that guarantee the highest cell viability. MTT tests proved the cell proliferation in the hydrogel, demonstrating an adequate mass transport and the absence of toxic product during the crosslinking and the degradation.

The most appropriate use of Hyaff120 ® seems to be as drug or cells carrier due to its feasibility of polymerization *in vivo* with a small UV light energy.

F.5 References

Ali Khademhosseini, G. Eng, et al. (2006). "Micromolding of photocrosslinkable hyaluronic acid for cell encapsulation and entrapment." Journal of Biomedical Materials Research Part A **79A**(3): 522-532.

Anderson, D. G., J. A. Burdick, et al. (2004). "MATERIALS SCIENCE: Smart Biomaterials." Science **305**(5692): 1923-1924.

Anna C. Jen, M. C. W. A. G. M. (1996). "Review: Hydrogels for cell immobilization." Biotechnology and Bioengineering **50**(4): 357-364.

Anseth, K. S., C. N. Bowman, et al. (1996). "Mechanical properties of hydrogels and their experimental determination." Biomaterials **17**(17): 1647-1657.

Anseth, K. S. and J. A. Burdick (2002). " New directions in photopolymerizable biomaterials." MRS Bulletin. **27**(2): 130-136.

Burdick, J. A., C. Chung, et al. (2005). "Controlled Degradation and Mechanical Behavior of Photopolymerized Hyaluronic Acid Networks." Biomacromolecules **6**(1): 386-391.

Chen, W. Y. J. and G. Abatangelo (1999). "Functions of hyaluronan in wound repair." Wound Repair and Regeneration **7**(2): 79-89.

Claycomb, W. C., N. A. Lanson, Jr., et al. (1998). "HL-1 cells: A cardiac muscle cell line that contracts and retains phenotypic characteristics of the adult cardiomyocyte." Proceedings of the National Academy of Sciences **95**(6): 2979-2984.

Cleland, R. (1970). "Ionic polysaccharides. IV. Free-rotation dimensions for disaccharide polymers. Comparison with experiment for hyaluronic acid." Biopolymers **9**: 811-824.

De Jong SJ, Van Eenderbrugh B, et al. (2001). "Physically crosslinked dextran hydrogels by stereocomplex formation of lactic acid oligomers: degradation and protein release behaviour." J Controlled Release **71**: 261-275.

Flory, P. (1953). Principles of polymer chemistry. , Cornell University Press, Ithaca, NY,.

Grijpma, D. W., Q. Hou, et al. (2005). "Preparation of biodegradable networks by photo-crosslinking lactide, [epsilon]-caprolactone and trimethylene carbonate-based oligomers functionalized with fumaric acid monoethyl ester." Biomaterials **26**(16): 2795-2802.

Hennink, W. E. and C. F. van Nostrum (2002). "Novel crosslinking methods to design hydrogels." Advanced Drug Delivery Reviews **54**: 13-36.

Hoffman, A. S. (2002). "Hydrogels for biomedical applications." Advanced Drug Delivery Reviews **54**(1): 3-12.

Hubbell, J. A. (1999). "Bioactive biomaterials." Current Opinion in Biotechnology **10**(2): 123-129.

Huglin MB, Rehab MM, et al. (1986). "Thermodynamic interactions in copolymeric hydrogels Macromolecules " **19**: 2986-2991.

Ingrid Zhang, K. K. S. D. A. E. (1996). "Hydrogels with enhanced mass transfer for transdermal drug delivery." Journal of Pharmaceutical Sciences **85**(12): 1312-1316.

J.A. Cadée, M. J. A. v. Luyn, et al. (2000). "In vivo biocompatibility of dextran-based hydrogels." Journal of Biomedical Materials Research **50**(3): 397-404.

Jennie Baier Leach, K. A. Bivens, et al. (2003). "Photocrosslinked hyaluronic acid hydrogels: Natural, biodegradable tissue engineering scaffolds." Biotechnology and Bioengineering **82**(5): 578-589.

Kamphuis, H., R. J. J. Jongschaap, et al. (1984). "A transient-network model describing the rheological behaviour of concentrated dispersions." Rheologica Acta **23**(4): 329-344.

Lapcik, L., S. De Smedt, et al. (1998). "Hyaluronan: Preparation, Structure, Properties, and Applications." Chem. Rev. **98**(8): 2663-2684.

Marsano, E., S. Gagliardi, et al. (2000). "Behaviour of gels based on (hydroxypropyl) cellulose methacrylate." Polymer **41**: 7691-7698.

Nettles, D. L., T. P. Vail, et al. (2004). "Photocrosslinkable Hyaluronan as a Scaffold for Articular Cartilage Repair." <u>Annals of Biomedical Engineering</u> **32**(3): 391-397.

Penn, M. and E. Topol (2007). The Challenge for Stem Cell Therapy. <u>Stem Cells And Myocardial Regeneration</u>**:** 1-6.

Peppas, N. A. and J. J. Sahlin (1996). "Hydrogels as mucoadhesive and bioadhesive materials: a review." <u>Biomaterials</u> **17**: 1553-1561.

Ratner, B. D. (2002). "Reducing capsular thickness and enhancing angiogenesis around implant drug release systems." <u>Journal of Controlled Release</u> **78**(1-3): 211-218.

Stocum, D. L. (1998). "Regenerative biology and engineering: strategies for tissue restoration." <u>Wound Repair and Regeneration</u> **6**(4): 276-290.

Toole, B. P. (2004). "Hyaluronan: from extracellular glue to pericellular cue." <u>Nat Rev Cancer</u> **4**(7): 528-539.

Zhao, X. (2006). " Synthesis and characterization of a novel hyaluronic acid hydrogel. ." <u>J Biomater Sci Polymer</u> **17**(4): 419-433.

Ringraziamenti

E crescendo impari che la felicità non e' quella delle grandi cose…

Fino a pochi minuti fa sentivo solo la stanchezza, e la frenesia, quella tipica dalle scadenze importanti, e la preoccupazione, per i mille errori che rileggendo avrei trovato nonostante tutto. Poi l'ho vista nelle mie mani.. ne ho sentito il peso… l'ho sfogliata… ed è stata gioia!

In questi fogli leggo le speranze, gli entusiasmi, le delusioni, il duro lavoro, le risate … i ricordi delle persone che mi hanno accompagnato per questi tre anni e che sono con me ora … e mi sento molto fortunata! GRAZIE!

Ringrazio Nicola perché il dottorato è stato sul serio un'opportunità, grazie per le discussioni mai sterili, per la fiducia, per l'entusiasmo, le energie e l'impegno che poni nello scegliere e sostenere questo gruppo di ricerca perché rimanga così armonioso e ricco.

Ringrazio tutti i membri del BioEra lab e ho le lacrime a ricordarne i motivi. Se c'è una nota di tristezza in questa fine dottorato è proprio nel lasciare voi. Credo nella particolare bellezza di questo gruppo sia a livello umano che professionale. Grazie per i consigli, le discussioni critiche, le risate, i DIPIC channel, i commenti muti ma comprensibili, le foto originali, l'aperitivo dopo lavoro, i filmati delle celluline, la generosità, l'entusiasmo e la partecipazione… vi porto con un sorriso nel cuore.

Un grazie a Chris e Sharon che hanno condiviso la mia fatica americana e a Nina per essere stata la mia base d'affetti in trasferta, ricorderò ora con affetto e un sorriso le notti passate sui divani del MIT sorpresi dall'alba a studiare.

Grazie ai tecnici che per anni mi hanno visto correre su e giù per i corridoi con progetti che sembravano nascere già in ritardo.

Grazie alla mia famiglia che ha saputo mettere amore e dolce rispetto anche nell'accettare scelte molto lontane e difficili. Grazie per l'ascolto nelle situazioni più complicate, la mia serenità e la mia forza hanno basi nel vostro affetto. Un grazie a Laura per la partecipazione e il sostegno sempre presente anche da lontano.

Un grazie agli amici, che mi fanno sentire così ricca. Un grazie particolare in questo momento ad Alberto per la armonia quasi magica di casa Rigallo e l'aiuto concreto, a Frombol perché c'è, per le chiacchiere mai banali e per le risate, a Opimo per i giri in moto all'avventura, ad Anna guru del mio cuore, a Elly per il rilassato abbandono che solo una vera amicizia può permettere, a Betta per la gioia del ritrovarsi, a Sundru per le ciaccole, a

Maura per le risate girly, a Cecilia per la comprensione e gli spunti di riflessione, anche da molto lontano… ma comunque a tutti GRAZIE: vi sento sempre così vicini.

Con grande affetto

Elisa

Amo tutto ciò che è stato,
tutto quello che non è più,
il dolore che ormai non mi duole,
l'antica e erronea fede,
l'ieri che ha lasciato dolore,
quello che ha lasciato allegria
solo perché è stato, è volato
e oggi è già un altro giorno.

Fernando Pessoa